CHALMERS

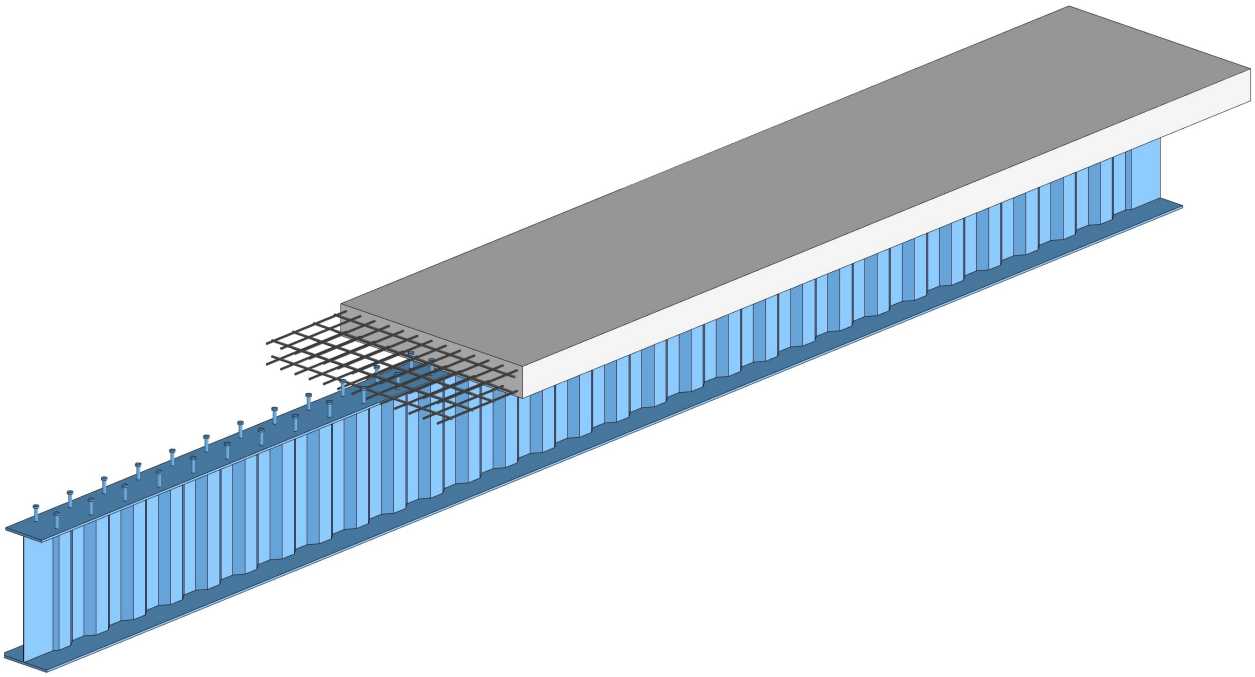

# Design Tool for the Ultimate Bending Resistance of Steel-Concrete Composite Bridge Girders with Flat and Corrugated Web Plates made of Stainless Steel

Master's thesis in Master Program Structural Engineering and Building Technology

ALBIN KARLSSON
GUSTAV FRIMAN

DEPARTMENT OF ARCHITECTURE AND CIVIL ENGINEERING

CHALMERS UNIVERSITY OF TECHNOLOGY
Gothenburg, Sweden 2023
www.chalmers.se

Master's thesis 2023

# Design Tool for the Ultimate Bending Resistance of Steel-Concrete Composite Bridge Girders with Flat and Corrugated Web Plates made of Stainless Steel

ALBIN KARLSSON

GUSTAV FRIMAN


CHALMERS
UNIVERSITY OF TECHNOLOGY

Department of Architecture and Civil Engineering
*Division of Structural engineering*
Lightweight Structures
Chalmers University of Technology
Gothenburg, Sweden 2023

Design Tool for the Ultimate Bending Resistance of Steel-Concrete Composite Bridge Girders with Flat and Corrugated Web Plates made of Stainless Steel
ALBIN KARLSSON
GUSTAV FRIMAN



Supervisor: Senior Lecturer Mozhdeh Amani, Department of Architecture and Civil Engineering, Civil Structures department at COWI
Examiner: Senior Lecturer Mozhdeh Amani, Department of Architecture and Civil Engineering

Master's Thesis 2023
Department of Architecture and Civil Engineering
Division of Structural Engineering
Lightweight Structures
Chalmers University of Technology
SE-412 96 Gothenburg
Telephone +46 31 772 1000

Cover: AN ILLUSTRATION OF A STEEL-CONCRETE COMPOSITE BEAM WITH A CORRUGATED WEB.

Gothenburg, Sweden 2023

Design Tool for the Ultimate Bending Resistance of Steel-Concrete Composite Bridge Girders with Flat and Corrugated Web Plates made of Stainless Steel
ALBIN KARLSSON
GUSTAV FRIMAN
Department of Architecture and Civil Engineering
Division of Structural Engineering
Lightweight Structures
Chalmers University of Technology

# Abstract

Stainless steel may be a relatively expensive material choice, however, its remarkable and sustainable material properties can make it a great option for steel-concrete composite beams in bridge construction. Stainless steel provides a ductile behaviour with substantial strain hardening, and if combined with a corrugated web, the plastic capacity can be utilized even further. Eurocode only provides an analytical calculation method for carbon steel beams with an elastic perfectly plastic calculation model, furthermore, corrugated webs are completely disregarded in bending. For a beam with stainless steel and a corrugated web, this provided method is especially conservative.

The aim of this master's thesis was to develop a design tool capable of calculating the ultimate bending capacity for beams with different materials and geometry, also, incorporating behaviour models from recent research of corrugated beams and stainless steel.

The tool was tested for stability with shifting location of the neutral axis and the bending capacity was verified with a comparison to finite element analysis in a case study. The resulting comparisons between the design tool and finite element analysis suggest that the tool preforms satisfactory with bending moment capacities closer to the simulations compared to the conservative Eurocode models. This imply that the elastic perfectly plastic calculation model is not recommended for beams with stainless steel and high levels of strain hardening.

Even though the design tool is stable and yield good results, parts of it still needs additional validation and development. More research in this topic is needed in order to get a better understanding of the actual behaviour of this type of beams. At the moment the available research is limited, especially for steel-concrete composite beams with corrugated webs.

Keywords: Steel-concrete composite beam, Stainless steel, Strain hardening, Corrugated web, Ultimate bending capacity, Design tool

Beräkningsverktyg för den Ultimata Böjkapaciteten för Samverkansbalkar med Släta och Korrugerade Livsplåtar av Rostfritt Stål
ALBIN KARLSSON
GUSTAV FRIMAN
Institutionen för Arkitektur och Samhällsbyggnadsteknik
Avdelningen för Konstruktionsteknik
Forskargruppen för Lättviktskonstruktioner
Chalmers Tekniska Högskola

# Sammanfattning

Rostfritt stål kan vara ett relativt dyrt materialval, men med sina unika materialegenskaper kan det vara ett utmärkt alternativ för samverkansbalkar av stål och betong inom brokonstruktion. Rostfritt stål ger ett segt verkningssätt med betydande töjningshårdning, i kombination med korrugerade livsplåtar kan den plastiska kapaciteten utnyttjas ytterligare. Eurocode tillhandahåller endast en analytisk beräkningsmetod för kolstålbalkar med en elasto-plastisk beräkningsmodell, samtidigt som de korrugerade livsplåtarna bortses helt i böjning. För en balk med rostfritt stål och en korrugerad livsplåt är denna metod särskilt konservativ.

Syftet med denna masteruppsats var att utveckla ett designverktyg som kan beräkna den ultimata böjningskapaciteten för balkar med olika material och geometrier. Genom att inkludera beräkningsmodeller från den senaste forskningen inom korrugerade livsplåtar och rostfritt stål.

Designverktyget testades för stabilitet med olika positioner av neutrallagret och böjkapaciteten verifierades med en jämförelse mot resultat från finita element analyser i en fallstudie. De resulterande jämförelserna mellan designverktyget och finita element analysen tyder på att verktyget presterar tillfredsställande med böjmomentkapaciteter närmare simuleringarna jämfört med de konservativa Eurocodemodellerna. Detta innebär att den elasto-plastiska beräkningsmodellen inte rekommenderas för balkar med rostfritt stål och höga nivåer av töjningshårdning.

Även om designverktyget ger numeriskt stabila och goda resultat behöver delar av det fortfarande ytterligare validering och utveckling. Mer forskning inom ämnet behövs fortfarande för att få en bättre förståelse av det faktiska beteendet hos denna typ av balkar. För närvarande är den tillgängliga forskningen begränsad, speciellt för samverkansbalkar med korrugerade livsplåtar.

Nyckelord: Samverkansbror i stål och betong, Rostfritt stål, Töjningshårdning, Korrugerade livsplåtar, Ultimat böjningskapacitet, Design verktyg

# Acknowledgements

This master's thesis was carried out at the Civil Structures department at COWI in Gothenburg, in collaboration with the department of Architecture and Civil Engineering at Chalmers University of Technology. The thesis was conducted between January 2023 to June 2023 at the master's program Structural Engineering and Building Technology.

Several people have given valuable guidance and discussions during the work of this thesis. Firstly, we would like to thank our supervisor and examiner Senior Lecturer Mozhdeh Amani for a constant enthusiastic support over mail and meetings throughout this thesis work.

Furthermore, we would like to send our gratitude to the supervisors at COWI, Jonas Zachrisson, Filip Nilenius and Mattias Öst for being available and helpful every week with their expertise and encouragement. Also, thanks to the department of Civil Structures at COWI for a welcoming and motivating workspace with a special thanks for the fika every Thursday.

We would also like to thank two more individuals that were helpful, thanks to Katherine Cashell, Associate Professor in Structural Engineering at UCL, for the input on the continued strength method and on our implementation and development. Also, thanks to Amer Ali, Structural Engineer at WSP, for the shared experience of the finite element analysis of his master's thesis from last year.

Lastly, we tank our friends and opponents Alexander Sandström and Gustav Kullander for their continuous support and input during the thesis work and during our entire master's studies.

Albin Karlsson and Gustav Friman, Gothenburg, June 2023

# List of Acronyms

Below is the list of acronyms that have been used throughout this thesis listed in alphabetical order:

| | |
|---|---|
| CDP | Concrete damage plasticity |
| CS | Carbon steel |
| CSM | Continuous strength method |
| CSW | Corrugated steel webs |
| FE | Finite element |
| FEM | Finite element method |
| EPP | Elastic perfectly plastic |
| LPF | Load proportionality factor |
| NA | Neutral axis |
| PW | Partial web contribution for corrugated webs |
| SLS | Serviceability limit state |
| SS | Stainless steel |
| ULS | Ultimate limit state |

# Nomenclature

Below is the nomenclature of indices, sets, parameters, and variables that have been used throughout this thesis.

## Roman upper-case letters

| | |
|---|---|
| $A$ | Elongation after fracture for the steel |
| $A_{fl}$ | Cross-section area of the lower flange |
| $A_{re}$ | Minimum reinforcement area |
| $A_s$ | Cross-section area of the steel girder |
| $A_{steel}$ | Cross-section area of the steel girder |
| $A_w$ | Cross-section area of the web |
| $E_{cm}$ | Mean Young's modulus of elasticity for concrete |
| $E$ | Young's modulus of elasticity |
| $G$ | Shear modulus |
| $G_F$ | Fracture energy of the concrete |
| $N_c$ | Compressive force on the concrete |
| $M_{CSM}$ | Ultimate moment capacity calculated with the CSM model |
| $M_{EC}$ | Ultimate moment capacity calculated with model given by Eurocode |
| $M_{EPP}$ | Ultimate moment capacity calculated with the EPP model |
| $M_{Pl}$ | Plastic bending moment capacity |
| $M_{SHA,D}$ | Ultimate moment capacity calculated with the detailed model by Shamass and Cashell (2019) |
| $M_{SHA,S}$ | Ultimate moment capacity calculated with the simplified model by Shamass and Cashell (2019) |
| $M_u$ | Ultimate moment capacity given by test or simulation |
| $L$ | Length of the beam |
| $V_{Ed}$ | Vertical shear acting in the cross-section |

| | |
|---|---|
| $V_{L,Ed}$ | Resulting longitudinal shear force in the shear connection |
| $V_{Rd}$ | Vertical shear resistance of the cross-section |

## Roman lower-case letters

| | |
|---|---|
| $a$ | Spacing between parallel beams |
| $a_1$ | Length of a flat fold in the corrugation |
| $a_3$ | Corrugation depth |
| $b_1$ | The length of the outstanding concrete |
| $b_2$ | The length of the outstanding concrete |
| $b_c$ | Effective width of the concrete slab |
| $b_{eff}$ | Effective concrete width |
| $b_{eff,1}$ | Effective concrete width in mid-span |
| $b_{fu}$ | Width of the upper steel flange |
| $b_{fl}$ | Width of the lower steel flange |
| $d_c$ | Plasticity variable for the damaged concrete in compression |
| $d_{head}$ | Diameter of the stud head |
| $d_{stud}$ | Diameter of the stud shank |
| $d_t$ | Plasticity variable for the damaged concrete in tension |
| $e_d$ | Distance form stud edge to edge of the steel flange |
| $e_E$ | Distance from centre of the stud to edge of the concrete slab |
| $e_L$ | Longitudinal stud spacing |
| $e_s$ | Distance from bottom of stud head to lower layer of reinforcement |
| $e_T$ | Transverse stud spacing |
| $f_{0.2}$ | 0.2% proof strength of the steel |
| $f_c$ | Concrete compressive strength |
| $f_{cd}$ | Design compression capacity of the concrete |
| $f_{ck}$ | Characteristic concrete compressive strength |
| $f_{cm}$ | Mean concrete compressive strength |
| $f_{ctk0.05}$ | 5% Characteristic concrete tensile strength |
| $f_{ctk0.95}$ | 95% Characteristic concrete tensile strength |
| $f_{ctm}$ | Mean concrete tensile strength |
| $f_{sd}$ | Ultimate design capacity of the shear reinforcement |
| $f_u$ | Nominal ultimate capacity of the steel |

| | |
|---|---|
| $f_{ub}$ | Ultimate strength for bolts and shear connectors |
| $f_y$ | Nominal yield capacity of the steel |
| $f_{yb}$ | Yield strength for bolts and shear connectors |
| $h$ | Crack band width of the concrete |
| $h_{stud}$ | Total length of the stud |
| $h_w$ | Height of the steel web |
| $k_s$ | Rotational stiffness per unit length along the top steel flange |
| $n$ | Strain hardening exponent |
| $n_0$ | Modular ratio for short term loading of the concrete |
| $n_L$ | Modular ratio for long term loading of the concrete |
| $m$ | Strain hardening exponent |
| $t$ | Nominal thickness of the steel element |
| $t_c$ | Thickness of the concrete slab |
| $t_{fu}$ | Thickness of the upper steel flange |
| $t_{fl}$ | Thickness of the lower steel flange |
| $t_{head}$ | Thickness of the stud head |
| $t_w$ | Thickness of the steel web |
| $t_{w,eff}$ | Effective web thickness |
| $y_{0.2}$ | Location in the cross-section where the steel strain is equal to the yield strain |
| $y_1$ | Location of the neutral axis from the top of the concrete |
| $y_2$ | Distance between the neutral axis and the distributed stress |

# Greek letters

| | |
|---|---|
| $\alpha$ | Corrugation angle |
| $\beta$ | Reduction factor for reduced plastic behaviour |
| $\gamma_c$ | Partial factor for concrete |
| $\gamma_{M0}$ | Resistance of cross-section to excessive yielding including local buckling |
| $\gamma_{M1}$ | Resistance of members to instability assessed by member checks |
| $\gamma_{M2}$ | Resistance of cross-section in tension to fracture |
| $\gamma_s$ | Partial factor for reinforcement |
| $\gamma_V$ | Partial factor for shear connectors |

| | |
|---|---|
| $\delta_{uk}$ | Characteristic slip capacity in the shear connector |
| $\varepsilon$ | Reference factor for cross-section classification |
| $\varepsilon_2$ | Stain in location $y_2$ |
| $\varepsilon_u$ | Ultimate steel strain |
| $\nu$ | Poisson's ratio |
| $\nu_a$ | Poisson's ratio of the steel |
| $\rho_w$ | Minimum transverse reinforcement ratio |
| $\sigma_{cm}$ | Distributed compressive stress |
| $\sigma_m$ | Distributed compressive stress |
| $\sigma_{max}$ | Stress in the bottom of the steel girder |
| $\sigma_{tm}$ | Distributed tensile stress |
| $\varphi(t, t_0)$ | Creep coefficient at time t for load applied at $t_0$ |
| $\chi_{c,g}$ | Shear buckling reduction factor, for global buckling |
| $\chi_{c,l}$ | Shear buckling reduction factor, for local buckling |

# Contents

# List of Figures

# List of Tables

# 1
# Introduction

This first chapter provides a brief background of the thesis topic and clarifies the aim of the study and what methods and limitations that the work is performed with.

## 1.1 Background

Steel-concrete composite bridges has been an effective and sustainable approach for a long time. The combination of different materials allows for unique and smart designs that can satisfy structures need by utilizing the superior properties for each material. These structures can be further optimized with the availability of the different types of steel and concrete. One interesting choice for the steel is stainless steel, its response is highly ductile but during large deformations it also performs with significant strain hardening. Which is a sought-after property during ultimate loading just before collapse. Even with these benefits, a reason for the lack of presence of stainless steel in construction is the high initial investment costs. However, recent studies have shown that beams in composite structures with corrugated webs and stainless steel can be designed with a reduced material consumption. Also, the use of corrugated webs has demonstrated an increase in the activation of the strain hardening, due to its flexibility. Steel-concrete composite bridges already have a design procedure given in Eurocode, only considering carbon steel. A complete cross-section analysis in Eurocode for ultimate limit state during plastic effects completely disregards any positive extra capacity from strain hardening. Design cases where stainless steel with corrugated webs seems appropriate will therefore lead to conservative capacity calculations. Further refined methods to take the strain hardening effect into account has recently been developed. Compared to Eurocode that limits the moment resistance to the plastic resistance, these methods may provide a more accurate representation of the stainless steel real load carrying capacity.

## 1.2 Aim

The aim of this master's thesis is to develop a design tool that should be able to determine the ultimate load carrying capacity for steel-concrete composite bridges in bending. The tool should be able to handle members with both flat and corrugated webs of both carbon steel and stainless steel, while also considering the effects of strain hardening for stainless steel.

## 1.3 Objectives

The thesis objective is to investigate the potential of the proposed design methods that are able to take the positive strain hardening effect into account. Information and data about these properties and design methods will be collected and incorporated into the design tool. This further developed design process for steel-concrete composite bridges using stainless steel and corrugated webs may lead to a reduced material consumption and increase its usage in construction. The developed tool and the resulting designs will be validated by comparing its capacity to a finite element analysis.

## 1.4 Method

The thesis is executed in the following steps:
- A literature study of the design models for steel-concrete composite bridges
- Development of a parameterized design tool for the ultimate bending capacity of beams with flat or corrugated webs and made of stainless steel or carbon steel
- Numerical finite element modelling and analysis of the composite action in girders and comparing to existing experimental data to validate the numerical model.
- A case study to evaluate the developed design tool and comparing the results with finite element analyses.

## 1.5 Limitations

This master's thesis is executed with the following limitations:
- The design of the steel-concrete composite beams are done as simply supported cases.
- The capacity calculations are performed in the ultimate limit state, only for plastic cases.
- The web corrugation will be limited to trapezoidal corrugation.
- Only beams with constant height will be taken into account.
- The steel flanges and web is considered to be of the same material and strength.

# 2
# Theory

This chapter presents information about the fundamental theory about steel-concrete composite bridges, stainless steel and corrugated webs from previous studies and standards that are used in construction today. It is divided in to three main sections that will cover the theory behind composite bridges, corrugated webs, and stainless steel.

## 2.1 Steel-concrete composite bridges

The structure of a steel-concrete composite bridge consists of beam elements with steel girders and a concrete deck on top. Both materials collaborates and act together by utilizing each superior load bearing property. The composite beam is primarily exposed to bending moments, but the composite action allows for the steel to carry the tension with its high tensile strength while the concrete manage the compression with its great compression strength. This considerate material usage results in an efficient and cost-effective bridge design and a significant capacity increase compared to other non-composite designs. However, for the composite action to be possible the steel girder and concrete slab ought to be linked together with shear connectors. The connection transfer shear forces between the materials and prevents any separation or slip. In the Figure 2.1 the components of a steel-concrete composite beam can be seen in a schematic illustration (Hällmark, 2020).

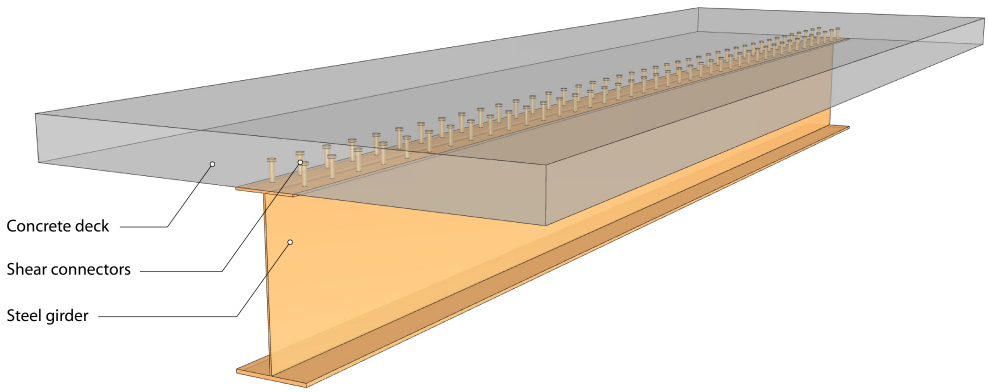


**Figure 2.1:** *Illustration showcasing the different parts of a steel-concrete composite beam*

Even though the steel-concrete composite concept was developed already in the mid-19th century it was not established and recognised in construction in Sweden until the late 1980s. Before that, steel and concrete bridges was built with no composite action. In current design practice, composite action is almost required for steel-concrete composite bridges (Hällmark, 2020). Considering the benefits from composite structures, designing a bridge is still no easy task. Bridges creates crucial connections for the infrastructure by overcoming a broad variety of obstacles with different limitations for the design. The steel-concrete composite bridge is a flexible concept and can be adapted to the surrounding with its light structure, slim height, and longer spans. The flexibility trait can however lead to complicated situations when looking for optimal solutions for a bridge design (Vayas & Iliopoulos, 2013).

### 2.1.1 Structural concept advantages

The composite bridge concept exhibits several benefits compared to non-composite constructions. Ellobody (2014) lifts further advantages of the composite structures, they have a higher strength compared to the structure self-weight than reinforced concrete bridges. The composite structure is easily prefabricated with its slim and light design. It can be transported and erected with many installation alternatives, such as, by cranes, slide-in techniques and launching. The fast construction process results in less time for the workers in a hostile environment, less closure of surrounding infrastructure, and reduced labour costs. Some sites also require lighter structures because of poor ground conditions. Once the composite bridge is erected, the steel girders will provide support to the subsequent operations, which further reduces impact on the surrounding by reducing the need of big form works or scaffolding. After the bridge has been built it can be strengthened with additional stiffeners, repaired if needed, recycled, or even modified in case the bridge needs a widening to accommodate extra traffic lanes. Ellobody (2014) continues to compare composite bridges to steel bridges and provides benefits in favour of the composite design. The composite bridge utilizes the exceptional properties of both materials and therefore have a higher strength, higher ductility, higher stiffness, higher fire resistance, and a higher seismic loading resistance.

### 2.1.2 Composite action

It is crucial that the composite beam has a sufficient connection between the different materials for the concept of composite action to work. The connection means that the materials will act as a single element in the structure. Without an interaction the materials would act individually. The connection between the girder and the slab needs to be designed to handle any potential shear coming from the design loads. There are many available types of shear connectors such as perfobond strips, T-connectors, welded studs and looped bars. By far, the most common shear connector is the welded shear studs. Besides shear forces, the shear connectors should be able to prevent separation of the steel girder and concrete deck. If the connectors are designed with sufficient strength the beam can be assumed to perform with full composite action. However, the assumption of either full action or no action at

all are two extreme cases. In reality there will always be some slip effect even if the shear connectors are designed with high strength. Also, there will always be friction in cases where no connectors are utilized. In situations where the shear connectors do not have enough strength for full composite action, the beam will act with partial composite action. This is allowed in design if additional requirements are fulfilled. Parts of the steel girder will be compressed, and the concrete will be subjected to tension and will lead to a risk for buckling and cracking, which need to be considered in design. Figure 2.2 illustrates the difference between composite action and no composite action together with the sectional strains depending on the connection restraint degree (Hällmark, 2020).

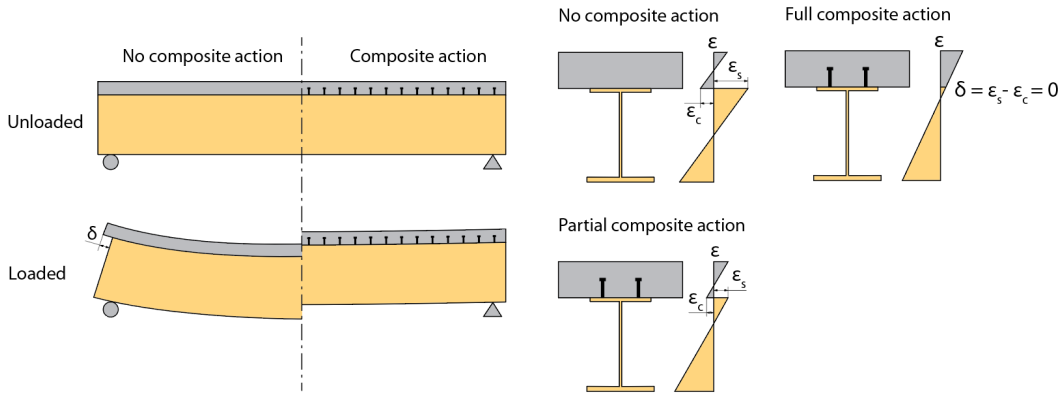


**Figure 2.2:** *Difference between different levels of restraint degree for the composite action, redrawn from (Hällmark, 2020)*

The slip that occurs for beams without full composite action is the difference between the steel strain and the concrete strain, since both materials are assumed to work individually without any friction. With full composite action the load will be shared depending on the flexural stiffness for the steel girder and concrete slab separately. The assumption of full composite action results in a slip that is equal to zero, and the strength completely depends on the global cross-section. This allows for the same assumption as in the Euler-Bernoulli beam theory, that plane sections will remain plane during bending (Hällmark, 2020).

## 2.2 Corrugated webs

In current practice I-girders with flat plate webs are one of the most commonly used type of cross-sections when it comes to the use of steel in bridge girders. These types of cross-sections are generally built up with deep and thin webs that may lead to instability issues such as shear buckling or flexural buckling. This instability phenomenon is prevented by the use of web stiffeners, either transverse or longitudinal that act as stabilisation of the cross-section. An alternative method to handle them is replacing the convectional flat webs with ones that are corrugated.

Corrugated web steel girders have been used in many bridges all over the world. The first example when it was used for a composite bridge is the Maupre bridge in

France. The main advantage of corrugated webs is that they have a higher out-of-plane stiffness compared to flat webs (Inaam & Upadhyay, 2022). This also leads to that girders with corrugated webs have a higher shear buckling strength compared to ones with flat webs (He et al., 2012). This makes it possible to create steel girders with slim webs without using stiffeners (Elgaaly & Seshadri, 1997). Studies have shown that by replacing stiffened flat webs with corrugated webs an increased fatigue resistance of about 50% and a reduction in self-weight around 30-50% can be reached (Moga et al., 2017). This makes the use of corrugated webs in combination with stainless steel an attractive option as the reduction in self-weight, hence material use, may somewhat cancel out the higher investment cost of stainless steel.

There are however some disadvantages with corrugated webs. Due to the corrugation, the web gets a low axial rigidity called the "accordion effect" (Inaam & Upadhyay, 2022). This results in a low flexural stiffness for the web and is therefore not considered when calculating the bending moment capacity of the girder according to SS-EN 1993-1-5 (2006). Due to the irregularities and eccentricities of the connection between the corrugated web and the flanges, local buckling can appear in the flanges. This is related to the larger overhangs of the flanges when the web corrugates and no longer lie in the middle of the flange (Elamary et al., 2017).

### 2.2.1 Manufacturing, types and design of corrugated webs

The most common corrugation geometries are either sinusoidal or trapezoidal. The sinusoidal corrugation is formed just like a sinus wave with a given amplitude and wavelength, an example and general geometric notations can be seen in Figure 2.3. The trapezoidal webs are more commonly used than the sinusoidal webs and have a higher capacity potential when thin webs are used (Karlsson, 2018). An example with general geometric notations of a trapezoidal web corrugation can be seen in Figure 2.4. Both types of are usually manufactured by cold bending to prevent loss of steel ductility and surface cracks (Steffner & Öman, 2021). In this master's thesis, only webs with trapezoidal corrugation will be studied due to it being the most common type in practice.

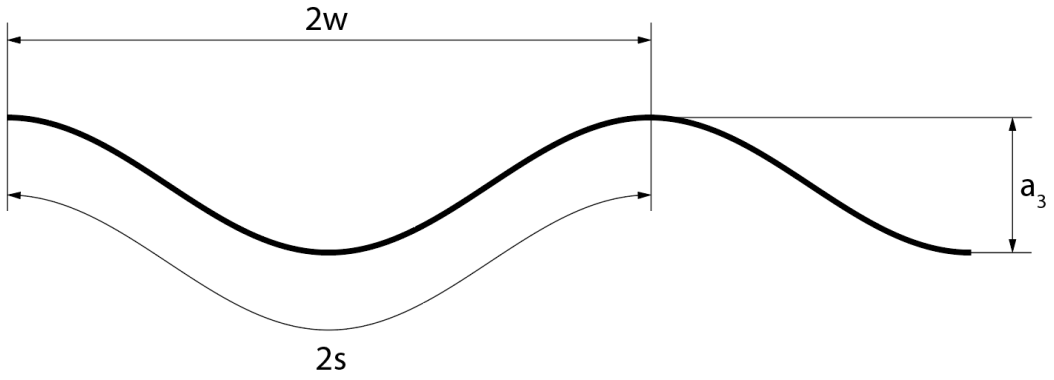


**Figure 2.3:** *Illustration and geometrical notations for a sinusoidal web*

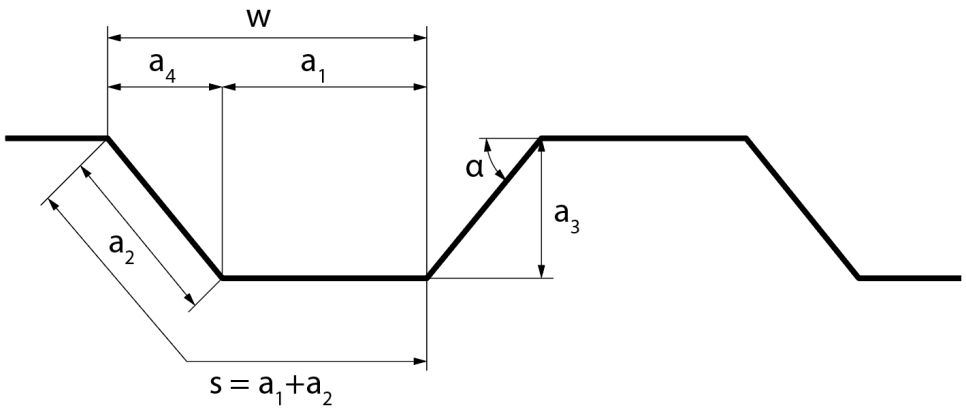


**Figure 2.4:** *Illustration and geometrical notations for a trapezoidal web*

Previous studies have been performed on the effect of the different parameters of the corrugated webs on ultimate shear capacity by Luo and Edlund (1996). The conclusions of the study are summarised and can be seen in Table 2.1. Further investigation on this topic was performed in a master's thesis by Karlsson (2018). Karlsson (2018) saw similar results as Luo and Edlund (1996) for most parameters but Karlsson (2018) also gathered additional understanding of the effects of the corrugation angle and length of the flat fold. It was found that the shear capacity from corrugation angle continues to increase up to approximately 50°. Also that the length of the flat folds and corrugation angle is the most influential parameters when performing design of shear capacity for beams with corrugated webs.

**Table 2.1:** *Geometrical parameters and their effect on ultimate shear capacity (Luo & Edlund, 1996)*

| **Geometrical parameter** | **Effect on ultimate shear capacity** |
|---|---|
| Web thickness, $t_w$ | Increased with increased web thickness |
| Web height, $h_w$ | Increased with increased web height |
| Corrugation depth, $a_3$ | Small or no effect |
| Corrugation angle, $\alpha$ | Small increase with increased corrugation angle |
| Length of flat fold, $a_1$ | Decreased with increased length |

## 2.3 Stainless steel

Stainless steel is a family name for a group of steels manufactured to be highly corrosion and heat resistant. They come with varying alloy element additions that affects the material properties such as strength, corrosion resistance, ductility and weldability. The wide range of stainless steel types and grades provide materials that can fit different site atmospheres. All stainless steel grades contain a minimum amount of 10.5% chromium, which is the added content that effects the stability of the corrosion resistance. Further property modification can be done with additional alloys, for example molybdenum and nitrogen. However, improved material properties results in a higher price (SCI, 2018).

A combination of a clean stainless steel surface with chromium and exposure to an oxidizing environment will lead to a tight and transparent, chromium-rich oxide film on the steel surface. Any potential cuts or scratches of the film are ineffective as it will reform immediately when subjected to oxygen. When the stainless steel is equipped with enough corrosion resistance, it will no longer react to the surrounding environment. Hence, the protective film is referred to as a passive film (SCI, 2018).

Stainless steel is a practical material and is recommended for buildings or structures that are subjected to intense environments with pollution, de-icing salts or coastal atmosphere. Stainless steel has also shown to compete with carbon steel in both environmental impact and long-term cost. The initial price of stainless steel material is substantially higher than carbon steel with similar properties. Stainless steel however comes with several cost-effective advantages in the long run, such as not needing corrosion resistance coating, avoiding normal and coating maintenance and avoiding component replacements as a result of corrosion. This in turn reduces downtime due to the reduced maintenance. Also, stainless steel provides a high strength and can therefore be designed with smaller cross-sections, which leads to lower material usage. The high durability gives the material a long service life, and at end-of-life, it is still fully recyclable (SCI, 2018).

### 2.3.1 Stainless steel types

The stainless steel products are divided in types which have further variations called grades which provide alternative choices for all potential environmental conditions. The stainless steel types that are most commonly used in structural application are austenitic, ferritic and duplex steels (SCI, 2018).

The stainless steel type with the highest frequent use in construction is austenitic steels, they consist of 17-18% chromium and additions of 8-11% nickel. The atomic structure is face-centered which leads to a highly ductile material that is easily weldable. Compared to carbon steel it has a great toughness when susceptible to a wide temperature range. The remarkable ductility gives the steel a good formability and a great elongation before any possible fracture (SCI, 2018).

Another type of stainless steel is the ferritic steels, it contains about 10.5-19% chromium and possibly small amounts of nickel additions. This type of steel has an atomic structure similar to that of carbon steels, body-centred, which also yields comparable formability. Ferritic stainless steels are cheaper compared to austenitic steels with the same corrosion resistance. However, while this type of steel is not commonly used in load-bearing construction, it is still used in the industry for cladding, roofing, water pipes, elevators, and other indoor applications (SCI, 2018).

The third stainless steel type is duplex steels, also called austenitic-ferritic stainless steel explained by its combined microstructure of the previous steel types. Duplex steels have 20-16% chromium, 1-8% nickel, 0.05-5% molybdenum and 0.05-3%

nitrogen. Duplex steels have a remarkably high strength, double the strength of austenitic and have therefore increased in demand for load-bearing structures. The considerable strength also allows for a reduced cross-section which makes it suitable for bridges that can be sensitive to self-weight. Even though duplex steel has a high ductility, the formability falls behind as a result of the high strength. Further properties worth noting are the good weldability and resistance against stress corrosion cracking (SCI, 2018).

### 2.3.2 Material behaviour

By comparing stainless steel and carbon steel a clear difference in material behaviour can be seen in the stress-strain curve. Comparisons of the stress-strain curves of both materials are illustrated in Figure 2.5 and 2.6. The most noticeable difference, and also the most important, is the shape of the curves. The carbon steel curve shows the initial linear elastic part up to the clearly identifiable yield strength. After the yield strength is reached it flattens out until the strain hardening effect initiates. Stainless steel however shows a more rounded response with no clear yield strength. The yield strength is instead defined by the 0.2% proof strength. The method to finding the proof strength is illustrated in Figure 2.7. After yielding it is clear that stainless steel exhibit substantial plastic strain hardening (SCI, 2018).

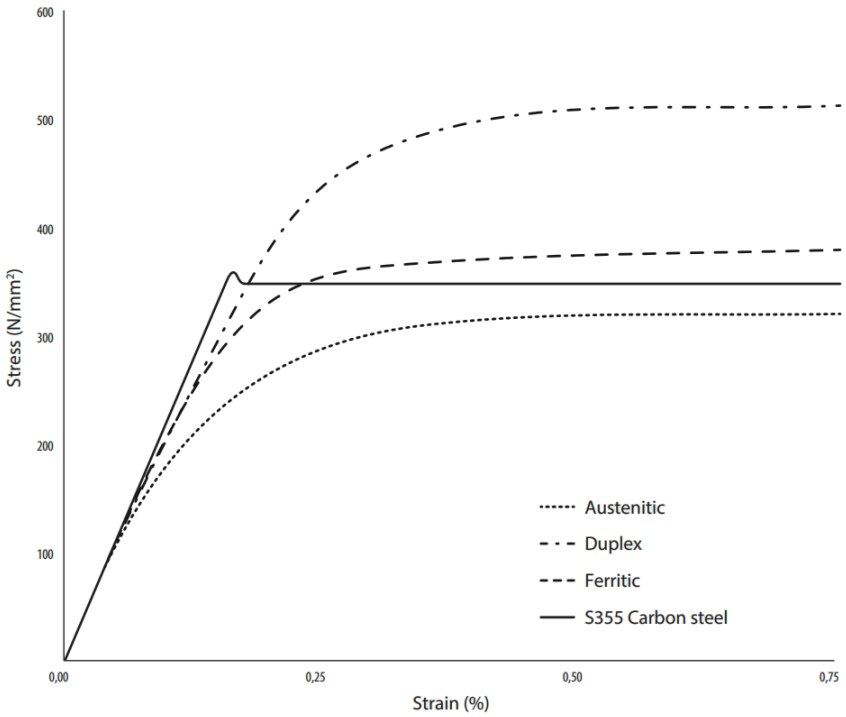


**Figure 2.5:** *Stress-strain curves for carbon steel and stainless steel up to a 0,75% strain (SCI, 2018)*

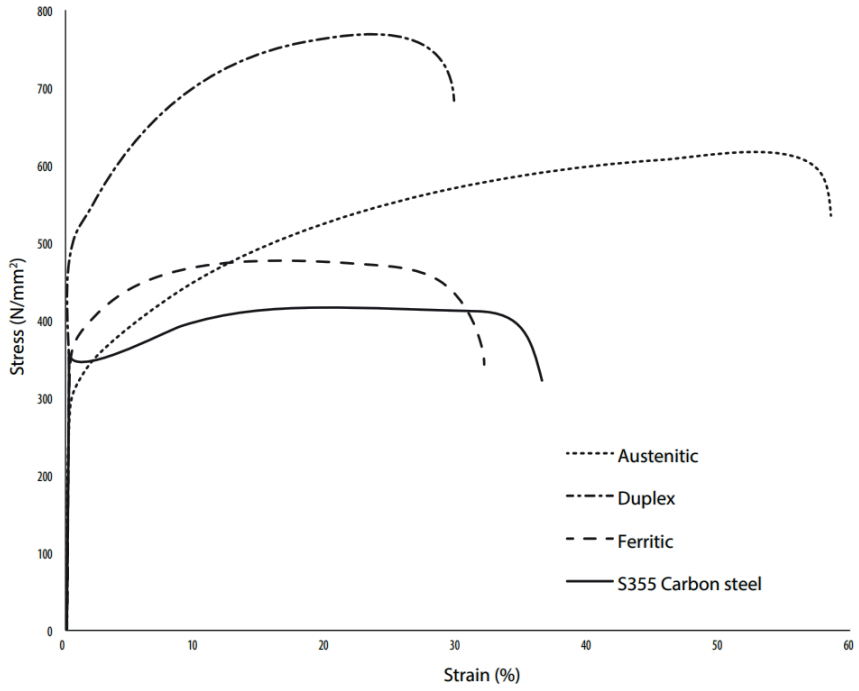


**Figure 2.6:** *Stress-strain curves for carbon steel and stainless steel for the full strain range (SCI, 2018)*

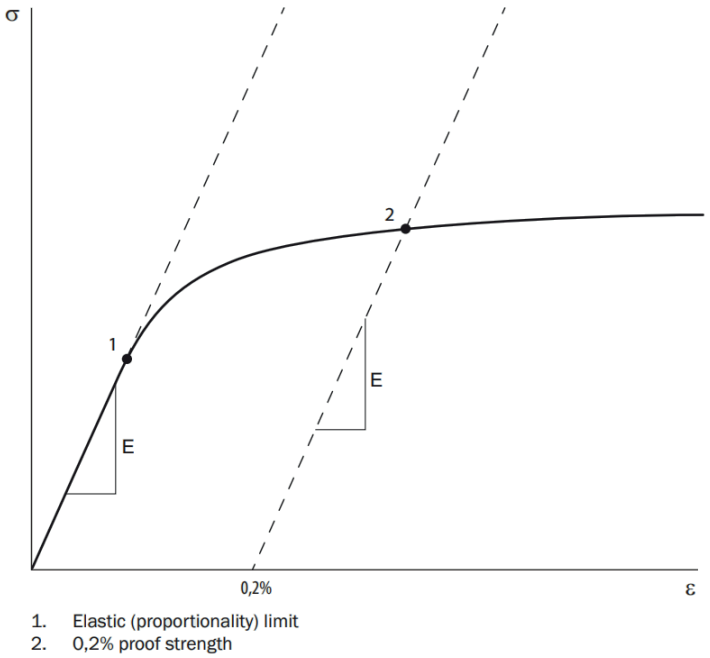


**Figure 2.7:** *Graph illustrating the definition of 0,2% proof strength (SCI, 2018)*

#### 2.3.2.1 Manufacturing of stainless steel

The stainless steel metallurgy is complex compared to carbon steel and the material properties of the final steel product after the manufacturing process can be altered. Depending on the sought after dimension, an early discussion with potential fabricators is recommended to get the correct information about size limits. The manufacturing methods for steel is either cold forming or hot rolling. Products that are produced are bars, sheets or plates but with further techniques even more elements can be fabricated. Such techniques are bending, pressing, deep drawing and pressing for cold forming. For even more products, cold forming techniques are bending, pressing, spinning and deep drawing. Depending on the quantity and size of the needed structural elements, some manufacturing techniques may be more economically beneficial. Stainless steel will require higher forming loads because of the higher strength compared to carbon steel. However, the high ductility allows for smaller corner radii when forming the element. One effect of cold forming is cold working which enhances the strength and reduces the ductility of the steel by plastic deformations. Cold working also increases the anisotropy of compression and tension strengths which can alter the stress-strain characteristics. The compression strength will be lower than the tensile strength and it is important to be careful and use the correct strength values in design (SCI, 2018).

When dealing with larger production, hot rolling is generally the most cost effective. It is also the production of choice when the steel thickness is too large for cold forming. By adding welding, larger structural member can be produced. The material strength values given in design is usually in annealed condition. Annealing is a heat treatment that can be used after cold working or welding to relieve stresses and return the steel to a more ductile and workable state. Cold worked sections are though rarely annealed when delivered and it can be conservative designing such a section with annealed strength values (SCI, 2018).

### 2.3.3 Corrosion durability

Stainless steels are fabricated to be highly resistant to corrosion and in general it will have a satisfactory performance for the majority of environments. Each grade under the steel types will have a slight difference in performance, and the most important step for a desired result is to carefully select one that is appropriate for the given site. Steels that contain more chromium, molybdenum and nitrogen will have a higher corrosion resistance. Duplex steels will therefore have a higher corrosion resistance compared to the other stainless steel types. If the steel still is prone to corrosion, it may be a result of wrongly assessed environment, unsuitable manufacturing techniques, a flawed design or poor workmanship. When detailing for a good corrosion control, appropriate measures should be taken to avoid surface contamination by having a smooth surface finish and design to prevent moisture and dirt entrapment. Also, consideration is necessary for the different types of corrosion that can occur by preventative detailing (SCI, 2018).

Some possible corrosion types are pitting, crevice, bimetallic (galvanic) and inter-

granular corrosion. Pitting corrosion is when the passive layer breaks down locally and form localised corrosion pits. The pitting is however often superficial and will not impose a reduction of the cross-section, although it can reduce the visual value for the architectural features. The next corrosion type, crevice corrosion, can be more severe depending on the geometry. It will occur in unsealed crevices with a continuous existence of a water film where deeper and tighter crevices will result in worse corrosion. Bimetallic corrosion will happen if two metals with dissimilar nobility are in contact together as an electrolyte. This condition induces a current which flows from the anode, the less noble metal to the cathode, the more noble metal. Eventually, the cathode will start to corrode. Any filler part that connects to the stainless steel should therefore be at least as noble as the stainless steel. Other methods to prevent bimetallic corrosion can be to add insulation between the metals or to coat or paint the most noble metal. The last mentioned corrosion type, intergranular corrosion can happen by prolonged heating that sensitize the material. However, it is no longer common with a modernised steel fabrication process (SCI, 2018).

# 3
# Design procedure used today

This chapter presents and explains how design of a steel-concrete composite beam is to be carried out based on current standards used in Sweden. It will cover what parameters and checks that have to be considered and how different designs and materials influence the procedure.

## 3.1 Basis for design

When designing a bridge, all potential events and their requirements has to be considered. This includes requirements in structural resistances, durability and serviceability which are accomplished by following appropriate standards and regulations for design, production and service. The design is done by considering the bridge in different limit states, serviceability and ultimate limit state (SLS and ULS). The bridge in SLS concerns the functionality and usability during normal use. Some of the considered factors are deformations, cracking and vibrations (Vayas & Iliopoulos, 2013). While ULS concerns structural failure for the safety of the users and the structure itself. Failures considered in ULS design include loss of global equilibrium, collapse or excessive deformations of the superstructure, failure due to fatigue and failure of the substructure (Vayas & Iliopoulos, 2013).

In design of a new bridge, the main standard that is used in Sweden is Eurocode. These guidelines and regulations cover topics such as materials, loads, safety and structure verification for design (Vayas & Iliopoulos, 2013). All standards from Eurocode that has to be considered for design of steel-concrete composite bridge and what they cover can be seen in Table 3.1.

**Table 3.1:** *List of Eurocode standards used for design of steel-concrete composite bridges*

| Eurocode | Standard | Part |
|---|---|---|
| SS-EN 1990 | Basis of structural design | - |
| SS-EN 1991 | Actions on structures | Part 1-1: Self-weight<br>Part 1-4: Wind actions<br>Part 1-5: Thermal actions<br>Part 2: Traffic loads on bridges |
| SS-EN 1992 | Design of concrete structures | Part 1-1: General rules<br>Part 2: Concrete bridges |
| SS-EN 1993 | Design of steel structures | Part 1-1: General rules<br>Part 1-5: Plated structural elements<br>Part 1-8: Design of joints<br>Part 1-9: Fatigue<br>Part 1-11: Design of structures with tension components<br>Part 2: Steel bridges |
| SS-EN 1994 | Design of composite steel and concrete structures | Part 2: General rules and rules for bridges |
| SS-EN 1998 | Design of structures for earthquake resistance | Part 1: Seismic actions<br>Part 2: Bridges |

Along with the Eurocode standards, nations can have their own addition, which are called the *National Annex*. The National Annex have country specific parameters and data that is either not covered in Eurocode or only given as recommended values (Vayas & Iliopoulos, 2013). In Sweden the national annex for bridge design is TRVINFRA-00227 (2022).

## 3.2 Material properties

Material properties for the materials that are used for steel-concrete composite bridges are presented in this section. That include parameters for concrete, carbon steel and stainless steel elements. Strength properties should be used as design values according to SS-EN 1990 (2002), design values are calculated by using equation 3.1.

$$X_d = \eta \frac{X_k}{\gamma_m} \tag{3.1}$$

where,

$X_d$ is the design value of the property for the material;

$\eta$ is the mean value of the conversion factor considering effects of volume and scale, effects of moisture and temperature and any other relevant parameters;

$X_k$ is the characteristic value of the property for the material;

$\gamma_m$ is the partial factor for the material property considering the possible deviation of a material property and the random part of the conversion factor $\eta$.

### 3.2.1 Concrete

SS-EN 1994-2 (2005) states that only normal concrete of classes between C20/25 and C60/75 are covered by the standards for design of composite bridges. It also states that properties and safety factors should be taken according to SS-EN 1992-1-1 (2005). Characteristic strengths and Young's modulus for named concrete classes can be seen in Table 3.2. Additionally, the Poisson's ratio should be taken as 0.2 for uncracked concrete and 0 for cracked concrete. According to SS-EN 1992-1-1 (2005) the partial factor $\gamma_C$ should be used for normal concrete and is equal to 1.5.

**Table 3.2:** *Characteristic strengths and Young's modulus of concrete in MPa (SS-EN 1992-1-1, 2005)*

| **Grade** | $\boldsymbol{f_{ck}}$ | $\boldsymbol{f_{cm}}$ | $\boldsymbol{f_{ctm}}$ | $\boldsymbol{f_{ctk,0.05}}$ | $\boldsymbol{f_{ctk,0.95}}$ | $\boldsymbol{E_{cm}}$ $\boldsymbol{x10^3}$ |
|---|---|---|---|---|---|---|
| C20/25 | 20 | 28 | 2.2 | 1.5 | 2.9 | 30 |
| C25/30 | 25 | 33 | 2.6 | 1.8 | 3.3 | 31 |
| C30/37 | 30 | 38 | 2.9 | 2.0 | 3.8 | 33 |
| C35/45 | 35 | 43 | 3.2 | 2.2 | 4.2 | 34 |
| C40/50 | 40 | 48 | 3.5 | 2.5 | 4.6 | 35 |
| C45/55 | 45 | 53 | 3.8 | 2.7 | 4.9 | 36 |
| C50/60 | 50 | 58 | 4.1 | 2.9 | 5.3 | 37 |
| C55/67 | 55 | 63 | 4.2 | 3.0 | 5.5 | 38 |
| C60/75 | 60 | 68 | 4.4 | 3.1 | 5.7 | 39 |

#### 3.2.1.1 Long term effects of concrete

Concrete as a material suffer from long term effects due to creep and shrinkage, both of which have effects when concrete is used in composite bridges. According to SS-EN 1994-2 (2005) the creep can be handled by using a long term loading modular ratio $n_L$, for composite bridges, which can be calculated by using equation 3.2.

$$n_L = n_0(1 + \Psi_L \varphi(t, t_0)) \tag{3.2}$$

where,

| | |
|---|---|
| $n_0$ | is the modular ratio $E_a/E_{cm}$ for short term loading; |
| $E_{cm}$ | is the Young's modulus of the concrete for short term loading; |
| $E_s$ | is the Young's modulus of the steel; |
| $\Psi_L$ | is a load dependent creep multiplier taken as 1.1 for permanent loads, 0.55 for primary and secondary effects of shrinkage and 1.5 for prestressing by imposed deformations; |
| $\varphi(t, t_0)$ | is the creep coefficient at time $t$ for load applied at $t_0$. |

The creep coefficient, $\varphi(t, t_0)$, should be determined using methods presented in Annex B of SS-EN 1992-1-1 (2005). The coefficient is dependent on time, load and moisture in the environment and can be calculated using equation 3.3.

$$\varphi(t, t_0) = \varphi_0 \cdot \beta_c(t, t_0) \tag{3.3}$$

where,

| | |
|---|---|
| $\varphi_0$ | is the notional creep coefficient; |
| $\beta_c(t, t_0)$ | is a coefficient describing the creep development in time after loading. |

The total effect of shrinkage consists of two components, drying and autogenous shrinkage. The drying shrinkage is a long process as it depends on water migrating from the concrete. While the autogenous shrinkage is a much faster response as it occurs when the concrete hardens, where the main effect happens during the days immediately after casting (SS-EN 1992-1-1, 2005). The total shrinkage strain is determined by equation 3.4.

$$\varepsilon_{cs} = \varepsilon_{cd} + \varepsilon_{ca} \tag{3.4}$$

where,

| | |
|---|---|
| $\varepsilon_{cs}$ | is the total strain due to shrinkage; |
| $\varepsilon_{cd}$ | is the strain due to drying shrinkage; |
| $\varepsilon_{ca}$ | is the strain due to autogenous shrinkage. |

### 3.2.2 Carbon steel

TRVINFRA-00227 (2022) specifies no limitation on what grades of structural carbon steel that is allowed for design of bridges. However, it states that regardless of what steel is used it has to be designed for corrosion class C4. TRVINFRA-00227 (2022) also declares that a minimum steel thickness of 4 mm is allowed for design.

In SS-EN 1994-2 (2005) it is stated that the standards only cover use of structural carbon steel with a nominal yield strength lower than 460 MPa, and that material parameters should be taken in accordance with SS-EN 1993. Nominal yield and ultimate tensile strength for covered steel grades in accordance with SS-EN 1993-1-1 (2022) are presented in Table 3.3. Additional material parameters for the structural steel can be seen in Table 3.4.

**Table 3.3:** *Nominal yield and ultimate tensile strength of structural carbon steel (SS-EN 1993-1-1, 2022)*

| **Steel Grade** | **Nominal thickness of the element** $t$ [mm] | | | |
|---|---|---|---|---|
| | $t \leq 40$ mm | | 40 mm $< t \leq 80$ mm | |
| | $f_y$ [N/mm$^2$] | $f_u$ [N/mm$^2$] | $f_y$ [N/mm$^2$] | $f_u$ [N/mm$^2$] |
| S235 | 235 | 360 | 215 | 360 |
| S275 | 275 | 390 | 245 | 370 |
| S355 | 355 | 490 | 325 | 470 |
| S420 | 420 | 510 | 390 | 490 |
| S460 | 460 | 540 | 410 | 510 |

**Table 3.4:** *Additional material parameters of structural carbon steel (SS-EN 1993-1-1, 2022)*

| | |
|---|---|
| Young's modulus, E | 210 GPa |
| Poisson's ratio, $\nu$ | 0.3 |
| Shear modulus, G | 81 GPa |

Partial factors used for design of carbon steel structures and when they are applicable should be taken from TSFS 2018:57 (2018) according to TRVINFRA-00227 (2022) and can be seen in Table 3.5.

**Table 3.5:** *Partial factors for structural carbon steel (TSFS 2018:57, 2018)*

| **Partial Factor** | **Description** | **Value** |
|---|---|---|
| $\gamma_{M0}$ | Resistance of cross-sections to excessive yielding including local buckling | 1.0 |
| $\gamma_{M1}$ | Resistance of members to instability assessed by member checks | 1.0 |
| $\gamma_{M2}$ | Resistance of cross-sections in tension to fracture | $\min \begin{cases} 0.9 f_u / f_y \\ 1.1 \end{cases}$ |

#### 3.2.2.1 Reinforcement steel

SS-EN 1994-2 (2005) states that material parameters for reinforcing carbon steel used in composite structures should be taken according to SS-EN 1992-1-1 (2005) or SS-EN 1992-2 (2005) for ductility classification. SS-EN 1992-1-1 (2005) declares that only carbon steel reinforcement with specified yield strength in the range of 400 to 600 MPa and that a partial factor $\gamma_s$ equal to 1.15 should be used. Also it is recommended to use a Young's modulus of 200 GPa, but SS-EN 1994-2 (2005)

states that the same Young's modulus as the structural steel may be used for the reinforcement in design. SS-EN 1992-2 (2005) recommends that carbon reinforcement of ductility class B or C should be used to assure sufficient ductility.

#### 3.2.2.2 Shear connectors

According to SS-EN 1994-2 (2005) structural capacities of shear connectors should be taken from SS-EN 1993-1-8 (2005) which is listed in Table 3.6. For design the partial factor $\gamma_V$ should be used as 1.25 for shear connections according to SS-EN 1994-2 (2005).

**Table 3.6:** *Nominal yield and ultimate tensile strength for bolts and shear connectors (SS-EN 1993-1-8, 2005)*

| **Bolt class** | 4.6 | 4.8 | 5.6 | 5.8 | 6.8 | 8.8 | 10.9 |
|---|---|---|---|---|---|---|---|
| $f_{yb}[MPa]$ | 240 | 320 | 300 | 400 | 480 | 640 | 900 |
| $f_{ub}[MPa]$ | 400 | 400 | 500 | 500 | 600 | 800 | 1000 |

### 3.2.3 Stainless steel

SS-EN 1993-1-4 (2006) gives the design condition and parameters that is needed for design when stainless steel is used. On the contrary to structural carbon steel TRVINFRA-00227 (2022) gives a limitation in what structural stainless steel grades that are allowed to be used in different corrosion classes. Stainless steels of grades 1.4462, 1.4529, 1.4539, 1.4410 and 1.4547 are allowed to be in corrosion category C5 without any protection while 1.4162, 1.4362, 1.4401, 1.4404, and 1.4571 are allowed for C4 without any protection. Partial factors allowed to use for structural stainless steel given by TSFS 2018:57 (2018) can be seen in Table 3.7. Nominal yield and ultimate tensile strength for structural stainless steel according to SS-EN 1993-1-4 A1 (2015) are presented in Table 3.8 and additional material parameters according to SS-EN 1993-1-4 (2006) can be seen in Table 3.9.

**Table 3.7:** *Partial factors for structural stainless steel (TSFS 2018:57, 2018)*

| **Partial Factor** | **Description** | **Value** |
|---|---|---|
| $\gamma_{M0}$ | Resistance of cross-sections to excessive yielding including local buckling | 1.0 |
| $\gamma_{M1}$ | Resistance of members to instability assessed by member checks | 1.0 |
| $\gamma_{M2}$ | Resistance of cross-sections in tension to fracture | 1.2 |

**Table 3.8:** *Nominal yield and ultimate tensile strength for structural stainless steel (SS-EN 1993-1-4 A1, 2015)*

| Type of stainless steel | Grade | Product form | | | | | | | |
|---|---|---|---|---|---|---|---|---|---|
| | | Cold rolled strip | | Hot rolled strip | | Hot rolled plate | | Bars, rods and sections | |
| | | Nominal thickness $t$ | | | | | | | |
| | | $t \leq 8$ mm | | $t \leq 13.5$ mm | | $t \leq 75$ mm | | $t \leq 250$ mm | |
| | | $f_y$ | $f_u$ | $f_y$ | $f_u$ | $f_y$ | $f_u$ | $f_y$ | $f_u$ |
| | | MPa | MPa | MPa | MPa | MPa | MPa | MPa | MPa |
| Ferritic steel | 1.4003 | 280 | 450 | 280 | 450 | 250 | 450 | 260 | 450 |
| | 1.4016 | 260 | 450 | 240 | 450 | 240 | 430 | 240 | 400 |
| | 1.4512 | 210 | 380 | 210 | 380 | – | – | – | – |
| Austenitic steel | 1.4306 | 220 | 520 | 200 | 520 | 200 | 500 | 180 | 460 |
| | 1.4307 | | | | | | | 175 | 500 |
| | 1.4541 | | | | | | | 190 | 500 |
| | 1.4301 | 230 | 540 | 210 | 520 | 210 | 520 | | |
| | 1.4401 | 240 | 530 | 220 | 530 | 220 | 520 | 200 | 500 |
| | 1.4404 | | | | | | | | |
| | 1.4539 | | | | | | | 230 | 530 |
| | 1.4571 | | 540 | | 540 | | | 200 | 500 |
| | 1.4432 | 240 | 550 | 220 | 550 | 220 | 520 | | |
| | 1.4435 | | | | | | | | |
| | 1.4311 | 290 | 550 | 270 | 550 | 270 | 550 | 270 | 550 |
| | 1.4406 | 300 | 580 | 280 | 580 | 280 | 580 | 280 | 580 |
| | 1.4439 | 290 | | 270 | | 270 | | | |
| | 1.4529 | – | – | – | – | 300 | 650 | 300 | 650 |
| | 1.4547 | 320 | 650 | 300 | 650 | | | | |
| | 1.4318 | 350 | 650 | 330 | 650 | 330 | 630 | – | – |
| Duplex steel | 1.4062 | 530 | 700 | 480 | 680 | 450 | 650 | 380 | 650 |
| | 1.4162 | 530 | 700 | 480 | 680 | 450 | 650 | 450 | 650 |
| | 1.4482 | 500 | 700 | 480 | 660 | 450 | 650 | 400 | 650 |
| | 1.4662 | 550 | 750 | 550 | 750 | 480 | 680 | 450 | 650 |
| | 1.4362 | 450 | 650 | 400 | 650 | 400 | 630 | 400 | 600 |
| | 1.4462 | 500 | 700 | 460 | 700 | 460 | 640 | 450 | 650 |

**Table 3.9:** *Additional material parameters for structural stainless steel (SS-EN 1993-1-4, 2006)*

| | |
|---|---|
| Young's modulus, E | 200 GPa for all austenitic and duplex grades excluding 1.4539, 1.4529 and 1.4547<br>195 GPa for austenitic grades 1.4539, 1.4529 and 1.4547<br>220 GPa for ferritic grades |
| Poisson's ratio, $\nu$ | 0.3 |
| Shear modulus, G | $\frac{E}{2(1+\nu)}$ |

#### 3.2.3.1 Shear connectors

When using stainless steel beams, it is important to make all details such as fasteners, studs, bolts and cross-beams made of stainless steel as well to prevent the risk of forming a galvanic cell (SCI, 2018). Stainless steel bolts and studs are grouped based on what type of stainless steel they have and the chemical composition of the specific chosen material. Each group have a specific property class and strength depending on the production method used for the connector (SS-EN ISO 3506-1, 2020). Nominal yield strength and nominal ultimate tensile strength and grouping of the connectors can be seen in Table 3.10 according to SS-EN ISO 3506-1 (2020).

**Table 3.10:** *Grading and nominal yield strength and nominal ultimate tensile strengths of stainless steel bolts, screws and studs (SS-EN ISO 3506-1, 2020)*

| **Stainless steel grade** | | **Property class** | **Production method** | **Yield strength [MPa]** | **Ultimate tensile strength [MPa]** |
|---|---|---|---|---|---|
| Austenitic | A1<br>A2<br>A3 | 50 | Soft hot-pressed | 210 | 500 |
| | | 70 | Cold-formed | 450 | 700 |
| | | 80 | Cold-formed high strength | 600 | 800 |
| | A4<br>A5 | 50 | Soft hot-pressed | 210 | 500 |
| | | 70 | Cold-formed | 450 | 700 |
| | | 80 | Cold-formed high strength | 600 | 800 |
| | | 100 | Cold-formed high strength | 800 | 1000 |
| | A8 | 70 | Cold-formed | 450 | 700 |
| | | 80 | Cold-formed high strength | 600 | 800 |

| | | | | | |
|---|---|---|---|---|---|
| | | 100 | Cold-formed high strength | 800 | 1000 |
| Duplex | D2<br>D4<br>D6<br>D8 | 70 | Cold-formed | 450 | 700 |
| | | 80 | Cold-formed | 600 | 800 |
| | | 100 | Cold-formed high strength | 800 | 1000 |
| Martensitic | C1 | 50 | Soft hot-pressed | 250 | 500 |
| | | 70 | Quenched | 410 | 700 |
| | | 110 | Quenched | 820 | 1100 |
| | C3 | 80 | Quenched | 640 | 800 |
| | C4 | 50 | Soft hot-pressed | 250 | 500 |
| | | 70 | Quenched | 410 | 700 |
| Ferritic | F1 | 45 | Soft hot-pressed | 250 | 450 |
| | | 60 | Cold-formed | 410 | 600 |

## 3.3 Design procedure

This section presents sectional checks, parameters and theories that are used for design of steel-concrete composite bridges according to SS-EN 1994-2 (2005). SS-EN 1994-2 (2005) states that effects of action may be calculated by elastic analysis even while resistances of the cross-section is done by plastic or non-linear analysis.

### 3.3.1 Effective width of the concrete flange

Due to the shear lag effect in the concrete flange introduced by in plane shear, SS-EN 1994-2 (2005) states that an effective flange width should be used for design of steel-concrete composite bridges. The effective width of the concrete flange that is allowed to be used varies along the beam and is narrower at the support regions due to higher shear forces, this is illustrated in Figure 3.1. For elastic analysis, SS-EN 1994-2 (2005) declares that a constant effective width of $b_{eff,1}$, illustrated in Figure 3.1, may be used over the entire span for members supported at both ends. The effective width can be calculated according to equation 3.5.

$$b_{eff} = b_0 + \sum b_{ei} \tag{3.5}$$

where,

$b_0$ is the distance between the centres of the outstanding shear connectors;

$b_{ei}$ is the effective width of the concrete flange on each side of the web and is taken as $L_e/8$, but not greater than $b_1$;

$b_1$ is the geometrical width of the concrete flange and should be taken as the distance between the outstanding shear connectors and the mid-point to adjacent girder or free edge;

$L_e$ is the approximate distance between zero bending moment sections, for typical continuous composite beams and cantilevers it may be taken according to Figure 3.1.

The effective width at end supports may be determined according to equation 3.6.

$$b_{eff} = b_0 + \sum \beta_i b_{ei} \tag{3.6}$$

with,

$$\beta_i = (0.55 + 0.025 L_e/b_{ei}) \leq 1.0 \tag{3.7}$$

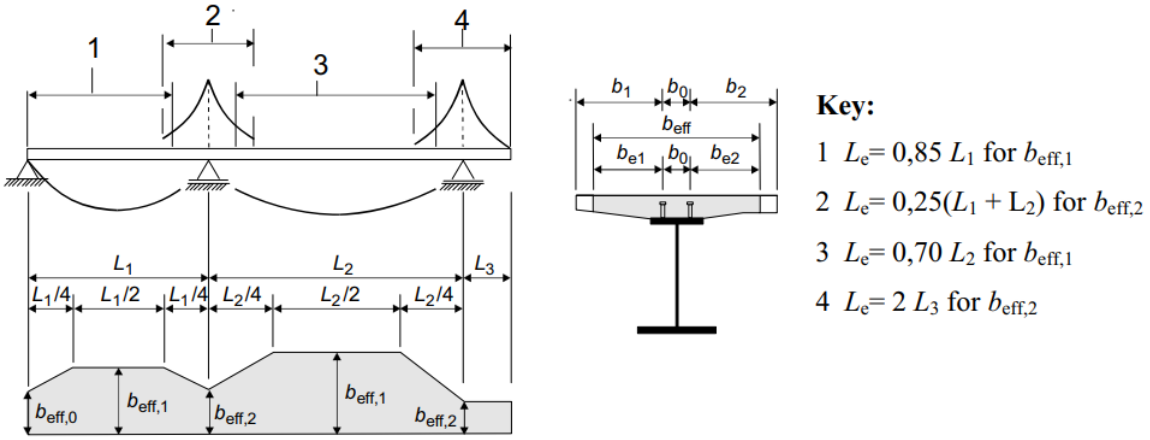


**Figure 3.1:** *Illustration of equivalent spans and effective width of the concrete flange (SS-EN 1994-2, 2005)*

If the beam is in cross-section class 1 or 2 and have reinforcement bars in tension, the effective concrete flange should be provided with a minimum reinforcement area $A_{re}$ (SS-EN 1994-2, 2005). The minimum area is calculated using equation 3.8.

$$A_{re} \geq \rho_s \cdot A_c \tag{3.8}$$

with,

$$\rho_s = \delta \frac{f_y}{235} \frac{f_{ctm}}{f_{sk}} \sqrt{k_c} \tag{3.9}$$

where,

$A_c$ is the area of the effective concrete flange;
$f_y$ is the nominal yield strength of the structural steel in MPa;
$f_{sk}$ is the characteristic yield strength of the reinforcement;
$f_{ctm}$ is the mean tensile strength of the concrete;
$k_c$ is a coefficient for the stress distribution prior to cracking, in this thesis conservatively set to 1;
$\rho$ is a coefficient equal to 1.0 for Class 2 and 1.1 for Class 1, in this thesis conservatively always used equal to 1.1.

### 3.3.2 Cross-section classification

Determining the cross-section class for a cross-section is vital for design of members that consist of steel elements that are subjected to compression, either pure compression or compression due to bending. The classes tells if the cross-section should be designed through plastic or elastic analysis and also checks the risk for local buckling of the elements. Cross-sections in Class 1 and 2 develop full plastic bending resistance, in Class 3 develop elastic bending resistance and in Class 4 the cross-section are subjected to local buckling before full elastic capacity can be reached (Vayas & Iliopoulos, 2013). According to SS-EN 1994-2 (2005) the cross-section classes for the steel parts in compression should be done according to SS-EN 1993-1-1 (2022) for carbon steel and SS-EN 1993-1-4 (2006) for stainless steel. The cross-section class of the beam is determined based on the steel element with the lowest cross-section class. The classification is based on the slenderness and material properties of the compressed part and therefore a reference factor, $\varepsilon$, that takes the material properties into account is used. The reference factor is different for carbon steel and stainless steel. Expressions for the two can be found in equation 3.10 for carbon steel and equation 3.11 for stainless steel.

$$\varepsilon = \sqrt{\frac{235}{f_y}}, \qquad \text{for carbon steel} \tag{3.10}$$

$$\varepsilon = \sqrt{\frac{235}{f_y}\frac{E}{210000}}, \qquad \text{for stainless steel} \tag{3.11}$$

where,

$f_y$ is the yield strength of the material in MPa;
$E$ is the Young's modulus of the material in MPa.

The checks and limitations for determining the cross-section class for internal and external compressed parts of carbon steel can be seen in Table A.1 and A.2 respectively and the same can be seen for stainless steel in Table A.3-A.6 in Appendix A.

For composite cross-sections, if the flange loaded in compression is connected to the concrete slab, it may be assumed to be in Class 1 if the shear connection is executed according to part 6.6.5.5 in SS-EN 1994-2 (2005). Beams with webs in cross-section

Class 3 may be considered as Class 2 if both the flanges are classified as either Class 1 or 2 according to SS-EN 1994-2 (2005). Due to this, the most common cross-section classes for composite cross-section in sagging bending are Class 1 or Class 2. Since the compressed flange is connected to the concrete and only parts of the web will be loaded in compression (Vayas & Iliopoulos, 2013).

### 3.3.3 Cross-sectional constants

The composite cross-section is composed of a steel girder with either corrugated or flat web and the effective concrete slab, presented in section 3.3.1. The sectional constants are calculated by transforming the entire cross-section to an equivalent steel cross-section. This is performed by using the modular ratios $n_L$ for long term loading and $n_0$ for short term loading for the concrete, see section 3.2.1.1. As stated before, according to SS-EN 1994-2 (2005) the contribution of the web should be neglected when designing a beam with a corrugated web in bending, hence the web is then not a part of the sectional constants. The cross-sectional area of a composite section is calculated according to equation 3.12 and the centre of gravity is calculated according to equation 3.15.

$$A_{tot} = A_s + \frac{A_c}{n_i} \tag{3.12}$$

with,

$$A_s = t_{fu} \cdot b_{fu} + t_{fl} \cdot b_{fl} + t_w \cdot h_w \tag{3.13}$$

$$A_c = b_{eff,1} \cdot t_c \tag{3.14}$$

where,

| | |
|---|---|
| $A_{tot}$ | is the total area of the composite cross-section; |
| $A_s$ | is the area of the steel girder; |
| $A_c$ | is the area of the effective concrete slab; |
| $n_i$ | is the modular ratio for either long or short term; |
| $t_{fu}$ | is the thickness of upper steel flange; |
| $b_{fu}$ | is the width of the upper steel flange; |
| $t_{fl}$ | is the thickness of the lower steel flange; |
| $b_{fl}$ | is the width of the lower steel flange; |
| $t_w$ | is the thickness of the steel web, $t_w$=0 for corrugated webs; |
| $h_w$ | is the height of the steel web; |
| $b_{eff,1}$ | is the effective width of the concrete flange; |
| $t_c$ | is the thickness of the concrete slab. |

$$z_{tp,tot} = \frac{A_s \cdot z_{tp,s} + \frac{A_c}{n_i} \cdot z_{tp,c}}{A_{tot}} \tag{3.15}$$

with,

$$z_{tp,s} = \frac{t_{fu} \cdot b_{fu} \cdot \left(\frac{t_{fu}}{2} + h_w + t_{fl}\right) + t_{fl} \cdot b_{fl} \cdot \frac{t_{fl}}{2} + h_w \cdot t_w \cdot \left(\frac{h_w}{2} + t_{fl}\right)}{A_s} \tag{3.16}$$

$$z_{tp,c} = \frac{t_c}{2} + t_{fu} + t_{fl} + h_w \tag{3.17}$$

where,

| | |
|---|---|
| $z_{tp,tot}$ | is the centre of gravity for the total composite cross-section from the bottom flange of the steel girder; |
| $z_{tp,s}$ | is the centre of gravity of the steel girder from the bottom of the steel girder; |
| $z_{tp,c}$ | is the centre of gravity of the concrete flange from the bottom of the steel girder. |

The static moment of the concrete slab is determined by using equation 3.18.

$$S_{1,i} = \frac{A_c}{n_i} \cdot (z_{tp,c} - z_{tp,tot}) \tag{3.18}$$

The moment of inertia of the composite cross-section around the strong axis (y-axis) is calculated according to equation 3.19.

$$I_{y,tot,i} = I_{y,s} + A_s \cdot (z_{tp,s} - z_{tp,tot})^2 + \frac{I_{y,c}}{n_i} + \frac{A_c}{n_i} \cdot (z_{tp,c} - z_{tp,tot})^2 \tag{3.19}$$

with,

$$\begin{aligned} I_{y,s} = {} & \frac{b_{fu} \cdot t_{fu}^3}{12} + \frac{b_{fl} \cdot t_{fl}^3}{12} + \frac{t_w \cdot h_w^3}{12} + b_{fu} \cdot t_{fu} \cdot \left(\frac{t_{fu}}{2} + h_w + t_{fl} - z_{tp,s}\right)^2 \\ & + b_{fl} \cdot t_{fl} \cdot \left(\frac{t_{fl}}{2} - z_{tp,s}\right)^2 + t_w \cdot h_w \cdot \left(\frac{h_w}{2} + t_{fl} - z_{tp,s}\right)^2 \end{aligned} \tag{3.20}$$

$$I_{y,c} = \frac{b_{eff,1} \cdot t_c^3}{12} \tag{3.21}$$

where,

| | |
|---|---|
| $I_{y,tot,i}$ | is the moment of inertia of the composite cross-section; |
| $I_{y,s}$ | is the moment of inertia of the steel girder; |
| $I_{y,c}$ | is the moment of inertia of the concrete flange. |

### 3.3.4 Effects of creep

For composite bridges the effect of creep is captured by the modular ratio described in section 3.2.1.1. The ratio varies over time to capture the stiffness reduction of the concrete. For statically determined systems, such as simply supported beams in

one span, the reduced concrete stiffness will lead to increased deflections and stress redistribution within the cross-section. As the steel will carry more load when the concrete loses stiffness (Vayas & Iliopoulos, 2013). This phenomenon is illustrated in Figure 3.2. As the concrete is loaded in compression and stay uncracked for these types of systems no change in internal forces will occur and hence secondary effect due to creep can be disregarded (Vayas & Iliopoulos, 2013).

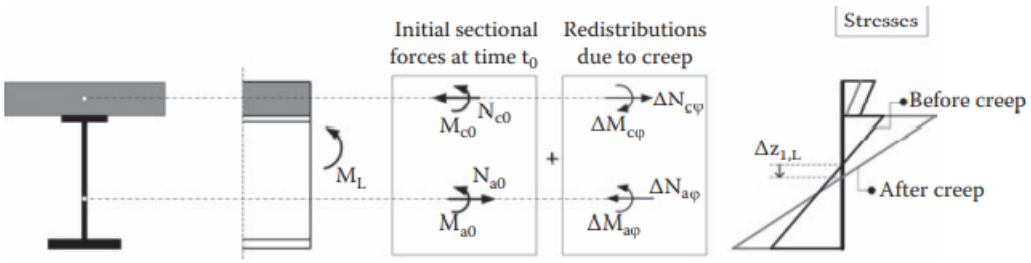


**Figure 3.2:** *Stress redistribution due to creep for composite bridges (Vayas & Iliopoulos, 2013)*

### 3.3.5 Effects of shrinkage

Shrinkage will result in a shortening of the concrete flange, see section 3.2.1.1. The shear connectors will prevent the shortening, hence, introduce a tension force in the gravity centre of the concrete. This results in a balancing compression force and moment in the composite section (Vayas & Iliopoulos, 2013). The introduced force and moment due to the concrete shrinkage are calculated according to equation 3.22 and 3.23, and illustrated in Figure 3.3.

$$N_{sh} = -\varepsilon_{cs} \cdot \frac{n_0}{n_s} \cdot E_{cm} \cdot A_c \tag{3.22}$$

$$M_{sh} = N_{sh} \cdot (z_{tp,tot} - z_{tp,c}) \tag{3.23}$$

where,

| | |
|---|---|
| $N_{sh}$ | is the shrinkage force; |
| $\varepsilon_{cs}$ | is the shrinkage strain, see section 3.2.1.1; |
| $n_0$ | is the short term modular ratio, see section 3.2.1.1; |
| $n_s$ | is the long term modular ratio for shrinkage, see section 3.2.1.1; |
| $E_{cm}$ | is the mean elasticity of concrete; |
| $A_c$ | is the effective cross-section area of the concrete, see equation 3.3.1; |
| $M_{sh}$ | is the moment caused by the shrinkage force; |
| $z_{tp,tot}$ | is the centre of gravity of the composite section from the bottom of the steel girder, see equation 3.15; |
| $z_{tp,c}$ | is the centre of gravity of the concrete flange from the bottom of the steel girder, see equation 3.17. |

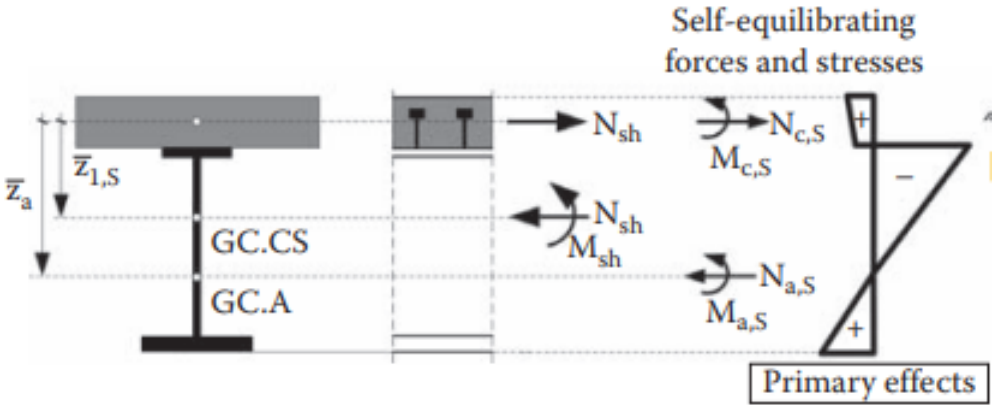


**Figure 3.3:** *Primary effects due to shrinkage (Vayas & Iliopoulos, 2013)*

The resulting force and moment are the primary effects of shrinkage, as for the effect of creep only the primary effects of shrinkage have to be considered for design of statically determined structures (Vayas & Iliopoulos, 2013).

### 3.3.6 Design of shear connectors

The shear connectors together with the transverse reinforcement are designed to transfer the longitudinal shear forces, without considering the natural bond between them (SS-EN 1994-2, 2005). The connection should also prevent separation of the concrete and steel while having a sufficient deformation capacity to justify any inelastic redistribution. SS-EN 1994-2 (2005) states that if the connector have a characteristic slip capacity $\delta_{uk}$ of at least 6 mm, the connector may be considered as ductile.

#### 3.3.6.1 Dimension and spacing of headed studs

Headed studs can have multiple shapes, sizes and orientation in order to fulfil the requirement stated before. SS-EN 1994-2 (2005) gives a few limitations and recommendations on both dimension and spacing of the headed studs. A headed stud is illustrated in Figure 3.4 and limitations of the stud dimensions according to SS-EN 1994-2 (2005) are presented in Table 3.11.

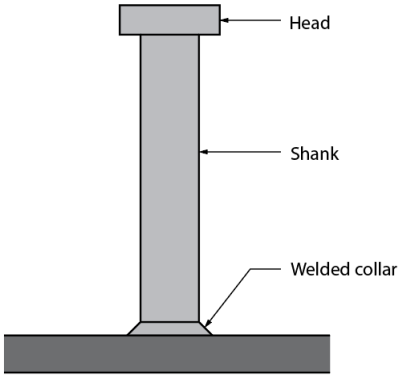


**Figure 3.4:** *Illustration of a headed stud*

**Table 3.11:** *Dimensions of headed studs with limitations (SS-EN 1994-2, 2005)*

| Index | Description | Limitation |
|---|---|---|
| $d_{stud}$ | Diameter of the stud shank | $d_{stud} \leq 2.5t_{fu}$ if not placed directly over the web |
| $h_{stud}$ | Total length of the stud | $h_{stud} \geq 3d_{stud}$ |
| $d_{head}$ | Diameter of the stud head | $d_{head} \geq 1.5d_{stud}$ |
| $t_{head}$ | Thickness of the stud head | $t_{head} \geq 0.4d_{stud}$ |

The spacing of the studs and detailing of the shear connections for solid concrete slabs are illustrated in Figure 3.5 and presented in Table 3.12 according to SS-EN 1994-2 (2005)

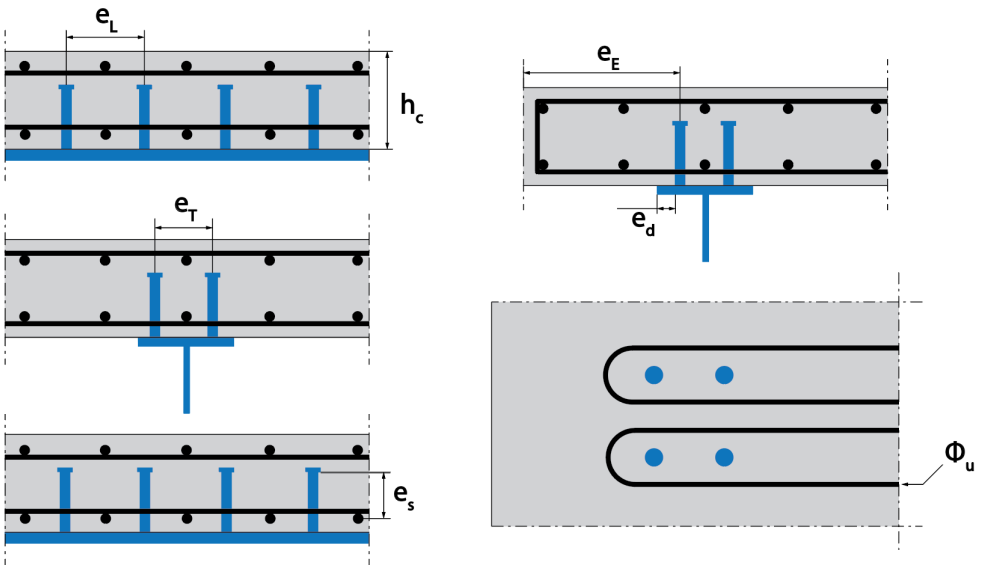


**Figure 3.5:** *Spacing and detailing of headed stud shear connection, redrawn from (Vayas & Iliopoulos, 2013)*

**Table 3.12:** *Spacing and detailing of headed stud shear connections (SS-EN 1994-2, 2005)*

| Index | Description | Limitation |
|---|---|---|
| $e_L$ | Longitudinal spacing | $5d_{stud} \geq e_L \leq min\{4h_c, 800mm\}$ |
| $e_T$ | Transverse spacing | $e_T \geq 2.5d_{stud}$ |
| $e_d$ | Distance form stud edge to edge of the steel flange | $e_d \geq 25mm$ |
| $e_s$ | Distance from bottom of stud head to lower layer of reinforcement | $e_s \geq 30mm$ |
| $e_E$ | Distance from centre of the stud to edge of the concrete slab | $e_E \geq 300mm$ |

If the upper steel flange is classified to Class 3 or 4 but taken as Class 1 or 2 due to the shear connection, $e_L$ and $e_d$ should be maximum $22 \cdot t_{fu}\sqrt{235/f_y}$ and $22 \cdot t_{fu}\sqrt{235/f_y}$ respectively (SS-EN 1994-2, 2005). Additionally, if the $e_E$ is less than 300 mm additional u-bars have to be provided around the studs of a minimum $0.5d_{stud}$ in diameter. The shear studs should also be placed closer than $6d_{stud}$ from the concrete edge to prevent splitting.

#### 3.3.6.2 Shear capacity of a headed stud

The shear capacity of a stud is designed according to SS-EN 1994-2 (2005) with the equations 3.24 and 3.25 where the capacity should be taken as the smallest of the two. Equation 3.24 refers to shear failure of the stud and equation 3.25 refers to crushing failure of the concrete around the stud shank.

$$P_{Rd} = \frac{0.8 \cdot f_u \cdot \pi \cdot d_{stud}^2}{4 \cdot \gamma_V} \tag{3.24}$$

$$P_{Rd} = \frac{0.29 \cdot \alpha \cdot d_{stud}^2\sqrt{f_{ck} \cdot E_{cm}}}{\gamma_V} \tag{3.25}$$

with,

$$\alpha = \begin{cases} 0.2\left(\frac{h_{stud}}{d_{stud}} + 1\right) & \text{for } 3 \leq h_{stud}/d_{stud} \leq 4 \\ 1 & \text{for } h_{stud}/d_{stud} > 4 \end{cases} \tag{3.26}$$

where,

| | |
|---|---|
| $f_u$ | is the ultimate tensile strength of the stud material, but not greater than 500 MPa; |
| $d_{stud}$ | is the shank diameter of the stud, 16 mm $\leq d_{stud} \leq$ 25 mm; |
| $\gamma_V$ | is the partial factor for design of studs, recommended value is 1.25; |
| $f_{ck}$ | is the characteristic cylinder compressive capacity of the concrete at considered age, with density grater than 1750 $kg/m^3$; |
| $E_{cm}$ | is the Young's modulus of the concrete; |
| $h_{stud}$ | is the height of the stud. |

The total shear capacity against longitudinal shear is determined according to equation 3.27. The longitudinal shear is an effect of the transverse shear forces acting on the cross-section, and for an elastic analysis the relation between the two is presented in equation 3.28 (Vayas & Iliopoulos, 2013).

$$V_{L,Rd} = \frac{P_{Rd} \cdot n}{e_L} \tag{3.27}$$

where,

| | |
|---|---|
| $V_{L,Rd}$ | is the capacity of the headed stud connection for longitudinal shear; |
| $P_{Rd}$ | is the shear capacity of an individual headed stud, see equation 3.21 and 3.22; |
| $n$ | is the number of studs in one cross-section; |
| $e_L$ | is the longitudinal spacing of the studs, see section 3.3.6.1. |

$$V_{L,Ed} = \frac{V_{Ed} \cdot S}{I} \tag{3.28}$$

where,

| | |
|---|---|
| $V_{L,Ed}$ | is the resulting longitudinal shear force; |
| $V_{Ed}$ | is the transverse shear force; |
| $S = S_{1,i}$ | is the static moment of the concrete slab, see section 3.3.3; |
| $I = I_{y,tot,i}$ | is the moment of inertia of the composite structure, see section 3.3.3. |

#### 3.3.6.3 Shear capacity of the concrete slab

In addition to design of the shear connectors, the concrete slab and transverse reinforcement should be designed to prevent failure and splitting of the concrete slab due to longitudinal shear according to SS-EN 1994-2 (2005). The shear failure can occur i different places in the concrete slab and the different shear planes are illustrated in Figure 3.6.

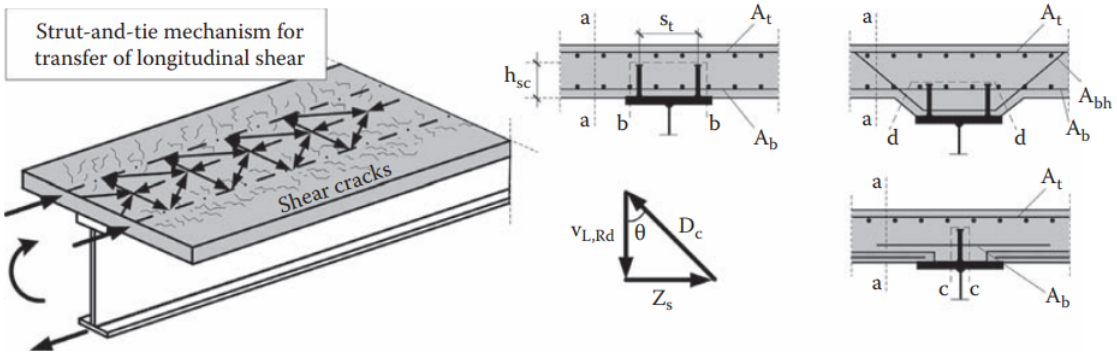


**Figure 3.6:** *Failure modes due to longitudinal shear for the concrete slab (Vayas & Iliopoulos, 2013)*

The shear flow acting in section a-a when the concrete flange is in compression may be taken according to equation 3.29, the rest of the sections should be design for the same shear flow as a the headed studs, $V_{L,Ed}$.

$$V_{Lc,Ed} = V_{L,Ed}\frac{A_{cp,eff}}{A_{c,tot,eff}} \tag{3.29}$$

where,

| | |
|---|---|
| $V_{Lc,Ed}$ | is the longitudinal shear acting in section a-a; |
| $V_{L,Ed}$ | is the longitudinal shear acting in the shear connection, see equation 3.28; |
| $A_{cp,eff}$ | is the area of the concrete cut by section a-a; |
| $A_{c,tot,eff}$ | is the total effective area of the concrete slab, see section 3.3.1. |

A strut and tie mechanism is formed in the concrete slab to carry the longitudinal shear, illustrated in Figure 3.6. The resistance of the compression strut in concrete is calculated with equation 3.30 and the capacity of the tensile ties of reinforcement is calculated with equation 3.32.

$$V_{c,Rd} = v \cdot f_{cd} \cdot L_v \cdot \frac{1}{cot(\theta) + cot(\theta)^{-1}} \tag{3.30}$$

with,

$$v = 0.6 \cdot \left(1 - \frac{f_{ck}}{250}\right) \tag{3.31}$$

where,

| | |
|---|---|
| $V_{c,Rd}$ | is the crushing capacity of the concrete strut; |
| $v$ | is the reduction factor of concrete cracked in shear; |
| $f_{cd}$ | is the design compression capacity of the concrete; |
| $L_v$ | is the length of the shear failure section, presented in Table 3.13; |
| $\theta$ | is the angle of the compression strut, taken as $1.0 \leq cot(\theta) \leq 2.5$ (TSFS 2018:57, 2018); |
| $f_{ck}$ | is the characteristic compression capacity of the concrete. |

$$V_{s,Rd} = \frac{A_{sf}}{s_f} \cdot f_{sd} \cdot cot(\theta) \tag{3.32}$$

where,

| | |
|---|---|
| $V_{s,Rd}$ | is the capacity of the reinforcement ties; |
| $A_{sf}/s_f$ | is the the effective transverse reinforcement per unit length, see Table 3.14; |
| $f_{sd}$ | is the ultimate design capacity of the reinforcement. |

**Table 3.13:** *Length of the longitudinal shear failure sections (Vayas & Iliopoulos, 2013)*

| **Section** | $\boldsymbol{L_v}$ |
|---|---|
| a-a | $t_c$ |
| b-b | $2 \cdot h_{stud} + e_T + d_{head}$ |
| c-c | $2 \cdot h_{stud} + d_{head}$ |

**Table 3.14:** *Effective transverse reinforcement per unit length for different shear failure section (SS-EN 1994-2, 2005)*

| **Section** | $\boldsymbol{A_{sf}/s_f}$ |
|---|---|
| a-a | $A_b + A_t$ |
| b-b | $2A_b$ |
| c-c | $2A_b$ |

Additionally minimum transverse reinforcement ratio should be provided in accordance with TSFS 2018:57 (2018). The ratio is calculated using equation 3.33.

$$\rho_w = (0.10 + 0.05h/b_w) \tag{3.33}$$

### 3.3.7 Bending capacity

SS-EN 1994-2 (2005) presents three different methods for calculating the bending capacity of a steel-concrete composite bridge. The methods are based on rigid-plastic theory, elastic theory and non-linear theory, where the two later can be used

for all cross-sections while rigid-plastic theory only is allowed for cross-sections in Class 1 or 2. For all methods the tensile strength of the concrete is neglected and the cross-section is assumed to remain plane in bending, if the shear connection is well designed (SS-EN 1994-2, 2005).

#### 3.3.7.1 Plastic bending capacity

When calculating the plastic bending capacity of a composite cross-section, full interaction between the steel girder, concrete flange and steel reinforcement is assumed. The steel girder and reinforcement are assumed to have their respective yield strengths, $f_{yd}$ and $f_{sd}$ in either tension or compression. For sagging bending the contribution of the reinforcement may be neglected when calculating the bending moment capacity. The compressed concrete is taken as a block with a stress of 0.85 times the design cylinder concrete compression strength, $f_{cd}$, from the top of the concrete to the neutral axis. An example of a plastic stress distribution in a composite cross-section in sagging bending can be seen in Figure 3.7.

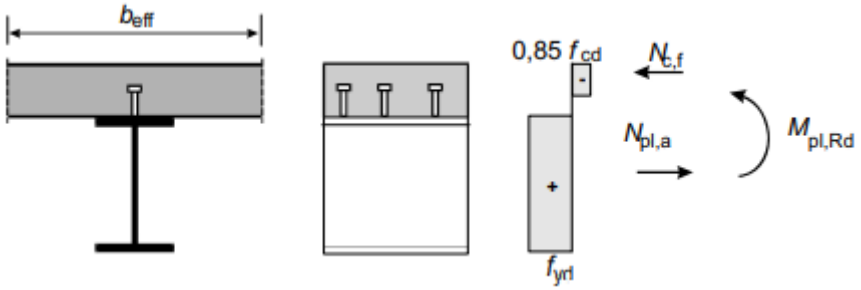


**Figure 3.7:** *Example of a plastic stress distribution for a composite cross-section in sagging bending (SS-EN 1994-2, 2005)*

When steel girders of class S420 or S460 is used, the plastic bending capacity should be reduced with a factor $\beta$ if the ratio of the distance between the top of the concrete slab and the neutral axis is greater than 0.15. If it the ratio exceeds 0.4, the bending moment capacity should be determined via either non-linear or elastic analysis (SS-EN 1994-2, 2005). An example of a plastic stress distribution and a graph for determining the reduction factor $\beta$ can be seen in Figure 3.8.

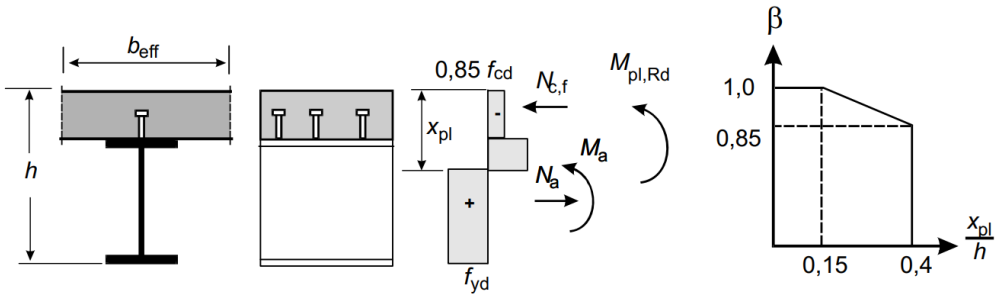


**Figure 3.8:** *Example of a plastic stress distribution and reduction factor $\beta$ for high strength steel and cross-section with deep neutral axis (SS-EN 1994-2, 2005)*

If the section is loaded in a combination of bending moments and vertical shear, the plastic bending capacity should be re-evaluated if the vertical shear $V_{Ed}$ exceeds 50% of the shear resistance $V_{Rd}$. If the cross-section is in Class 1 or 2 the plastic bending capacity should be determined with a reduced yield strength of the steel in the areas loaded in shear, according to equation 3.34. An example of this can be seen in Figure 3.9. If the cross-section instead would be in Class 3 or 4 the plastic bending moment capacity should be determined with equation 3.36. The shear capacity should be taken as the smallest of the vertical shear capacity and the shear buckling resistance. These can be determined according to SS-EN 1993-1-1 (2022) and SS-EN 1993-1-5 (2006) respectively when carbon steel is used and SS-EN 1993-1-4 (2006) for the vertical shear capacity when stainless steel is used.

$$f_{yd,red} = (1 - \rho) f_{yd} \tag{3.34}$$

with,

$$\rho = (2 \cdot V_{Ed}/V_{Rd} - 1)^2 \tag{3.35}$$

where,

| | |
|---|---|
| $f_{yd,red}$ | is the reduced design yield strength of the structural steel; |
| $f_{yd}$ | is the design yield strength of the structural steel; |
| $V_{Ed}$ | is the vertical shear acting in the cross-section; |
| $V_{Rd}$ | is the vertical shear resistance of the cross-section. |

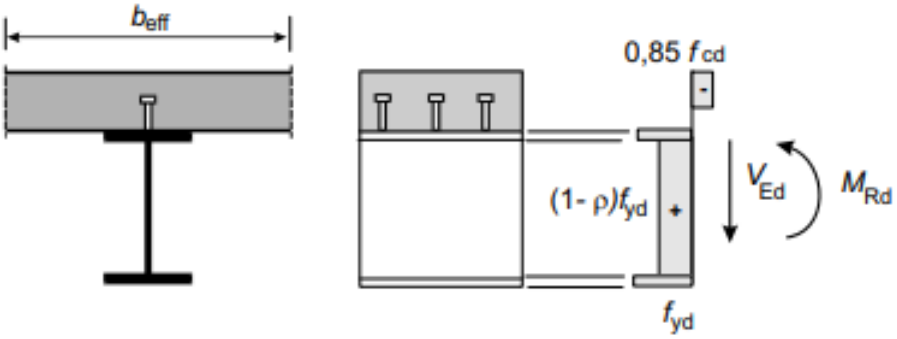


**Figure 3.9:** *Example of a plastic bending distribution adjusted due the effect of vertical shear for a cross-section in Class 1 or 2 (SS-EN 1994-2, 2005)*

$$\bar{\eta}_1 + \left(1 - \frac{M_{f,Rd}}{M_{pl,Rd}}\right) \cdot (2\bar{\eta}_3 - 1)^2 \leq 1.0 \qquad \text{for } \bar{\eta}_1 \geq \frac{M_{f,Rd}}{M_{pl,Rd}} \tag{3.36}$$

with,

$$\bar{\eta}_1 = \frac{M_{Ed}}{M_{pl,Rd}} \tag{3.37}$$

$$\bar{\eta}_3 = \frac{V_{Ed}}{V_{bw,Rd}} \tag{3.38}$$

where,

$M_{f,Rd}$ is the design plastic moment capacity of the effective flanges;
$M_{pl,Rd}$ is the design plastic moment capacity of the effective cross-section with the whole web regardless of its section class;
$M_{Ed}$ is the bending moment acting in the cross-section;
$V_{Ed}$ is the vertical shear acting in the cross-section;
$V_{bw,Rd}$ is the design vertical shear buckling resistance of the web.

#### 3.3.7.2 Non-linear bending capacity

When determining the non-linear bending capacity of a composite cross-section SS-EN 1994-2 (2005) states that the stress-strain curves for each included material should be considered. The strain in the bonded reinforcement should also be taken as the mean strain in the surrounding concrete, both when in tension and compression. The stress-strain curve for the compressed concrete should be taken from section 3.1.7 in SS-EN 1992-1-1 (2005) and the bi-linear stress-strain curve for the reinforcement steel should be taken according to section 3.2.7 in SS-EN 1992-1-1 (2005). The bi-linear stress-strain for the structural steel should be taken according to section 7.3.3(4) in SS-EN 1993-1-1 (2022) considering the method of construction.

SS-EN 1994-2 (2005) give a simplified method that can be used for determining the non-linear bending capacity for a cross-section in Class 1 or 2 by considering the compressive force acting on the concrete $N_c$. The bending capacity is calculated according to equation 3.39 and 3.40 and illustrated in Figure 3.10 for propped and unpropped construction method.

$$M_{Rd} = M_{a,Ed} + (M_{el,Rd} - M_{a,Ed})\frac{N_c}{N_{c,el}} \qquad for\ N_c \leq N_{c,el} \tag{3.39}$$

$$M_{Rd} = M_{el,Ed} + (M_{pl,Rd} - M_{el,Ed})\frac{N_c - N_{c,el}}{N_{c,f}N_{c,el}} \qquad for\ N_{c,el} \leq N_c \leq N_{c,f} \tag{3.40}$$

with,

$$M_{el,Rc} = M_{a,Ed} + k \cdot M_{c,Ed} \tag{3.41}$$

where,

$M_{Rd}$ is the design non-linear moment capacity of the composite cross-section;
$M_{a,Ed}$ is the design bending moment applied to the structural steel before composite action is established;
$M_{el,Rd}$ is the design elastic moment capacity of the composite cross-section;
$N_c$ is the compressive force acting on the concrete;
$N_{c,el}$ is the compressive force acting on the concrete corresponding to the moment $M_{el,Rd}$;
$M_{pl,Rd}$ is the design plastic moment capacity of the composite cross-section;
$N_{c,f}$ is the compressive force acting on the concrete corresponding to the moment $M_{pl,Rd}$;
$k$ is a factor used to accommodate the maximum stresses in the composite cross-section for elastic bending capacity, see section 3.3.7.3.

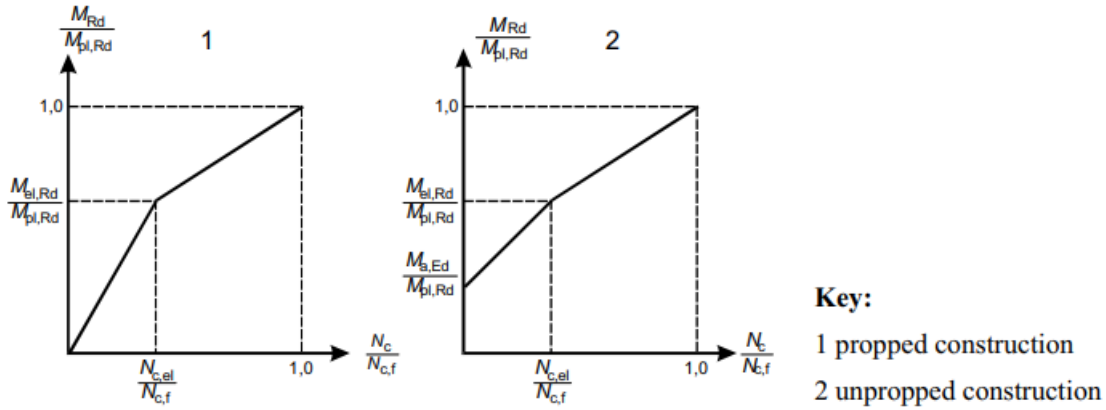


**Figure 3.10:** *Simplified non-linear bending capacity relation for propped and unpropped construction (SS-EN 1994-2, 2005)*

#### 3.3.7.3 Elastic bending capacity

When determining the elastic bending capacity of a composite cross-section according to SS-EN 1994-2 (2005), the effective dimensions of the concrete slab and the steel parts in cross-section class 4 should be used. The effects of creep should be handled with modular ratios presented in section 3.2.1.1 and additionally steel flanges in compression should be checked against lateral-torsional buckling. Stresses in the loaded parts should be limited to the design yield capacity of the material of said part. That means $f_{yd}$ for the structural steel, $f_{cd}$ for the concrete in compression and $f_{sd}$ for the reinforcement.

#### 3.3.7.4 Lateral-torsional buckling

Lateral-torsional buckling may develop in steel-concrete composite beams and have to be handled in accordance with SS-EN 1993-1-1 (2022). SS-EN 1994-2 (2005) states that the a steel flange connected to a laterally stiff concrete flange with shear connections may be considered laterally stable. For cross-sections in Class 1, 2 or 3 the resulting capacity against lateral-torsional buckling should be determined using equation 3.42.

$$M_{b,Rd} = \chi_{LT} \cdot M_{Rd} \tag{3.42}$$

where,

| | |
|---|---|
| $M_{b,Rd}$ | is the design moment capacity against lateral-torsional buckling; |
| $\chi_{LT}$ | is the reduction factor for lateral-torsional buckling, determined according to SS-EN 1993-1-1 (2022); |
| $M_{Rd}$ | is the design moment capacity of the composite section. |

For sections where the top steel flange is connected to the concrete flange, the lower steel flange is laterally restrained and the web stiffened at supports. The elastic critical moment may be determined based on the "continuous inverted-U frame"

model. The U-frame model is based on applying a rotational stiffness $k_s$ per unit length at the level of the top steel flange of a lone beam, illustrated in Figure 3.11. The rotational stiffness $k_s$ is calculated according to equation 3.43.

$$k_s = \frac{k_1 \cdot k_2}{k_1 + k_2} \tag{3.43}$$

with,

$$k_1 = \alpha E_a \cdot I_2 / a \tag{3.44}$$

$$k_2 = \frac{E_a t_w^3}{4(1 - \nu_a^3) h_s} \tag{3.45}$$

where,

| | |
|---|---|
| $k_s$ | is the rotational stiffness per unit length along the top steel flange; |
| $k_1$ | is the flexural stiffness of the cracked concrete slab in the direction transverse to the steel girder; |
| $k_2$ | is the flexural stiffness of the steel web; |
| $\alpha$ | is $\begin{cases} 2 & \text{for and edge beam} \\ 3 & \text{for and inner beam} \\ 4 & \text{for and inner beam with four or more similar beams} \end{cases}$ |
| $E_a \cdot I_2$ | is the "cracked" flexural stiffness per unit length of the concrete, defined in section 1.5.2.12 in SS-EN 1994-2 (2005); |
| $a$ | is the spacing between parallel beams; |
| $t_w$ | is the thickness of the steel web; |
| $\nu_a$ | is the Poisson's ratio of the steel; |
| $h_s$ | is the total height of the steel girder. |

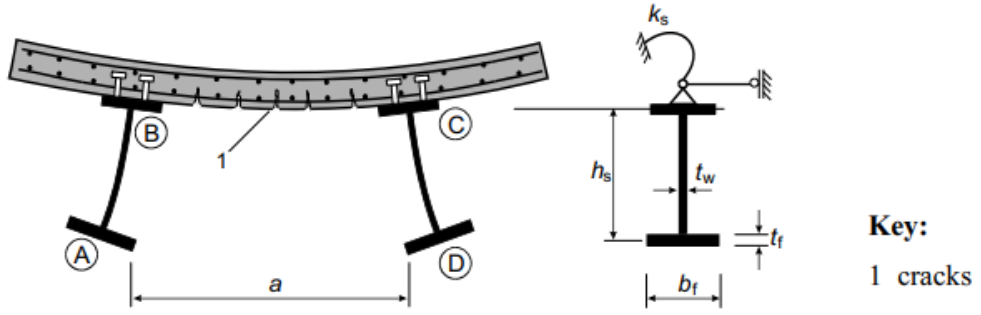


**Figure 6.10: U-frame model**

**Figure 3.11:** *Illustration of the U-frame model (SS-EN 1994-2, 2005)*

### 3.3.8 Shear buckling

In addition to the local and lateral torsional buckling the web have to be checked and designed for shear buckling according to SS-EN 1993-1-5 (2006). For stiffened flat webs the check for shear buckling is done by considering the web as an equivalent

orthotropic plate. If the equation 3.46 is fulfilled the stiffened flat web can be assumed to be prevented from shear buckling.

$$\frac{h_w}{t_w} \leq \frac{31}{\eta}\varepsilon\sqrt{k_\tau} \tag{3.46}$$

with,

$$\varepsilon = \sqrt{\frac{235}{fy}\frac{E}{210}} \tag{3.47}$$

$$\begin{aligned} k_\tau &= 5.34 + 4.0\left(\frac{h_w}{a}\right)^2 + k_{\tau sl} \quad \text{when } a/h_w \geq 1 \\ k_\tau &= 4.0 + 5.34\left(\frac{h_w}{a}\right)^2 + k_{\tau sl} \quad \text{when } a/h_w < 1 \end{aligned} \tag{3.48}$$

where,

| | |
|---|---|
| $h_w$ | is the height of the web; |
| $t_w$ | is the thickness of the web; |
| $\eta$ | is a coefficient, recommended to be taken as 1.2 for steel grades up to S460 and 1.0 for higher grades; |
| $a$ | is the distance between the vertical stiffeners; |
| $k_{\tau sl}$ | is a coefficient set to 0 as simplification. |

For corrugated webs the shear buckling is handled by the corrugated web itself instead of using stiffeners. SS-EN 1993-1-5 (2006) covers two different types of web shear buckling, local and global. Where the local buckling is buckling in a fold of the corrugated web and global buckling is buckling in the web as a whole. The shear buckling is handled by calculating a reduced shear capacity of the web using equation 3.49.

$$V_{Rd} = \chi_c \frac{f_{yw}}{\gamma_{M1}\sqrt{3}} h_w t_w \tag{3.49}$$

where,

| | |
|---|---|
| $\chi_c$ | is the shear buckling reduction factor taken as the smallest of $\chi_{c,l}$ and $\chi_{c,g}$; |
| $f_{yw}$ | is the nominal yield strength of the structural steel in the web; |
| $\gamma_{M1}$ | is the partial factor for structural steel, see section 3.2.2 and 3.2.3. |

The reduction factors for the local ($\chi_{c,l}$) and global ($\chi_{c,g}$) web shear buckling are determined by using equation 3.50 and 3.53 respectively.

$$\chi_{c,l} = \frac{1.15}{0.9 + \overline{\lambda}_{c,l}} \leq 1.0 \tag{3.50}$$

with,

$$\overline{\lambda}_{c,l} = \sqrt{\frac{f_y}{\tau_{cr,l}\sqrt{3}}} \tag{3.51}$$

$$\tau_{cr,l} = 4.83E\left(\frac{t_w}{a_{max}}\right)^2 \tag{3.52}$$

where,

$a_{max}$ is the larger of the length of the flat ($a_1$) and inclined ($a_2$) folds in the corrugated web, see Figure 2.4.

$$\chi_{c,g} = \frac{1.5}{0.5 + \overline{\lambda}_{c,g}^2} \leq 1.0 \tag{3.53}$$

with,

$$\overline{\lambda}_{c,g} = \sqrt{\frac{f_y}{\tau_{cr,g}\sqrt{3}}} \tag{3.54}$$

$$\tau_{cr,g} = \frac{32.4}{t_w h_w^2}\sqrt[4]{D_x D_z^3} \tag{3.55}$$

$$D_x = \frac{Et_w^3}{12\left(1-\nu_a^2\right)}\frac{w}{s} \tag{3.56}$$

$$D_z = \frac{EI_z}{w} \tag{3.57}$$

where,

$\nu_a$ is the Poisson's ratio for the structural steel in the web;

$w$ is the longitudinal length of half a wavelength of the corrugation, see Figure 2.4;

$s$ is the actual length of half a wavelength of the corrugation, see Figure 2.4;

$I_z$ is the moment of inertia of half a wavelength of the corrugation like illustrated in Figure 4.1.

# 4

# Recent research

Current standards suggest analytical solutions for stainless steel-concrete composite beams with corrugated webs that are highly conservative. Ongoing research are developing methods to utilize the significant plastic capacity of stainless steel and the bending capacity of the corrugated webs. This chapter presents these important material or geometrical properties and also the methods taking the effects into account.

## 4.1 Corrugated webs

With full-scale experiments together with an analytical study, Elamary et al. (2017) aimed to define the flexural capacity for conventional I-beams with both corrugated and flat webs. Four different test specimen was fabricated with corrugated and flat webs, different flange compactness and with similar geometrical parameters to get comparable results. The study concluded that a steel beam with a corrugated web has a flexural strength 10-20% lower than a beam with a flat web. A finite element model built up of shell elements was analysed to simulate and to verify the results from the four-point bending experiments. The material mechanical properties were taken directly from tension coupon tests from each experimental beam and then used for the finite element model. This verification comparison resulted in a similar and satisfactory result.

Elamary et al. (2017) continued by studying the behaviour for steel-concrete composite beams with corrugated webs. Experimental measures showed how the corrugated web affected the flexural capacity and behaviour of the beam.

An analytical limit state nominal moment capacity was calculated using current standard code practice for the tested beams to compare with the experimental results. The capacities were calculated on the basis of partial shear connection while considering the full thickness of the corrugated web. However, the moment capacity was reduced by multiplying the tensile force in the steel with 0.85. The calculation gave a nominal moment capacity of 84.3 kNm which was 95% of the experimental maximum moment. Elamary et al. (2017) then concluded that the flexural capacity reduction from a corrugated web compared to a flat web can be the same for both steel beams and steel-concrete composite beams.

### 4.1.1 Accordion effect

The lower flexural capacity from a corrugated web is directly connected to the accordion effect. The accordion effect is the high longitudinal flexibility that emerges depending on the corrugation geometry. Axial stresses will therefore easily contract or stretch the element, which is why previous studies and design codes suggest that the flexural capacity from the web is negligible and can be disregarded. In order to avoid such conservative assumptions, Inaam and Upadhyay (2022) studied the accordion effect for beams with trapezoidal corrugated webs and laterally restrained compact flanges. The numerically based study proposed a new approach that considers a reduced web thickness instead of completely neglecting it. This applied participation factor parameter can give material and economical savings as a result of a better bending capacity in design.

Inaam and Upadhyay (2022) introduced an initial theoretical test together with a numerical analysis in order to conclude how different corrugations profiles will provide different axial rigidity. The theoretical element can be seen in Figure 4.1 and correspond to half of a corrugation wavelength. The stretching or contracting deformation from an axial force can be derived from Castigliano's Second Theorem together for half a wavelength which leads to the equation 4.1.

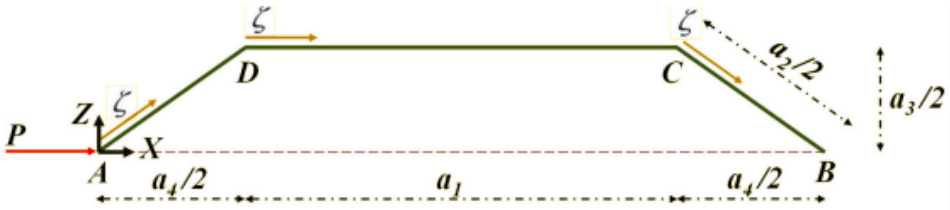


**Figure 4.1:** *Corrugated steel web unit for analytical calculation (Inaam & Upadhyay, 2022)*

$$\delta = 2n \cdot \frac{P \cdot (a_1 + a_4)}{A \cdot E} \tag{4.1}$$

where,

| | |
|---|---|
| $\delta$ | is the axial deformation of the corrugated web; |
| $a_1$ | is the length of the longitudinal corrugation fold; |
| $a_4$ | is the longitudinal length of the inclined corrugation fold; |
| n | is the number of corrugation wavelength halves; |
| P | is the applied axial force; |
| A | is the sectional area; |
| E | is the Young's modulus. |

The numerical part of the corrugation profile investigation is shown in Figure 4.2 with geometry, applied load and the numerical results. The stress intensity from the axial load is noticeably lower for the inclined corrugation folds compared to the

longitudinal folds. As a result of the longitudinal folds' eccentricity from the middle axis, the inclined folds are also subjected to a rotational moment in addition to a minor axial stress. Three corrugation profiles with the same span length where studied and the resulting deformations can be seen in Table 4.1, with these results it was concluded that a coarse corrugation will have less longitudinal stiffness compared to a dense corrugation (Inaam & Upadhyay, 2022).

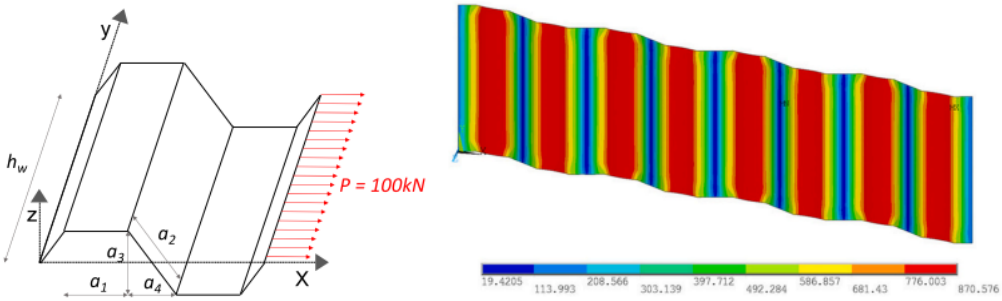


**Figure 4.2:** *Applied axial load and the resulting stress intensity in the corrugated web (Inaam & Upadhyay, 2022)*

**Table 4.1:** *Theoretical and numerical results for trapezoidal corrugated webs with axial loading (Inaam & Upadhyay, 2022)*

| Axial Extension [mm] | | | | | |
|---|---|---|---|---|---|
| Type | Fold width ($a_1$) | Plane web Theoretical (a) | CSW Theoretical (b) | CSW Numerical | (b)/(a) |
| CSW-1 | 75 | 0.24 | 20.06 | 18.36 | 84.67 |
| CSW-2 | 150 | 0.24 | 79.59 | 72.60 | 335.87 |
| CSW-3 | 300 | 0.24 | 317.68 | 290.89 | 1340.68 |

### 4.1.2 Web participation

With a geometrical investigation from a numerical study of the accordion effect, Inaam and Upadhyay (2022) introduced a web participation ratio expressed as $t_{w,eff}/t_w$ with the effective web thickness $t_{w,eff}$ that can contribute to the flexural resistance, in addition to the flanges. When the total moment capacity is known from a numerical analysis, the effective web thickness can be calculated via equations 4.2 and 4.3.

$$t_{w,eff} = \frac{4 \cdot (Z_{num} - b_f \cdot t_f \cdot (h_w + t_f))}{h_w^2} \tag{4.2}$$

with,

$$Z_{num} = \frac{M_{num}}{f_y} \tag{4.3}$$

where,

| | |
|---|---|
| $M_{num}$ | is the total moment resistance from a numerical analysis; |
| $f_y$ | is the yield strength of the material; |
| $b_f$ | is the flange width; |
| $t_f$ | is the flange thickness; |
| $h_w$ | is the web height. |

From the tests included in the study by Inaam and Upadhyay (2022), it was concluded that some geometrical parameters had a higher impact on the effective web participation ratio than others. These parameters and their effects are as follows:

- The corrugation angle ($\alpha$) highly influence the web profile and may also affect if the flanges classes as compact or not. With a lower angle, the beam will act more like a conventional flat web beam with no accordion effect. Thus, higher angles will lead to a worse flexural capacity.
- The flange width and thickness both have a significant affect on the moment capacity. However, a change of flange width will still result in roughly the same accordion behaviour and therefore, the same web participation ratio. A flange thickness increase on the other hand will significantly raise the web participation.
- The web height, thickness and corrugation geometry are shown to affect the accordion behaviour. With increased web height, the web participation for flexural resistance will decrease, and the opposite for the thickness. A thicker web will increase the web participation.
- The web slenderness ratio ($h_w/t_w$) is also relevant for the web participation. A more slender web will result in a higher accordion effect, thus, a decrease in web participation ratio.

The corrugation geometry is shown to have a vast influence on the accordion effect and thus, a dimensionless parameter is needed to quantify it. This is when the enclosing effect can be utilized, see equation 4.4. However, the enclosing effect cannot be used independently to determine the accordion effect. Both the flange width and the corrugation angle are needed in conjunction to the enclosing effect to not get multiple resulting values. Inaam and Upadhyay (2022) defines a supplementary parameter, the outstand ratio seen in equation 4.5, which considers both the flange width and the corrugation angle. With the experimental data, it was noticed that the outstand ratio had a substantial influence on the accordion effect, and therefore, also the web participation. The outstand ratio is simply the long flange outstand divided with the short flange outstand and is further simplified and derived to the equation 4.5.

$$R = \frac{(a_1 + a_4) \cdot a_3}{(a_1 + 2a_4) \cdot b_f} \tag{4.4}$$

$$O = \frac{b_f + a_3}{b_f - a_3} \tag{4.5}$$

where,

| | |
|---|---|
| $R$ | is the enclosing effect |
| $O$ | is the outstand ratio |
| $a_1$ | is the length of the longitudinal flat corrugation fold; |
| $a_3$ | is the corrugation width; |
| $a_4$ | is the longitudinal length of the inclined corrugation fold; |
| $b_f$ | is the flange width. |

It was observed from the numerical study that roughly 92% of the tests have a web participation factor above 0.1 where the total average was 0.184. It was therefore concluded that a web participation factor up to 30% can be utilized in design for moment resistance capacity calculation for trapezoidal corrugated beams. What factor that can be used for each specific case is determined based on the parameters outstand ration, enclosing effect and the slenderness. The limits for the different parameters and the applicable ratio of web participation can be seen in Table 4.2 (Inaam & Upadhyay, 2022).

**Table 4.2:** *Geometrical conditions and limits for partial web participation (Inaam & Upadhyay, 2022)*

| $t_{w,eff}/t_w$ | $h_w/t_w$ | R | O |
|---|---|---|---|
| 0.1 | $\leq 150$ | $< 0.18$ | $\leq 1.6$ |
| 0.2 | $\leq 125$ | $< 0.13$ | $\leq 1.2$ |
| 0.3 | $\leq 90$ | $< 0.09$ | $\leq 1.1$ |

## 4.2 Stainless steel

The use of stainless steel in construction have increased rapidly in the last few years due to an increased desire for sustainable structures. Stainless steel is used because of its great material properties and resistances against fire, corrosion and fatigue. As stainless steel does not need any protection against corrosion, it has been shown that the life cycle cost can be lower for stainless steel structures compared to similar structures with carbon steel. The increased use has also led to an increased interest in the usability and behaviour of stainless steel in the latter years (Shamass & Cashell, 2019).

### 4.2.1 Design of stainless steel members

The current procedure for design of stainless steel structures is based on the concept of cross-section classification presented in SS-EN 1993-1-4 (2006). The current standards are derived on limited testing of stainless steel structures and based on the elastic-plastic behaviour of carbon steel (Afshan & Gardner, 2013). This is however not the behaviour that can be observed for stainless steel. Stainless steel shows a

highly non-linear behaviour early in the stress-strain relationship and also a substantial strain hardening prior to failure (Shamass & Cashell, 2019).

Afshan and Gardner (2013) evaluated the current design method given by SS-EN 1993-1-4 (2006) by comparing the ultimate bending capacities of 65 tested stainless steel beams. The test results were normalized with the plastic bending capacity of the beams and plotted against the slenderness of the cross-sections shown in Figure 4.3. The comparison shows that design codes given by SS-EN 1993-1-4 (2006) predicts conservative capacities all over the slenderness spectrum, specially for stocky cross-sections.

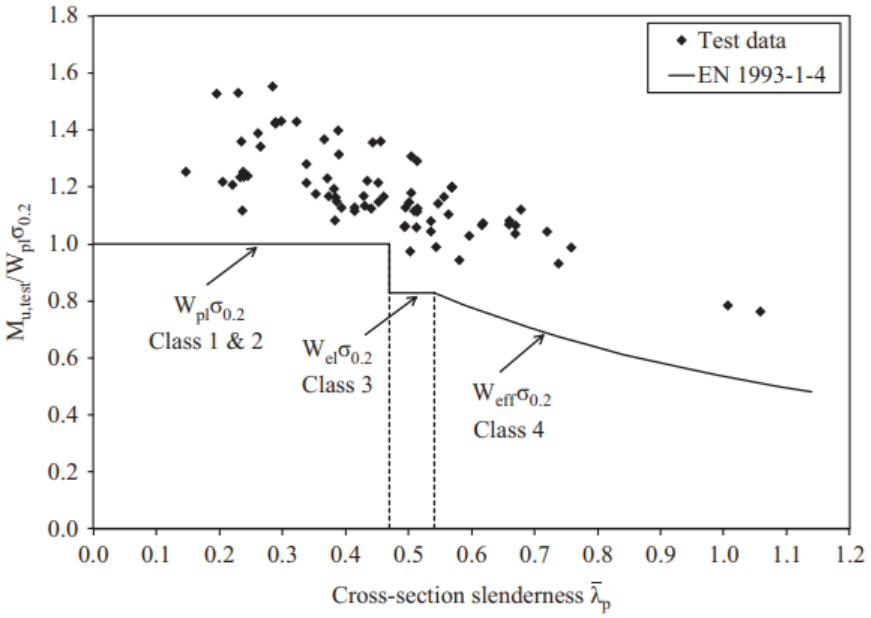


**Figure 4.3:** *Comparison of bending capacity of 65 tested beams and design methods by SS-EN 1993-1-4 (2006) (Afshan & Gardner, 2013)*

#### 4.2.1.1 New design models for stainless steel

Afshan and Gardner (2013) proceeded to construct a new design method called the continuous strength method (CSM) to predict the effects and capacities due to strain hardening. The CSM considers the slenderness and deformation capacity of the cross-section as well as the non-linear behaviour of the stainless steel. It was compared to the test results and values determined by methods given by SS-EN 1993-1-4 (2006) as shown in Figure 4.4. The comparison showed that the CSM gives a more accurate mean resistance as well as less scattered results than SS-EN 1993-1-4 (2006) (Afshan & Gardner, 2013).

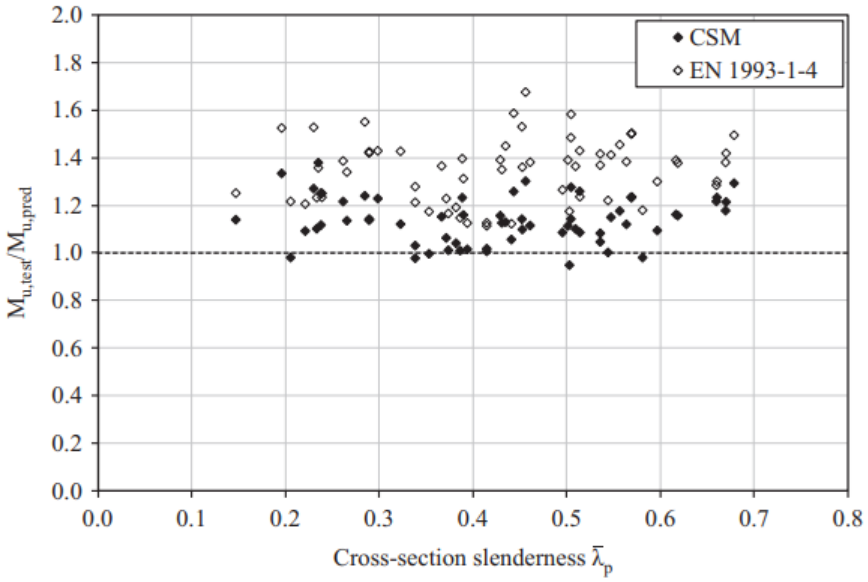


**Figure 4.4:** *Comparison of bending capacity of 65 tested beams with SS-EN 1993-1-4 (2006) and CSM predictions (Afshan & Gardner, 2013)*

For design of composite bridges of stainless steel and concrete SS-EN 1994-2 (2005) gives similar guidelines of using the cross-section classification and limiting the plastic capacities to a rigid-plastic analysis. This completely neglects the effect of strain hardening that may occur and hence, gives conservative results when using highly ductile materials such as stainless steel (Shamass & Cashell, 2019).

Shamass and Cashell (2019) developed the CSM and came up with a new analytical method that considers the effect of strain hardening for stainless steel-concrete composite bridges. The new method can be used for any type of steel material as long as an appropriate material model can be provided. The method provides two different models that can be used to predict the bending capacity of the composite bridge, one detailed and one simplified model.

The material model for the steel used by Shamass and Cashell (2019) is one derived in a previous study by Abdella (2006). The most common and previously used model for modelling the non-linear stress-strain relation of a steel is the Ramberg-Osgood model. The main disadvantage with the Ramberg-Osgood model is that it is an highly non-linear and implicit function that is hard and time consuming to use in practice (Abdella, 2006). Abdella (2006) derived a closed-form inversion of the Ramberg-Osgood model that could be used to relate the stress directly to the strain of the steel over the entire stress range of the steel. A two parted expression of the full-range stress-strain curve for steel was created based on the power law assumption. The expressions were validated against the fully iterated numerical solutions of the full-range stress-strain curves. The comparison was done for 15 different materials and showed that the inversion expressions came extraordinarily close to the numerical solutions with maximum divergence of 10% (Abdella, 2006).

The prediction method presented by Shamass and Cashell (2019) was developed with the assumption that the neutral axis is located in the concrete, that there is negligible slip between the concrete and steel girder due to the shear connectors and that the effect of the reinforcement is ignored. The strain distribution and resulting stress distribution in the cross-section for the detailed model can be seen in Figure 4.5.

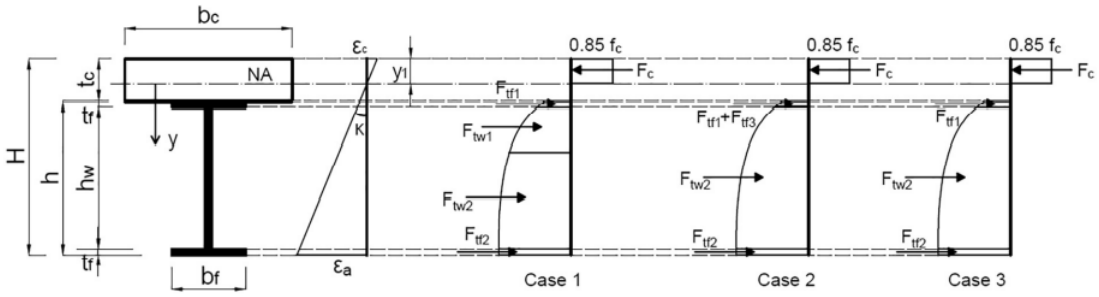


**Figure 4.5:** *Strain and stress distribution for the detailed CSM model (Shamass & Cashell, 2019)*

The model consists of three different cases depending on the location of $y_{0.2}$, where the steel strain equals the yield-strain of the steel. Case 1 is when $y_{0.2}$ is located in the steel web, case 2 is when $y_{0.2}$ is located in the upper steel flange and case 3 is when $y_{0.2}$ is located in the concrete slab. The internal forces and moments needed for calculating the bending moment capacity for the different cases and how they are calculated can be seen in Table 4.3.

**Table 4.3:** *Internal forces and moments for the detailed CSM model (Shamass & Cashell, 2019)*

| | **Case 1** | **Case 2** | **Case 3** |
|---|---|---|---|
| $F_C$ | $0.85 \cdot f_c \cdot b_c \cdot y_1$ | $0.85 \cdot f_c \cdot b_c \cdot y_1$ | $0.85 \cdot f_c \cdot b_c \cdot y_1$ |
| $M_C$ | $0.85 \cdot f_c \cdot b_c \cdot \frac{y_1^2}{2}$ | $0.85 \cdot f_c \cdot b_c \cdot \frac{y_1^2}{2}$ | $0.85 \cdot f_c \cdot b_c \cdot \frac{y_1^2}{2}$ |
| $F_{tf1}$ | $\int_{t_c - y_1}^{t_c - y_1 + t_f} b_f \sigma_1(\varepsilon) dy$ | $\int_{t_c - y_1}^{y_{0.2}} b_f \sigma_1(\varepsilon) dy$ | $\int_{t_c - y_1}^{t_c - y_1 + t_f} b_f \sigma_2(\varepsilon) dy$ |
| $M_{tf1}$ | $\int_{t_c - y_1}^{t_c - y_1 + t_f} b_f \sigma_1(\varepsilon) y dy$ | $\int_{t_c - y_1}^{y_{0.2}} b_f \sigma_1(\varepsilon) y dy$ | $\int_{t_c - y_1}^{t_c - y_1 + t_f} b_f \sigma_2(\varepsilon) y dy$ |

| | | | |
|---|---|---|---|
| $F_{tf2}$ | $\int_{H-t_f-y_1}^{H-y_1} b_f\sigma_1(\varepsilon)dy$ | $\int_{H-t_f-y_1}^{H-y_1} b_f\sigma_2(\varepsilon)dy$ | $\int_{H-t_f-y_1}^{H-y_1} b_f\sigma_2(\varepsilon)dy$ |
| $M_{tf2}$ | $\int_{H-t_f-y_1}^{H-y_1} b_f\sigma_1(\varepsilon)ydy$ | $\int_{H-t_f-y_1}^{H-y_1} b_f\sigma_2(\varepsilon)ydy$ | $\int_{H-t_f-y_1}^{H-y_1} b_f\sigma_2(\varepsilon)ydy$ |
| $F_{tf3}$ | $-----$ | $\int_{y_{0.2}}^{t_c-y_1-t_f} t_w\sigma_2(\varepsilon)dy$ | $-----$ |
| $M_{tf3}$ | $-----$ | $\int_{y_{0.2}}^{t_c-y_1-t_f} t_w\sigma_2(\varepsilon)ydy$ | $-----$ |
| $F_{tw1}$ | $\int_{t_c-y_1-t_f}^{y_{0.2}} t_w\sigma_1(\varepsilon)dy$ | $-----$ | $-----$ |
| $M_{tw1}$ | $\int_{t_c-y_1-t_f}^{y_{0.2}} t_w\sigma_1(\varepsilon)ydy$ | $-----$ | $-----$ |
| $F_{tw2}$ | $\int_{y_{0.2}}^{H-t_f-y_1} t_w\sigma_2(\varepsilon)dy$ | $\int_{t_c-y_1+t_f}^{H-t_f-y_1} t_w\sigma_2(\varepsilon)dy$ | $\int_{t_c-y_1+t_f}^{H-t_f-y_1} t_w\sigma_2(\varepsilon)dy$ |
| $M_{tw2}$ | $\int_{y_{0.2}}^{H-t_f-y_1} t_w\sigma_2(\varepsilon)dy$ | $\int_{t_c-y_1+t_f}^{H-t_f-y_1} t_w\sigma_2(\varepsilon)dy$ | $\int_{t_c-y_1+t_f}^{H-t_f-y_1} t_w\sigma_2(\varepsilon)dy$ |

The main drawback with the detailed model is that it is time consuming as the capacity is determined by the influence of each element in the cross-section and requires integration to find the force in each element. Thus, Shamass and Cashell (2019) developed a simplified model. The main assumption of the simplified model is that the entire steel section is stressed to a constant level of $\sigma_m$ that is defined by the stress at 60 % of the steel beam height (Shamass & Cashell, 2019). The stain and resulting stress distribution for the simplified model can be seen in Figure 4.6.

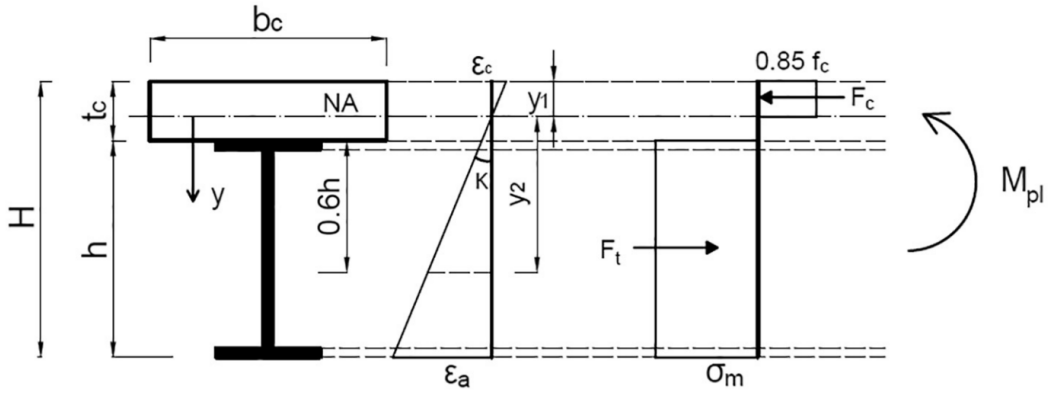


**Figure 4.6:** *Strain and stress distribution for the simplified model (Shamass & Cashell, 2019)*

The plastic bending capacity for a steel-concrete cross-section using the simplified method is calculated by finding the location of the distributed stress, $\sigma_m$, illustrated in Figure 4.6. The location is calculated according to equation 4.6.

$$y_2 = t_c + 0.6h - y_1 \tag{4.6}$$

where,

| | |
|---|---|
| $y_2$ | is the distance between the neutral axis and $\sigma_m$; |
| $t_c$ | is the thickness of the concrete slab; |
| $h$ | is the height of the steel girder; |
| $y_1$ | is the location of the neural axis from the top of the composite cross-section. |

Then location of the neutral axis is determined by setting up an equilibrium of the horizontal forces and solving for $y_1$ according to 4.7 and 4.8.

$$F_c = F_t \Rightarrow f_c \cdot y_1 \cdot b_c = A_s \sigma_m \tag{4.7}$$

$$y_1 = \frac{A_s}{0.85 \cdot f_c \cdot b_c} \sigma_m \tag{4.8}$$

where,

| | |
|---|---|
| $F_c$ | is the balancing compressive force acting in the cross-section; |
| $F_t$ | is the balancing tensile force acting in the cross-section; |
| $f_c$ | is the compressive strength of the concrete; |
| $b_c$ | is the width of the effective concrete slab; |
| $A_s$ | is the cross-sectional area of the steel girder. |

In order to calculate $\sigma_m$ the strain $\varepsilon_2$ in position $y_2$ have to be determined first. $\varepsilon_2$ can be calculated using equation 4.9 and 4.10.

$$\varepsilon_2 = \kappa \cdot y_2 \tag{4.9}$$

$$\kappa = min \begin{cases} \kappa_c = \dfrac{\varepsilon_{cu}}{y_1} \\ \kappa_a = \dfrac{\varepsilon_u}{H - y_1} \end{cases} \tag{4.10}$$

where,

| | |
|---|---|
| $\kappa$ | is the curvature due to bending in the cross-section; |
| $\varepsilon_{cu}$ | is the ultimate strain for the concrete; |
| $H$ | is the total height of the cross-section, including both the steel girder and concrete flange; |
| $\varepsilon_u$ | is the ultimate strain for the steel. |

When $\varepsilon_2$ is known $\sigma_m$ can be determined using inversion model of the steel mentioned in this section according to equation 4.11 or 4.12 depending on if the steel has yielded or not.

$$\sigma_m = \sigma_{0.2} \frac{r\left(\dfrac{\varepsilon_2}{\varepsilon_{0.2}}\right)}{1 + (r-1)\left(\dfrac{\varepsilon_2}{\varepsilon_{0.2}}\right)^p} \quad \text{for } \varepsilon_2 \leq \varepsilon_{0.2} \tag{4.11}$$

$$\sigma_m = \sigma_{0.2} \left( 1 + \frac{r_2\left(\dfrac{\varepsilon_2}{\varepsilon_{0.2}} - 1\right)}{1 + (r^* - 1)\left(\dfrac{\dfrac{\varepsilon_2}{\varepsilon_{0.2}} - 1}{\dfrac{\varepsilon_u}{\varepsilon_{0.2}} - 1}\right)^{p^*}} \right) \quad \text{for } \varepsilon_2 \geq \varepsilon_{0.2} \tag{4.12}$$

where,

| | |
|---|---|
| $\sigma_{0.2}$ | is the 0.2% proof strength of the steel; |
| $\varepsilon_{0.2}$ | is the actual strain at 0.2% proof strength of the steel. |

The rest of the parameters for the material models can be calculated according to equations 4.13-4.25.

$$\varepsilon_{0.2} = \frac{\sigma_{0.2}}{E} + 0.002 \tag{4.13}$$

$$r = \frac{E \cdot \varepsilon_{0.2}}{\sigma_{0.2}} \tag{4.14}$$

$$p = r\frac{1 - r_2}{r - 1} \tag{4.15}$$

$$r_2 = \frac{E_2 \cdot \varepsilon_{0.2}}{\sigma_{0.2}} \tag{4.16}$$

$$E_2 = \frac{E}{1 + 0.002n/e} \tag{4.17}$$

$$e = \frac{\sigma_{0.2}}{E} \tag{4.18}$$

$$r^* = \frac{E_2(\varepsilon_u - \varepsilon_{0.2})}{\sigma_u - \sigma_{0.2}} \tag{4.19}$$

$$\varepsilon_u = min \begin{cases} 1 - \dfrac{\sigma_{0.2}}{\sigma_u} \\ A \end{cases} \tag{4.20}$$

$$p^* = r^* \frac{1 - r_u}{r^* - 1} \tag{4.21}$$

$$r_u = \frac{E_u(\varepsilon_u - \varepsilon_{0.2})}{\sigma_u - \sigma_{0.2}} \tag{4.22}$$

$$E_u = \frac{E_2}{1 + (r^* - 1)m} \tag{4.23}$$

$$m = 1 + 3.5\frac{\sigma_{0.2}}{\sigma_u} \tag{4.24}$$

$$\sigma_u = \sigma_{0.2} \frac{1 - 0.0375(n - 5)}{0.2 + 185e} \tag{4.25}$$

where,

| | |
|---|---|
| $A$ | is the elongation of the steel after fracture; |
| $n$ | is the strain hardening exponent; |
| $E_2$ | is the inclination of the stress-strain curve at $\varepsilon_{0.2}$; |
| $E_u$ | is the inclination of the stress-strain curve at $\varepsilon_u$. |

The other parameters $r$, $r_2$, $r^*$, $r_u$, $p$ and $p^*$ are ones that need to be calculated to derive the full-range stress-strain curve of the steel. The elongation of the steel after fracture A and the strain hardening exponent n are both material parameters that are listed in Eurocode. The elongation of the steel after fracture can be found for most grades in SS-EN 10088-2 (2019), values of the elongation for the grades covered by SS-EN 1993-1-4 A1 (2015) can be found in Table 4.6. According to SCI (2018), the values and equations presented in Eurocode are based on low number of tests and not completely accurate. SCI (2018) presents a new table and equation of the strain hardening exponent that is to be incorporated in a future edition of the Eurocode standard. The table and equation for the strain hardening exponent covered in SS-EN 1993-1-4 (2006) can be seen in Table 4.4 and equation 4.26. And

the new recommendations by SCI (2018) can be seen in Table 4.5 and equation 4.27.

$$n = \frac{ln(20)}{ln(f_y/R_{p0.01})} \tag{4.26}$$

$$n = \frac{ln(4)}{ln(f_y/R_{p0.05})} \tag{4.27}$$

where,

$R_{p0.01}$ is the 0.01 % proof stress.
$R_{p0.05}$ is the 0.05 % proof stress.

**Table 4.4:** *Values of the strain hardening exponent, n (SS-EN 1993-1-4, 2006)*

| Steel grade | Coefficient $n$ | |
|---|---|---|
| | Longitudinal direction | Transverse direction |
| 1.4003 | 7 | 11 |
| 1.4016 | 6 | 14 |
| 1.4512 | 9 | 16 |
| 1.4301 | 6 | 8 |
| 1.4306 | | |
| 1.4307 | | |
| 1.4318 | | |
| 1.4541 | | |
| 1.4401 | 7 | 9 |
| 1.4404 | | |
| 1.4432 | | |
| 1.4435 | | |
| 1.4539 | | |
| 1.4571 | | |
| 1.4462 | 5 | 5 |
| 1.4362 | | |

**Table 4.5:** *Values of the strain hardening exponent, n (SCI, 2018)*

| Steel type | Coefficient $n$ |
|---|---|
| Ferritic | 14 |
| Austenitic | 7 |
| Duplex | 8 |

**Table 4.6:** *Values of the elongation after fracture, A (SS-EN 10088-2, 2019)*

| Steel grade | Product form | Coefficient $A$ | |
|---|---|---|---|
| | | Nominal thickness $t$ | |
| | | $t < 3$ mm | $t \geq 3$ mm |
| 1.4003 | C | 20 | 20 |
| | H | | |
| | P | 18 | 18 |
| 1.4016 | C | 20 | 20 |
| | H | 18 | 18 |
| | P | 20 | 20 |
| 1.4512 | C | 25 | 25 |
| | H | | |
| 1.4306 | C | 45 | 45 |
| | H | | |
| | P | | |
| 1.4307 | C | 45 | 45 |
| | H | | |
| | P | | |
| 1.4541 | C | 40 | 40 |
| | H | | |
| | P | | |
| 1.4301 | C | 45 | 45 |
| | H | | |
| | P | | |
| 1.4401 | C | 40 | 40 |
| | H | | |
| | P | 45 | 45 |
| 1.4404 | C | 40 | 40 |
| | H | | |
| | P | 45 | 45 |
| 1.4539 | C | 35 | 35 |
| | H | | |
| | P | | |
| 1.4571 | C | 40 | 40 |
| | H | | |
| | P | | |
| 1.4432 | C | 40 | 40 |
| | H | | |
| | P | 45 | 45 |
| 1.4435 | C | 40 | 40 |
| | H | | |
| | P | 45 | 45 |
| 1.4311 | C | 40 | 40 |
| | H | | |
| | P | | |

| | | | |
|---|---|---|---|
| 1.4406 | C | 40 | 40 |
| | H | | |
| | P | | |
| 1.4439 | C | 35 | 35 |
| | H | | |
| | P | 40 | 40 |
| 1.4529 | P | 40 | 40 |
| 1.4547 | C | 35 | 35 |
| | H | | |
| | P | 40 | 40 |
| 1.4318 | C | 35 | 40 |
| | H | | |
| | P | 45 | 45 |
| 1.4062 | C | 20 | 20 |
| | H | 30 | 30 |
| | P | | |
| 1.4162 | C | 20 | 30 |
| | H | 30 | |
| | P | | |
| 1.4482 | C | 20 | 30 |
| | H | 30 | |
| | P | | |
| 1.4662 | C | 20 | 25 |
| | H | – | |
| | P | | |
| 1.4362 | C | 20 | 20 |
| | H | | |
| | P | 25 | 25 |
| 1.4462 | C | 20 | 20 |
| | H | 25 | 25 |
| | P | | |

C = Cold rolled strip; H = Hot rolled strip;
P = Hot rolled plate

SCI (2018) also presents new equations for calculating the parameters m and $\varepsilon_u$ that will be included in a upcoming edition of the Eurocode standard. The new equations for m and $\varepsilon_u$ can be seen in equations 4.28 and 4.29.

$$m = 1 + 2.8\frac{\sigma_{02}}{\sigma_u} \tag{4.28}$$

$$\varepsilon_u = \min \begin{cases} 1 - \dfrac{\sigma_{02}}{\sigma_u} \\ 0.6 \cdot \left(1 - \dfrac{\sigma_{02}}{\sigma_u}\right) \\ A \end{cases} \tag{4.29}$$

Once all the parameters, stresses and strains are determined the plastic moment capacity can then be calculated using the equation 4.30.

$$M_{pl} = \sigma_m \cdot A_s(H - h/2 - y_1/2) \tag{4.30}$$

Shamass and Cashell (2019) compared the results given by the derived method with results from non-linear finite element analysis for two different models for six different grades of stainless-steel. The comparison showed that the method performed well, always predicting the ultimate strength within 5% of the ones computed in the FE analysis. Both the detailed and simplified models were tested, and both showed similar results, the simplified model were within 2% of the detailed model for all cases. Hence, Shamass and Cashell (2019) concluded that the simplified model was accurate and can be used to predict the ultimate bending capacity of stainless steel-concrete composite bridges.

### 4.2.2 Experimental testing

Zhou et al. (2021) performed a study where the response in shear and bending of stainless steel-concrete composite beams was analysed by experimental, analytic and numerical testing. In the study, eighteen beams with various shear connections and loading setups were analysed, where eight of them were tested in bending. The variations of the eight beams tested in bending can be seen in Table 4.7 and the geometry and configuration of the tests can be seen in Figure 4.7.

**Table 4.7:** *Details for the beam specimen used in experimental testing (Zhou et al., 2021)*

| **Specimen** | **Steel material** | $\boldsymbol{L_e}$ [m] | $\boldsymbol{a}$ [m] | **Loading method** | **Connector type** | **Connection degree** |
|---|---|---|---|---|---|---|
| CSSB1-BF | LD2101 | 5.8 | 2 | FPL | Bolt | Full |
| CSSB2-SF | LD2101 | 5.8 | 2 | FPL | Stud | Full |
| CSSB3-BP | LD2101 | 5.8 | 2 | FPL | Bolt | Partial |
| CSSB4-SP | LD2101 | 5.8 | 2 | FPL | Stud | Partial |
| CSSB5-BF | A304 | 5.8 | 2 | FPL | Bolt | Full |
| CSSB6-BF | D2205 | 5.8 | 2 | FPL | Bolt | Full |
| CSSB7-BF | LD2101 | 2 | 1 | TPL | Bolt | Full |
| CSSB8-SF | LD2101 | 2 | 1 | TPL | Stud | Full |
| FPL: Four-point loading; TPL: Three point loading | | | | | | |

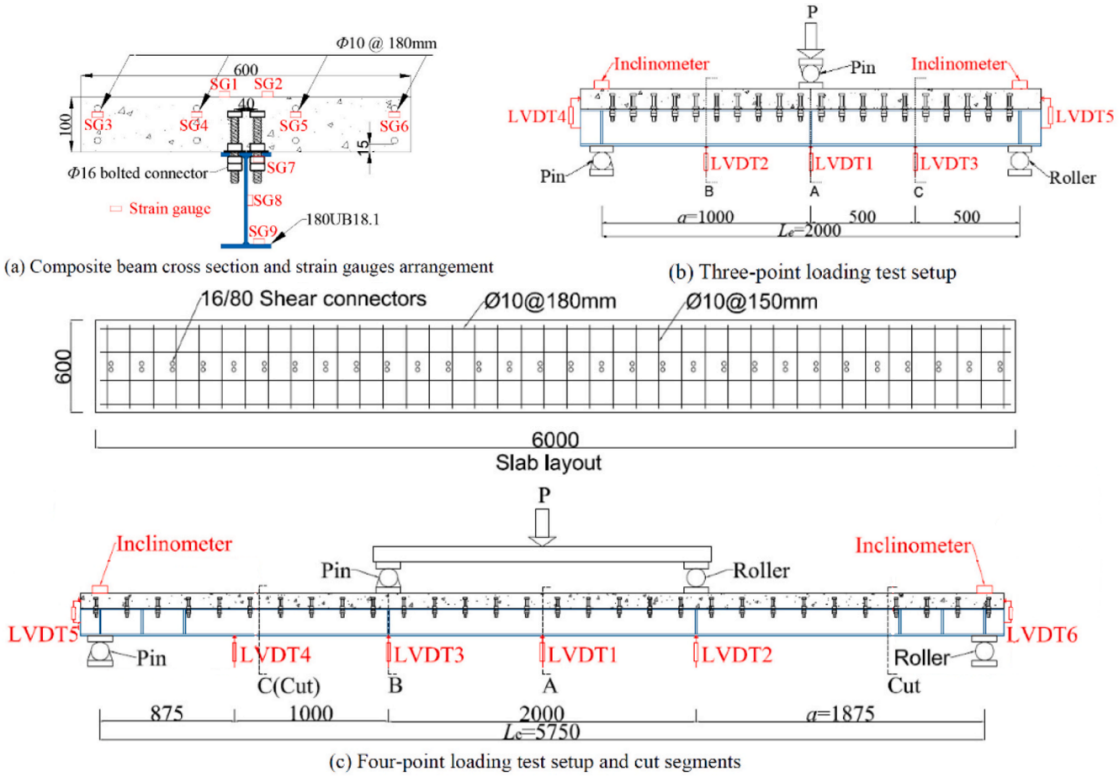


**Figure 4.7:** *Configuration and geometry of the experimental bending tests (Zhou et al., 2021)*

The resulting moment-displacement curves from the experimental test of the eight specimens can be seen in Figure 4.8. The moment capacities were then compared to values calculated with analytical methods. Three analytical models were used, the first was a rigid-plastic model given by SS-EN 1994-2 (2005) and the other two were the detailed and simplified model by Shamass and Cashell (2019) presented in section 4.2.1.1. The results from the test and the three methods can be seen in Table 4.8.

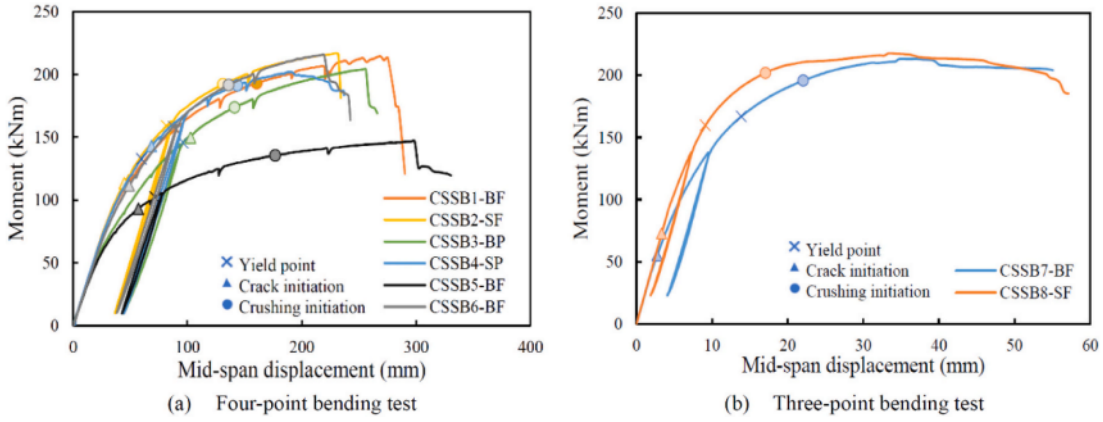


**Figure 4.8:** *Moment-displacement curves for the tested specimens (Zhou et al., 2021)*

**Table 4.8:** *Moment capacities form testing and analytical models (Zhou et al., 2021)*

| Beam | $M_u$ [kNm] | $M_{EC}$ [kNm] | $M_u/M_{EC}$ | $M_{SHA,D}$ [kNm] | $M_u/M_{SHA,D}$ | $M_{SHA,S}$ [kNm] | $M_u/M_{SHA,S}$ |
|---|---|---|---|---|---|---|---|
| CSSB1-BF | 204 | 177 | 115% | 190 | 107% | 190 | 108% |
| CSSB2-SF | 206 | 177 | 116% | 190 | 109% | 190 | 109% |
| CSSB3-BP | 194 | 170 | 114% | 175 | 111% | 175 | 111% |
| CSSB4-SP | 192 | 165 | 116% | 170 | 113% | 170 | 113% |
| CSSB5-BF | 139 | 118 | 118% | 126 | 110% | 125 | 112% |
| CSSB6-BF | 205 | 177 | 115% | 190 | 108% | 190 | 108% |
| CSSB7-BF | 213 | 175 | 122% | 190 | 112% | 190 | 112% |
| CSSB8-SF | 218 | 175 | 124% | 190 | 115% | 190 | 115% |

As seen in Figure 4.8 the beams show remarkable strain hardening and high level of ductility beyond the yield-point. The strain hardening effect can also be seen in the results presented in Table 4.8 where the capacity given by SS-EN 1994-2 (2005) is between 14-24 % lower than the measured result. The improved models presented by Shamass and Cashell (2019) does however improve the estimation substantially as they take the underestimation to 7-15 % compared to the tests. It can also be observed that both the detailed and simplified models yield similar results and only using the simplified method is sufficient.

## 4.3 Finite element modelling of steel-concrete composite bridges

Ali and Abudaher (2022) performed a master's thesis where a method of how to model steel-concrete composite bridges was adopted and evaluated. The method was created for handling bridges with both flat and corrugated webs of carbon or stainless steel. It was validated against multiple experimental tests and the FE method perform and showed good agreement with the test results. From the results Ali and Abudaher (2022) observed that the level of strain hardening activation was larger for the beams with corrugated webs compared to the ones with flat webs. The reason for this was concluded to be the increased flexibility and ductility given by the corrugated webs.

# 5
# Design tool development

This chapter will cover how the design tool should be used, what it covers and what different design choices can be made and what they entail. The tool is built up in multiple Python modules linked together, all Python modules can be found in Appendix E. The tool is made up of a set of equations and algorithms that computes the ultimate plastic moment capacity based on the geometry and materials of the beam.

## 5.1 Design tool structure

The design tool is built up in three parts, the first one being the main tool where all inputs and choices should be stated. The second part is a library of equations that is used in the main tool to perform all necessary calculations and the third is a library of material properties from Eurocode standards for the different materials. The structure of the tool is illustrated in Figure 5.1.

### 5.1.1 Inputs

The tool requires a number of user defined geometrical and material inputs in order to calculated the plastic moment capacity, these are presented in Table 5.1.

**Table 5.1:** *User defined inputs needed for the design tool*

| | |
|---|---|
| **Cross-section geometry** | |
| $b_{fu}$, $t_{fu}$, $b_{fl}$, $t_{fl}$, $h_w$, $t_w$ & $t_c$ | Presented in section 3.3.3 |
| **Corrugation geometry for corrugated web** | |
| $\alpha$, $a_1$ & $a_3$ | Presented in section 2.2 |
| **Global geometry** | |
| $L$, $b_1$ & $b_2$ | Presented in section 3.3.1 |
| **Used materials** | |
| Material types and grades eg. C35/45, S355, 1.4162 | Presented in section 3.2 |

The defined cross-sectional inputs are used to calculate and derive the rest of the values and dimension of the cross-section, such as total height and areas. The corrugation values are used to derive the rest of the corrugation geometry and the global geometry values are used for calculating the effective width of the concrete

for the beam. The material inputs are used to gather material constants from the library implemented in the tool taken from Eurocode standards.

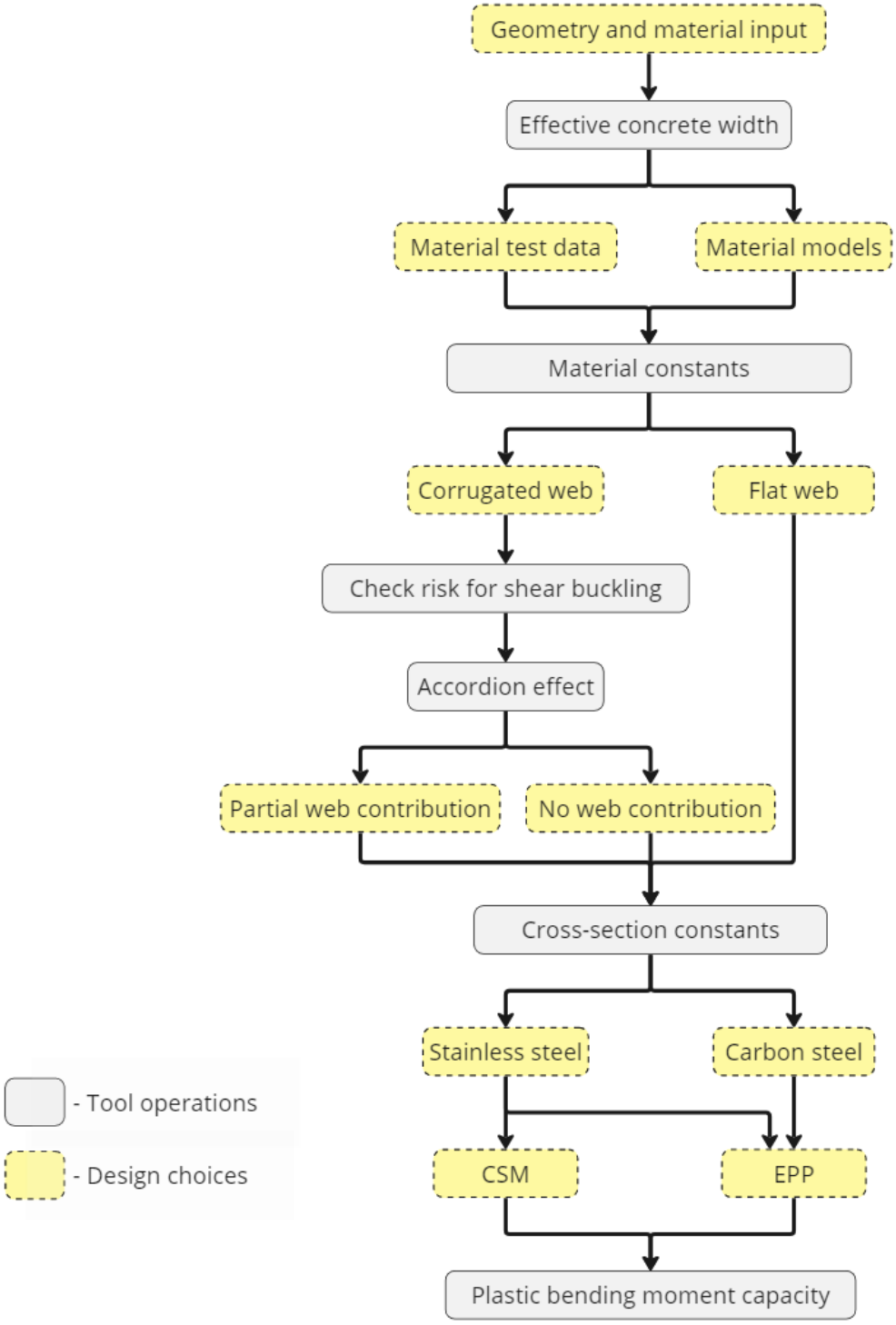


**Figure 5.1:** *Illustration of the general design tool structure*

### 5.1.2 Design choices and tool operations

The tool is versatile and can take multiple different design methods and considerations into account when calculating the plastic moment capacity of a steel-concrete composite beam.

Once the tool has been given proper and correct inputs it starts by defining the effective width of the concrete flange. It can be done, either by using the method given by SS-EN 1994-2 (2005) presented in section 3.3.1, based on the global geometry or by using a chosen effective width.

The next choice is how the material properties and behaviour should be gathered by the tool. The tool can do this in two ways, using material models or using data from material tests. If material models are chosen, the tool gathers material constants from the Eurocode library based on defined material classes and generates the material behaviour with analytical equations. If material test data is provided with material behaviour as a stress-strain curve, the tool gathers the material constants based on the provided data. The main advantage of providing test data is that steel grades that is not covered or given conservative values in Eurocode can be used for predicting the moment capacity. Apart from that, either choice should yield similar accuracy and results.

The next choice affecting the tools operations is what web type is used. The choice of web type will affect two different aspects, the first is the check of shear buckling risk and the second is what web thickness is considered for calculating the cross-sectional constants. The risk of shear buckling is checked for the corrugated web based on the corrugation and web geometry as presented in section 3.3.8. The risk of shear buckling is not checked for flat webs as they can be stabilized with vertical and horizontal stiffeners. When a flat web is used, the entire defined web thickness is considered, while for corrugated webs another design choice has to be made in order to decide what web thickness should to be considered. The choice refers to how the accordion effects of the corrugated web should be treated. One option is to treat it as suggested in SS-EN 1993-1-5 (2006), by neglecting the web and not consider any contribution. The other option is to analyse the corrugation and web geometry to find an effective width of the web that can be utilized in bending according to section 4.1.1. Once the shear buckling and web thickness is checked, the necessary cross-sectional constants are calculated by the tool.

After the cross-sectional constants are calculated, the tool can calculate the plastic bending moment capacity of the beam. Two different models for the calculations can be used, the first is the elastic perfectly plastic (EPP) model given in SS-EN 1994-2 (2005). The second model is a variation of the simplified model for the CSM created by Shamass and Cashell (2019) taking strain hardening of the steel into account. The models used in the tool are presented and discussed further in section 5.2. What model that is or can be used in the tool depends on what steel type was chosen in the material inputs. If stainless is used either model can be used, while carbon steel only can be used for the EPP model.

## 5.2 Calculation models

The two calculation models incorporated in the tool are both plastic models although they differ both in the models and the calculation methods. The models and their calculation methods are described in this section.

### 5.2.1 Calculation model EPP

The EPP model given by SS-EN 1994-2 (2005) is presented in section 3.3.7.1 and the calculation method and all its steps is presented in Figure 5.2.

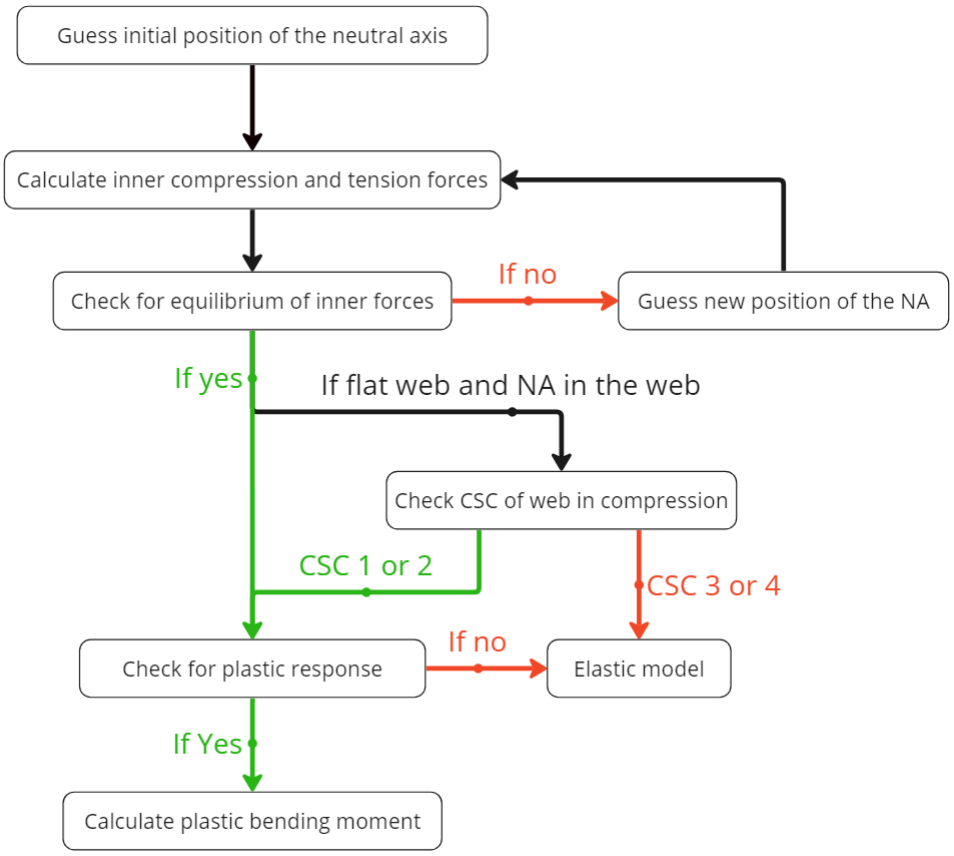


**Figure 5.2:** *Representation of the calculation method for the EPP model*

The first part of the calculation method is to find the location of the neutral axis (NA), this is done by iterating the location of the NA, $y_1$. The iteration starts by setting the position of the NA at the top of the cross-section and calculating the inner compression and tension forces. If the compression and tension are within a prescribed difference of each other, $y_1$ is found. Otherwise, a new location is generated by moving down the NA a defined step. All steel parts are assumed to be stressed to its yield strength regardless if it is in tension or compression. The compressed concrete parts are assumed to be stressed up to 0.85 times its mean

compressive strength.

When $y_1$ is found, the cross-section is checked to see if it is within the plastic work range. This is done by first checking the cross-section class to see that plastic calculation are allowed according to SS-EN 1994-2 (2005), described in section 3.3.2. If it is acceptable the section is validated to have a plastic behaviour. This is done by calculating the ratio of $y_1$ and the total height of the cross-section to find a reduction factor $\beta$ for the moment capacity, described in section 3.3.7.1.

If the checks for plastic response are satisfactory the plastic moment capacity $M_{pl}$ can be calculated by adding all the inner forces times their lever arm to the NA and then multiply it by the reduction factor $\beta$. If the input beam does not have a plastic behaviour, an elastic calculation model is needed, which is not within the scope of this thesis.

### 5.2.2 Calculation model CSM

When calculating with regards to additional plastic strain hardening capacity, the CSM is utilized. Furthermore, Shamass and Cashell (2019) developed the simplified analytic calculation based on CSM which were shown to give reliable result and is therefore implemented in the design tool. Similarly to the EPP calculation model, the NA location is iterated by moving it down if the inner force balance is not satisfied. The CSM does also check for plastic response, however, in as slightly different way than the EPP method. The CSM utilizes the curvature in the cross-section, which allows for a specific steel stress to be determined. If the steel stress at 60% of the steel height in tension surpass the yield strength, plastic response is assumed. When the location of the NA is found, the cross section class is controlled if parts of the web are compressed. Lastly, the moment capacity is calculated with the inner forces and their level arms. This methodology is clearly illustrated in Figure 5.3.

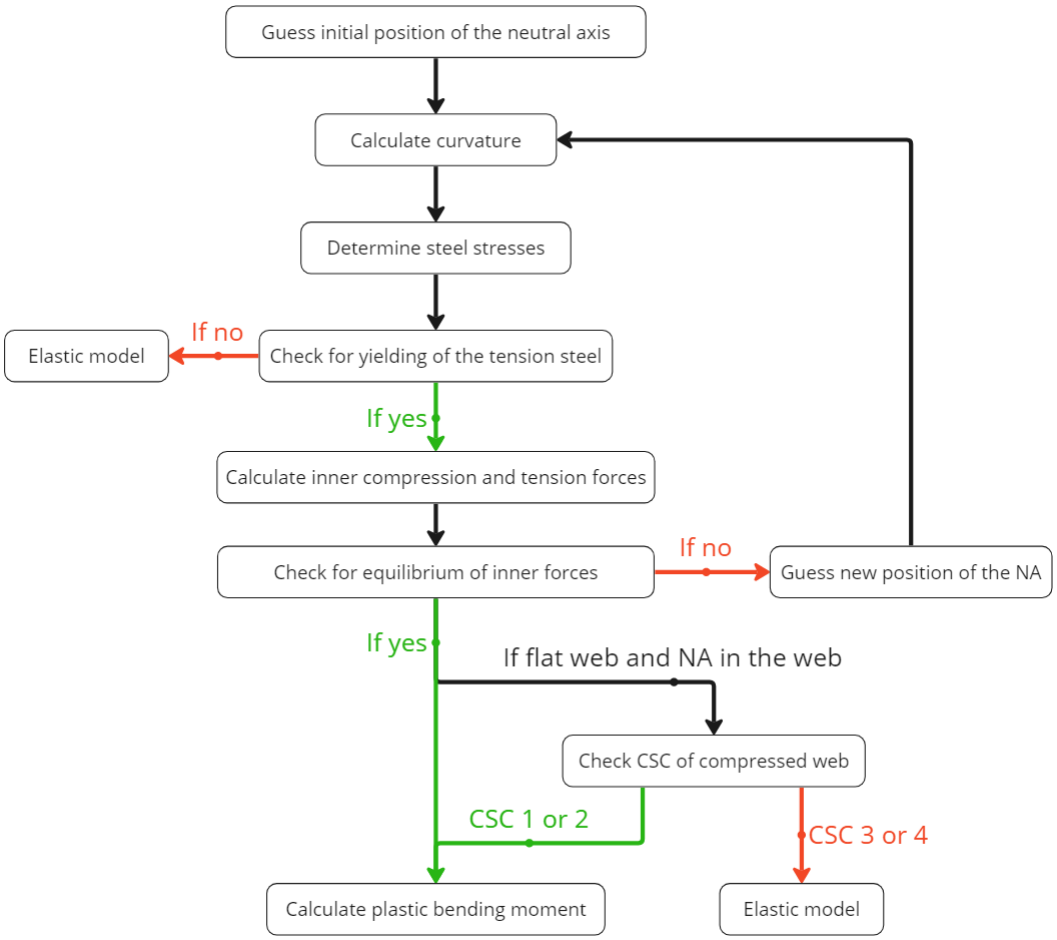


**Figure 5.3:** *Representation of the calculation method for the CSM model*

Depending on where the NA is located in the cross-section, slightly different calculation models are used. For the first case, with the NA in the concrete slab, the simplified CSM developed by Shamass and Cashell (2019) is used and can be seen in Figure 5.4. The entire steel girder is subjected to tension and in the calculations, the steel stress is set to be constant. The stress value is calculated from the curvature and the strain at 60% girder height, which is the same stress used to validate plastic response. The concrete compression block is, like in the EPP model, subjected to 0.85 time the compression strength only above the NA. The concrete in tension is assumed to be cracked and does not contribute to the bending moment capacity.

However, the case with the NA in the concrete is the only one that is covered by the research article and further development was needed for cases where the NA is in the steel flange or web. These models are inspired by the same ideas as the simplified model developed by Shamass and Cashell (2019). The new models can be seen in Figure 5.5 and 5.6. The applied stress for the steel parts is taken from 60% of the steel height in compression or tension. The internal cross-sectional forces for each block are listed in Table 5.2 for the three possible cases. With these, the ultimate plastic bending capacity can be calculated with the equations 5.1 to 5.3.

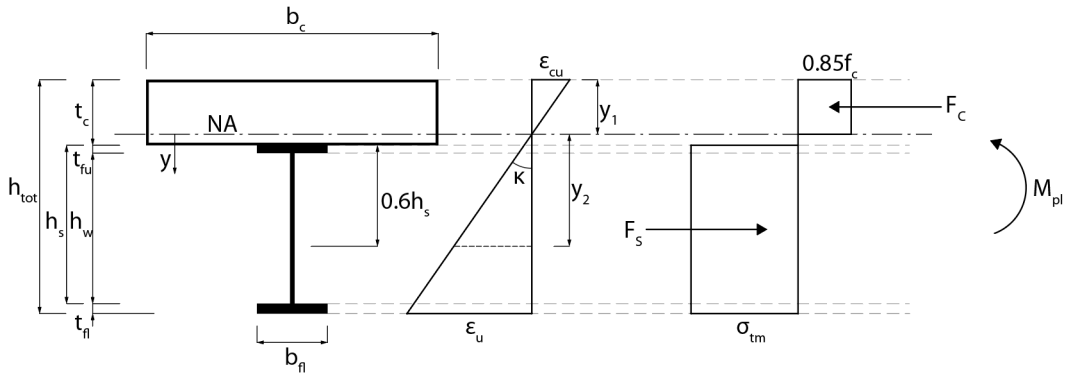


**Figure 5.4:** *Plastic calculation model when the NA is in the concrete*

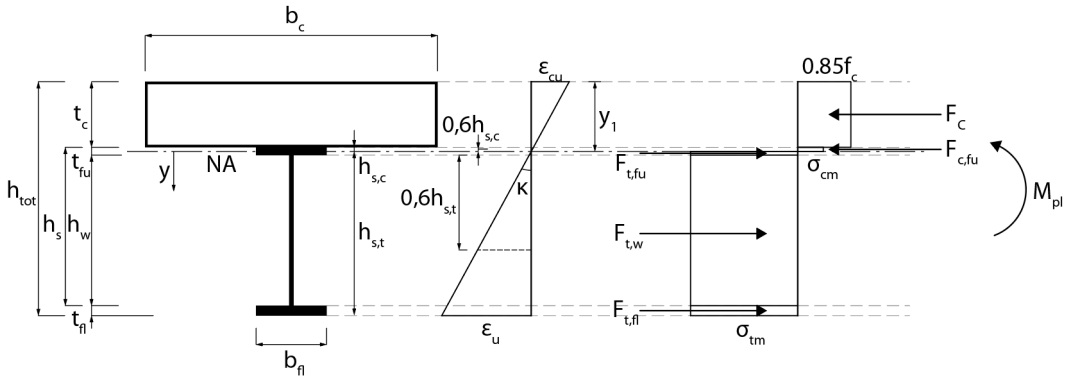


**Figure 5.5:** *Plastic calculation model when the NA is in the upper steel flange*

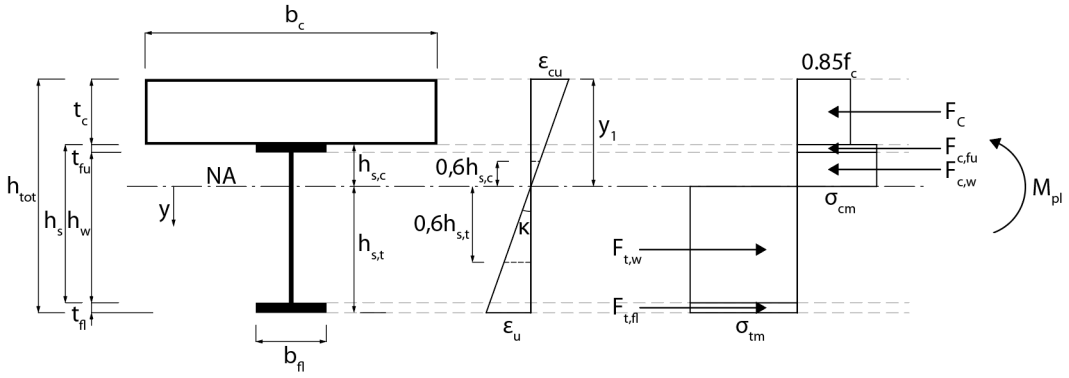


**Figure 5.6:** *Plastic calculation model when the NA is in the steel web*

**Table 5.2:** *Internal forces for the CSM models used in the tool*

| | **Case 1** | **Case 2** | **Case 3** |
|---|---|---|---|
| $F_C$ | $0.85 \cdot f_c \cdot b_c \cdot y_1$ | $0.85 \cdot f_c \cdot b_c \cdot t_c$ | $0.85 \cdot f_c \cdot b_c \cdot t_c$ |
| $F_S$ | $A_s \cdot \sigma_{tm}$ | – | – |
| $F_{c,f_u}$ | – | $b_{fu} \cdot (y_1 - t_c) \cdot \sigma_{cm}$ | $b_{fu} \cdot t_{fu} \cdot \sigma_{cm}$ |
| $F_{t,f_u}$ | – | $b_{fu} \cdot (t_c + t_{fu} - y_1) \cdot \sigma_{tm}$ | – |
| $F_{c,w}$ | – | – | $t_w \cdot (y_1 - t_c - t_{fu}) \cdot \sigma_{cm}$ |
| $F_{t,w}$ | – | $t_w \cdot h_w \cdot \sigma_{tm}$ | $t_w \cdot (h_{tot} - t_{fl} - y_1) \cdot \sigma_{tm}$ |
| $F_{t,f_l}$ | – | $b_{fl} \cdot t_{fl} \cdot \sigma_{tm}$ | $b_{fl} \cdot t_{fl} \cdot \sigma_{tm}$ |

The location of the NA, $y_1$, is solved by finding equilibrium between the compression and tension forces acting in the cross-section. The plastic bending capacity is then calculated as a sum of each force times its lever arm to the NA. The equations for the plastic moment capacities for the for case 1−3 can be seen in equations 5.1−5.3 where the forces are listed in table 5.2.

$$M_{pl} = F_C \cdot \frac{y_1}{2} + F_S \cdot \left( h_{tot} - y_1 - \frac{h_s}{2} \right) \tag{5.1}$$

$$\begin{aligned} M_{pl} = F_C \cdot \left( y_1 - \frac{t_c}{2} \right) + F_{c,f_u} \cdot \frac{y_1 - t_c}{2} + F_{t,f_u} \cdot \frac{t_c + t_{fu} - y_1}{2} + \\ F_{t,w} \cdot \left( h_{tot} - t_{fl} - \frac{h_w}{2} - y_1 \right) + F_{t,f_l} \cdot \left( h_{tot} - \frac{t_{fl}}{2} - y_1 \right) \end{aligned} \tag{5.2}$$

$$\begin{aligned} M_{pl} = F_C \cdot \left( y_1 - \frac{t_c}{2} \right) + F_{c,f_u} \cdot \left( y_1 - t_c - \frac{t_{fu}}{2} \right) + F_{c,w} \cdot \frac{y_1 - t_c - t_{fu}}{2} + \\ F_{t,w} \cdot \frac{h_{tot} - y_1 - t_{fl}}{2} + F_{t,f_l} \cdot \left( h_{tot} - \frac{t_{fl}}{2} - y_1 \right) \end{aligned} \tag{5.3}$$

where,

| | |
|---|---|
| $f_c$ | is the compressive strength of the concrete; |
| $b_c$ | is the width of the effective concrete flange, see section 3.3.1; |
| $y_1$ | is the location of the NA from the top of the concrete; |
| $t_c$ | is the thickness of the effective concrete flange; |
| $A_s$ | is the cross-sectional area of the steel girder; |

$b_{fu}$ is the width of the upper steel flange;
$\sigma_{cm}$ is the distributed compressive stress in the steel;
$t_{fu}$ is the thickness of the upper steel flange;
$\sigma_{tm}$ is the distributed tensile stress in the steel;
$t_w$ is the thickness of the steel web;
$h_w$ is the height of the steel web;
$h_{tot}$ is the total height of the composite beam;
$t_{fl}$ is the thickness of the lower steel flange;
$b_{fl}$ is the width of the lower steel flange;
$h_s$ is the total height of the steel girder.

## 5.3 Evaluation of the tool and the new models

In order to evaluate the tool and the new calculation models, a small study was conducted to see how they performed for different case. This was done by comparing the results for multiple similar beam designs with the location of the neutral axis (NA) in different parts of the beams. Starting with a generated cross-section with the NA in the concrete. Then by increasing the size of the lower steel flange in increments, shifting the NA from the concrete into the steel. The study was done for beams with corrugated web without considering any partial participation of the web. The dimension of the start cross-section, apart for ones for the lower steel flange, and materials used can be seen in Table 5.4. The dimensions of the lower flange, location of the NA, moment capacity and more results gathered from the study can be seen in Table 5.5 and Table 5.6. Table 5.5 covers the beams when the location of the NA moves from the concrete to the upper flange and Table 5.6 when it moves from the upper flange to the web.

**Table 5.4:** *Dimensions and materials for initial generated cross-section for the evaulation of the tool*

| **Geometry** | |
|---|---|
| $b_{fu}$ | 300 mm |
| $t_{fu}$ | 20 mm |
| $t_w$ | 8 mm |
| $h_w$ | 1000 mm |
| $t_c$ | 100 mm |
| $b_c$ | 1980 mm |
| **Materials** | |
| Steel | 1.4162 |
| Concrete | C40/50 |

**Table 5.5:** *Results for when the NA goes from the concrete to the steel flange*

| **Beam** | **1** | **2** | **3** | **4** |
|---|---|---|---|---|
| NA location | Concrete | | Upper flange | |
| $y_1$ [mm] | 96.9 | 99.8 | 101.2 | 102.5 |
| $b_{fl}$ [mm] | 320 | 340 | 360 | 380 |
| $t_{fl}$ [mm] | 20 | 20 | 20 | 20 |
| $A_{fl}$ [$mm^2$] | 6400 | 6800 | 7200 | 7600 |
| $A_{fl}/A_{fl1}$ | 100.0% | 106.3% | 112.5% | 118.8% |
| $M_{pl}$ [kNm] | 3839.9 | 4049.1 | 4261.1 | 4473.4 |
| $M_{pl}/M_{pl1}$ | 100.0% | 105.4% | 111.0% | 116.5% |

**Table 5.6:** *Results for when the NA goes from the steel flange to the steel web*

| **Beam** | **5** | **6** | **7** | **8** | **9** | **10** |
|---|---|---|---|---|---|---|
| NA location | Upper flange | | | Web | | |
| $y_1$ [mm] | 116.8 | 118.7 | 119.7 | 125.1 | 141 | 156 |
| $b_{fl}$ [mm] | 400 | 420 | 430 | 435 | 440 | 445 |
| $t_{fl}$ [mm] | 30 | 30 | 30 | 30 | 30 | 30 |
| $A_{fl}$ [$mm^2$] | 12000 | 12600 | 12900 | 13050 | 13200 | 13350 |
| $A_{fl}/A_{fl1}$ | 187.5% | 196.9% | 201.6% | 203.9% | 206.3% | 208.6% |
| $M_{pl}$ [kNm] | 6805.4 | 7115.3 | 7269.8 | 7327.6 | 7348.7 | 7374.5 |
| $M_{pl}/M_{pl1}$ | 177.2% | 185.3% | 189.3% | 190.8% | 191.4% | 192.0% |

To see the changes and to be able to compare the different cases both the area of the lower flange and the moment capacity was normalised against the values of the initial cross-section. The normalised values for the moment and the area can be seen in Figure 5.7 and 5.8 for when the NA moves into the flange and then into the web.

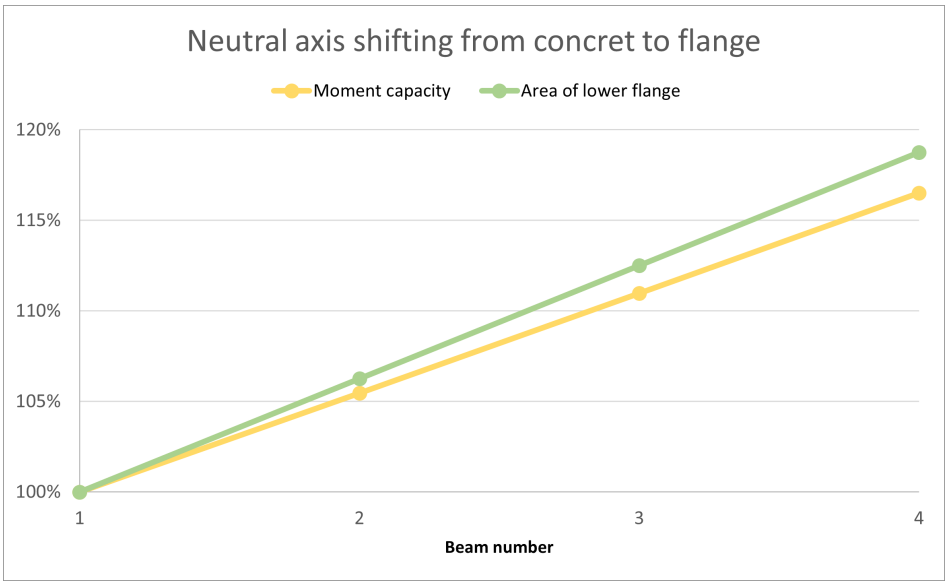


**Figure 5.7:** *Comparison of the change in moment capacity and area of the lower flange for cases when the NA moves from the concrete to the flange*

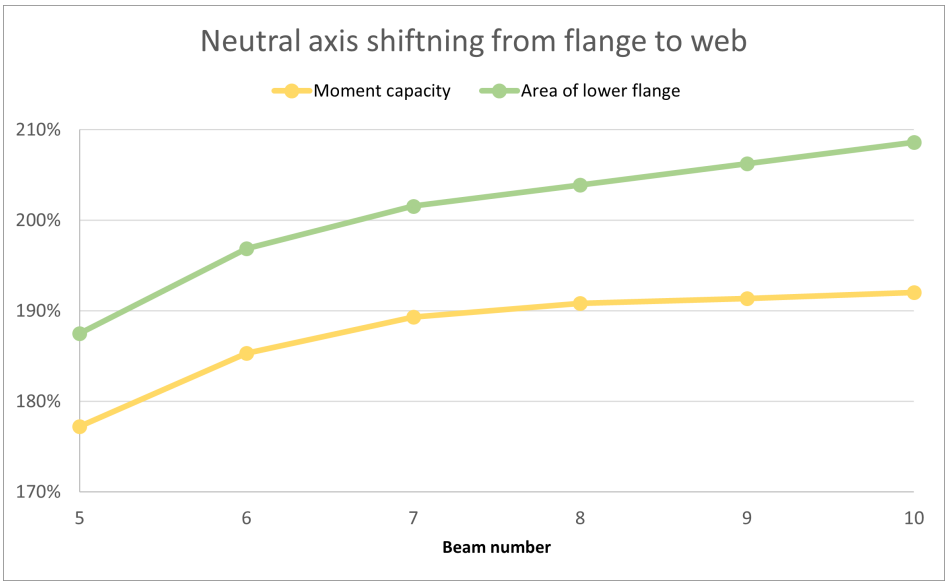


**Figure 5.8:** *Comparison of the change in moment capacity and area of the lower flange for cases when the NA moves from the flange to the web*

The results for all the cases shows that the lower flange area and moment capacity changes in similar way between the different beams. However, it can also be seen that when the area of the lower flange increases the difference in the normalised values for the area and moment capacity increases. This increased difference is expected and comes from the reduced amount of strain hardening as the NA goes deeper into the beam. The results of the study shows that the tool and the new models performs well and is able to work for the different beams with varying location of the NA.

# 6
# Finite element analysis

This chapter presents how the finite element (FE) analysis was created, performed and what results was gathered from the analysis. The FE analysis was performed in the FE software Abaqus. The master's thesis by Ali and Abudaher (2022) investigated how to analyse and model a steel-concrete composite bridge in Abaqus. The same modelling methodology was used in this thesis, with a few slight differences.

## 6.1 Finite element model

This section covers how the model and analysis was built up in the software and how the different parts and materials were modelled.

### 6.1.1 Element types

The model of steel-concrete composite bridge was built as an assembly of the different parts with different properties and element types. The concrete slab was modelled with solid 3D elements (C3D8R) and the structural steel parts, such as the web, flanges, and vertical stiffeners, were modelled with shell elements with reduced integration points (S4R). Examples of the concrete and structural steel elements can be seen in Figure 6.1 and 6.2 respectively.

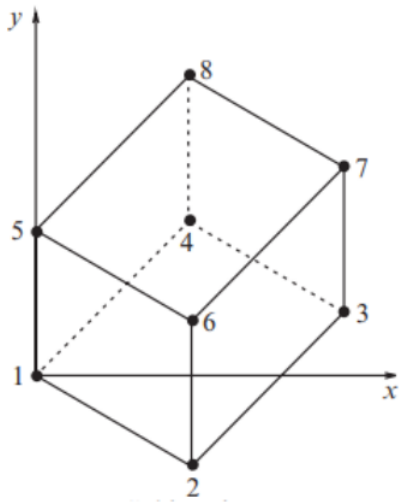


**Figure 6.1:** *Illustration of a solid 3D element (C3D8R)(Ellobody, 2014)*

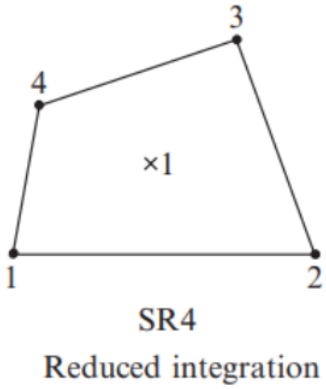


**Figure 6.2:** *Illustration of a shell element with reduced integration points(S4R) (Ellobody, 2014)*

The steel rebars were modelled with truss elements (T3D2) embedded in the concrete slab. An example of a truss element can be seen in in Figure 6.3.

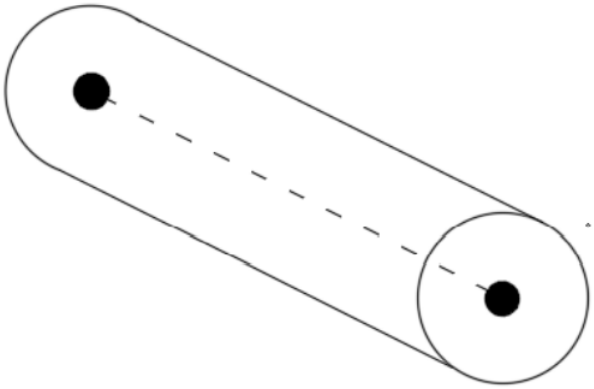

**Figure 6.3:** *Illustration of a truss element (T3D2) (Mendis et al., 2018)*

### 6.1.2 Shear connection in finite analysis

As mentioned in section 2.1.2, the shear connection is crucial for the composite action and the behaviour of the beam. Ali and Abudaher (2022) explains that the connection behaviour of the load-slip can be simulated in finite element by modelling with springs. Rigid springs for the vertical loads and non-linear springs for the longitudinal slip. In a recent study it was shown that the slip behaviour in the shear connection will affect the bending moment capacity and the ductility. However, an increasing degree of shear interaction will eventually lead to a converging moment capacity with a continuing decrease in deflection. Since the moment capacity is the main property studied in this thesis, the shear connection can therefore be modelled as a tie interaction instead of using springs. This will simulate a full interaction connection with no possible slip, resulting in less deflection compared to real test data, but with an unchanged and reliable bending moment capacity (Ali & Abudaher, 2022).

### 6.1.3 Material models

The material used in the FE analysis include concrete, carbon steel and stainless steel. The different materials all need their own material model or models in Abaqus. The material models used in the FE analysis are presented and described in this section.

#### 6.1.3.1 Concrete

The material behaviour of the concrete was modelled using the concrete damage plasticity (CDP) model. The CDP model introduce the non-elastic behaviour of the concrete by combining the isotropic damaged elasticity and the isotropic tensile and compressive plasticity (Hafezolghorani et al., 2017). The uniaxial compressive and tensile response of the concrete introduced in the CDP model can be seen in Figure 6.4 and 6.5 respectively.

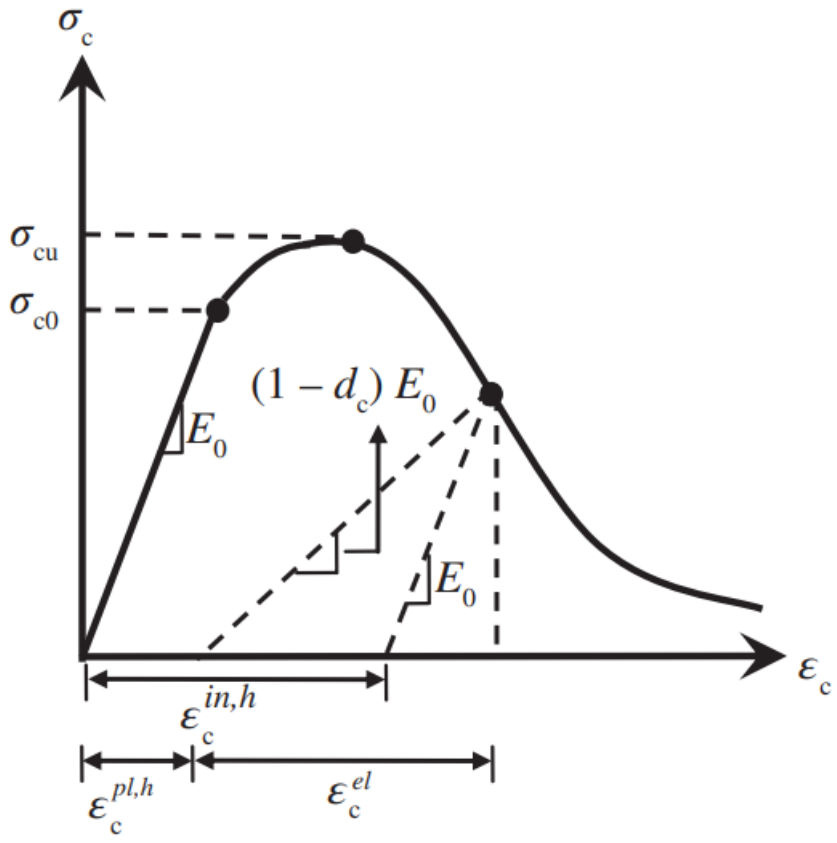


**Figure 6.4:** *Compressive response of the concrete under uniaxial loading for the CDP model (Hafezolghorani et al., 2017)*

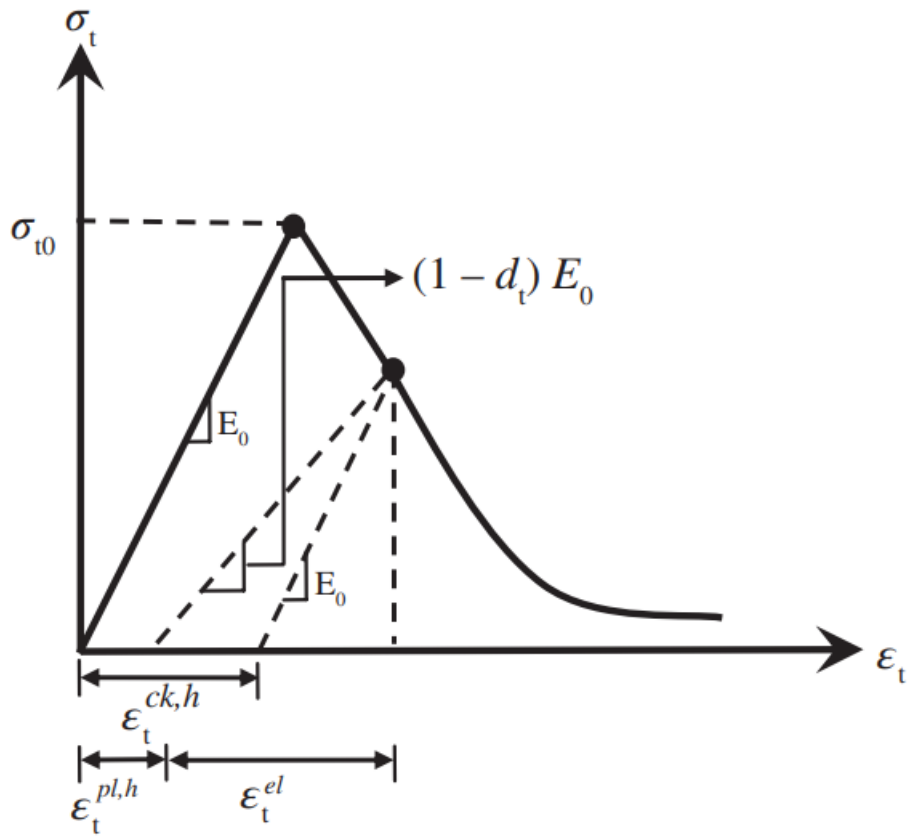


**Figure 6.5:** *Tensile response of the concrete under uniaxial loading for the CDP model (Hafezolghorani et al., 2017)*

The tensile and compressive behaviour is characterised by the reduction in elastic stiffness as the strains get larger. The reduction can be described with the two plasticity variables $d_c$ and $d_t$ for compressive and tensile damage. The two variables $d_c$ and $d_t$ is determined with equation 6.1 and 6.2.

$$d_c = 1 - \frac{\sigma_c}{\sigma_{cu}} \tag{6.1}$$

$$d_t = 1 - \frac{\sigma_t}{\sigma_{t0}} \tag{6.2}$$

where,

| | |
|---|---|
| $\sigma_c$ | is the active compressive stress on the concrete; |
| $\sigma_{cu}$ | is the ultimate compressive capacity of the concrete; |
| $\sigma_t$ | is the active tensile stress on the concrete; |
| $\sigma_{t0}$ | is the ultimate tensile capacity of the concrete. |

The compressive behaviour of the concrete is obtained using the relationship given in SS-EN 1992-1-1 (2005) for non-linear structural analysis, using equation 6.3.

$$\sigma_c = f_{cm} \cdot \frac{k\eta - \eta^2}{1 + (k-2)\eta} \tag{6.3}$$

with,

$$\eta = \frac{\varepsilon_c}{\varepsilon_{c1}} \tag{6.4}$$

$$k = 1.05 \cdot E_{cm} \cdot \frac{|\varepsilon_{c1}|}{f_{cm}} \tag{6.5}$$

where,

| | |
|---|---|
| $\varepsilon_{c1}$ | is the strain at the peak stress according to Table 3.1 in SS-EN 1992-1-1 (2005); |
| $f_{cm}$ | is the mean compressive strength of the concrete. |

In this study only concrete grade C40/50 and a tested concrete type by Zhou et al. (2021) were studied in the case studies and validation. The stress-strain curve for the concrete in compression for the studied concrete grades can be seen in Figure 6.6. All material properties, stresses, strains and damage values are listed in Table C.1 and C.3 in Appendix C.

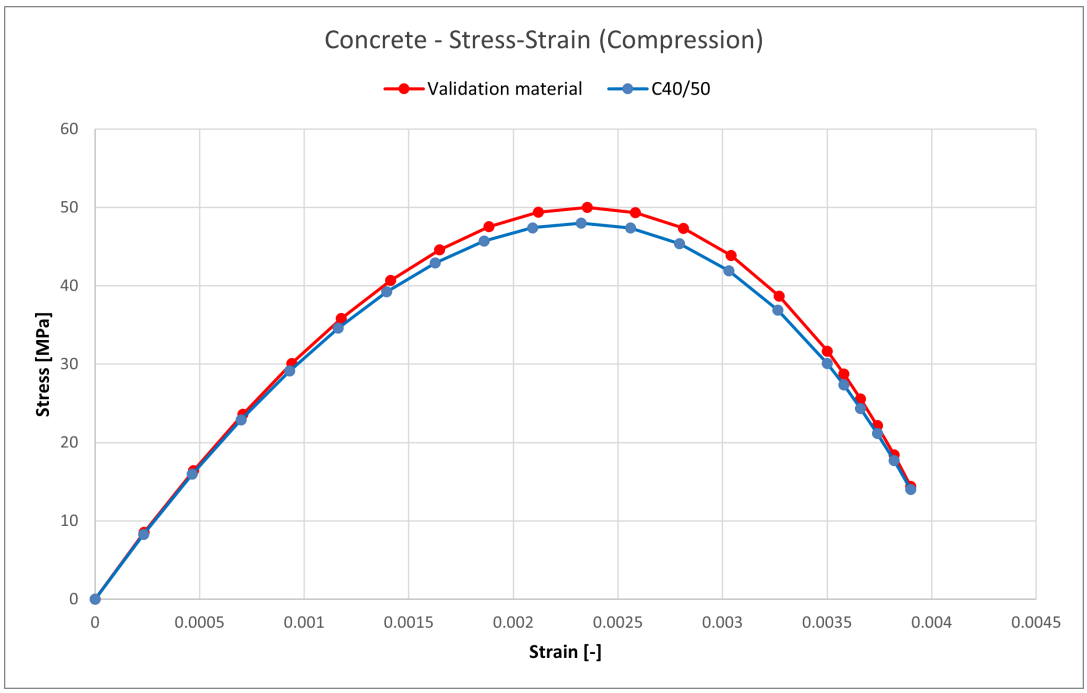


**Figure 6.6:** *Stress-strain curve for studied concrete grades in compression*

The tensile behaviour of the concrete is obtained by using the value of the fracture energy and ultimate tensile strength of the concrete. Using a linear relation the ultimate tensile cracking strain is calculated using equation 6.6.

$$\varepsilon_{su} = \frac{2 \cdot G_F}{f_{ctm}} \cdot \frac{1}{h} \tag{6.6}$$

where,

| | |
|---|---|
| $\varepsilon_{su}$ | is the ultimate tensile cracking strain of the concrete; |
| $G_F$ | is the fracture energy of the concrete; |
| $f_{ctm}$ | is the mean tensile strength of the concrete; |
| $h$ | is the crack band width. |

The stress-strain curve of the concrete in tension for the studied concrete grades can be seen in Figure 6.7. The material properties, stresses, strains and damage values is listed in Table C.2 and C.4 in Appendix C.

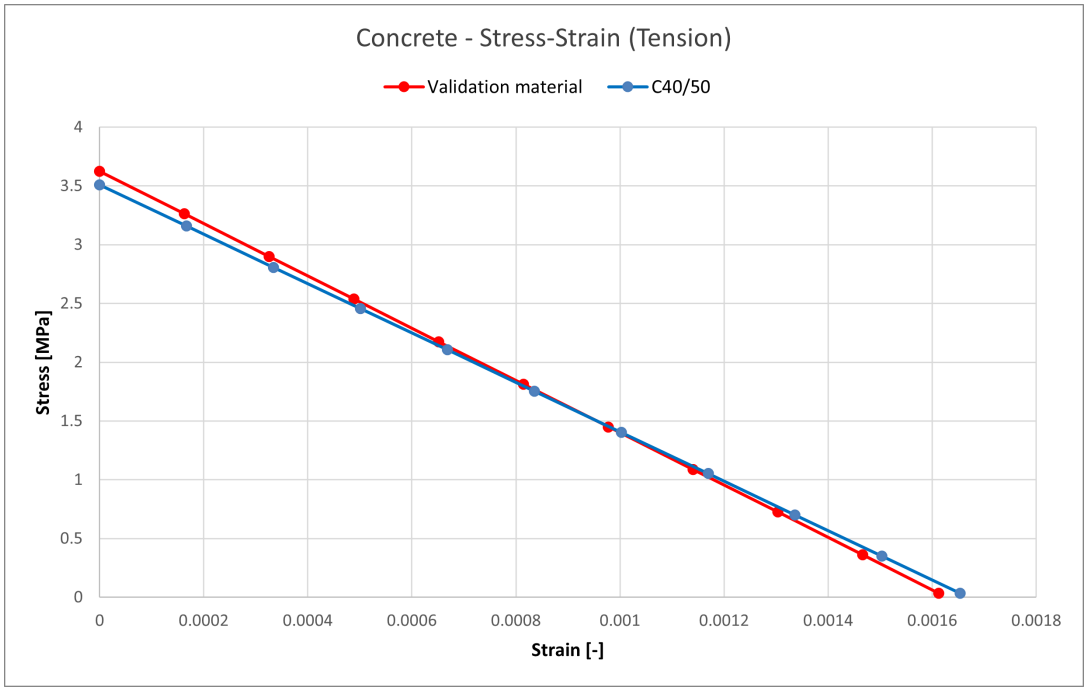


**Figure 6.7:** *Stress-strain curve for studied concrete grades in tension*

Additionally to the tensile and compressive behaviour, the CDP model requires more parameters in order to define the yield surface in the concrete. These parameters are presented in Table 6.1 together with the used values. The implemented values were taken from Jankowiak and Lodygowski (2005), as was done in last year's thesis by Ali and Abudaher (2022).

**Table 6.1:** *Additional parameters used in the CDP model (Jankowiak & Lodygowski, 2005)*

| Dilation angle | Eccentricity | $f_{b0}/f_{c0}$ | k | Viscosity |
|---|---|---|---|---|
| 38 | 1 | 1.12 | 0.667 | 0.003 |

#### 6.1.3.2 Carbon steel

The behaviour of the structural carbon steel and reinforcement was modelled using the bi-linear stress-strain curve given in SS-EN 1993-1-5 (2006). The engineering strains was obtained based on the ultimate and yield strength of the steel according to equation 6.7 and 6.8. Where equation 6.7 is used for stresses up to the yield strength and equation 6.8 is used for stresses between the yield and ultimate strength.

$$\varepsilon = \frac{f_y}{E} \tag{6.7}$$

$$\varepsilon = \frac{f_y}{E} + \frac{f_u - f_y}{\frac{E}{100}} \tag{6.8}$$

where,

| | |
|---|---|
| $\varepsilon$ | is the engineering strain; |
| $f_y$ | is the yield strength of the steel; |
| $f_u$ | is the ultimate strength ; |
| $E$ | is the Young's modulus of the concrete. |

The engineering stress-strain curve was then converted to true stress-strain curves to be input to Abaqus. The true stresses and strains is calculated using equation 6.9 and 6.10 respectively.

$$\sigma_{true} = \sigma \cdot (1 + \varepsilon) \tag{6.9}$$

$$\varepsilon_{true} = ln(1 + \varepsilon) \tag{6.10}$$

The plastic true strain is then calculated using equation 6.11.

$$\varepsilon_{true,pl} = ln(1 + \varepsilon) - \frac{\sigma_{true}}{E} \tag{6.11}$$

In this study structural steel of grade S460 as well as reinforcement of grade B500B were used. The true stress-strain curves for these steels can be seen in Figure 6.8. The material properties and all stress and strain values are listed in Table C.5 - C.5 in Appendix C.

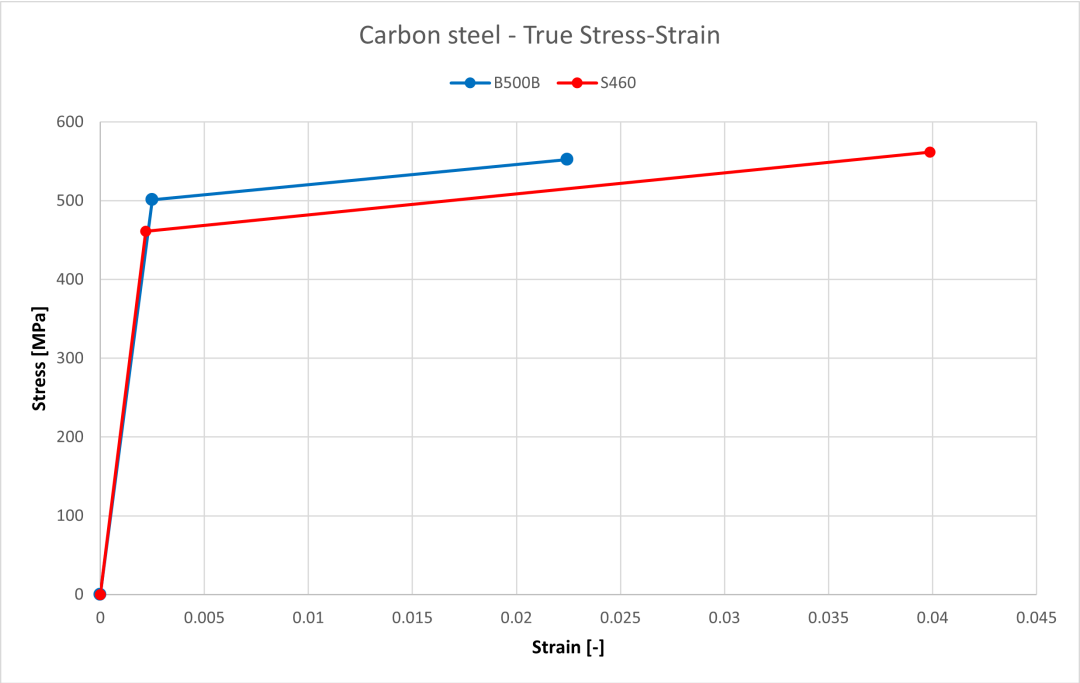


**Figure 6.8:** *True stress-strain curve for studied carbon steels*

#### 6.1.3.3 Stainless steel

To capture and utilize the plastic capacity of stainless steel, the same material model as in the design tool was implemented when computing the engineering material curves for the FE analysis. This calculation method is previously described in section 4.2. Before inputting the material model into Abaqus, the engineering stresses and strains were recalculated to the true stress and strain values. The same equations used for carbon steel are used for the conversion for the stainless steel, see equation 6.9 and 6.10. The plastic strain was determined with equation 6.11 and used to describe the material behaviour in the FE analysis. This study include the stainless steel grade 1.4162 and three tested steels by Zhou et al. (2021), two structural and one reinforcement steel. The true stress-strain curves can be seen in Figure 6.9 and all the material properties, stress and strain values are listed in Table C.7 - C.10 in Appendix C.

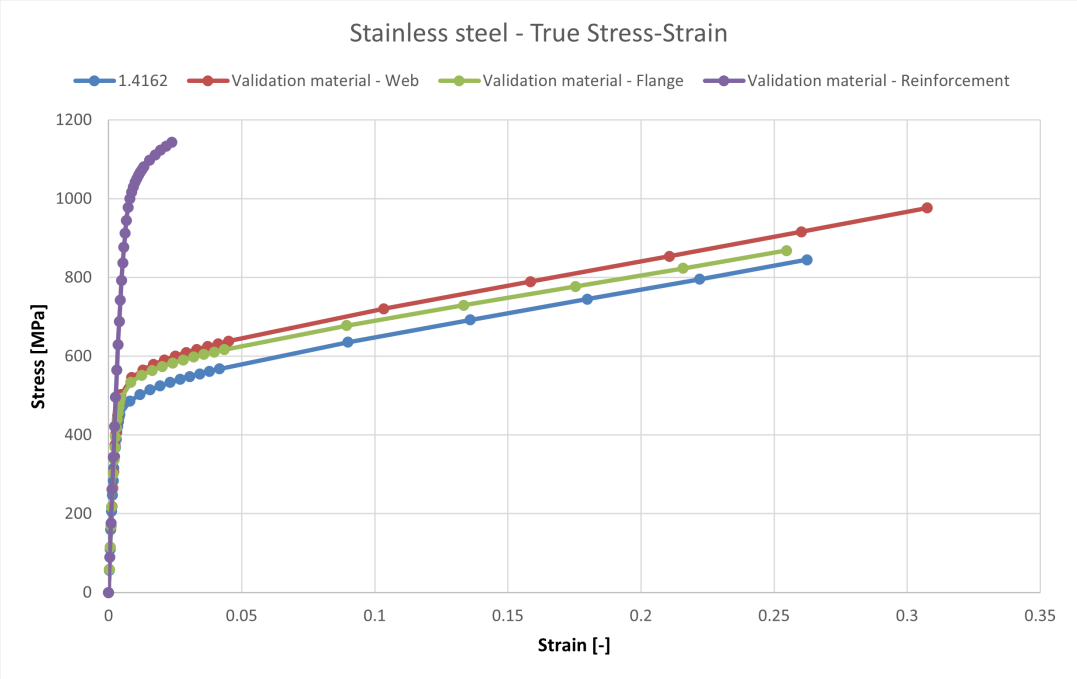


**Figure 6.9:** *True stress-strain curves for studied stainless steels*

### 6.1.4 Modelling in Abaqus

The modelling process in finite element was inspired from the master's thesis by Ali and Abudaher (2022) with some minor differences. The complete beam was parameterized in Grasshopper and the elements was imported as parts into Abaqus. This allowed for a quick and flexible process when running different geometries or implementing changes. The assembly of the elements can be seen in Figure 6.10 where all the thicknesses of the shells are shown. Stiffeners was added to prevent any undesirable buckling failure and to redistribute stresses from the locations with concentrated forces around the supports and the applied loads. For the beams with a flat web, stiffeners were distributed along the beam where shear forces are acting. The geometry of the stiffeners was adapted to be as deep as the upper flange and were extended over the entire web depth, to prevent a unsuitable mesh.

Similarly to Ali and Abudaher (2022), the analysis was performed with the Riks method that successively increase the arc length in increments and simultaneously calculates a solution for the deflection and the load proportionality factor (LPF).

The assembly with boundary conditions and loads can be seen in Figure 6.11 and 6.11. Partitions was used to apply constraints for the beam and also to get a more controlled mesh around locations with higher importance.

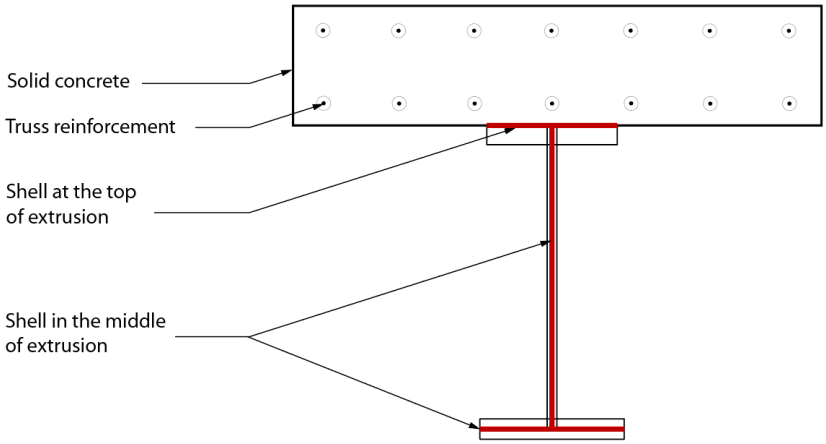


**Figure 6.10:** *Illustration of the assembly of the elements in Abaqus*

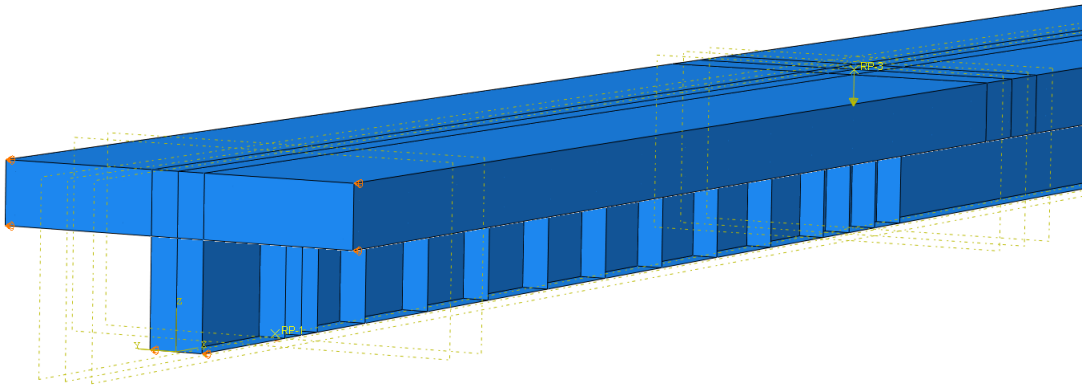

**Figure 6.11:** *Finite model with boundary conditions and loads from Abaqus*

## 6.2 Validation of methodology

The applied FE modelling process was verified by simulating one of the experimental tests performed by Zhou et al. (2021). Compared to other available research, these beams that were tested are the closest to the beams studied in this thesis. The beam specimens, setup and results is previously presented in 4.2.2. The specimen chosen for the finite element verification was CSSB2-SF. It was loaded with a four-point bending setup with studs in the shear connection and the steel girder section was a 180UB18.1 girder with the stainless steel LD2101. Coupon specimen was extracted from the steel elements and tested which gave the following material data in Table 6.2. The concrete strength was assessed by compressing cylinders which resulted in an ultimate capacity of 42 MPa. This value was used as the characteristic compressive capacity and additional needed strength classes was calculated with the analytical relations given in SS-EN 1992-1-1 (2005). The calculated stress-strain curve for each material and the parameters is presented in Appendix C.

**Table 6.2:** *Experimental steel material data (Zhou et al., 2021)*

| Element | E [GPa] | $f_{0.2}$ [MPa] | $f_u$ [MPA] | $\varepsilon_u$ [-] | n [%] | m [%] |
|---|---|---|---|---|---|---|
| Web | 191 | 500 | 718 | 0.36 | 8.01 | 3.44 |
| Flange | 201 | 490 | 673 | 0.29 | 7.08 | 3.55 |
| Reinforcement | 201 | 938 | 1116 | 0.024 | 4.81 | 3.94 |

### 6.2.1 Convergence study

A convergence study was carried out in order to find a mesh that yields satisfactory results with a reasonable computational time. During the study, it was noted that the analysis was extremely sensitive to minor changes to the mesh or the concrete tension properties. The convergence was controlled for the ultimate moment capacity and for the bending moment when the mid deflection was 50mm and 100mm, these results can be seen in Figure 6.12,6.13 and 6.14. Controlling the convergence in both the elastic and plastic moments confirm there is no numerical problems in the analysis for either case. The graphs shows that the model converges at a mesh size of 40mm, coarser meshes than 60 does not result in a wanted behaviour with too large deflections and finer meshes can eventually end up with numerical problems and stop before reaching failure. A similar mesh ratio with regards to the geometry was used for the case study in section 7.1.1.2.

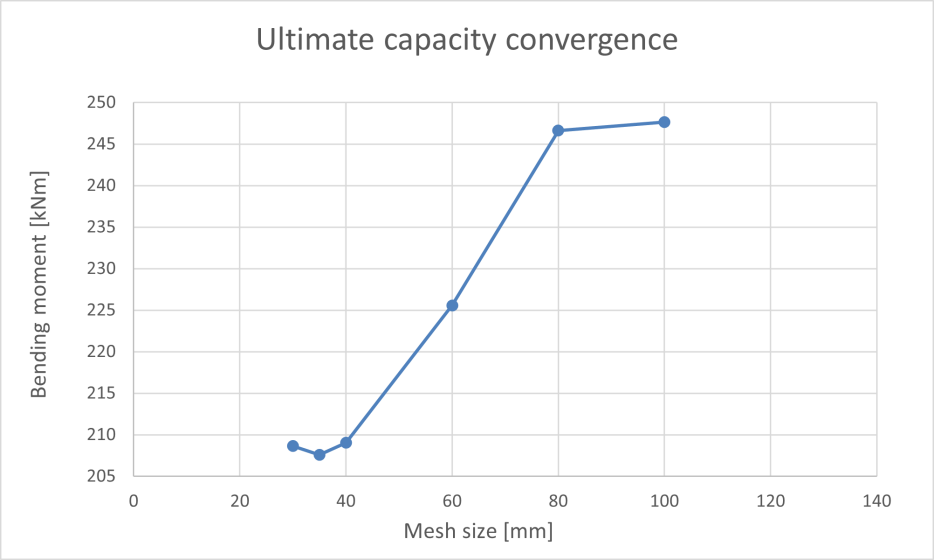


**Figure 6.12:** *Convergence study on ultimate capacity*

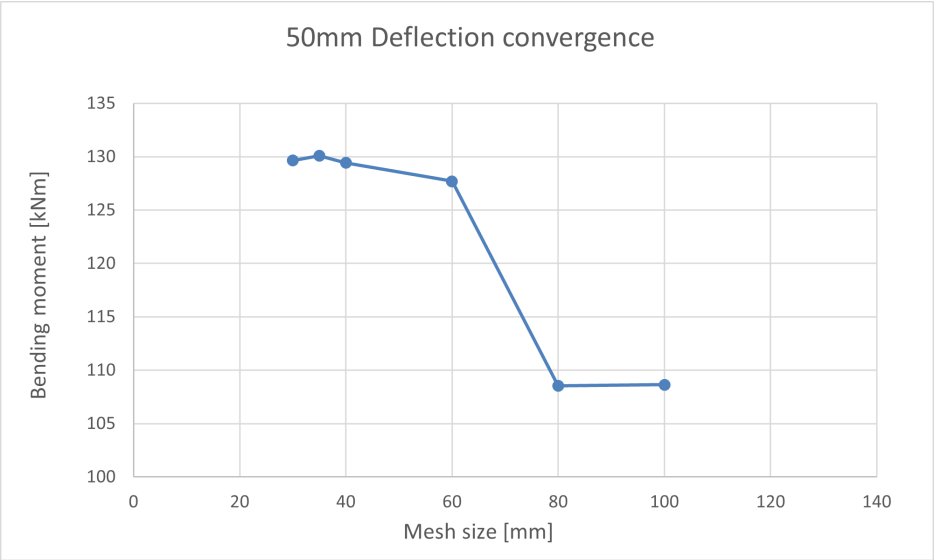


**Figure 6.13:** *Convergence study on moment at 50 mm deflection*

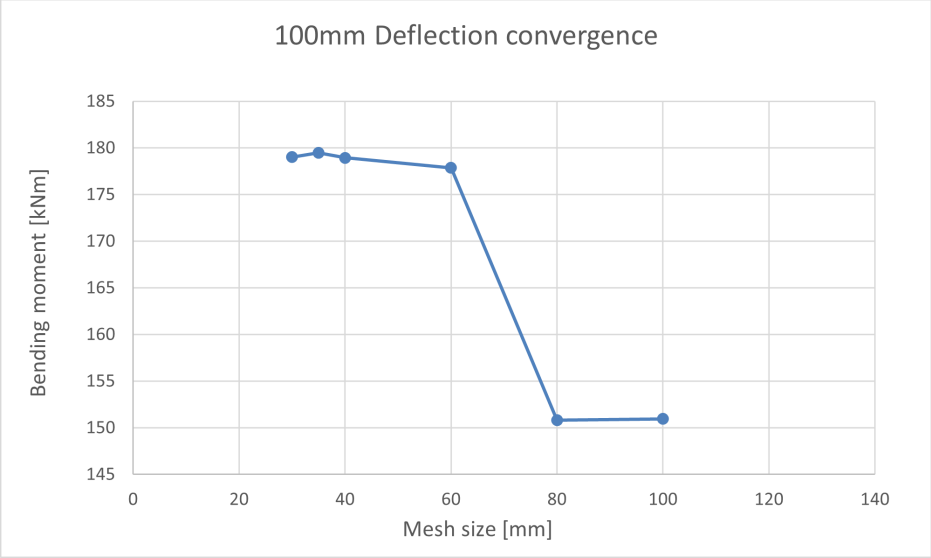


**Figure 6.14:** *Convergence study on moment at 100 mm deflection*

### 6.2.2 Validation results

The resulting behaviour from the FE-analysis with a mesh size of 30 mm can be seen in Figure 6.15. The bending moment capacity from the analysis is 208.6 kNm, a 1.28% difference compared to the experimental test beam produced by Zhou et al. (2021), this is more than acceptable. The deflection is shown to be 19.3% lower for the analysis, 187.2 mm compared to 231.9 mm. This is an expected results as the shear connection is modelled as a tie constraint, which will affect the flexural behaviour and reduce deflections. At the increment of failure, the steel stresses can be seen in Figure 6.16. The steel yielding is evaluated by limiting the stress values to the yield stress of the steel. The majority of the steel girder is yielding and the strain

hardening effect is therefore active. Also, the failure mode is crushing of the concrete, seen in Figure 6.17. The concrete crushing is illustrated by limiting the longitudinal strain to the strain value ultimate compression strength of the concrete. With both the bending moment capacity and the failure mode matching the experimental test, it was concluded that the applied finite modelling procedure was validated.

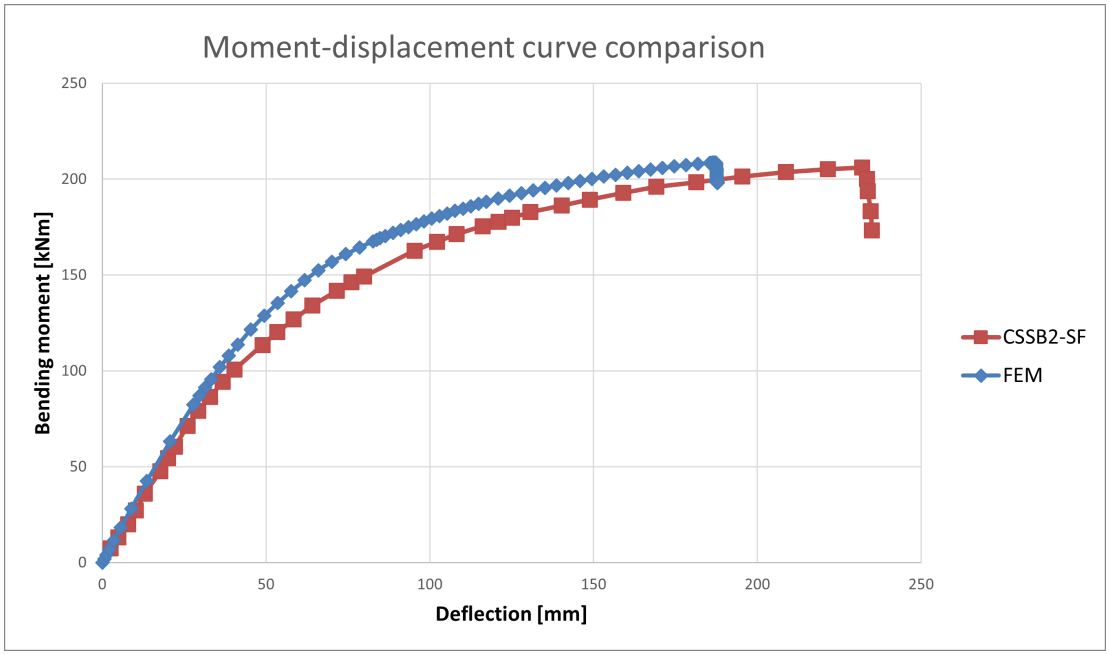


**Figure 6.15:** *Moment-displacement curves for FE simulation and test by Zhou et al. (2021)*

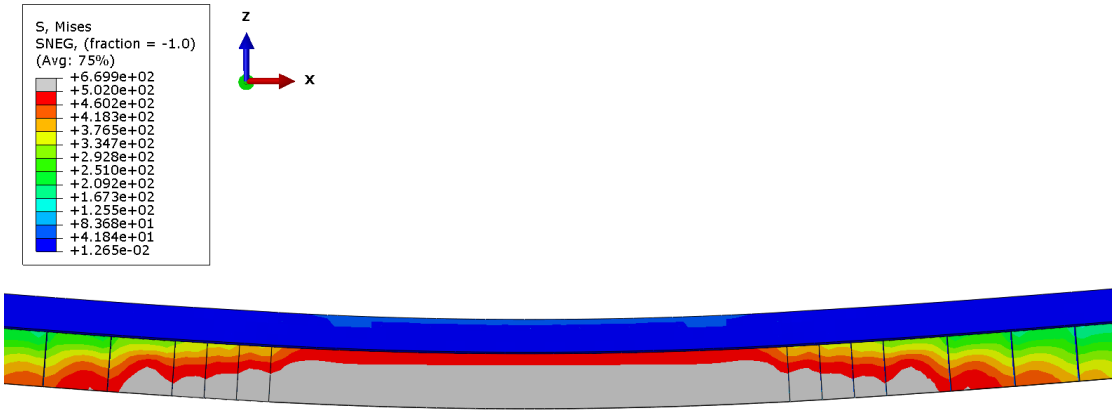


**Figure 6.16:** *Steel yielding during failure from the 30mm mesh size analysis*

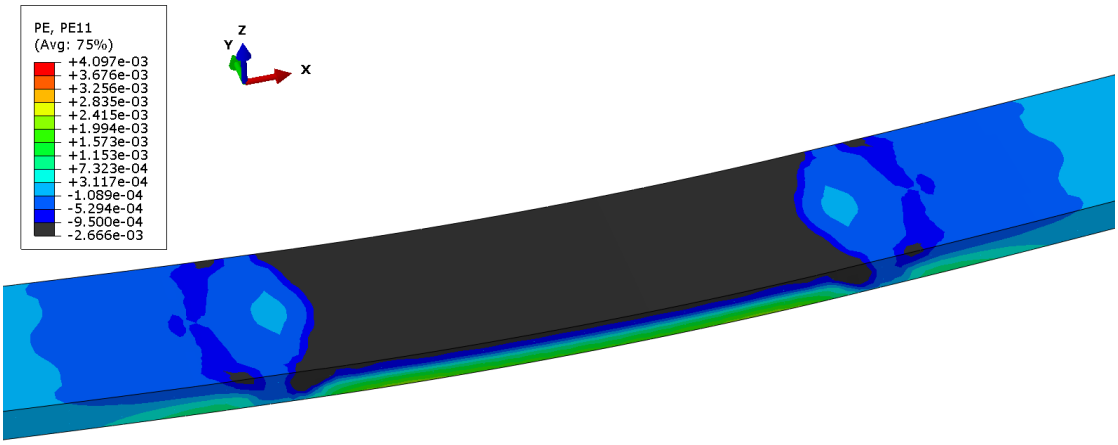


**Figure 6.17:** *Concrete crushing during failure from the 30mm mesh size analysis*

# 7
# Results

This chapter presents the results of case study beams analysed with finite element and comparisons to the performance of the developed design tool. Also, FE-results from previous research and master's thesis were compared to the design tool results for further potential discussions. An additional study is presented comparing the implemented calculation models and how the capacity is affected when changing the web from flat to corrugated.

## 7.1 Ultimate bending moment capacity

As the FE-analysis methodology has been validated to yield satisfactory results, this section shows two studies comparing the design tool ultimate bending moment results to the numerical FE ultimate capacity.

### 7.1.1 Case study

A case study was carried out in order to validate the design tool and prove the effects of strain hardening. The beam designs were first created with the tool and later introduced into FE to validate the results given by the tool.

#### 7.1.1.1 Beam design

The beams used in the study were chosen out of multiple designs generated by using the tool. The designs were all created to have the same bending moment capacity at 10 MNm ± 10 kNm while trying to reduce the amount of steel in the cross-section. Some geometrical limitations were set to prevent unreasonable beam designs. The designs were also created and analysed using the different models and materials in the tool, spanning from cases with corrugated webs and stainless steel while considering strain hardening and partial web contribution to cases with flat webs and and carbon steel while using the EPP calculation model. The materials used and dimensions of the effective concrete flange for the beams can be seen in Table 7.1 and all the designs for the different cases can be seen in Table D.1 - D.4 in Appendix D. The dimensions and types of the beams chosen for the case study in finite element are presented in Table 7.2. The two beams with flat webs share the same dimension and are only separated by the steel type. This was done in order to capture and see the differences between the carbon steel and stainless steel due to strain hardening.

**Table 7.1:** *Common material and geometry data for all case study beams*

| **Steel** | |
|---|---|
| Stainless steel grade | 1.4162 |
| $f_y$ | 450 MPa |
| $f_u$ | 650 MPa |
| Carbon steel grade | S460 |
| $f_y$ | 460 MPa |
| **Concrete** | |
| Grade | C40/50 |
| $t_c$ | 300 mm |
| $b_c$ | 3500 mm |

**Table 7.2:** *Chosen case study beams*

| | **Beam 1** | **Beam 2** | **Beam 3** | **Beam 4** | **Beam 5** |
|---|---|---|---|---|---|
| Web design | Corrugated | Corrugated | Corrugated | Flat | Flat |
| Steel type | Stainless | Stainless | Stainless | Stainless | Carbon |
| $b_{fu}$ [mm] | 300 | 300 | 506 | 300 | 300 |
| $t_{fu}$ [mm] | 12 | 12 | 20 | 12 | 12 |
| $b_{fl}$ [mm] | 496 | 548 | 506 | 300 | 300 |
| $t_{fl}$ [mm] | 20 | 20 | 20 | 12 | 12 |
| $t_w$ [mm] | 7 | 8 | 8 | 12 | 12 |
| $h_w$ [mm] | 1400 | 1200 | 1200 | 1194 | 1194 |
| $\alpha$ [°] | 36 | 36 | 36 | - | - |
| $a_1$ [mm] | 95 | 120 | 120 | - | - |
| $a_3$ [mm] | 55 | 50 | 50 | - | - |
| $A_{\text{steel}}$ | 23320 | 24160 | 29840 | 29840 | 21528 |
| $A_{fl}/A_{\text{steel}}$ | 42.5% | 45.4% | 33.9% | 16.7% | 16.7% |
| $A_w/A_{\text{steel}}$ | 42.0% | 39.7% | 32.2% | 66.6% | 66.6% |

The chosen designs differentiates against each other in a couple of ways, firstly beam 1-3 have corrugated webs while beam 4 and 5 have flat webs. This resulted in a vast difference in how the steel is distributed in the cross-section. Looking at the beams with corrugated webs, the cross-sectional area of the steel web and lower flange make up very similar portions of the total steel area but for the beams with flat webs this is not the case. These beams have a much larger ratio of the steel area in the web and very small flanges.

The plastic bending moment capacity for the chosen beams for the calculation models they were created with can be seen in Table 7.3. As mentioned previously, all beams except beam 5 that is made of carbon steel have a similar moment capacity. All cases also have the neutral axis located in the concrete.

**Table 7.3:** *Plastic bending moment capacity and calculation model used for the chosen beams from the tool*

| Beams | Caclulation model | $M_{pl}$ [kNm] | $t_{w,eff}$ [mm] | $y_1$ [mm] |
|---|---|---|---|---|
| Beam 1 | C-CSM | 9991 | 0 | 63.9 |
| Beam 2 | C-CSM,PW | 10006 | 0.8 | 72.1 |
| Beam 3 | C-CSM,PW | 10001 | 0.8 | 96.4 |
| Beam 4 | F-CSM | 10001 | 12 | 97.7 |
| Beam 5 | F-EPP | 8590 | 12 | 83.2 |

#### 7.1.1.2 Finite element results

The FE results for the case study are presented as the bending moment-displacement curves for all the beams in Figure 7.1 - 7.5, where the curves are compared against the results from the tool for each beam. All the values of bending moment and displacements from the FE analysis for all the runs can be seen in Table E.2 - E.6 in Appendix E.

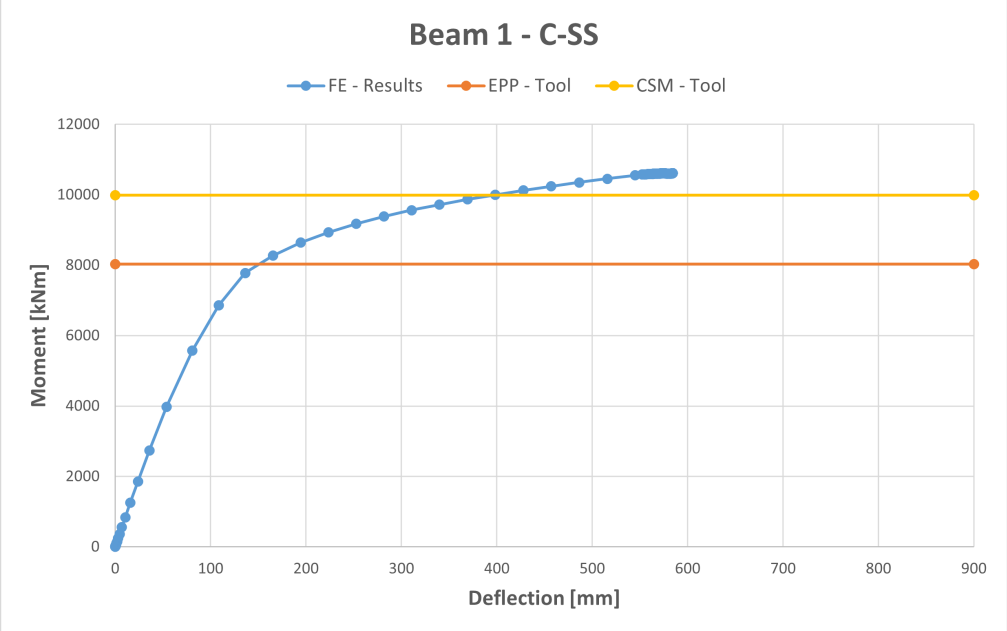


**Figure 7.1:** *Moment-displacement curve from FE-analysis for Beam 1*

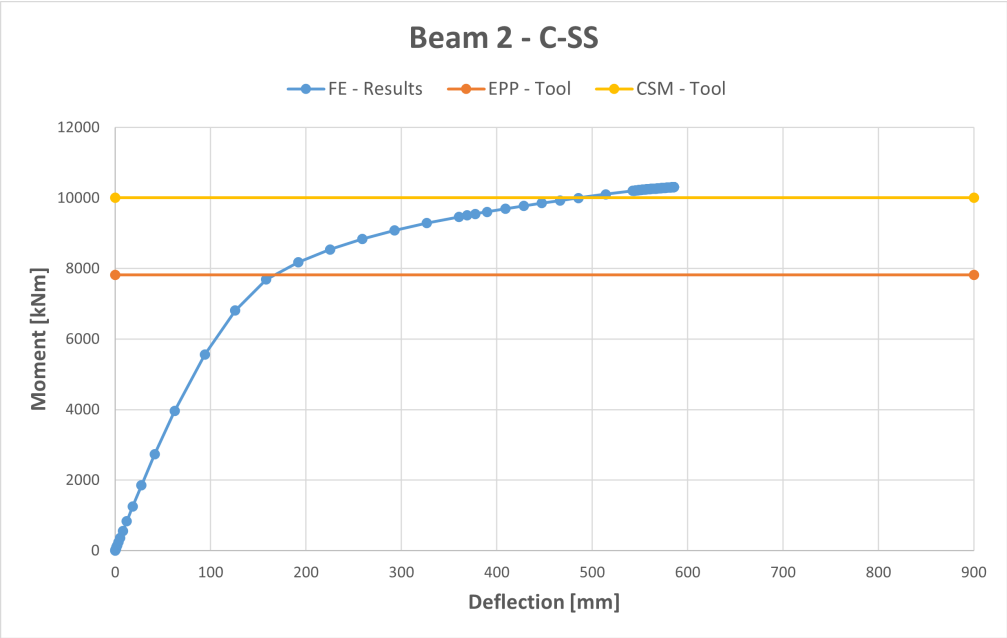


**Figure 7.2:** *Moment-displacement curve from FE-analysis for Beam 2*

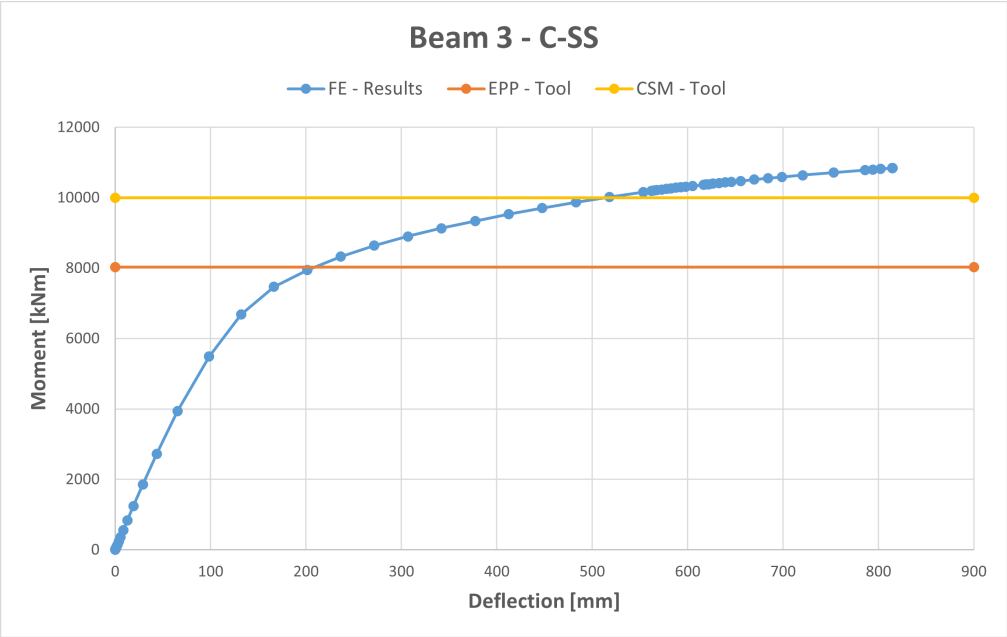


**Figure 7.3:** *Moment-displacement curve from FE-analysis for Beam 3*

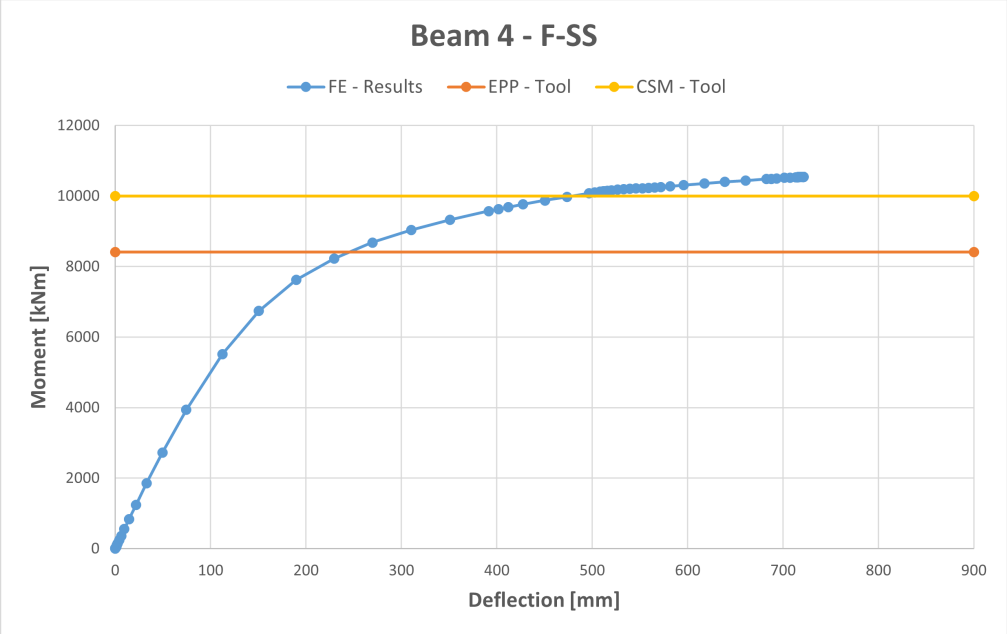


**Figure 7.4:** *Moment-displacement curve from FE-analysis for Beam 4*

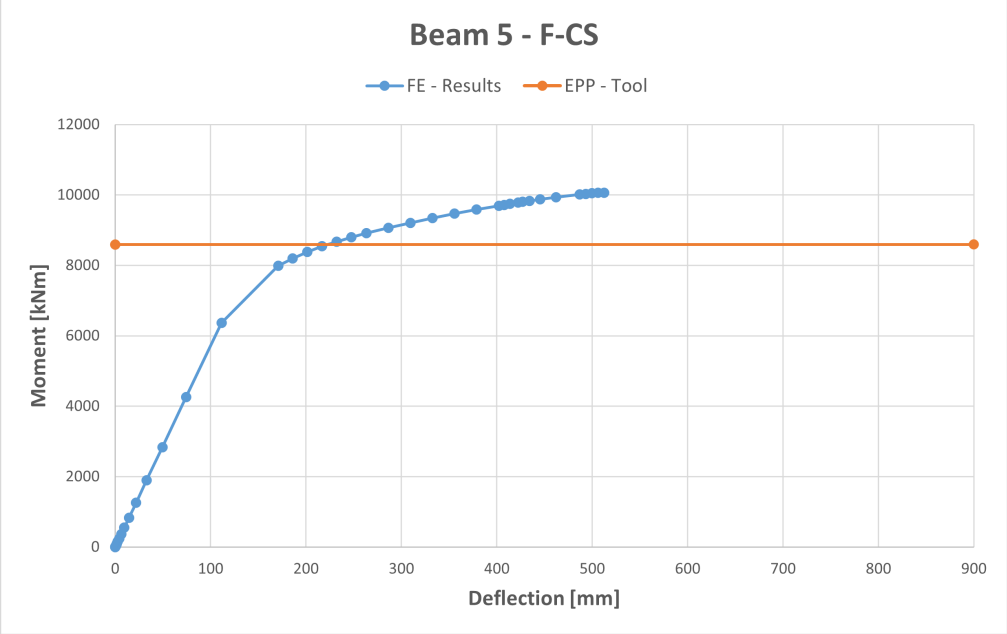


**Figure 7.5:** *Moment-displacement curve from FE-analysis for Beam 5*

The simulations for all the beams exceed the design tool results and with a satisfactory behaviour. The CSM calculation model predicts capacities close to the numerical analysis, but are still on the safe side, which are a great result. However, it should be noted that the moment-displacement curves show no drop at the end. During the case study, numerical problems occurred where the analyses did not run all the way to a capacity drop, it simply stopped. Therefore, it is not possible to conclude that the beam has failed. This could mean that the beams possess higher

capacities than shown from the FE results.

The outputs for beam 3 and beam 4 can be seen below, the deflection is plotted in Figure 7.6 and 7.7. It can be observed that the corrugated beam is more flexible with a higher deflection even though they were designed with the same moment capacity. The von Mises stresses can be seen in Figure 7.8 and 7.9. For beam 3, the stresses in the web are more concentrated in the middle where the beam is subjected to pure bending moment, compared to beam 4. A reason for this is the accordion effect of the corrugated web. The same stresses limited to the true yield stress can be seen in Figure 7.10 and 7.11. The accordion effect has a considerable influence on the yielding of the beams. Both beams are subjected to a similar maximum stress but show a large difference in what parts of the steel that has yielded, and how the strain hardening is activated. The corrugated web stretches with the accordion effect and develop more yielding in the flanges even though the flanges are wider and thicker. While the flat web yield over a larger area and carry a bigger portion of the load. The longitudinal strains in the concrete is shown in Figure 7.12 and 7.13. It can be observed that crushing of the concrete has been initiated at the edge where the load is applied. However, the concrete has significantly less crushing compared to the beam that was used to validated the FEM process in section 6.2.2. This is also a sign that the numerical analysis for the case study beams may not have fully reached its ultimate capacity.

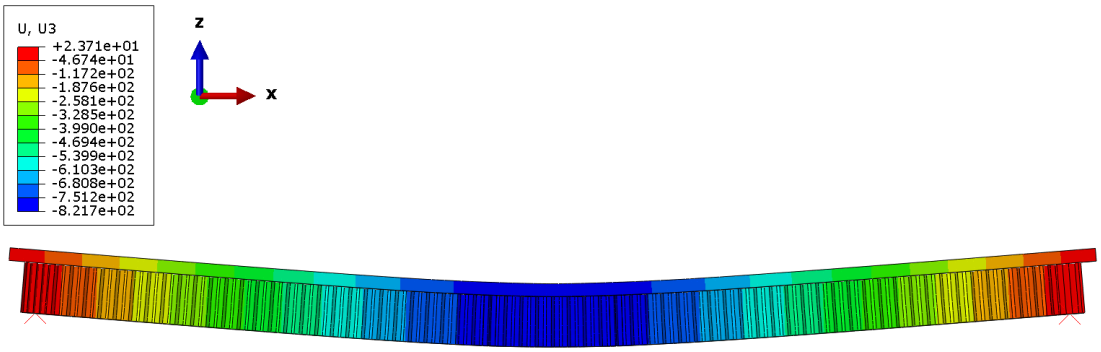


**Figure 7.6:** *Deflection for beam 3*

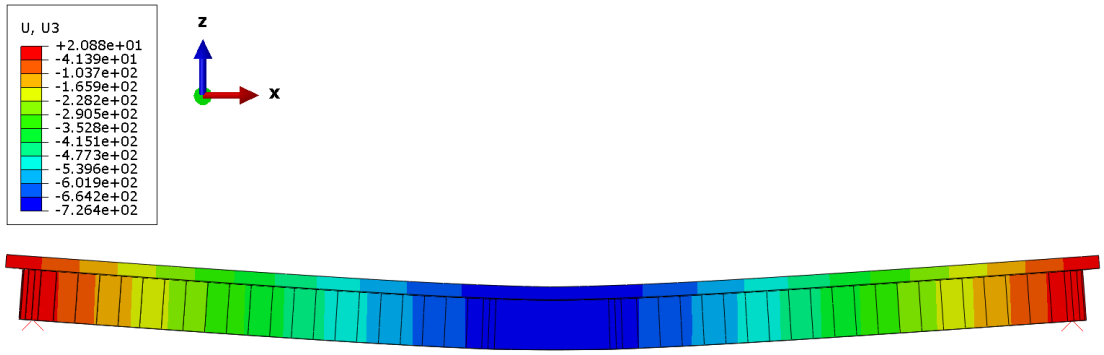


**Figure 7.7:** *Deflection for beam 4*

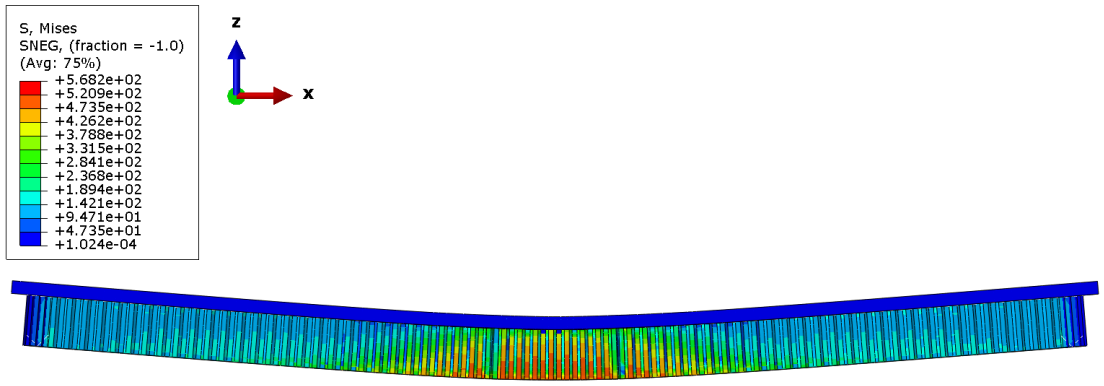


**Figure 7.8:** *Global stress distribution for beam 3*

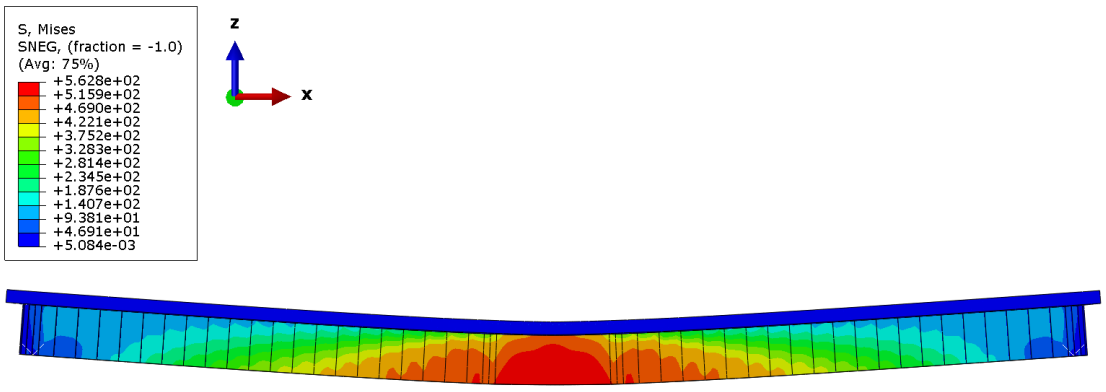


**Figure 7.9:** *Global stress distribution for beam 4*

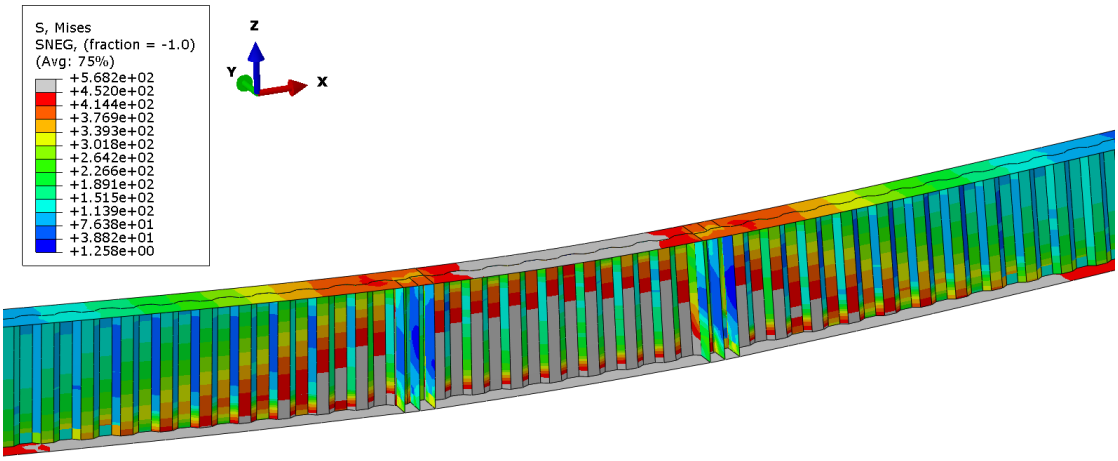


**Figure 7.10:** *Steel yielding for beam 3*

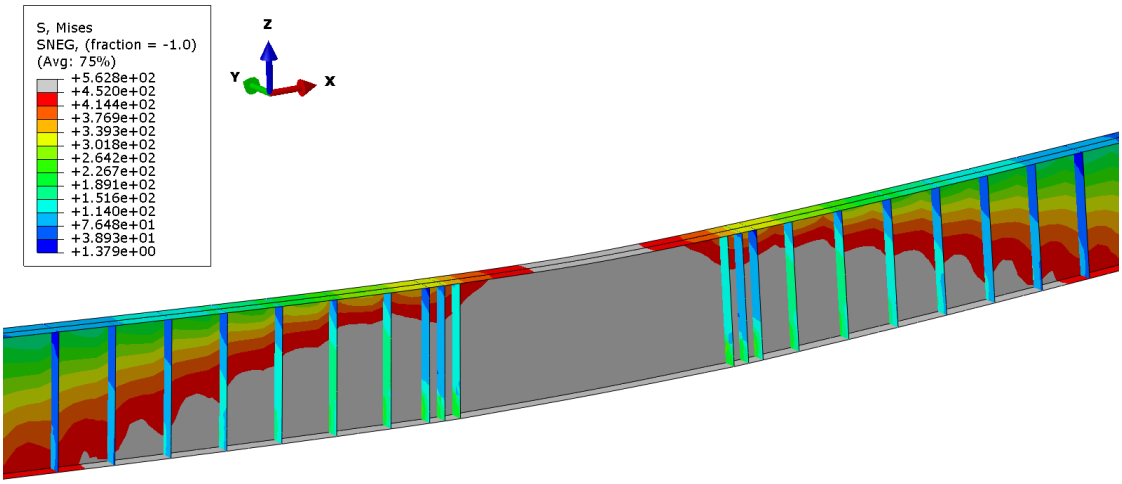


**Figure 7.11:** *Steel yielding for beam 4*

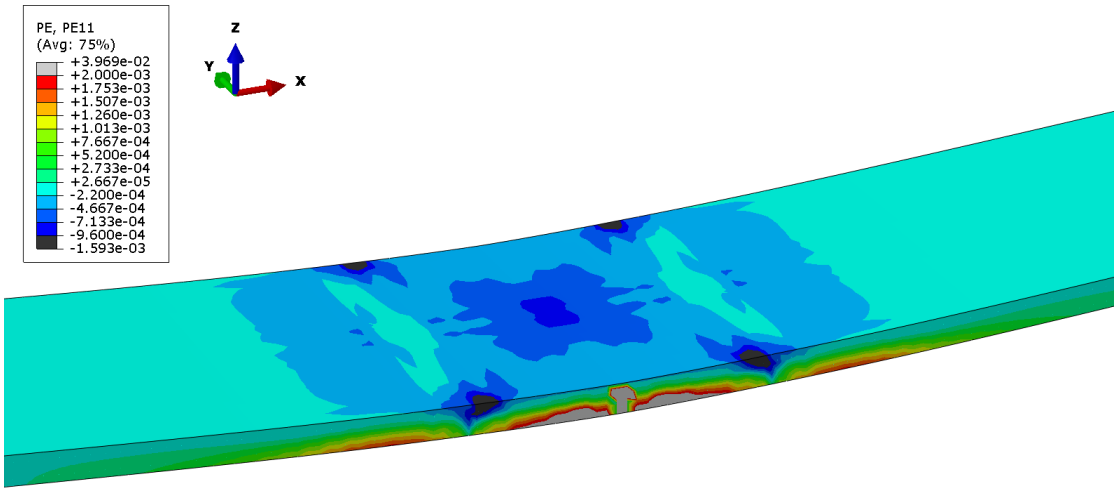


**Figure 7.12:** *Concrete crushing of beam 3*

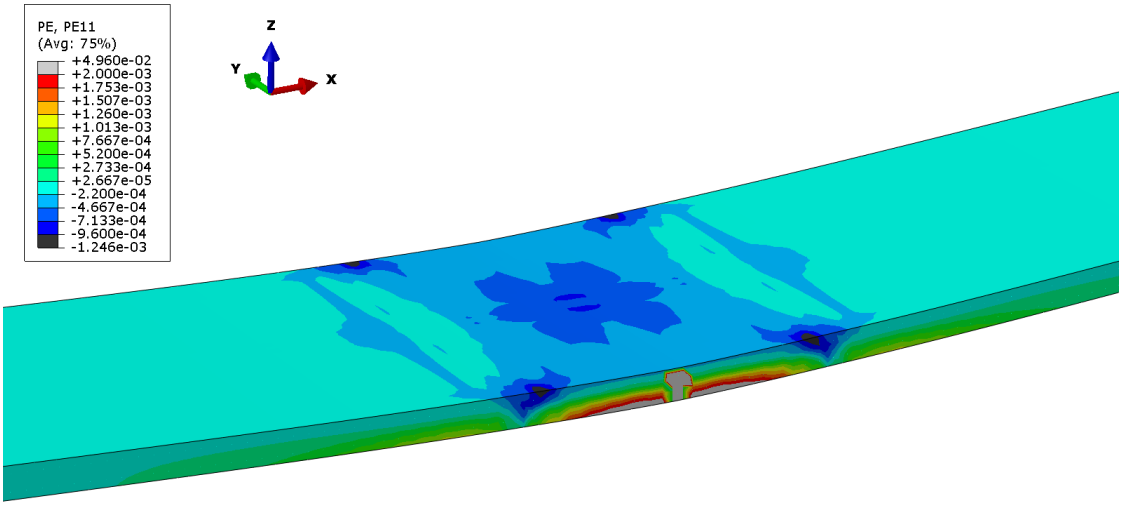


**Figure 7.13:** *Concrete crushing of beam 4*

The ultimate bending moments from the FE analyses are compared to the ones from the tool for the different beams and calculation models, this comparison can be seen in Table 7.4 and Figure 7.14. The results shows that the EPP calculation model gives moment capacities 24.1-25.9% lower than the FE results for the corrugated beams and 14.7-20.2% for the flat beams. The CSM model resulted in bending moments only 5.8-11.4% difference without and 2.9-7.7% with partial web contribution for the cases with corrugated webs. For beam 4, the CSM model is within 5.1% of the simulation results. It can also be observed that for beam 5 made of carbon steel, the results given by the EPP model is also still a bit conservative.

**Table 7.4:** *Comparison of ultimate moment capacity from the tool and FE-analysis*

| | **Beam 1** | **Beam 2** | **Beam 3** | **Beam 4** | **Beam 5** |
|---|---|---|---|---|---|
| $M_u$ [kNm] | 10610 | 10310 | 10841 | 10544 | 10065 |
| $M_{\text{EPP}}$ [kNm] | 8027 | 7822 | 8031 | 8412 | 8590 |
| $M_{\text{EPP}}/M_u$ | 75.7% | 75.9% | 74.1% | 79.8% | 85.3% |
| $M_{\text{CSM}}$ [kNm] | 9991 | 9602 | 9601 | 10001 | - |
| $M_{\text{CSM}}/M_u$ | 94.2% | 93.1% | 88.6% | 94.9% | - |
| $M_{\text{CSM,PW}}$ [kNm] | 9991 | 10006 | 10001 | - | - |
| $M_{\text{CSM,PW}}/M_u$ | 94.2% | 97.1% | 92.3% | - | - |

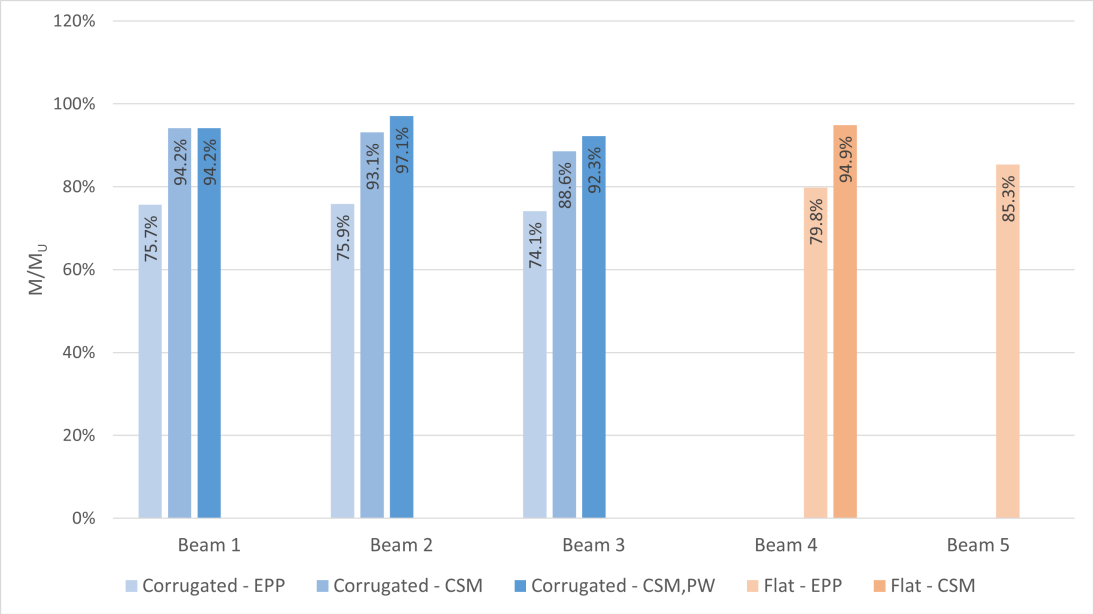


**Figure 7.14:** *Comparison of the moment capacities from the tool and the simulations for the beams in the case study*

### 7.1.2 Additional comparisons of the ultimate moment capacity

In addition to the validation against the FE simulations for the beams in the case study, the design tool results were compared against an experimental test and simulation results from previous research. The compared test result is from the same beam used in the FE method validation, beam specimen CSSB2-SF from Zhou et al. (2021). The other numerical simulation results are from the master's thesis by Ali and Abudaher (2022) that used a similar method of FE modelling as in this thesis. The geometries and materials for all the beams are presented in Table D.5 and D.6 in Appendix D. The ultimate moment capacities for these beams from the test and simulations can be seen in Table 7.5.

**Table 7.5:** *Ultimate bending moment capacity from experimental test by Zhou et al. (2021) and simulations by Ali and Abudaher (2022)*

| **Beams** | $M_u$ [kNm] | **Source** |
|---|---|---|
| CSSB2-SF | 206 | (Zhou et al., 2021) |
| G1-F | 4757.62 | (Ali & Abudaher, 2022) |
| G1-C | 3881.87 | (Ali & Abudaher, 2022) |
| G2-F | 4033.18 | (Ali & Abudaher, 2022) |
| G2-C | 2852.43 | (Ali & Abudaher, 2022) |
| 100-262-1-F | 91273.38 | (Ali & Abudaher, 2022) |
| 100-262-1-C | 72263.22 | (Ali & Abudaher, 2022) |

As for the case study beams, the different beams in this additional study were put into both calculation models in the design tool. The capacity for the beams with flat webs were calculated for both the EPP and CSM model, while the capacity for the corrugated beams also were calculated with and without partial web contribution for the CSM model. The results of the runs in the tool for and comparison against the test and simulation results for the beams with flat webs can be seen in Table 7.6 and in Table 7.7 for the ones with corrugated webs. The comparison of the moment capacities for all beams can also be seen in Figure 7.15.

**Table 7.6:** *Comparison of results from the tool with test and simulation results for the beams with flat webs*

| | **CSSB2-SF** | **G1** | **G2** | **100-262-1-F** |
|---|---|---|---|---|
| $M_u$ [kNm] | 206 | 4757.62 | 4033.18 | 91273.38 |
| | | **EPP** | | |
| $M_{\text{EPP}}$ [kNm] | 173.94 | 4236.75 | 3428.38 | 82989.27 |
| $y_1$ [mm] | 50.67 | 185.18 | 67.4 | 337.87 |
| $M_{\text{EPP}}/M_u$ | 84.4% | 89.1% | 85.0% | 90.9% |
| | | **CSM** | | |
| $M_{\text{CSM}}$ [kNm] | 191.77 | 4693.75 | 3998.54 | 89364.29 |
| $y_1$ [mm] | 55.6 | 196.97 | 79.5 | 521.58 |
| $M_{\text{CSM}}/M_u$ | 93.1% | 98.6% | 99.1% | 97.9% |

**Table 7.7:** *Comparison of results from the tool with test and simulation results for the beams with corrugated webs*

| | **G1** | **G2** | **100-262-1-C** |
|---|---|---|---|
| $M_u$ [kNm] | 3881.87 | 2852.43 | 72263.22 |
| **EPP** | | | |
| $M_{\text{EPP}}$ [kNm] | 3129.25 | 1815.07 | 63689.29 |
| $y_1$ [mm] | 124.14 | 34.59 | 305.53 |
| $M_{\text{EPP}}/M_u$ | 80.4% | 63.6% | 88.1% |
| **CSM** | | | |
| $M_{\text{CSM}}$ [kNm] | 3482.33 | 2225.43 | 71034.42 |
| $y_1$ [mm] | 140.33 | 42.75 | 328.64 |
| $M_{\text{CSM}}/M_u$ | 89.7% | 78.0% | 98.3% |
| **CSM,PW** | | | |
| $M_{\text{CSM,PW}}$ [kNm] | 3482.33 | 2225.43 | 71034.42 |
| $y_1$ [mm] | 140.33 | 42.75 | 328.64 |
| $M_{\text{CSM,PW}}/M_u$ | 89.7% | 78.0% | 98.3% |

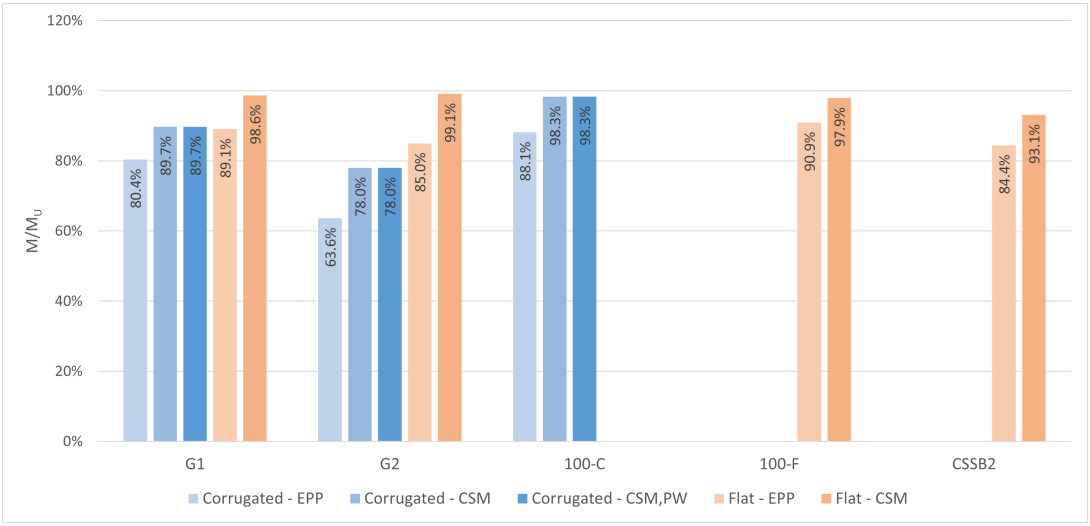


**Figure 7.15:** *Comparison of the moment capacities from the tool and the simulations and test for the beams in the additional validation*

The comparison shows a sublime agreement in the results given from the tool with the CSM model and the results from the tests and simulations for the beams with flat webs. With the biggest difference of 6.9% for beam CSSB2-SF while the others were within 2.1% of the simulation results. This good agreement is shown even as the location of the neutral axis shifts between the concrete and steel for the different beams. A substantial increase in plastic bending moment capacity can also be seen when comparing the results for $M_{\text{EPP}}$ and $M_{\text{CSM}}$, proving the positive effects of strain hardening. The results for the beams with corrugated webs show a much larger spread in the results. The difference in capacity given by the tool with the CSM model and the simulations vary between 1.7 % and 22% for the different

beams. However, all cases do still show a considerable increase in capacity due to strain hardening.

## 7.2 Design tool studies

In addition to the study of the ultimate moment capacity, the tool was used to evaluate the effects of the different calculation models and the influence of the different web types. This was done by using the dimensions of beam 1-4 used in the case study, presented in Table 7.1 and 7.2. The geometries of the beams were analysed with both flat and corrugated webs to create more results for the comparison. The results given by the tool for the geometries for the different web types and calculation models are presented in 7.8.

**Table 7.8:** *Results given by the design tool for different web types and calculation models*

| **Flat web EPP** | | | | | |
|---|---|---|---|---|---|
| **Beams** | $t_{w,eff}$ [mm] | $y_1$ [mm] | $M_{pl}$ [kNm] | $\sigma_m$ [MPa] | $\sigma_{max}$ [MPa] |
| **Beam 1** | 7 | 88.2 | 12183 | 450 | 450 |
| **Beam 2** | 8 | 91.3 | 11446 | 450 | 450 |
| **Beam 3** | 8 | 112.8 | 11596 | 450 | 450 |
| **Beam 4** | 12 | 81.4 | 8412 | 450 | 450 |
| **Flat web CSM** | | | | | |
| **Beam 1** | 7 | 106.1 | 14546 | 541 | 558 |
| **Beam 2** | 8 | 108.8 | 13525 | 536 | 552 |
| **Beam 3** | 8 | 132.5 | 13468 | 529 | 544 |
| **Beam 4** | 12 | 97.7 | 10001 | 540 | 556 |
| **Corrugated web EPP** | | | | | |
| **Beam 1** | 0 | 51.1 | 8027 | 450 | 450 |
| **Beam 2** | 0 | 55 | 7822 | 450 | 450 |
| **Beam 3** | 0 | 76.5 | 8031 | 450 | 450 |
| **Beam 4** | 0 | 27.2 | 2901 | 450 | 450 |
| **Corrugated web CSM** | | | | | |
| **Beam 1** | 0 | 63.9 | 9991 | 563 | 582 |
| **Beam 2** | 0 | 67.9 | 9602 | 555 | 573 |
| **Beam 3** | 0 | 92.3 | 9601 | 543 | 559 |
| **Beam 4** | 0 | 35.4 | 3744 | 585 | 606 |
| **Corrugated web CSM, Partial web contribution** | | | | | |
| **Beam 1** | 0 | 63.9 | 9991 | 563 | 582 |
| **Beam 2** | 0.8 | 72.1 | 10006 | 553 | 570 |
| **Beam 3** | 0.8 | 96.4 | 10001 | 541 | 557 |
| **Beam 4** | 1.2 | 41.8 | 4424 | 577 | 597 |

The results shows how the moment capacity changes between cases for the different beam geometries. The stresses $\sigma_m$ are the stress in the steel that is used for calculat-

ing the moment capacity and $\sigma_{max}$ are the stress at the bottom of the cross-section. The stress values indicates that even if the neutral axis in in the concrete the steel still have a lot of excess capacity, as the case with the highest stress only reaches 606 MPa and the ultimate capacity is 650 MPa. However, the stress values also indicates that all cases in the CSM models show a great level of strain hardening as all of them reaches stresses well over the yield stress of 450 MPa.

### 7.2.1 Calculation model comparison

From the results presented in Table 7.8, a comparison of plastic moment capacities calculated with the EPP and CSM models for flat and corrugated webs was performed. The comparison can be seen in Table 7.9 and Figure 7.16. The results shows that all beams have an increased moment capacity due to the strain hardening. It can also be observed that the capacity increase is larger for the beams when a corrugated web is used and even larger when partial web contribution is considered. Especially large is the increase for beam 4 when strain hardening and partial web contribution is considered.

**Table 7.9:** *Comparison of moment capacity given by the EPP and CSM models for beams with corrugated and flat webs in the tool*

| | **Flat web** | **Corrugated web** | |
|---|---|---|---|
| | $M_{CSM}/M_{EPP}$ | $M_{CSM}/M_{EPP}$ | $M_{CSM,PW}/M_{EPP}$ |
| **Beam 1** | 119.40 % | 124.47 % | 124.47 % |
| **Beam 2** | 118.16 % | 122.76 % | 127.92 % |
| **Beam 3** | 116.14 % | 119.55 % | 124.53 % |
| **Beam 4** | 118.89 % | 129.06 % | 152.50 % |

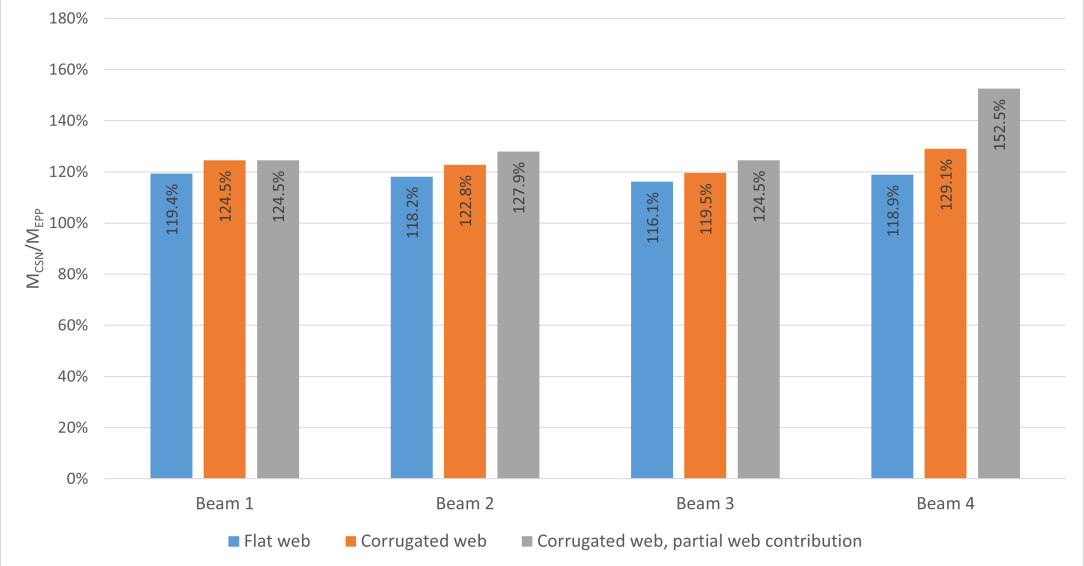


**Figure 7.16:** *Comparison of the moment capacities given by the EPP and CSM calculation models in the tool*

### 7.2.2 Web shape comparison

A comparison of how the moment capacity was affected by different web types was also conducted based on the same results, presented in 7.8. The comparison can be seen in Table 7.10 and Figure 7.17. This comparison shows how the capacity changes if the same dimensions are used for a beam with a corrugated web compared to one with a flat web. Beam 1, 2 and 3 shows a similar reduction of around 25-30% when going from a flat to corrugated web. But beam 4 shows a much greater loss of around 60%.

**Table 7.10:** *Comparison of the results for the different web types*

| | **Beam 1** | **Beam 2** | **Beam 3** | **Beam 4** |
|---|---|---|---|---|
| $M_{F,CSM}$ [kNm] | 14546 | 13525 | 13468 | 10001 |
| $M_{C,CSM}$ [kNm] | 9991 | 9602 | 9601 | 3744 |
| $M_{C,CSM}/M_{F,CSM}$ | 68.7% | 71.0% | 71.3% | 37.4% |
| $M_{C,CSM,PW}$ [kNm] | 9991 | 10006 | 10001 | 4424 |
| $M_{C,CSM,PW}/M_{F,CSM}$ | 68.7% | 74.0% | 74.3% | 44.2% |

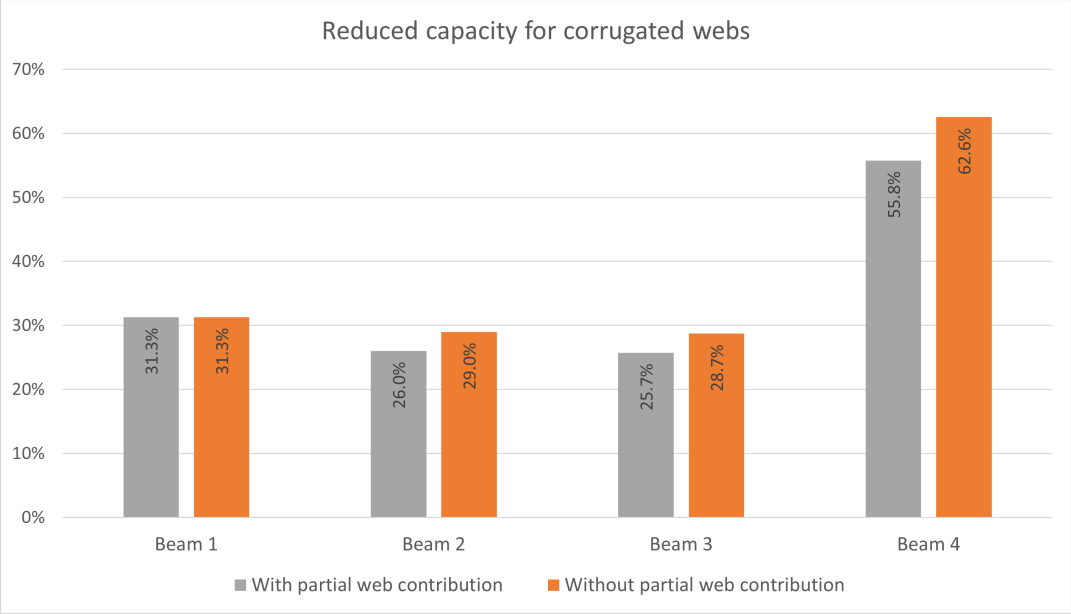


**Figure 7.17:** *Comparison of the reduction in moment capacity when going from a flat to a corrugated web from the tool*

# 8

# Discussion

The discussions, observations and conclusions seen and drawn are all based on the results presented in chapter 5, 6 and 7.

## 8.1 Validation of the tool

Looking at all the results from the tool compared to simulations and tests, both from the case study and the additional validation against previous simulations and test, the tool shows good accuracy.

The comparison of the case study shows that the tool comes within 5.1% of the simulation result for the beam with a flat web for the CSM model. While the EPP model predicts values of 20.2% and 14.7% lower than the simulations for the beam with stainless and carbon steel, respectively. This shows how important the incorporation of strain hardening in the calculation models is, especially when stainless steel is used. For the beams with corrugated webs, the tool is within 11.4% without partial web contribution and 7.6% with partial web contribution for the CSM model. The EPP model is in this case predicting capacities around 25% lower than the simulation results, which is even more inaccurate than for the beams with flat webs. This shows the increased activation of strain hardening with corrugate webs and promising results for the theory of partial web contribution. Both of which are neglected in the EPP model from Eurocode.

Looking at the results of the additional validation, a similar behaviour can be observed. The results for the beams with flat webs are extremely accurate, within 7% for the CSM model while the EPP model gives results 9.1-15.6% lower than the experimental test and simulations. For the beams with corrugated webs, a big discrepancy can be observed for results of the different beams. The tool results are within 1.7% of the simulations for beam 100-262-1 and only 22% for beam G2. The difference might come from the vast variation in design of these two beams. The cross-sectional web area of beam G2 stand for almost 50% of the total steel area, while for beam 100-262-1 this ratio is only around 10%. This will lead to a substantial difference in capacity as the steel area in the web is completely neglected in the tool calculation, as none of the beams in the additional validation reaches the criteria for partial web contribution. The EPP model does in this case also predict conservative results ranging from 11.9% for beam 100-262-1 and 36.4% for beam G2.

Looking at the results for all the beams from both validations, the results are overall good. For the beams with flat webs the CSM is never further than 7% away from the values given by the experimental test and simulations. This lines up well with what previous studies of the model by Shamass and Cashell (2019) and Zhou et al. (2021). These studies have shown the CSM model gives moment capacities within 5% and 7-15% of simulations in the respective studies.

The case study results show an overall slightly better correlation compared to the additional validation, especially for the beams with corrugated webs. One reason for this comes down to the FE simulations and modelling method used in this study. The convergence study and validation of the CSSB2-SF beam shows that the methodology used can give results that agrees with the experimental result and behaviour. This was achieved by introducing the steel into Abaqus with a much lower yield-point than the normal 0.2% prof-strength in order to capture the highly non-linear material behaviour of the stainless-steel. For the case study, the simulations reached and exceeded the results given by the tool to later stop without showing a drop in load. This makes it difficult to tell if the final value given in the simulation is the ultimate moment capacity of the beam or not. But what it shows is that the beams can withstand at least these loads. Some potential reasons for the aborting analyses can be numerical problems in the FE simulations or that the mesh in the steel girder sometimes became distorted due to the corrugated web and vertical stiffeners. It was also observed that the simulation was extremely sensitive to how the concrete in tension was model both for the geometry and the material behaviour. One last thing could be that the beams failed due to a non-expected failure mode, even though the beams were designed, modelled and stiffened to prevent other failure modes than bending failure. While using the CSM in the design tool, the applied stress will be calculated from either a concrete crushing failure at the top or a steel tension failure in the bottom. It should be noted that no other failure mode is taken into account in the design tool. This is why it is important to prevent other possible failure modes in the FE-analysis.

The incorporated plastic calculations in the design tool uses the simplified CSM. This method multiplies the steel height with a factor of 0.6 and finds the stress at that location. This specific stress is applied over the entire steel girder for the bending moment capacity calculation. However, this factor has only previously been verified for beams with flat webs and with the NA in the concrete. As the tool was meant to manage more cases, such as when the NA is located in the steel and beams with corrugated webs. The factor 0.6 was also used for these cases and for the development of the additional calculation models. The tool results with this assumption were promising, however, further studies and validations are needed to confirm this assumption, specially for cases with a corrugated web.

## 8.2 Comparison of different calculation models

The results in Table 7.9 shows how the tool moment capacities change between the EPP model to the CSM model. For all beams, the increase in moment capacity when

considering strain hardening is larger for the cases with corrugated webs than with flat webs. This correlates with the observations found by Ali and Abudaher (2022), that the beams with corrugated webs show a more flexible and ductile behaviour and hence, a greater activation of strain hardening in the steel. It can also be noted that the choice of incorporating partial web contribution leads to an additional increase in moment capacity for the beams where it is applicable. The largest increase is for beam 4, this comes down to the fact that this beam has a thicker web compared to the others and therefore get a bigger increase of the effective web thickness. Beam 4 does also have a deep and slender steel girder, with a deep but thick web and small upper and lower flanges. This will lead to a bigger portion of total capacity coming from the web, so activating a partial thickness of the web will have a great impact on the capacity.

## 8.3 Comparison of results for flat and corrugated webs

The comparison of moment capacity from the tool when going from a flat to a corrugated web with the same dimension, presented in Table 7.10, shows some variation for the different beams. Beam 1, 2 and 3 shows similar reductions in moment capacity, while beam 4 shows much larger decrease. The larger decrease for beam 4 is probably due to the web dimension as discussed earlier. When its deep and thicker web is not, or only partially considered, the beam loses a vast part of its capacity. Regardless, all beams show a decrease around or larger than 25%, which is larger than what Elamary et al. (2017) concluded. This indicates that there might be some inaccuracies in the values predicted by the tool. The model used for the flat webs in the tool is as previously stated well studied and validated and is assumed to give accurate results, which also can be seen in the tool validation in this study. However, the model is not previously assessed for cases with corrugated webs which suggests that this might be where the main part of the difference comes from.

As both the model with and without partial web contribution show larger differences than 10-20% the inaccuracy can come down to two things. It can be either that the criteria for the partial web contribution or the CSM model for corrugated webs is too conservative.

## 8.4 Evaluation of the new calculation models

The evaluation of the new models when the NA is located in the steel presented in section 5.3 show a promising result and a stable behaviour. The cases 1-4 where the NA moves from the concrete to the steel show a good correlation between the increase in moment capacity and increase in area of the lower flange. For cases 5-10, where the NA shifts between the steel flange and web the difference between the increase in flange are and moment capacity is larger. For these beams the steel

area of the lower flange becomes a larger portion of the total steel area in the cross-section, around 50% compared to around 35% for cases 1-5. This leads to the flange becoming more impactful in the overall moment capacity. The NA moving down also limits the moment capacity from the lower flange in two ways, by reducing the distributed steel stress $\sigma_m$ and shortening the lever arm for the lower steel flange. These two observation combined explains the larger difference in the flange area and moment capacity ratios.

## 8.5 Observations when generating the case study beams

During the development of the case study beams, multiple cross-sections were tested for the different calculation models of the tool. The goal was to find good designs reaching the target moment capacity while trying to keep the steel use in the cross-section as low as possible. This procedure resulted in a plethora of tested designs that are presented in Table D.1 - D.4 in Appendix D. During this procedure, a couple of interesting observations regarding how the different types of beams behaved were detected. The first observation was that, in general the beams with flat webs could be altered to use less steel in the cross-section than the beams with corrugated webs. This is however only when the ultimate bending capacity is considered and only based on the steel area in the cross-section. For real designed beams, which are designed for additional phenomenon, comparing to total steel volume might be more interesting. This would make it possible to include the steel in vertical and horizontal stiffeners and the actual length of the corrugated web to capture the true steel consumption.

Another observation was how the final designs of the beams with the different web types differed from each other. The beams with flat webs ended up with small steel flanges and a deep web, as this was the most material efficient design. Without any geometrical limitations, this would mean that the most "optimal" beam according to the design tool would have unrealistically deep web with tiny flanges. For the beams with corrugated webs, this was not the case. The most material efficient designs were found with an equally sized top flange as the ones with flat webs but with a limited web height and instead increasing size of the lower steel flange. This can be due to the fact that the steel in the web itself is not fully considered in the bending moment capacity. After a certain web height, increasing it even further would only lead to a decrease in capacity. The decrease comes from a reduced strain hardening in the bottom flange due to increased stiffness of the cross-section and the location of the neutral axis shifting downwards.

It was also observed that when trying to activate a partial contribution of the corrugated web, the steel area increased. This comes down to the fact that in order to reach the minimum web slenderness criteria, presented in Table 4.2, the web height had to be limited. This limitation in web height led to that the overall performance

and activation of strain hardening was lowered in such a way that the minor increase in web contribution was not beneficial.

The last observation that was found when trying to optimize the activation of strain hardening as much as possible, by making the cross-sections fail due to tensile rapture in the steel. This proved to be particularly difficult to attain due to the vast difference in ultimate strain of the concrete around 0.35% and the stainless steel around 18-45%. In order to attain this behaviour, both extremely small steel flanges and a very thin and deep web had to be used, sizes of which in combination are neither reasonable nor feasible in a real design case. Hence concluding that the highly ductile behaviour of the stainless steel will almost always lead to a failure govern by concrete crushing for steel-concrete composite beams in bending.

## 8.6 Further development and future studies

The results and observation from this thesis are overall satisfactory, but still further development and studies are needed of the models and methods presented and used. As the FE simulations proved to be more unstable and not always performing as wanted. Therefore, it could be good to evaluate the FE procedure further to gain a deeper understanding of the behaviour.

The tool and the incorporated models show a promising behaviour, especially for beams with flat webs. For beams with corrugated webs and for cases when the NA enters the steel girder, more testing is needed to validate or potentially alter the models. The results for the beams with corrugated webs altogether are slightly further away from the simulations results than beams with flat webs. One suggestion is making an alteration to the calculation models, by changing at what location the steel stress value is evaluated. Instead of using a constant of 0.6, the factor could instead be variable. For example, it could be dependent on the location of the NA or geometrical parameters of the corrugation design. One other option is looking over the limits or how the partial web contribution is applied. In this thesis, only three of the seven studied beams with corrugated webs could benefit of partial web contribution. Making the limits slightly less strict or depend on different factors are two suggestions that can be examined. As the results from this thesis show, once the partial web contribution is utilized the results from the tool gets closer to the simulation results.

The models for when the NA is located in the steel established in this thesis have also been put through limited testing. The results from this test were promising, but they do still need further validation and balancing.

In its current state, the tool and the calculation models used in it are intended to be used as a part of ongoing research. However, the long-term goal is to change the models and methods recommended in the Eurocode standards for design. Based on the results and experience gathered during the work with this thesis, some potential

ways on how this can be done are suggested. The positive effects of strain hardening of the stainless steel could be implemented by replacing the EPP model in Eurocode with the CSM models used in this thesis. But only once all the calculation models are fully validated and tested. One other way could be to create an additional factor used for the current EPP model if stainless steel is used. This factor could be dependent on how deep into the beam the NA is located and based on this, either increase or reduce the moment capacity in line with the predicted added capacity due to strain hardening. For corrugated webs, the theory of a partial web contribution thickness has shown promising results and if studied further, this could directly be implemented in the Eurocode standards.

Outside of the scope of this thesis are some topics that might be interesting to investigate further. One could be to implement strain hardening also for the carbon steel. As could be seen in the case study for beam 5, the EPP model was also quite conservative, even when carbon steel was used. It would also be interesting to do full scale experimental testing of stainless steel-concrete beams to see how they behave. As there is a lack of such test results right now.

# 9
# Conclusion

The aim of this master's thesis was to develop a design tool that should be able to determine the ultimate bending capacity of steel-concrete composite bridge beams. It should be able to handle both carbon and stainless steel with flat or corrugated web plates, while considering strain hardening for stainless steel. From the studies and observation in this thesis, the tool is concluded to be able to perform with satisfactory accuracy. The tool and the calculation models do however need some additional testing, balancing and validation for specific designs and cases.

The method of modelling and the simulating in finite element proved to be more difficult and sensitive than expected and could use some further development. However, the results for both ultimate capacity and deflections were still satisfactory for the aim of this study.

The design tool results also show a large impact of including strain hardening for the stainless steel for the ultimate bending capacity. Especially for beams with corrugated webs, due to their increased flexibility with and without considering partial web contribution. Current standards given by Eurocode neglect both the effects of strain hardening and the contribution of the corrugated web plates in bending. By using the models for the continuous strength method and considering a partial web contribution, a more accurate capacity and higher material utilization can be achieved. Therefore, the design models for calculation of the plastic bending moment capacity given by Eurocode needs to be updated, for both stainless steel and beams with corrugated webs.

The designs and resistances studied in this thesis are limited to only the ultimate bending resistance of the beams. More developed designs with consideration of all potential failure modes during all phases from construction to demolition might behave differently. Leading to different observations and results than the ones achieved in this thesis.

# References


Abdella, K. (2006). Inversion of a full-range stress-strain relation for stainless steel alloys. *International Journal of Non-Linear Mechanics*, *41*(3). https://doi.org/10.1016/j.ijnonlinmec.2005.10.002

Afshan, S., & Gardner, L. (2013). The continuous strength method for structural stainless steel design. *Thin-Walled Structures*, *68*. https://doi.org/10.1016/j.tws.2013.02.011

Ali, A., & Abudaher, H. (2022). *Finite element analysis and design models for composite action in stainless steel corrugated web i girders bridges* [Master Thesis, Chalmers University of Technology]. Chalmers. https://odr.chalmers.se/handle/20.500.12380/305750

Elamary, A. S., Saddek, A. B., & Alwetaishi, M. (2017). Effect of corrugated web on flexural capacity of steel beams. *International Journal of Applied Engineering Research*, *12*(4), 470–481. http://www.ripublication.com

Elgaaly, M., & Seshadri, A. (1997). Girders with Corrugated Webs under Partial Compressive Edge Loading. *Journal of Structural Engineering*, *123*(6). https://doi.org/10.1061/(asce)0733-9445(1997)123:6(783)

Ellobody, E. (2014). *Finite Element Analysis and Design of Steel and Steel-Concrete Composite Bridges*. Elsevier. https://doi.org/10.1016/C2013-0-01336-9

Hafezolghorani, M., Hejazi, F., Vaghei, R., Jaafar, M. S. B., & Karimzade, K. (2017). Simplified damage plasticity model for concrete. *Structural Engineering International*, *27*(1). https://doi.org/10.2749/101686616X1081

Hällmark, R. (2020). *Composite bridges: Innovative ways of achieving composite action* [Doctoral Thesis, Luleå University of Technology]. DiVA. http://www.diva-portal.org/smash/record.jsf?pid=diva2%3A1249244&dswid=7363

He, J., Liu, Y., Chen, A., & Yoda, T. (2012). Mechanical behavior and analysis of composite bridges with corrugated steel webs: State-of-the-art. *International Journal of Steel Structures*, *12*(3). https://doi.org/10.1007/s13296-012-3003-9

Inaam, Q., & Upadhyay, A. (2022). Accordion effect in bridge girders with corrugated webs. *Journal of Constructional Steel Research*, *188*. https://doi.org/10.1016/j.jcsr.2021.107040

Jankowiak, T., & Lodygowski, T. (2005). Identification of parameters of concrete damage plasticity constitutive model. *Foundations of civil and environmental ...*, (6).

Karlsson, E. (2018). *Stainless steel bridge girders with corrugated webs* [Master's Thesis, Chalmers University of Technology]. Chalmers. https://odr.chalmers.se/items/24bb8a42-4acc-4e09-b869-5934db9c5eb6

Luo, R., & Edlund, B. (1996). Shear capacity of plate girders with trapezoidally corrugated webs. *Thin-Walled Structures*, *26*(1). https://doi.org/10.1016/0263-8231(96)00006-7

Mendis, A. S., Al-Deen, S., & Ashraf, M. (2018). Flexural shear behaviour of reinforced Crumbed Rubber Concrete beam. *Construction and Building Materials*, *166*. https://doi.org/10.1016/j.conbuildmat.2018.01.150

Moga, C., Guţiu, Ş. I., & Danciu, A. D. (2017). Material Consumption Reduction by Using Steel Girders with Corrugated Webs. *Procedia Engineering*, *181*. https://doi.org/10.1016/j.proeng.2017.02.384

SCI. (2018). *Design manual for structural stainless steel* (4 th).

Shamass, R., & Cashell, K. A. (2019). Analysis of stainless steel-concrete composite beams. *Journal of Constructional Steel Research*, *152*. https://doi.org/10.1016/j.jcsr.2018.05.032

SS-EN 10088-2. (2019). *Stainless steels - Part 2: Technical delivery conditions for sheet/plate and strip of corrosion resisting steels for general purposes*. SIS. https://www.sis.se/en/produkter/metallurgy/ferrous-metals/steels/ssen1008822014/

SS-EN 1990. (2002). *Eurocode - Basis of structural design*. SIS. https://www.sis.se/en/produkter/construction-materials-and-building/construction-industry/technical-aspects/ssen19902/

SS-EN 1992-1-1. (2005). *Eurocode 2: Design of concrete structures - Part 1-1: General rules and rules for buildings*. SIS. https://www.sis.se/en/produkter/construction-materials-and-building/construction-industry/technical-aspects/ssen1992112005a12014/

SS-EN 1992-2. (2005). *Eurocode 2: Design of concrete structures - Part 2: Concrete bridges - Design and detailing rules*. SIS. https://www.sis.se/en/produkter/construction-materials-and-building/construction-industry/technical-aspects/ssen199222005/

SS-EN 1993-1-1. (2022). *Eurocode 3 - Design of steel structures - Part 1-1: General rules and rules for buildings*. SIS. https://www.sis.se/en/produkter/construction-materials-and-building/structures-of-buildings/metal-structures/SS-EN-1993-1-12022/

SS-EN 1993-1-4. (2006). *Eurocode 3: Design of steel structures - Part 1-4: General rules - Supplementary rules for stainless steels*. SIS. https://www.sis.se/en/produkter/construction-materials-and-building/construction-industry/technical-aspects/ssen19931420062/

SS-EN 1993-1-4 A1. (2015). *Eurocode 3: Design of steel structures - Part 1-4: General rules - Supplementary rules for stainless steels* [Incorporating amendments June 2015]. SIS. https://www.sis.se/en/produkter/construction-materials-and-building/construction-industry/technical-aspects/ssen1993142006a12015/

SS-EN 1993-1-5. (2006). *Eurocode 3 - Design of steel structures - Part 1-5: Plated structural elements*. SIS. https://www.sis.se/en/produkter/construction-materials-and-building/construction-industry/technical-aspects/ssen19931520062/

SS-EN 1993-1-8. (2005). *Eurocode 3: Design of steel structures - Part 1-8: Design of joints*. SIS. https://www.sis.se/en/produkter/construction-materials-and-building/construction-industry/technical-aspects/ssen19931820052/

SS-EN 1994-2. (2005). *Eurocode 4 - Design of composite steel and concrete structures - Part 2: General rules and rules for bridges*. SIS. https://www.sis.se/en/produkter/construction-materials-and-building/construction-industry/technical-aspects/ssen199422005/

SS-EN ISO 3506-1. (2020). *Fasteners - Mechanical properties of corrosion-resistant stainless steel fasteners - Part 1: Bolts, screws and studs with specified grades and property classes*. SIS. https://www.sis.se/en/produkter/mechanical-systems-and-components-for-general-use/fasteners/bolts-screws-studs/ss-en-iso-3506-12020/

Steffner, J., & Öman, M. (2021). *Design of continuous composite road bridges* [Master Thesis, Chalmers University of Technology]. Chalmers. https://odr.chalmers.se/items/9f58d30d-0b60-49a4-848e-8dd3b6a89544

TRVINFRA-00227. (2022). *Bro och broliknande konstruktioner, Byggnad* [Version 3.0]. Trafikverket. https://puben.trafikverket.se/dpub/visa-dokument/ba27c7be-7cc4-486d-b13b-aae7e36571e5

TSFS 2018:57. (2018). *Transportstyrelsens föreskrifter och allmänna råd om tillämpning av eurokoder*. Transportstyrelsen. https://www.transportstyrelsen.se/TSFS/TSFS%202018_57.pdf

Vayas, I., & Iliopoulos, A. (2013). *Design of Steel-Concrete Composite Bridges to Eurocodes*. https://doi.org/10.1201/b15690

Zhou, Y., Uy, B., Wang, J., Li, D., Huang, Z., & Liu, X. (2021). Behaviour and design of stainless steel-concrete composite beams. *Journal of Constructional Steel Research*, *185*. https://doi.org/10.1016/j.jcsr.2021.106863

# A

# Eurocode cross-section classification

## A.1 Carbon steel

Limits and checks for cross-section classification for carbon steel according to SS-EN 1993-1-1 (2022) can be seen in Figure A.1 and A.2.

**Table A.1:** *Cross-section classification for internal compression component in carbon steel SS-EN 1993-1-1 (2022) Table 7.3*

| **Internal compression parts** | | | |
|---|---|---|---|
| 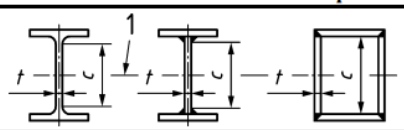 | | 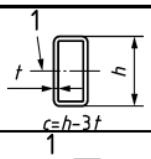 | |
| 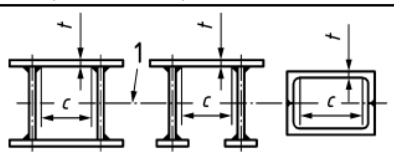 | | 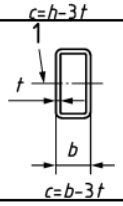 | |
| **Key**<br>1 Axis of bending | | | |
| | Part subject to bending | Part subject to compression | Part subject to bending and axial force |
| Stress distribution in parts (compression positive) | 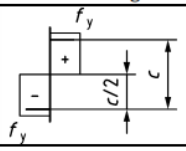 | 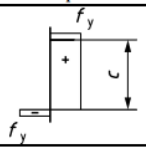 | 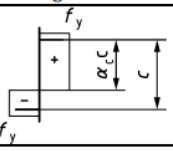 |
| Class 1 | $c/t \le 72\,\varepsilon$ | $c/t \le 28\,\varepsilon$ | $when\,\alpha_c > 0{,}5 : c/t \le \frac{126\,\varepsilon}{5{,}5\,\alpha_c - 1}$<br>$when\,\alpha_c \le 0{,}5 : c/t \le \frac{36\,\varepsilon}{\alpha_c}$ |
| Class 2 | $c/t \le 83\,\varepsilon$ | $c/t \le 34\,\varepsilon$ | $when\,\alpha_c > 0{,}5 : c/t \le \frac{188\,\varepsilon}{6{,}53\,\alpha_c - 1}$<br>$when\,\alpha_c \le 0{,}5 : c/t \le \frac{41{,}5\,\varepsilon}{\alpha_c}$ |
| Stress distribution in parts (compression positive) | 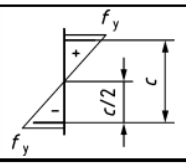 | 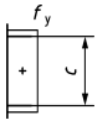 | 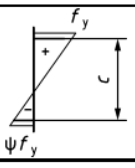 |

| | | | |
|---|---|---|---|
| Class 3 | $c/t \le 121\,\varepsilon$ | $c/t \le 38\,\varepsilon$ | when $\psi > -1$ : $c/t \le \dfrac{38\,\varepsilon}{0{,}608 + 0{,}343\,\psi + 0{,}049\,\psi^2}$<br>when $\psi \le -1$ [a] : $\dfrac{c}{t} \le 60{,}5\,\varepsilon\,(1-\psi)$ |
| For I or H sections with equal flanges, under axial force and bending moment about the main axis parallel to the flanges, the parameter $\alpha_c$ that defines the position of the plastic neutral axis may be calculated as follows:<br>If $N_{Ed} \ge c\,t_w f_y$ $\alpha_c = 1{,}0$<br>If $N_{Ed} \le -c\,t_w f_y$ $\alpha_c = 0$<br>In other cases: $\alpha_c = 0{,}5\left(1 + \dfrac{N_{Ed}}{c\,t_w\,f_y}\right)$<br>where $N_{Ed}$ is the design axial force taken as positive for compression and negative for tension. | | | |
| [a] $\psi \le -1$ and a compression stress of $\sigma_{com,Ed} = f_y$ applies where the tensile strain $\varepsilon_t > f_y/E$ | | | |

**Table A.2:** *Cross-section classification for external compression component in carbon steel SS-EN 1993-1-1 (2022) Table 7.4*

| **Outstand flanges** | | | |
|---|---|---|---|
| 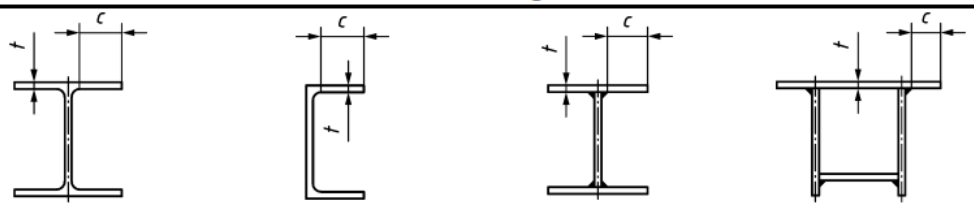 <br>Rolled sections | | Welded sections | |
| | Part in pure compression | Part subject to bending and axial force | |
| Stress distribution in parts (compression positive) | 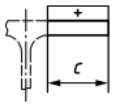 | 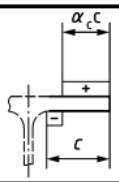 | 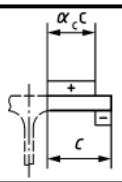 |
| Class 1 | $c/t \le 9\,\varepsilon$ | $c/t \le \dfrac{9\varepsilon}{\alpha_c}$ | $c/t \le \dfrac{9\varepsilon}{\alpha_c\sqrt{\alpha_c}}$ |
| Class 2 | $c/t \le 10\,\varepsilon$ | $c/t \le \dfrac{10\varepsilon}{\alpha_c}$ | $c/t \le \dfrac{10\varepsilon}{\alpha_c\sqrt{\alpha_c}}$ |
| Stress distribution in parts (compression positive) | 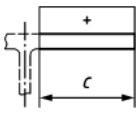 | 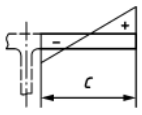 | 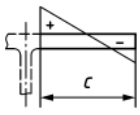 |
| Class 3 | $c/t \le 14\,\varepsilon$ | $c/t \le 21\,\varepsilon\sqrt{k_\sigma}$<br>For $k_\sigma$ see EN 1993-1-5 | |

## A.2 Stainless steel

Limits and checks for cross-section classification for stainless steel according to SS-EN 1993-1-4 (2006) can be seen in Figure A.3 and A.4 and updated limits according

to SS-EN 1993-1-4 A1 (2015) can be seen in Figure A.5 and A.5.

**Table A.3:** *Cross-section classification for internal compression component in stainless steel SS-EN 1993-1-4 (2006) Table 5.2*

**Internal compression parts**

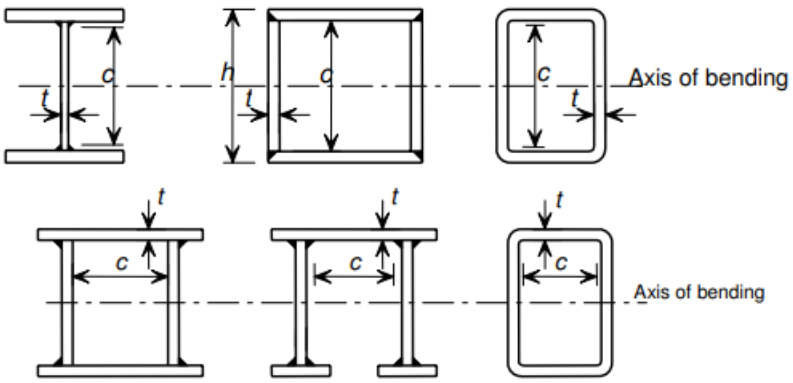


| Class | Part subject to bending | Part subject to compression | Part subject to bending and compression |
|---|---|---|---|
| Stress distribution in parts (compression positive) | 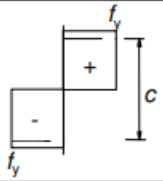 | 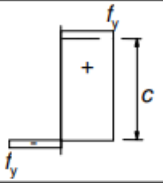 | 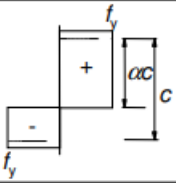 |
| 1 | $c/t \le 56{,}0\varepsilon$ | $c/t \le 25{,}7\varepsilon$ | $when\ \alpha > 0{,}5:\ c/t \le \frac{308\varepsilon}{13\alpha - 1}$<br>$when\ \alpha \le 0{,}5:\ c/t \le \frac{28\varepsilon}{\alpha}$ |
| 2 | $c/t \le 58{,}2\varepsilon$ | $c/t \le 26{,}7\varepsilon$ | $when\ \alpha > 0{,}5:\ c/t \le \frac{320\varepsilon}{13\alpha - 1}$<br>$when\ \alpha \le 0{,}5:\ c/t \le \frac{29{,}1\varepsilon}{\alpha}$ |
| Stress distribution in parts (compression positive) | 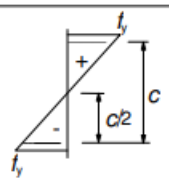 | 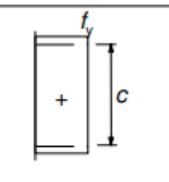 | 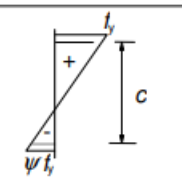 |
| 3 | $c/t \le 74{,}8\varepsilon$ | $c/t \le 30{,}7\varepsilon$ | $c/t \le 15{,}3\varepsilon\sqrt{k_\sigma}$<br>For $k_\sigma$ see EN 1993-1-5 |

$$\varepsilon = \left[\frac{235}{f_y}\frac{E}{210\,000}\right]^{0,5}$$

| Grade | 1.4301 | 1.4401 | 1.4462 |
|---|---|---|---|
| $f_y$ (N/mm$^2$) | 210 | 220 | 460 |
| $\varepsilon$ | 1,03 | 1,01 | 0,698 |

Note: For hollow sections, $c$ may conservatively be taken as ($h$-2$t$) or ($b$-2$t$).

**Table A.4:** *Cross-section classification for external compression component in stainless steel SS-EN 1993-1-4 (2006) Table 5.2*

**Outstand flanges**

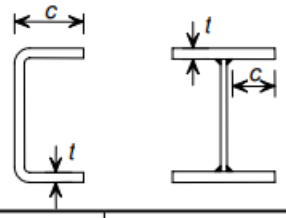


| Class | Section type | Part subject to compression | Part subject to bending and compression | |
|---|---|---|---|---|
| | | | Tip in compression | Tip in tension |
| Stress distribution in parts (compression positive) | | 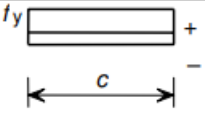 | 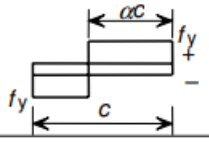 | 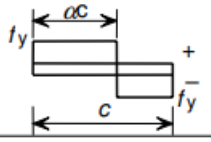 |
| 1 | Cold formed | $c/t \le 10\varepsilon$ | $c/t \le \frac{10\varepsilon}{\alpha}$ | $c/t \le \frac{10\varepsilon}{\alpha\sqrt{\alpha}}$ |
| | Welded | $c/t \le 9\varepsilon$ | $c/t \le \frac{9\varepsilon}{\alpha}$ | $c/t \le \frac{9\varepsilon}{\alpha\sqrt{\alpha}}$ |
| 2 | Cold formed | $c/t \le 10{,}4\varepsilon$ | $c/t \le \frac{10{,}4\varepsilon}{\alpha}$ | $c/t \le \frac{10{,}4\varepsilon}{\alpha\sqrt{\alpha}}$ |
| | Welded | $c/t \le 9{,}4\varepsilon$ | $c/t \le \frac{9{,}4\varepsilon}{\alpha}$ | $c/t \le \frac{9{,}4\varepsilon}{\alpha\sqrt{\alpha}}$ |
| Stress distribution in parts (compression positive) | | 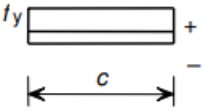 | 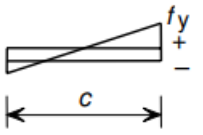 | 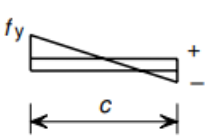 |
| 3 | Cold formed | $c/t \le 11{,}9\varepsilon$ | $c/t \le 18{,}1\varepsilon\sqrt{k_\sigma}$ For $k_\sigma$ see EN 1993-1-5 | |
| | Welded | $c/t \le 11\varepsilon$ | $c/t \le 16{,}7\varepsilon\sqrt{k_\sigma}$ For $k_\sigma$ see EN 1993-1-5 | |

$$\varepsilon = \left[\frac{235}{f_y}\frac{E}{210\,000}\right]^{0,5}$$

| Grade | 1.4301 | 1.4401 | 1.4462 |
|---|---|---|---|
| $f_y$ (N/mm$^2$) | 210 | 220 | 460 |
| $\varepsilon$ | 1,03 | 1,01 | 0,698 |

**Table A.5:** *Cross-section classification for external compression component in stainless steel SS-EN 1993-1-4 A1 (2015) section 9*

| ... | | | |
|---|---|---|---|
| Class | Part subject to bending | Part subject to compression | Part subject to bending and axial force |
| ... | | | |
| 1 | $c/t \leq 72\varepsilon$ | $c/t \leq 33\varepsilon$ | *when* $\alpha > 0{,}5$ : $c/t \leq \frac{396\varepsilon}{13\alpha - 1}$<br>*when* $\alpha \leq 0{,}5$ : $c/t \leq \frac{36\varepsilon}{\alpha}$ |
| 2 | $c/t \leq 76\varepsilon$ | $c/t \leq 35\varepsilon$ | *when* $\alpha > 0{,}5$ : $c/t \leq \frac{420\varepsilon}{13\alpha - 1}$<br>*when* $\alpha \leq 0{,}5$ : $c/t \leq \frac{38\varepsilon}{\alpha}$ |
| ... | | | |
| 3 | $c/t \leq 90\varepsilon$ | $c/t \leq 37\varepsilon$ | $c/t \leq 18{,}5\varepsilon\sqrt{k_\sigma}$<br>For $k_\sigma$ see EN 1993-1-5 |
| ... | | | |

**Table A.6:** *Cross-section classification for external compression component in stainless steel SS-EN 1993-1-4 A1 (2015) section 9*

| ... | | | | |
|---|---|---|---|---|
| Class | Section type | Part subject to compression | Part subject to bending and axial force | |
| | | | Tip in compression | Tip in tension |
| ... | | | | |
| 1 | Cold formed and welded | $c/t \leq 9\varepsilon$ | $c/t \leq \frac{9\varepsilon}{\alpha}$ | $c/t \leq \frac{9\varepsilon}{\alpha\sqrt{\alpha}}$ |
| 2 | Cold formed and welded | $c/t \leq 10\varepsilon$ | $c/t \leq \frac{10\varepsilon}{\alpha}$ | $c/t \leq \frac{10\varepsilon}{\alpha\sqrt{\alpha}}$ |
| ... | | | | |
| 3 | Cold formed and welded | $c/t \leq 14\varepsilon$ | $c/t \leq 21{,}0\varepsilon\sqrt{k_\sigma}$ For $k_\sigma$ see EN 1993-1-5 | |
| ... | | | | |

# B

# Design tool python code

## B.1 Material data module

```
# Master's Thesis
#
# Design Tool for Ultimate Bending Resistance of a Steel-Concrete Composite Beam
#
# Albin Karlsson & Gustav Friman
# June 2023
#
# ------------------------------------------------------------------------------
# MATERIAL CLASS MODULE
#
#   Contents:
#   0. Import Modules
#   1. Concrete material properties
#   2. Carbon-Steel material properties
#   3. Stainless-Steel material propertie
#   4. Material properties from test data
# ------------------------------------------------------------------------------
# Eurocode strandards used in this module:
# SS-EN 1992-1-1:2005
# SS-EN 1993-1-1:2022
# SS-EN 1993-1-4:2006
# SS-EN 1993-1-4:2006/A1:2015
# SS-EN 10088-2:2014
# ------------------------------------------------------------------------------
# 0. Import Modules
# ------------------------------------------------------------------------------

#General modules
import numpy as np
import pandas as pd

# ------------------------------------------------------------------------------
# 1. Concrete material properties
#
#   Input:
#       ConcreteGrade   Material grade:      ['C20/25',
#                                             'C25/30',
#                                             'C30/35',
#                                             'C35/45',
#                                             'C40/50',
#                                             'C45/55',
#                                             'C50/60',
#                                             'C55/67',
#                                             'C60/75']                [string, - ]
#
#   Output:
#       MtrlPar_c       Material properties [fck, fcm, fctm, fctk005, fctk095, Ecm,
#                                                                              eps_cu]
#       Where:
#           fck         Characteristic compression strength            [float, MPa]
#           fcm         Mean compressive strength                      [float, MPa]
#           fctm        Mean tensile strength                          [float, MPa]
```

```
#           fctk005     Characteristic tensile strength for 0.05%      [float, MPa]
#           fctk095     Characteristic tensile strength for 0.95%      [float, MPa]
#           Ecm         Young's modulus                                [float, MPa]
#           eps_cu      Ultimate concrete strain                       [float,  - ]
# ------------------------------------------------------------------------------

# Matrial properties - SS-EN 1992-1-1, Table 3.1
class Concrete:
    def __init__(self,ConcreteGrade):

        #                   'Grade',fck, fcm, fctm, fctk005, fctk095, Ecm, eps_cu
        Mtrl_c = np.array([['C20/25',20, 28,  2.2,  1.5,     2.9,     30,  0.0035],
                           ['C25/30',25, 33,  2.6,  1.8,     3.3,     31,  0.0035],
                           ['C30/37',30, 38,  2.9,  2.0,     3.8,     33,  0.0035],
                           ['C35/45',35, 43,  3.2,  2.2,     4.2,     34,  0.0035],
                           ['C40/50',40, 48,  3.5,  2.5,     4.6,     35,  0.0035],
                           ['C45/55',45, 53,  3.8,  2.7,     4.9,     36,  0.0035],
                           ['C50/60',50, 58,  4.1,  2.9,     5.3,     37,  0.0035],
                           ['C55/67',55, 63,  4.2,  3.0,     5.5,     38,  0.0032],
                           ['C60/75',60, 68,  4.4,  3.1,     5.7,     39, 0.0030]])


        #Row location for the given concrete type
        location_c = np.argwhere(Mtrl_c == ConcreteGrade)[:,0]

        #Output
        self.fck = float(Mtrl_c[location_c,1])
        self.fcm = float(Mtrl_c[location_c,2])
        self.fctm = float(Mtrl_c[location_c,3])
        self.fctk005 = float(Mtrl_c[location_c,4])
        self.fctk095 = float(Mtrl_c[location_c,5])
        self.Ecm = float(Mtrl_c[location_c,6])*1000
        self.eps_cu = float(Mtrl_c[location_c,7])

# ------------------------------------------------------------------------------
# 2. Carbon-Steel material properties
#
#   Input:
#       t               Plate thickness                                 [float, mm]
#       SteelGrade      Steel grade:        ['S235',
#                                            'S275',
#                                            'S355',
#                                            'S420',
#                                            'S460',
#                                            'S500',        OBS:higher grades than
#                                            'S550',            460 is not allowed
#                                            'S600',            for steel-concrete
#                                            'S620',               composite beams
#                                            'S650',         according to Eurocode
#                                            'S690',
#                                            'S700']                  [string, - ]
#
#   Output:
#       MtrlPar_cs      Material properties  [fy, fu, E]
#       Where:
#           fy          Yield strength                                  [float, MPa]
#           fu          Ultimate strength                               [float, MPa]
#           E           Modulus of elasticity                           [float, MPa]
# ------------------------------------------------------------------------------

# Nominal steel strenghts - SS-EN 1993-1-1, Table 5.1
class CarbonSteel:
    def __init__(self,SteelGrade,t):
        #                               [ t<=40 ][ 40<t<80 ]
        #                   'Grade',    fy,  fu,  fy,   fu
        Mtrl_cs = np.array([['S235',    235, 360, 215,  360],
                           ['S275',    275, 390, 245,  370],
                           ['S355',    355, 490, 325,  470],
                           ['S420',    420, 510, 390,  490],
                           ['S460',    460, 540, 410,  510],
```

```
                            ['S500',   500, 580, 450,  550],   # \
                            ['S550',   550, 600, 500,  600],   #  |
                            ['S600',   600, 650, 550,  650],   #   \ #See input
                            ['S620',   620, 700, 560,  660],   #   /
                            ['S650',   650, 700, '-',  '-'],   #  |
                            ['S690',   690, 770, 630,  710],   #  |
                            ['S700',   700, 750, '-',  '-']])  # /

        #Row location for the given steel grade
        location_cs = np.argwhere(Mtrl_cs == SteelGrade)[:,0]

        #Strength dependant on thickness
        if t <= 40:
            fy = Mtrl_cs[location_cs,1]
            fu = Mtrl_cs[location_cs,2]
        elif 40 < t < 80:
            fy = Mtrl_cs[location_cs,3]
            fu = Mtrl_cs[location_cs,4]
        else:
            print('OBS: Invalid plate thickness for Carbon-Steel,'
                'please lower the thickness below 80mm')

        #Invalid steel and thickness
        if fy == '-' or fu == '-':
            print('OBS: Invalid Carbon-Steel grade for the given plate thickness,',
                'please lower thickness below 40mm or change steel grade')

        #Young's modulus and poisson's ratio - SS-EN 1993-1-1, Section 5.2.5
        E = 210000

        #Output
        self.fy = float(fy)
        self.fu = float(fu)
        self.E = E

# ------------------------------------------------------------------------------
# 3. Stainless-Steel material properties
#
#   Input:
#       t               Plate thickness                                 [float, mm ]
#       ProductForm     ColdRolledStip, HotRolledStrip,
#                       HotRolledPlate, Bars/Rods/Sections              [string, - ]
#       SteelGrade      Ferritic:           ['1.4003',
#                                            '1.4016',
#                                            '1.4512']
#                       Austenitic:         ['1.4306',
#                                            '1.4307',
#                                            '1.4541',
#                                            '1.4301',
#                                            '1.4401',
#                                            '1.4404',
#                                            '1.4539',
#                                            '1.4571',
#                                            '1.4432',
#                                            '1.4435',
#                                            '1.4311',
#                                            '1.4406',
#                                            '1.4439',
#                                            '1.4529',
#                                            '1.4547',
#                                            '1.4318']
#                       Duplex:             ['1.4062',
#                                            '1.4162',
#                                            '1.4482',
#                                            '1.4662',
#                                            '1.4362',
#                                            '1.4462']                  [string, - ]
#
#   Output:
#       MtrlPar_ss              Material properties [StainlessType,fy, fu, A, n, E]
```

```
#       Where:
#           StainlessType       Austenitic, Ferritic, or Duplex         [string, - ]
#           fy                  Yield strength                          [float, MPa]
#           fu                  Ultimate strength                       [float, MPa]
#           A                   Elongation after fracture               [float,  - ]
#           n                   Strain hardening exponent               [float,  - ]
#           E                   Modulus of elasticity                   [float, MPa]
# ----------------------------------------------------------------------------------

# Material properties - SS-EN 1993-1-4, Table 2.1 with replacements according to
# SS-EN 1993 1-4 A and additions from SS-EN 10088-2, Table 7.
class StainlessSteel:
    def __init__(self, SteelGrade, t, ProductForm):
        #                               [ColdRolledStip,           HotRolledStrip,
           HotRolledPlate,    Bars/Rods/Sections]
        #                              [       t<=8        ] [       t<=13.5
     ] [       t<=75        ] [      t<=250     ]
        #                     'Grade'     fy      fu      A       fy      fu      A
          fy      fu      A       fy      fu      n   StainlessType
        Mtrl_ss = np.array([['1.4003',  280,    450,    20,     280,    450,    20,
         250,    450,    18,     260,    450,    14,    'Ferritic'],
                            ['1.4016',  260,    450,    20,     240,    450,    18,
         240,    430,    20,     240,    400,    14,    'Ferritic'],
                            ['1.4512',  210,    380,    25,     210,    380,    25,
         '-',    '-',    '-',    '-',    '-',    14,    'Ferritic'],
                            ['1.4306',  220,    520,    45,     200,    520,    45,
         200,    500,    45,     180,    460,     7,   'Austenitic'],
                            ['1.4307',  220,    520,    45,     200,    520,    45,
         200,    500,    45,     175,    500,     7,   'Austenitic'],
                            ['1.4541',  220,    520,    40,     200,    520,    40,
         200,    500,    40,     190,    500,     7,   'Austenitic'],
                            ['1.4301',  230,    540,    45,     210,    520,    45,
         210,    520,    45,     190,    500,     7,   'Austenitic'],
                            ['1.4401',  240,    530,    40,     220,    530,    40,
         220,    520,    45,     200,    500,     7,   'Austenitic'],
                            ['1.4404',  240,    530,    40,     220,    530,    40,
         220,    520,    45,     200,    500,     7,   'Austenitic'],
                            ['1.4539',  240,    530,    35,     220,    530,    35,
         220,    520,    35,     230,    530,     7,   'Austenitic'],
                            ['1.4571',  240,    540,    40,     220,    540,    40,
         220,    520,    40,     200,    500,     7,   'Austenitic'],
                            ['1.4432',  240,    550,    40,     220,    550,    40,
         220,    520,    45,     200,    500,     7,   'Austenitic'],
                            ['1.4435',  240,    550,    40,     220,    550,    40,
         220,    520,    45,     200,    500,     7,   'Austenitic'],
                            ['1.4311',  290,    550,    40,     270,    550,    40,
         270,    550,    40,     270,    550,     7,   'Austenitic'],
                            ['1.4406',  300,    580,    40,     280,    580,    40,
         280,    580,    40,     280,    580,     7,   'Austenitic'],
                            ['1.4439',  290,    580,    35,     270,    580,    35,
         270,    580,    40,     280,    580,     7,   'Austenitic'],
                            ['1.4529',  '-',    '-',    '-',    '-',    '-',    '-'
    ,    300,    650,    40,     300,    650,     7,   'Austenitic'],
                            ['1.4547',  320,    650,    35,     300,    650,    35,
         300,    650,    40,     300,    650,     7,   'Austenitic'],
                            ['1.4318',  350,    650,    35,     330,    650,    35,
         330,    630,    45,     '-',    '-',     7,   'Austenitic'],
                            ['1.4062',  530,    700,    20,     480,    680,    30,
         450,    650,    30,     380,    650,     8,       'Duplex'],
                            ['1.4162',  530,    700,    20,     480,    680,    30,
         450,    650,    30,     450,    650,     8,       'Duplex'],
                            ['1.4482',  500,    700,    20,     480,    660,    30,
         450,    650,    30,     400,    650,     8,       'Duplex'],
                            ['1.4662',  550,    750,    20,     550,    750,    25,
         480,    680,    25,     450,    650,     8,       'Duplex'],
                            ['1.4362',  450,    650,    20,     400,    650,    20,
         400,    630,    25,     400,    600,     8,       'Duplex'],
                            ['1.4462',  500,    700,    20,     460,    700,    25,
         460,    640,    25,     450,    650,     8,       'Duplex']])
```

```
        #Row location the for given steel grade
        location_ss = np.argwhere(Mtrl_ss == SteelGrade)[:,0]

        #Property dependant on thickness and manufacturing method
        if ProductForm == 'ColdRolledStip' and t<=8:
            fy = Mtrl_ss[location_ss,1]
            fu = Mtrl_ss[location_ss,2]
            A = Mtrl_ss[location_ss,3]
        elif ProductForm == 'HotRolledStrip' and t<=13.5:
            fy = Mtrl_ss[location_ss,4]
            fu = Mtrl_ss[location_ss,5]
            A = Mtrl_ss[location_ss,6]
        elif ProductForm == 'HotRolledPlate' and t<=75:
            fy = Mtrl_ss[location_ss,7]
            fu = Mtrl_ss[location_ss,8]
            A = Mtrl_ss[location_ss,9]
        elif ProductForm == 'Bars/Rods/Sections' and t<=250:
            fy = Mtrl_ss[location_ss,10]
            fu = Mtrl_ss[location_ss,11]
        else:
            print('OBS: Invalid Product form or thickness')

        #Invalid steel grade and thickness
        if fy == '-' or fu == '-' or A =='-':
            print('OBS: Invalid Stainless-Steel grade for the given thickness')

        #Young's modulus - SS-EN 1993-1-4, Section 2.1.3
        if Mtrl_ss[location_ss,13] == 'Ferritic':
            E = 220000
        elif (Mtrl_ss[location_ss,0] == '1.4539' or
              Mtrl_ss[location_ss,0] == '1.4529' or
              Mtrl_ss[location_ss,0] == '1.4547'):
            E = 195000
        else:
            E = 200000

        #Output
        self.fy = float(fy)
        self.fu = float(fu)
        self.A = float(A)/100
        self.StainlessType = Mtrl_ss[location_ss,13]
        self.E = E
        self.n = float(Mtrl_ss[location_ss,12])/100

# ------------------------------------------------------------------------------
# 4. Material properties from test data
#
#   Input:
#       Excel sheet     "MaterialData.xlsx": Make sure to use the correct path
#                                            in the "pd.read_excel" function
#       With:           Column 1: Strain                                [float,  % ]
#                       Column 2: Stress                                [float, MPa]
#
#   Output:
#       MtrlPar_ex      Material properties     [M_data, eps_02, eps_su, fy, fu, E]
#       Where:
#           M_data      Test data, strain-stress array   [[float, - ],[float, MPa]]
#           eps_02      Strain at 0,2% proof strength                   [float,  - ]
#           eps_su      Ultimate steel strain                           [float,  - ]
#           fu          Ultimate strength                               [float, MPa]
#           fy          Yield strength                                  [float, MPa]
#           E           Young's modulus                                 [float, MPa]
#------------------------------------------------------------------------------
# OBS:This section was writen based on the layout and values in the Excel-file
# provided, threfore this section will need to be adapted before use
# ------------------------------------------------------------------------------

class SteelDataEx:
    def __init__(self):
```

```
        #Import excel data
        Import = pd.read_excel(r'C:\Users\ALKAX\OneDrive - COWI\Exjobb\Design tool\
    Friman_Karlsson\MaterialData.xlsx')

        #Convert data to numpy array
        M_data = Import.to_numpy()
        M_data[:,0] = M_data[:,0]/100  #Convert strain from [%] to [-]

        #Young's modulus
        E_v = M_data[:,1]/M_data[:,0]/1000
        E = []
        for i in range(len(M_data)):
            if 190 <= E_v[i] <=225:
                E.append(E_v[i])
        E = np.average(E)

        #Ultimate capcity
        fu = max(M_data[:,1])
        fu_pos = np.argwhere(M_data == fu)[0,0]
        eps_su = M_data[fu_pos,0]

        #yield capacity
        for i in range(len(M_data)):
            eps = M_data[i,0]-M_data[i,1]/(E*1000)
            if eps >= 0.002:
                fy = M_data[i,1]
                eps_02 = M_data[i,0]
                break

        #Output
        self.M_data = M_data
        self.eps_02 = eps_02
        self.eps_su = eps_su
        self.fu = fu
        self.fy = fy
        self.E = E*1000
```

## B.2 Design function module

```
# Master's Thesis
#
# Design Tool for Ultimate Bending Resistance of a Steel-Concrete Composite Beam
#
# Albin Karlsson & Gustav Friman
# June 2023
#
# ------------------------------------------------------------------------------
# DESIGN FUNCTIONS MODULE
#
#   Contents
#   0. Import Modules
#   1. Web corrugation geometry
#   2. Effective concrete width
#   3. Cross section geometry
#   4. Abdella calculations
#   5. Moment calculation with EuroCode
#   6. Moment calculation with strainhardening
#
# ------------------------------------------------------------------------------
# Eurocode strandards used in this module:
# SS-EN 1993-1-5:2006
# SS-EN 1994-2:2005
# SS-EN 1993-1-4:2006
# SS-EN 1993-1-4:2006/A1:2015
# SS-EN 1993-1-1:2022
# ------------------------------------------------------------------------------
```

```
# 0. Import Modules
# ------------------------------------------------------------------------------

#General modules
import numpy as np
import pandas as pd

# ------------------------------------------------------------------------------
# 1 Web corrugation geometry
#
# This module calculates the geometrical properties of the corrugted web, checks
# for risk of shear-buckling and calculates the effective width of the web if
# corrugated webs are used.
#
#   Input:
#       WebShape        Web shape, 'C' or 'F'                          [string, -]
#       Accordion       Web contribution from accordion effect        [boolean, -]
#       a1              Flat fold length                               [float, mm]
#       a3              Corrugation depth                              [float, mm]
#       alpha           Corrugation angle                          [float, degrees]
#       bfu             Upper flange width                             [float, mm]
#       bfl             Lower flange width                             [float, mm]
#       hw              Web height                                     [float, mm]
#       tw              Web thickness                                  [float, mm]
#       fy              Yield strength                                [float, MPa]
#       E               Young's modulus                               [float, MPa]
#
#   Output:
#       CorrGeo         Corrugation class                              [a2, a4, w]
#       Where:
#           a2          Inclined fold length                           [float, mm]
#           a4          Inclined fold longitudinal length              [float, mm]
#           w           Corrugation length                             [float, mm]
#           tw          Effective web thickness                        [float, mm]
#
# Corrugation figure:
#                 _____a1____        _
#               /           \       |
#            a2/             \      |a3
#   ___________/_\alpha        \____|_______
#              |--|----------|
#               a4     a1
#              |-------------|
#                     w
# ------------------------------------------------------------------------------

class WebGeometry:
    def __init__(self,WebShape,Accordion,a1,a3,alpha,bfu,bfl,hw,tw,fy,E):

        # Corrugated web with accordion effect
        if WebShape == 'C':

            # Web geometry
            a2 = a3/np.sin(np.radians(alpha))
            self.a2 = a2
            a4 = a3/np.tan(np.radians(alpha))
            self.a4 = a4
            w = a1+a4
            self.w = w
            s = a2+a1
            self.s = s

            # Shear buckling - SS-EN 1993-1-5, Section D.2.2
            v = 0.3
            tau_cr_l = 4.83*E*(tw/max(a1, a2))**2
            lamb_l = np.sqrt(fy/(tau_cr_l*np.sqrt(3)))
            Chi_l = 1.15/(0.9+lamb_l)
            Dx = E*tw**3/(12*(1-v**2))*w/s
            Iz = tw*a3**2*(3*a1+a2)/12
            Dz = E*Iz/w
```

```
            tau_cr_g = 32.4/(tw*hw**2)*(Dx*Dz**3)**(1/4)
            lamb_g = np.sqrt(fy/(tau_cr_g*np.sqrt(3)))
            Chi_g = 1.15/(0.5+lamb_g**2)


            if Chi_g < 1 and Chi_l < 1:
                    print('Shear buckling in the corruated web:')
                    print('Global buckling may occur, lower hw or raise tw,a1,a3,')
                    print('Chi_g',Chi_g)
                    print('Local buckling may occur, raise tw or lower a1 and a3')
                    print('Chi_l',Chi_l)
            elif Chi_g < 1:
                    print('Shear buckling in the corruated web:')
                    print('Global buckling may occur, lower hw or raise tw,a1,a3,')
                    print('Chi_g',Chi_g)
            elif Chi_l < 1:
                    print('Shear buckling in the corruated web:')
                    print('Local buckling may occur, raise tw or lower a1 and a3')
                    print('Chi_l',Chi_l)

            if Accordion:

                # Parameters for effective web thickness
                bf = min(bfl, bfu)
                R = ((a1+a4)*a3)/((a1+2*a4)*bf)
                O = (bf+a3)/(bf-a3)
                slenderness = hw/tw

                # Conditions for web utilization
                #O: b/a=4.33 =>0.1*tw, b/a=6 =>0.2*tw, b/a=21 =>0.3*tw
                if slenderness <= 90 and R < 0.09 and O <= 1.1:
                    t_weff = 0.3*tw
                elif slenderness <= 125 and R < 0.13 and O <= 1.2:
                    t_weff = 0.2*tw
                elif slenderness <= 150 and R < 0.18 and O <= 1.6:
                    t_weff = 0.1*tw
                else:
                    t_weff = 0

                self.tw = round(t_weff,3)

            else:
            # Corrugated web with no accordion effect
                self.tw = 0

        # Flat web
        else:
            self.tw = tw

# ------------------------------------------------------------------------------
# 2. Effective concrete width
#
# This module calculates the effective width of the concrete to be considerd based
# on global dimensions for cases when the width is not prescribed.
#
#   Input:
#       b0                  Shear connector distance                    [float, mm]
#       L                   Span length                                 [float, mm]
#       girder_space        Girder to girder spacing                    [float, mm]
#       girder_space_edge   Girder to edge spacing                      [float, mm]
#
#   Output:
#       EffConc             Effective concrete width              [b_eff, b_eff_s]
#       Where:
#           b_eff           Effective concrete width, field             [float, mm]
#           b_eff_s         Effective concrete width, support           [float, mm]
# ------------------------------------------------------------------------------

# Calculation of effective width - SS-EN 1994-2, Section 5.4.1.2
class EffConcWidth:
```

```
    def __init__(self,b0,L,girder_space,girder_space_edge,girder_edge):
        # Simply supported span
        Le = L

        # Girder placed adjecent to an edge
        if girder_edge:
            b1 = girder_space/2-b0/2
            b2 = girder_space_edge-b0/2

        # Girder placed in the middle with no adjecent edge
        else:
            b1 = girder_space/2-b0/2
            b2 = girder_space/2-b0/2

        # Effective width for field
        be1 = min(Le/8, b1)
        be2 = min(Le/8, b2)
        self.b_eff = b0+be1+be2

        # Effective width over support
        B1 = min((0.55+0.025*Le/be1),1)
        B2 = min((0.55+0.025*Le/be2),1)
        self.b_eff_s = b0 + B1*be1 + B2*be2

# -----------------------------------------------------------------------------
# 3. Cross section geometry
#
# This sections the geometrical cross-sectional constants for the given
# cross-section.
#
#   Input:
#       bfu             Upper flange width                          [float, mm]
#       tfu             Upper flange thickness                      [float, mm]
#       bfl             Lower flange width                          [float, mm]
#       tfl             Lower flange thickness                      [float, mm]
#       tw              Web thickness                               [float, mm]
#       hw              Web height                                  [float, mm]
#       tc              Concrete height                             [float, mm]
#       bc              Effective width of the concrete flange      [float, mm]
#       Es              Young's modulus of the structural steel     [float, MPa]
#       Ec              Young's modulus of the concrete             [float, MPa]
#
#   Output:
#       CrossSecGeo     Cross section geometry              [As, hs, htot, z_tp_s]
#       Where:
#           As          Steel area                                  [float, mm^2]
#           hs          Total steel height                            [float, mm]
#           htot        Total height                                  [float, mm]
#           z_tp_s      Steel center of gravity from below            [float, mm]
#           Iy          Moment of inertia in the strong direction   [float, mm^4]
# -----------------------------------------------------------------------------

class SectionGeometry:
    def __init__(self,bfu,tfu,bfl,tfl,tw,hw,tc,bc,Es,Ec):
        # Steel area
        As_fu = bfu*tfu
        As_fl = bfl*tfl
        As_w = tw*hw
        As = As_fu+As_fl+As_w
        self.As = As

        # Heights
        hs = tfl+tfu+hw
        self.hs = hs
        self.htot = tc+hs

        # Center of gravity calculated form below
        z_tp_s = (tfu*bfu*(tfu/2+hw+tfl)+tfl*bfl*tfl/2+hw*tw*(hw/2+tfl))/As
        self.z_tp_s = z_tp_s
```

```
        # Inertia
        n = Es/Ec
        Ac = bc*tc
        Atot = As+Ac/n
        z_tp_c = hs+tc/2
        z_tp = (As*z_tp_s+Ac/n*z_tp_c)/Atot
        Iys = bfu*tfu**3/12+bfl*tfl**3/12+tw*hw**3/12+As_fu*(tfu/2+hw+tfl-z_tp_s)\
                **2+As_fl*(tfl/2-z_tp_s)**2+As_w*(hw/2+tfl-z_tp_s)**2
        Iyc = bc*tc**3/12
        Iy = Iys+As*(z_tp_s-z_tp)**2+Iyc/n+Ac/n*(z_tp_c-z_tp)**2
        self.Iy = Iy

# ------------------------------------------------------------------------------
# 4. Abdella calculations
#
# This module calculates the constatns used in for the non-linear stress-strain
# relationship of the stainless-steel.
#
#   Input:
#       fy              Yield strength                                  [float, MPa]
#       fu              Ultimate strength                               [float, MPa]
#       E               Young's modulus                                 [float, MPa]
#       A               Elongation after fracture                        [float, - ]
#       n               Strain hardening exponent                        [float, - ]
#       StainlessType   'Austenitic', 'Ferritic', or 'Duplex'           [string, - ]
#
#   Output:
#       Abdella         Material behaviour    [eps_su, eps_02, r_2, r_s, p_s, r, p]
#       Where:
#           eps_su      Ultimate steel strain                            [float, - ]
#           eps_02      Strain at 0,2% proof strength                    [float, - ]
#           r_2         Material behaviour parameter                     [float, - ]
#           r_s         Material behaviour parameter                     [float, - ]
#           p_s         Material behaviour parameter                     [float, - ]
#           r           Material behaviour parameter                     [float, - ]
#           p           Material behaviour parameter                     [float, - ]
# ------------------------------------------------------------------------------

class Abdella:
    def __init__(self,fy,fu,E,A,n,StainlessType):

        # Strain
        eps_02=fy/E+0.002
        if StainlessType == 'Ferritic':
            eps_su=min(0.6*(1-fy/fu),A)
        else:
            eps_su=min(1-fy/fu,A)

        # Material behaviour parameters
        r = E*eps_02/fy
        e = fy/E
        E_2 = E/(1+0.002*n/e)
        r_2 = E_2*eps_02/fy
        p = r*(1-r_2)/(r-1)
        r_s = E_2*(eps_su-eps_02)/(fu-fy)
        m = 1+2.8*fy/fu
        E_u = E_2/(1+(r_s-1)*m)
        r_u = E_u*(eps_su-eps_02)/(fu-fy)
        p_s = r_s*(1-r_u)/(r_s-1)

        # Output
        self.eps_su = eps_su
        self.eps_02 = eps_02
        self.r_2 = r_2
        self.r_s = r_s
        self.p_s = p_s
        self.r = r
        self.p = p

# ------------------------------------------------------------------------------
```

```
# 5. Moment calculation with EuroCode
#
# This module locates the location of the neutral axis and caluculates the plastic
# bending moment capacity ussing the elastic, perfectly plastic model recomended by
# eurocode.
#
#   Input:
#       er              Balance difference break value                  [float, N ]
#       E               Young's modulus                                [float, MPa]
#       htot            Total height                                    [float, mm]
#       tc              Concrete height                                 [float, mm]
#       bc              Effective concrete width                        [float, mm]
#       tfu             Upper flange thickness                          [float, mm]
#       bfu             Upper flange width                              [float, mm]
#       tfl             Lower flange thickness                          [float, mm]
#       bfl             Lower flange width                              [float, mm]
#       tw              Web thickness                                   [float, mm]
#       hw              Web height                                      [float, mm]
#       As              Steel area                                     [float, mm^2]
#       fy              Yield strength                                  [float, MPa]
#       fck             Characteristic compression strength             [float, MPa]
#       z_tp_s          Center of gravity for the steel                 [float, mm]
#       SteelType       Stainless or carbon ('SS' or 'CS')              [string, -]
#       WebShape        Flat or Corrugated ('F' or 'C')                 [string, -]
#
#   Output:
#       MomentCalcEC    Moment calculation                       [beta, M_pl, y1_0]
#       Where:
#           beta        Reduction factor for reduced plastic response   [float, - ]
#           M_pl        Plastic bending moment capacity                [float, kNm]
#           y1_0        Neutral axis from the top                       [float, mm]
# ------------------------------------------------------------------------------

# Calculation of plasic moment capacity using the recomended model in eurocode -
# SS-EN 1994-2, Section 6.2.1.2
class MomentCalcEC:
    def __init__(self,er,E,htot,tc,bc,tfu,bfu,tfl,bfl,tw,hw,As,fy,fck,z_tp_s,
                 SteelType,WebShape):

        # Starting values
        M_pl = 0
        y1_0 = 1

        # Loop to itterate the neutral axis
        for i in range(int(round(htot,0))*100):


            #---------------------- Neutral axis in  the concrete -----------------
            if y1_0 <= tc:

                sig_m = fy

                # Forces
                FC = y1_0*0.85*fck*bc
                FT = sig_m*As
                dF = np.abs(FC-FT)

                # Moment calculation if balance is found
                if dF < er:
                    M_pl = sig_m*As*((htot-z_tp_s-y1_0/2))
                    break

                # Continue itteration
                else:
                    y1_0 = y1_0+0.01
                    y1_0 = round(y1_0,2)

            #---------------------- Neutral axis in the steel ----------------------
            else:
```

```
sig_tm = fy
sig_cm = fy

# Forces
if y1_0 >= (tc+tfu):
    FC = 0.85*fck*tc*bc+tfu*bfu*sig_cm+tw*(y1_0-tc-tfu)*sig_cm
    FT = tw*(htot-tfl-y1_0)*sig_tm+tfl*bfl*sig_tm
else:
    FC = 0.85*fck*tc*bc+(y1_0-tc)*bfu*sig_cm
    FT = bfu*(tc+tfu-y1_0)*sig_tm+tw*hw*sig_tm+tfl*bfl*sig_tm
dF = np.abs(FT-FC)

# Moment calculation if balance is found
if dF < er:

    # Neural axis in the web
    if y1_0 > (tc+tfu):

        # Checks the cross-section class of web part in compresion
        # Flat web with stainless steel
        if SteelType == 'SS' and WebShape == 'F':

            # Check cross section class for the web -
            # SS-EN 1993-1-4, Table 5.2 with replacements according
            # to SS-EN 1993-1-4 A1
            eps_CSC = (235/fy*E/210000)**0.5
            alpha = (y1_0-tc-tfu)/hw
            if hw/tw <= 38*eps_CSC/alpha:
                M_pl = 0.85*tc*bc*fck*(y1_0-tc/2)\
                +bfu*tfu*sig_cm*(y1_0-tc-tfu/2)\
                +tw*(y1_0-tc-tfu)**2*sig_cm/2\
                +tw*(htot-tfl-y1_0)**2*sig_tm/2\
                +tfl*bfl*sig_tm*(htot-y1_0-tfl/2)
            else:
                print('Web not in CSC 1 or 2, Elastic repsonse')
                break

        # Flat web with carbon steel
        elif SteelType == 'CS' and WebShape == 'F':

            # Check cross section class for the web -
            # SS-EN 1993-1-1, Table 7.3
            eps_CSC = (235/fy)**0.5
            alpha = (y1_0-tc-tfu)/hw
            if hw/tw <= 41.5*eps_CSC/alpha:
                M_pl = 0.85*tc*bc*fck*(y1_0-tc/2)\
                +bfu*tfu*sig_cm*(y1_0-tc-tfu/2)\
                +tw*(y1_0-tc-tfu)**2*sig_cm/2\
                +tw*(htot-tfl-y1_0)**2*sig_tm/2\
                +tfl*bfl*sig_tm*(htot-y1_0-tfl/2)
            else:
                print('Web not in CSC 1 or 2, Elastic response')
                break

        # Corrugated web
        else:
            M_pl = 0.85*tc*bc*fck*(y1_0-tc/2)\
            +bfu*tfu*sig_cm*(y1_0-tc-tfu/2)\
            +tw*(y1_0-tc-tfu)**2*sig_cm/2\
            +tw*(htot-tfl-y1_0)**2*sig_tm/2\
            +tfl*bfl*sig_tm*(htot-y1_0-tfl/2)\

    # Neutral axis in in the flange
    else:
        M_pl = 0.85*tc*bc*fck*(y1_0-tc/2)\
        +bfu*(y1_0-tc)**2*sig_cm/2\
        +bfu*(tc+tfu-y1_0)**2*sig_tm/2\
        +tw*hw*sig_tm*(htot-tfl-hw/2-y1_0)\
        +tfl*bfl*sig_tm*(htot-y1_0-tfl/2)
```

```
                    break

                # Continue itteration
                else:
                    y1_0 = y1_0+0.01
                    y1_0 = round(y1_0,2)

        # Plasticity check with beta factor - SS-EN 1994-2, Figure 6.3
        if y1_0/htot <= 0.15:
            beta = 1
        elif y1_0/htot <= 0.4:
            beta = 1-(y1_0/htot-0.15)/(0.4-0.15)*(0.15)
        else:
            beta = 0
            print("Location of neutral axis too deep, Elastic response")

        # Output
        self.beta = beta
        self.M_pl = (beta*M_pl)/1000000
        self.y1_0 = y1_0


# ------------------------------------------------------------------------------
# 6. Moment calculation with strain hardening
#
# This moduel locates the possition of the neutral axis and calculates the plastic
# bending moment capacity considering strain hardening for stainless steel.
#
#   Input:
#       er              Balance difference break value                  [float, N ]
#       E               Young's modulus                                [float, MPa]
#       eps_cu          Ultimate concrete strain                        [float, - ]
#       eps_su          Ultimate steel strain                           [float, - ]
#       eps_y           Strain at yield strength                        [float, - ]
#       htot            Total height                                    [float, mm]
#       hs              Total Steel height                              [float, mm]
#       tc              Concrete height                                 [float, mm]
#       bc              Effective concrete width                        [float, mm]
#       tfu             Upper flange thickness                          [float, mm]
#       bfu             Upper flange width                              [float, mm]
#       tfl             Lower flange thickness                          [float, mm]
#       bfl             Lower flange width                              [float, mm]
#       tw              Web thickness                                   [float, mm]
#       hw              Web height                                      [float, mm]
#       As              Steel area                                     [float, mm^2]
#       fy              Yield strength                                  [float, MPa]
#       fck             Characteristic compression strength             [float, MPa]
#       r_2             Material behaviour parameter                    [float, - ]
#       r_s             Material behaviour parameter                    [float, - ]
#       p_s             Material behaviour parameter                    [float, - ]
#       r               Material behaviour parameter                    [float, - ]
#       p               Material behaviour parameter                    [float, - ]
#       z_tp_s          Center of gravity for the steel                 [float, mm]
#       SteelType       Stainless or carbon ('SS' or 'CS')              [string, -]
#       WebShape        Flat or Corrugated ('F' or 'C')                 [string, -]
#       M_data          Test data, strain-stress array    [[float, -],[float, MPa]]
#
#   Output:
#       MomentCalcSH    Moment calculation    [M_pl, y1_0]
#       Where:
#           M_pl        Plastic bending moment capacity                 [float, kNm]
#           y1_0        Neutral axis from the top                       [float, mm]
# ------------------------------------------------------------------------------

class MomentCalcSH:
    def __init__(self,er,E,eps_cu,eps_su,eps_y,htot,hs,tc,bc,tfu,bfu,tfl,bfl,tw,hw,
                 As,fy,fck,r_2,r_s,p_s,r,p,z_tp_s,SteelCurve,WebShape,M_data):

        #Strating values
        M_pl = 0
```

```
y1_0 = 1
sig_m = 0
sig_S = 0

#Loop to itterate the neutral axis
for i in range(int(round(htot,0))*100):

    #Curvature from cross sectional strain relation
    kc = eps_cu/y1_0
    ka = eps_su/(htot-y1_0)
    k = min(kc,ka)

    #----------------- Neutral axis in the concrete ----------------------
    if y1_0 <= tc:

        #Strain at 60% from NA
        eps_2 = k*(tc+0.6*hs-y1_0)

        # Stain at the bottom
        eps_S = k*(htot-y1_0)

        # Check if the steel yields at eps_2
        if eps_2 > eps_y:

            # Stress calculated from Abdella material behaviour
            if SteelCurve == 'Py':
                sig_m = fy*(1+(r_2*((eps_2/eps_y)-1))/(1+(r_s-1)\
                *((eps_2/eps_y-1)/(eps_su/eps_y-1))**p_s))
                sig_S = fy*(1+(r_2*((eps_S/eps_y)-1))/(1+(r_s-1)\
                *((eps_S/eps_y-1)/(eps_su/eps_y-1))**p_s))

            # Stress interpolated from material test data, excel
            else:
                for j in range(M_data.shape[0]):
                    if M_data[j,0]>eps_2:
                        sig_m = (eps_2-M_data[j-1,0])/(M_data[j,0]-\
                        M_data[j-1,0])*(M_data[j,1]-M_data[j-1,1])\
                        +M_data[j-1,1]
                        break
        else:
            print("Too low steel strain, Elastic response")
            break

        # Forces
        FC = y1_0*0.85*fck*bc
        FT = sig_m*As
        dF = np.abs(FC-FT)
        self.sig_m = sig_m
        self.sig_S = sig_S

        # Moment calculation
        if dF < er:
            M_pl = sig_m*As*((htot-z_tp_s-y1_0/2))
            break

        # Continue itteration
        else:
            y1_0 = y1_0+0.01
            y1_0 = round(y1_0,2)

    #-------------------Neutral axis in the steel -------------------------
    else:

        # Strain at 60% from NA
        eps_c = k*(y1_0-tc)*0.6
        eps_t = k*(htot-y1_0)*0.6
        eps_S = k*(htot-y1_0)

        # Check if the steel yields at eps_t
        if eps_t > eps_y:
```

```
        # Stress calculated from Abdella material behaviour
        if SteelCurve == 'Py':
            sig_tm = fy*(1+(r_2*((eps_t/eps_y)-1))/(1+(r_s-1)\
            *((eps_t/eps_y-1)/(eps_su/eps_y-1))**p_s))
            sig_cm = fy*(r*(eps_c/eps_y)/(1+(r-1)*(eps_c/eps_y)**p))
            sig_S = fy*(1+(r_2*((eps_S/eps_y)-1))/(1+(r_s-1)\
            *((eps_S/eps_y-1)/(eps_su/eps_y-1))**p_s))

        # Stress interpolated from material test data, excel
        else:
            for j in range(M_data.shape[0]):
                if M_data[j,0]>eps_c:
                    sig_cm = (eps_c-M_data[j-1,0])/(M_data[j,0]\
                    -M_data[j-1,0])*(M_data[j,1]-M_data[j-1,1])\
                    +M_data[j-1,1]
                    break
            for j in range(M_data.shape[0]):
                if M_data[j,0]>eps_t:
                    sig_tm = (eps_t-M_data[j-1,0])/(M_data[j,0]\
                    -M_data[j-1,0])*(M_data[j,1]-M_data[j-1,1])\
                    +M_data[j-1,1]
                    break
    else:
        print("Too low steel strain, Elastic response")
        break

    # Forces
    if y1_0 >= (tc+tfu):
        FC = 0.85*fck*tc*bc+tfu*bfu*sig_cm+tw*(y1_0-tc-tfu)*sig_cm
        FT = tw*(htot-tfl-y1_0)*sig_tm+tfl*bfl*sig_tm

    else:
        FC = 0.85*fck*tc*bc+(y1_0-tc)*bfu*sig_cm
        FT = bfu*(tc+tfu-y1_0)*sig_tm+tw*hw*sig_tm+tfl*bfl*sig_tm

    dF = np.abs(FT-FC)
    self.sig_m = sig_tm
    self.sig_S = sig_S

    # Moment calculation
    if dF < er:

        #Neutral axis in the web
        if y1_0 > (tc+tfu):

            # Flat web
            if WebShape == 'F':
                # SS-EN 1993-1-4, Table 5.2 with replacements according
                # to SS-EN 1993-1-4 A1
                eps_CSC = (235/fy*E/210000)**0.5
                alpha = (y1_0-tc-tfu)/hw
                if hw/tw <= 38*eps_CSC/alpha:
                    M_pl = 0.85*tc*bc*fck*(y1_0-tc/2)\
                    +bfu*tfu*sig_cm*(y1_0-tc-tfu/2)\
                    +tw*(y1_0-tc-tfu)**2*sig_cm/2\
                    +tw*(htot-tfl-y1_0)**2*sig_tm/2\
                    +tfl*bfl*sig_tm*(htot-y1_0-tfl/2)
                else:
                    print('Web not in CSC 1 or 2, Elastic response')
                    break

            # Corrugated web
            else:
                M_pl = 0.85*tc*bc*fck*(y1_0-tc/2)\
                +bfu*tfu*sig_cm*(y1_0-tc-tfu/2)\
                +tw*(y1_0-tc-tfu)**2*sig_cm/2\
                +tw*(htot-tfl-y1_0)**2*sig_tm/2\
                +tfl*bfl*sig_tm*(htot-y1_0-tfl/2)
```

```
                    # Neutral axis in the flange
                    else:
                        M_pl = 0.85*tc*bc*fck*(y1_0-tc/2)\
                        +bfu*(y1_0-tc)**2*sig_cm/2\
                        +bfu*(tc+tfu-y1_0)**2*sig_tm/2\
                        +tw*hw*sig_tm*(htot-tfl-hw/2-y1_0)\
                        +tfl*bfl*sig_tm*(htot-y1_0-tfl/2)
                    break

                # Continue itteration
                else:
                    y1_0 = y1_0+0.01
                    y1_0 = round(y1_0,2)

        # Output
        self.M_pl = M_pl/1000000
        self.y1_0 = y1_0
```

## B.3 Design tool module

```
# Master's Thesis
#
# Design Tool for Ultimate Bending Resistance of a Steel-Concrete Composite Beam
#
# Albin Karlsson & Gustav Friman
# June 2023
#
# ------------------------------------------------------------------------------
# DESIGN TOOL MODULE
#
#   Contents
#   0. Import Modules
#   1. Input data
#       1.1 Geometrical input data
#       1.2 Material imput data
#       1.3 Calculation input data
#   2. Parameters
#   3. Moment capacity calculation
#   4. Printing results
#
# ------------------------------------------------------------------------------

################################################################################
# 0. IMPORT MODULES
################################################################################

# General modules
import numpy as np
import pandas as pd
import matplotlib.pyplot as plt

# Modules developed for this thesis
import DesignFunctions as fun # Includes equations used for the calulations
import MaterialClass as mtrl # Includes material parameters for the different
                             # materials from Eurocode standards

################################################################################
# 1. INPUT DATA
################################################################################

# ------------------------------------------------------------------------------
# 1.1 Geometrical input data
#
# Corrugation figure:
#                   _____a1____          _
#                 /           \        |
```

```
#              a2/              \      |a3
#    ___________/_\alpha         \____|_______
#                |--|----------|
#                 a4     a1
#                |-------------|
#                       w
# ------------------------------------------------------------------------------
# Cross-Section
bfu = 300                        # Widths of upper flange                [float, mm]
tfu = 20                         # Thickness of upper flange             [float, mm]
bfl = 320                        # Widths of lower flange                [float, mm]
tfl = 20                         # Thickness of lower flange             [float, mm]
tw = 8                           # Thickness of web                      [float, mm]
hw = 1000                        # Height of web                         [float, mm]
tc = 100                         # Thickness of concrete slab            [float, mm]
A_steel = bfu*tfu+bfl*tfl+tw*hw

# Corrugation
WebShape = 'F'                  # 'C' for Corrugated or 'F' for Flat web [string, -]

Accordion = False             # True = Partial web contibution for corrugaterd webs,
                             # False = No web contribution for corrugated webs

alpha = 36                       # Corrugation angle of inclined part [float, degree]
a1 = 120                         # Flat fold length                      [float, mm]
a3 = 50                          # Corrugation depth                     [float, mm]

#Effective concrete width
Pick_bc = True                    # Ture = Prescribed effective cocnrete width,
                                  # False = Calculating effective concrete width

bc_pick = 1980                    # Presicribed concrete width            [float, mm]

# Dimension for calculation of effective concrete width (Pick_bc = False)
#Studs
b0 = (bfu-50)-20                  # Transverse C-C distance of the shear studs

L = 7000                          # Span                                  [float, mm]
girder_edge = True                # True = girder is at the edge,
                                  # False = girder is in the middle with no adjecent
                                  # edge
girder_space = 4000               # Girder spacing
girder_space_edge = 1500          # Girder spacing to the edge

# ------------------------------------------------------------------------------
# 1.2 Material input data
# ------------------------------------------------------------------------------
# SteelGrade, Both Stainless and Carbon
SteelType = 'SS'                  #'SS' for Stainless or 'CS' for Carbon  [string, -]
SteelCurve = 'Py'                 #'Py' for Python (material models)or 'Ex' for Excel
                                  # (test data)                           [string, -]

SteelGrade = '1.4162'             # Stainless or Carbon                 [string, -],
                                  # [see available grades in "MaterialClass.py"]
ProductForm = 'HotRolledPlate'    # Stainless manufacturing             [string, -],
                                  # [ColdRolledStip, HotRolledStrip,
                                  # HotRolledPlate, Bars/Rods/Sections

# Concrete
ConcreteGrade = 'C40/50'          # Concrete grade                      [string, -],
                                  # [see available grades in "MaterialClass.py"]

# ------------------------------------------------------------------------------
# 1.3 Calculation input data
# ------------------------------------------------------------------------------
# Calculation model
CalcModel = 'SH'              # 'EC' for EuroCode(EPP) and 'SH' for Strain hardening
er = 1e4                      # Allowed difference in the internal forces for
                              # capacity calculation                  [float, mm]
```

```
#############################################################################################
# 2. PARAMETERS
#############################################################################################
# For the result printing layout
print('#########################################################################')

# Effective concrete
EffConc = fun.EffConcWidth(b0,L,girder_space,girder_space_edge,girder_edge)
bc = EffConc.b_eff
if Pick_bc:
    bc = bc_pick

# Import material parameters from "MaterialClass.py"
MtrlPar_c = mtrl.Concrete(ConcreteGrade)
if SteelType == 'CS' and SteelCurve == 'Py':
    MtrlPar_cs = mtrl.CarbonSteel(SteelGrade,tw)
elif SteelType == 'SS' and SteelCurve == 'Py':
    MtrlPar_ss = mtrl.StainlessSteel(SteelGrade,tw,ProductForm)
    StainlessType = MtrlPar_ss.StainlessType
elif SteelCurve == 'Ex':
    MtrlPar_ex = mtrl.SteelDataEx()
else:
    print('Choose a correct input for "SteelType", and "SteelCurve"')

# Concrete parameters
eps_cu = MtrlPar_c.eps_cu

fck = MtrlPar_c.fck
Ec = MtrlPar_c.Ecm

# Start value in case of unused parameters
M_data = 0
eps_su = 0
r_2 = 0
r_s = 0
p_s = 0
r = 0
p = 0

# Parameters for stainless steel and Abdella material behaviour
if SteelType == 'SS' and SteelCurve == 'Py':

    # Material parameters
    fy = MtrlPar_ss.fy
    fu = MtrlPar_ss.fu
    E = MtrlPar_ss.E
    A = MtrlPar_ss.A
    n = MtrlPar_ss.n

    # Abdella parameters
    Abdella = fun.Abdella(fy,fu,E,A,n,StainlessType)
    r_2 = Abdella.r_2
    r_s = Abdella.r_s
    p_s = Abdella.p_s
    r = Abdella.r
    p = Abdella.p
    eps_su = Abdella.eps_su
    eps_y = Abdella.eps_02

# Material behaviour parameters from test data, excel
elif SteelCurve == 'Ex':
    fy = MtrlPar_ex.fy
    fu = MtrlPar_ex.fu
    E = MtrlPar_ex.E

    eps_su = MtrlPar_ex.eps_su
    eps_y = MtrlPar_ex.eps_02
    M_data = MtrlPar_ex.M_data

# Parameters for carbon steel
```

```
else: # SteelType == 'CS' and SteelCurve == 'Py'
    fy = MtrlPar_cs.fy
    fu = MtrlPar_cs.fu
    E = MtrlPar_cs.E
    eps_y = fy/E
    eps_su = 1

# Web geometry
WebGeo = fun.WebGeometry(WebShape,Accordion,a1,a3,alpha,bfu,bfl,hw,tw,fy,E)
tw = WebGeo.tw

# Cross section geometry
CrossSecGeo = fun.SectionGeometry(bfu,tfu,bfl,tfl,tw,hw,tc,bc,E,Ec)
htot = CrossSecGeo.htot
hs = CrossSecGeo.hs
As = CrossSecGeo.As
z_tp_s = CrossSecGeo.z_tp_s
Iy = CrossSecGeo.Iy
################################################################################
# 3. MOMENT CALCULATION
################################################################################

# Moment capacity calculations
if SteelType == 'CS' or CalcModel == 'EC':
    MomCalc = fun.MomentCalcEC(er,E,htot,tc,bc,tfu,bfu,tfl,bfl,tw,hw,As,fy,fck,
                               z_tp_s,SteelType,WebShape)
else:
    MomCalc = fun.MomentCalcSH(er,E,eps_cu,eps_su,eps_y,htot,hs,tc,bc,tfu,bfu,tfl,
                               bfl,tw,hw,As,fy,fck,r_2,r_s,p_s,r,p,z_tp_s,
                               SteelCurve,WebShape,M_data)

################################################################################
# 4. PRINTING RESULTS
################################################################################

# Print results
if MomCalc.M_pl != 0:
    print('##########################################################################')
    print('TOOL OUTPUTS')
    print('##########################################################################')
    print('--------------------------------------------------------------------------')
    print('Geometry')
    print('--------------------------------------------------------------------------')

    print('A_steel =',A_steel, 'mm^2')
    print('Iy = ',Iy/1000000000000, 'mm^4')
    print('tw_eff = ',tw, 'mm')
    print('bc_eff = ', bc, 'mm')

    print('--------------------------------------------------------------------------')
    print('Results')
    print('--------------------------------------------------------------------------')
    print('fy =',fy, 'MPa')
    print('fu =',fu, 'MPa')
    if SteelType == 'SS' and CalcModel == 'SH':
        print('Tensile stress at 0.6 =',MomCalc.sig_m, 'MPa')
        print('Tensile stress at bottom =',MomCalc.sig_S, 'MPa')
    else:
        print('Reduction factor for reduced plastic response =', MomCalc.beta)
    print('NA = ',MomCalc.y1_0, 'mm')
    print('M_pl = ',MomCalc.M_pl, 'kNm')
    print('##########################################################################')
else:
    print('##########################################################################')
```

# C
# Material data

## C.1 Concrete

**Table C.1:** *Material data for the concrete used by Zhou et al. (2021) in compression*

| $f_{cm}$ | | 50 | MPa |
|---|---|---|---|
| $E_{cm}$ | | 35654 | MPa |
| $\sigma$ $[MPa]$ | $\varepsilon$ $[-]$ | $\varepsilon_{inelastic}$ $[-]$ | $d_t$ $[-]$ |
| 0 | 0 | 0 | 0.0000 |
| 8.514424514 | 0.000235385 | -3.41903E-06 | 0.0000 |
| 16.40370113 | 0.00047077 | 1.06955E-05 | 0.0000 |
| 23.61985564 | 0.000706155 | 4.3689E-05 | 0.0000 |
| 30.1098762 | 0.00094154 | 9.70484E-05 | 0.0000 |
| 35.81503428 | 0.001176925 | 0.000172421 | 0.0000 |
| 40.67009276 | 0.00141231 | 0.000271636 | 0.0000 |
| 44.60237851 | 0.001647695 | 0.000396732 | 0.0000 |
| 47.53069191 | 0.00188308 | 0.000549987 | 0.0000 |
| 49.36401852 | 0.002118465 | 0.000733952 | 0.0000 |
| 50 | 0.00235385 | 0.0009515 | 0.0000 |
| 49.35858558 | 0.00258308 | 0.00119872 | 0.0128 |
| 47.35145739 | 0.00281231 | 0.001484244 | 0.0530 |
| 43.84183636 | 0.00304154 | 0.001811908 | 0.1232 |
| 38.67404766 | 0.00327077 | 0.002186079 | 0.2265 |
| 31.67014097 | 0.0035 | 0.002611748 | 0.3666 |
| 28.75682464 | 0.00358 | 0.002773458 | 0.4249 |
| 25.58572799 | 0.00366 | 0.002942397 | 0.4883 |
| 22.14682065 | 0.00374 | 0.003118848 | 0.5571 |
| 18.42954504 | 0.00382 | 0.003303107 | 0.6314 |
| 14.42278126 | 0.0039 | 0.003495484 | 0.7115 |

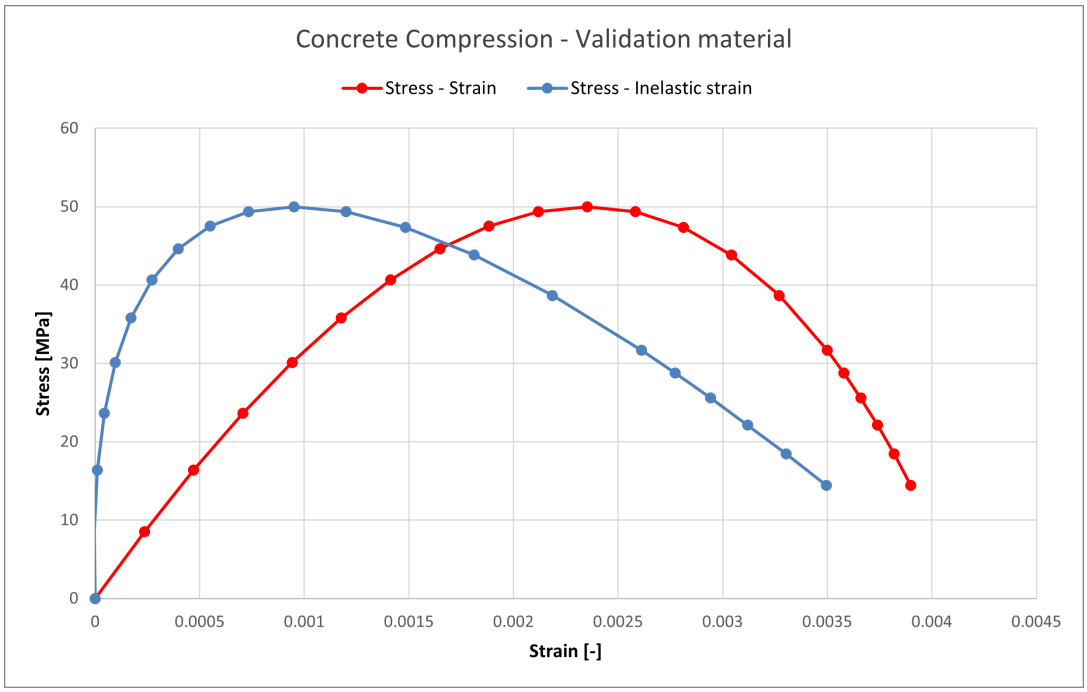


**Figure C.1:** *Stress-strain curves for the concrete used by Zhou et al. (2021) in compression*

**Table C.2:** *Material data for the concrete used by Zhou et al. (2021) in tension*

| | | |
|---|---|---|
| $G_F$ | 0.1476 | N/mm |
| $f_{ctm}$ | 3.62 | MPa |
| h | 50 | mm |
| $\sigma$ $[MPa]$ | $\varepsilon$ $[-]$ | $d_t$ $[-]$ |
| 3.6248 | 0 | 0 |
| 3.2623 | 0.0001629 | 0.1 |
| 2.8999 | 0.0003258 | 0.2 |
| 2.5374 | 0.0004887 | 0.3 |
| 2.1749 | 0.0006516 | 0.4 |
| 1.8124 | 0.0008145 | 0.5 |
| 1.4499 | 0.0009774 | 0.6 |
| 1.0874 | 0.0011403 | 0.7 |
| 0.7250 | 0.0013032 | 0.8 |
| 0.3625 | 0.0014661 | 0.9 |
| 0.0362 | 0.0016127 | 0.99 |

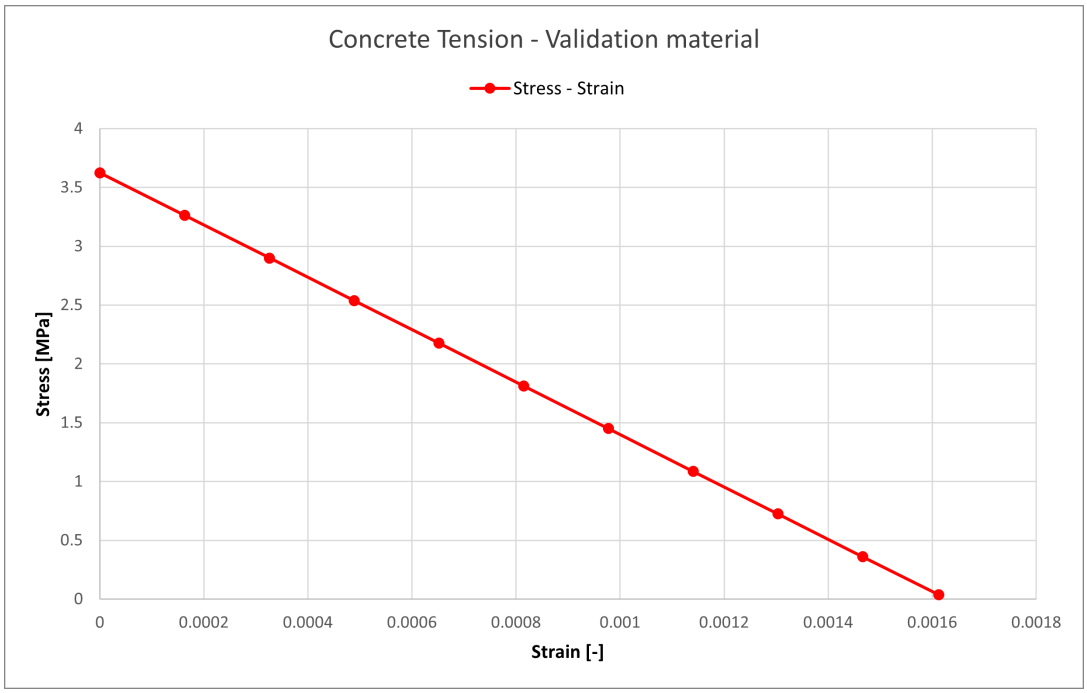


**Figure C.2:** *Stress-strain curves for the concrete used by Zhou et al. (2021) in tension*

**Table C.3:** *Material data for the concrete grade C40/50 in compression*

| $f_{cm}$ | 48 | MPa |
|---|---|---|
| $E_{cm}$ | 35220 | MPa |
| $\sigma$ $[MPa]$ | $\varepsilon$ $[-]$ | $\varepsilon_{inelastic}$ $[-]$ | $d_t$ $[-]$ |
| 0 | 0 | 0 | 0 |
| 8.288897443 | 0.000232425 | -2.91824E-06 | 0 |
| 15.93796529 | 0.00046485 | 1.23299E-05 | 0 |
| 22.90433985 | 0.000697275 | 4.69615E-05 | 0 |
| 29.14124126 | 0.0009297 | 0.000102305 | 0 |
| 34.59751579 | 0.001162125 | 0.000179812 | 0 |
| 39.21711242 | 0.00139455 | 0.000281075 | 0 |
| 42.9384824 | 0.001626975 | 0.00040784 | 0 |
| 45.69388826 | 0.0018594 | 0.000562032 | 0 |
| 47.40860591 | 0.002091825 | 0.000745772 | 0 |
| 48 | 0.00232425 | 0.000961406 | 0 |
| 47.36153785 | 0.0025594 | 0.001214683 | 0.013301295 |
| 45.37389328 | 0.00279455 | 0.001506268 | 0.054710557 |
| 41.91921111 | 0.0030297 | 0.001839505 | 0.126683102 |
| 36.86549786 | 0.00326485 | 0.002218143 | 0.231968795 |
| 30.064436 | 0.0035 | 0.002646393 | 0.373657583 |
| 27.32317691 | 0.00358 | 0.002804224 | 0.430767148 |
| 24.35336977 | 0.00366 | 0.002968545 | 0.49263813 |
| 21.14756752 | 0.00374 | 0.003139566 | 0.559425677 |
| 17.69799605 | 0.00382 | 0.003317508 | 0.631291749 |
| 13.99653598 | 0.0039 | 0.003502602 | 0.708405501 |

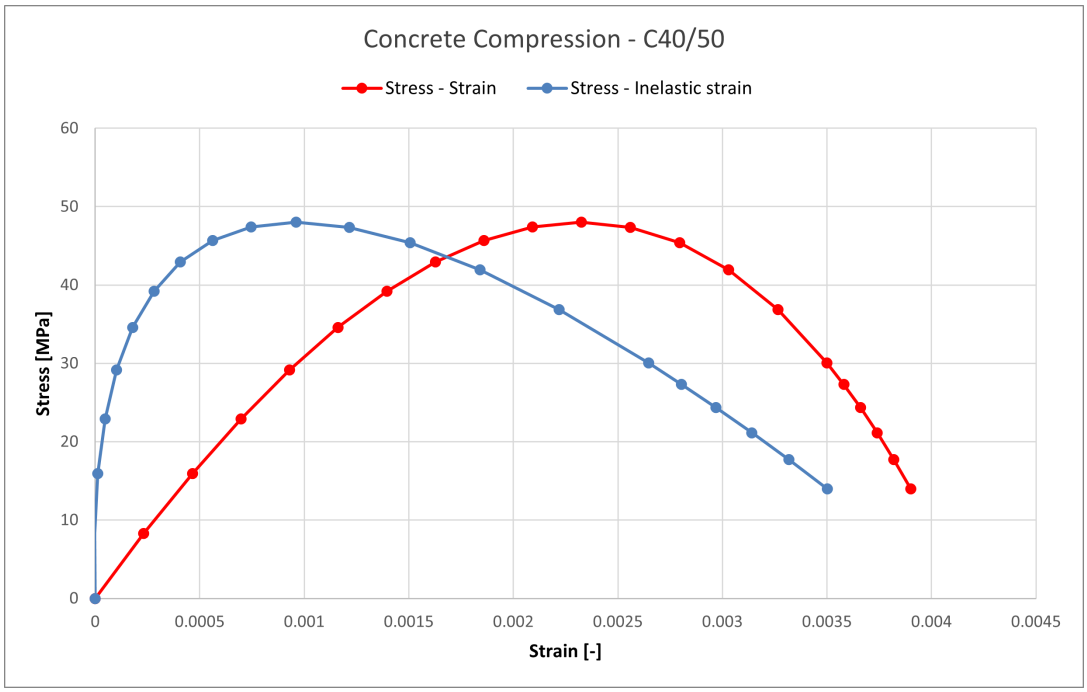


**Figure C.3:** *Stress-strain curves for the concrete grade C40/50 in compression*

**Table C.4:** *Material data for the concrete grade C40/50 in tension*

| | | |
|---|---|---|
| $G_F$ | 0.1465 | N/mm |
| $f_{ctm}$ | 3.51 | MPa |
| h | 50 | mm |
| $\sigma$ $[MPa]$ | $\varepsilon$ $[-]$ | $d_t$ $[-]$ |
| 3.5088 | 0 | 0 |
| 3.1579 | 0.00017 | 0.1 |
| 2.8071 | 0.00033 | 0.2 |
| 2.4562 | 0.00050 | 0.3 |
| 2.1053 | 0.00067 | 0.4 |
| 1.7544 | 0.00084 | 0.5 |
| 1.4035 | 0.00100 | 0.6 |
| 1.0526 | 0.00117 | 0.7 |
| 0.7018 | 0.00134 | 0.8 |
| 0.3509 | 0.00150 | 0.9 |
| 0.0351 | 0.00165 | 0.99 |

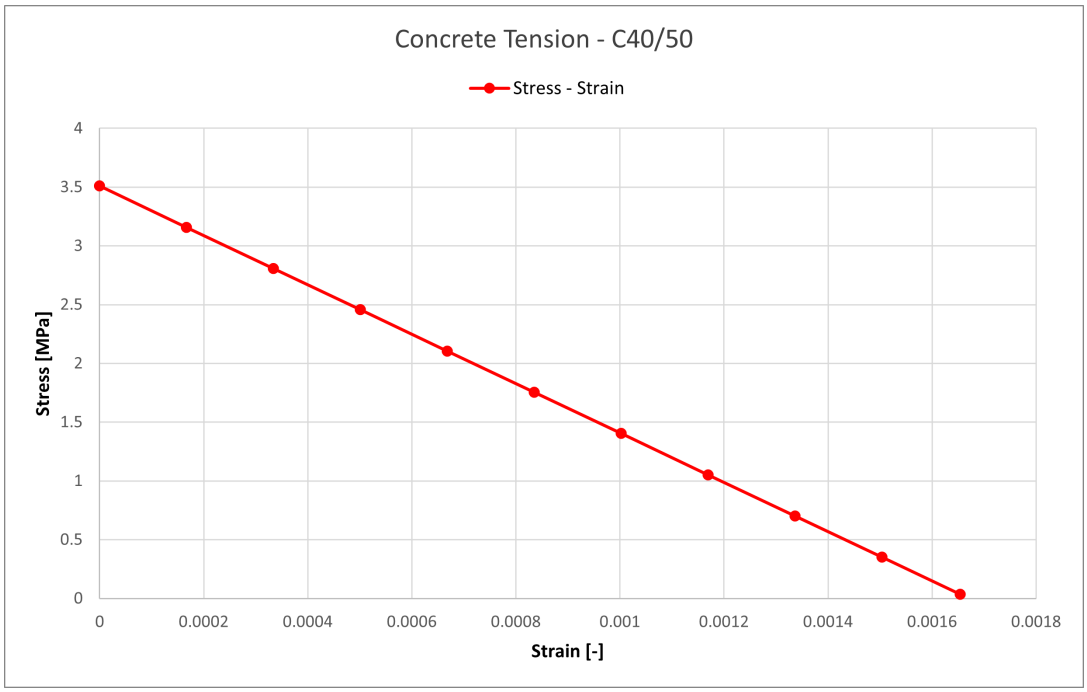


**Figure C.4:** *Stress-strain curves for the concrete grade C40/50 in tension*

## C.2 Carbon steel

**Table C.5:** *Material data for the reinforcement carbon steel B500B*

| | | |
|---|---|---|
| $f_y$ | 500 | MPa |
| $f_u$ | 540 | MPa |
| $E$ | 200000 | MPa |

| $\sigma\ [MPa]$ | $\varepsilon\ [-]$ | $\sigma_{true}\ [MPa]$ | $\varepsilon_{true}\ [-]$ | $\varepsilon_{true,pl}\ [-]$ |
|---|---|---|---|---|
| 0 | 0 | 0 | 0 | 0 |
| 500 | 0.0025 | 501.250 | 0.00249688 | 0 |
| 540 | 0.0227 | 552.258 | 0.022446189 | 0.01968490 |

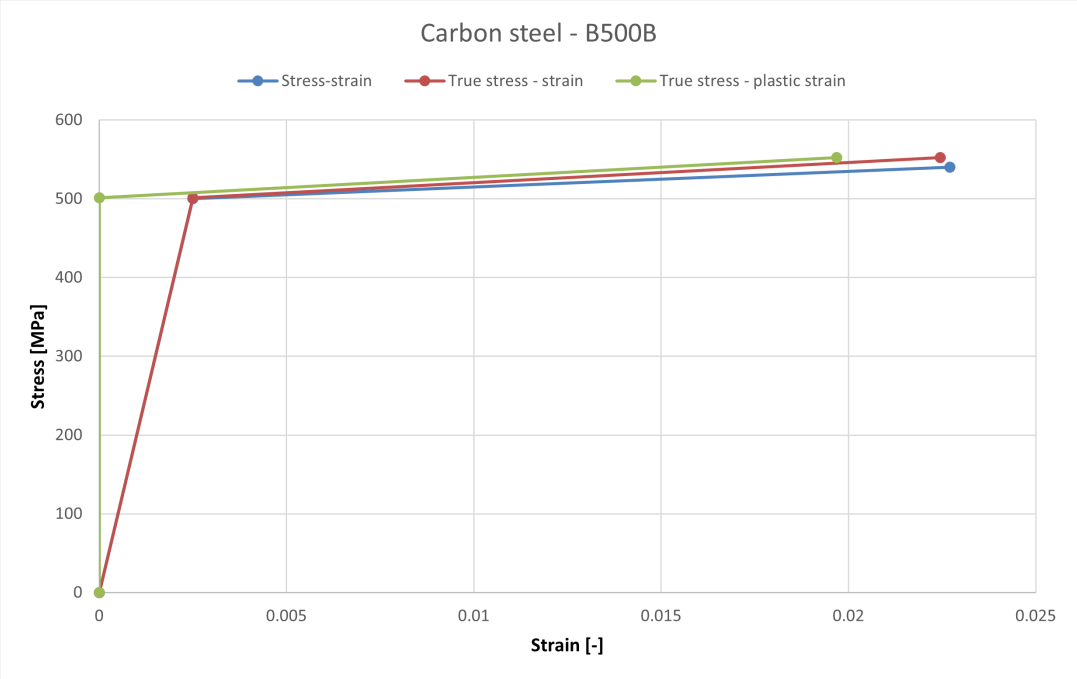


**Figure C.5:** *Stress-strain curves for the reinforcement carbon steel B500B*

**Table C.6:** *Material data for the structural carbon steel S460*

| | | |
|---|---|---|
| $f_y$ | 460 | MPa |
| $f_u$ | 540 | MPa |
| $E$ | 210000 | MPa |

| $\sigma\ [MPa]$ | $\varepsilon\ [-]$ | $\sigma_{true}\ [MPa]$ | $\varepsilon_{true}\ [-]$ | $\varepsilon_{true,pl}\ [-]$ |
|---|---|---|---|---|
| 0 | 0 | 0.00 | 0 | 0 |
| 460 | 0.002190476 | 461.01 | 0.002188081 | 0 |
| 540 | 0.040666667 | 561.96 | 0.039861533 | 0.037185533 |

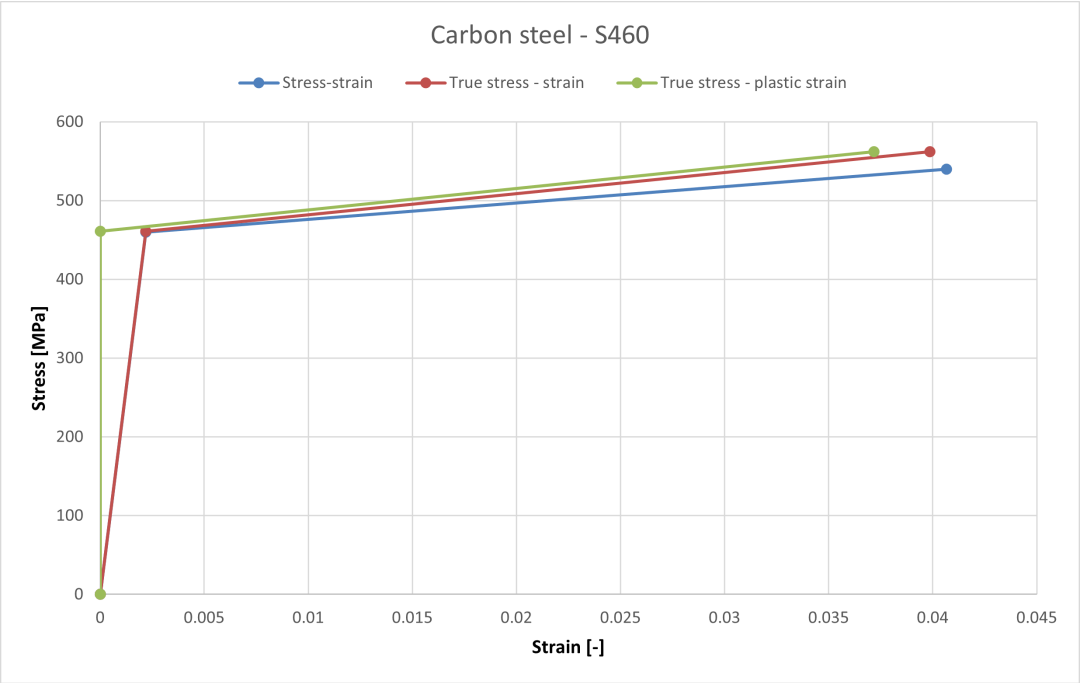


**Figure C.6:** *Stress-strain curves for the structural carbon steel S460*

## C.3 Stainless steel

**Table C.7:** *Material data for the structural stainless steel used by Zhou et al. (2021) in the web*

| | | |
|---|---|---|
| $f_y$ | 500 | MPa |
| $f_u$ | 718 | MPa |
| $E$ | 191000 | MPa |
| $A$ | 36 | % |
| $n$ | 8.01 | % |
| $m$ | 3.44 | % |
| $\varepsilon_{su}$ | 0.36 | [-] |

| $\sigma\ [MPa]$ | $\varepsilon\ [-]$ | $\sigma_{true}\ [MPa]$ | $\varepsilon_{true}\ [-]$ | $\varepsilon_{true,pl}\ [-]$ |
|---|---|---|---|---|
| 0 | 0 | 0 | 0 | 0 |
| 58.39561307 | 0.000307853 | 58.41 | 0.000307806 | 1.97571E-06 |
| 114.9469002 | 0.000615707 | 115.02 | 0.000615517 | 1.33306E-05 |
| 168.5334571 | 0.00092356 | 168.69 | 0.000923134 | 3.99449E-05 |
| 218.3985951 | 0.001231414 | 218.67 | 0.001230656 | 8.57998E-05 |
| 264.0684643 | 0.001539267 | 264.47 | 0.001538084 | 0.000153398 |
| 305.3028001 | 0.00184712 | 305.87 | 0.001845417 | 0.00024402 |
| 342.0493068 | 0.002154974 | 342.79 | 0.002152655 | 0.000357962 |
| 374.4000354 | 0.002462827 | 375.32 | 0.002459799 | 0.000494762 |
| 402.5514817 | 0.002770681 | 403.67 | 0.002766849 | 0.000653411 |
| 426.7700205 | 0.003078534 | 428.08 | 0.003073805 | 0.000832528 |
| 447.3634799 | 0.003386387 | 448.88 | 0.003380667 | 0.001030518 |
| 464.6588903 | 0.003694241 | 466.38 | 0.003687434 | 0.001245678 |
| 478.9858986 | 0.004002094 | 480.90 | 0.003994107 | 0.001476291 |
| 490.6650452 | 0.004309948 | 492.78 | 0.004300686 | 0.001720688 |
| 500 | 0.004617801 | 502.31 | 0.004607172 | 0.001977282 |
| 540.8556075 | 0.008773822 | 545.60 | 0.008735556 | 0.005879006 |
| 557.9203389 | 0.012929843 | 565.13 | 0.012846966 | 0.009888149 |
| 569.42896 | 0.017085864 | 579.16 | 0.016941542 | 0.0139093 |
| 578.2748816 | 0.021241885 | 590.56 | 0.021019421 | 0.017927491 |
| 585.5340026 | 0.025397906 | 600.41 | 0.025080738 | 0.021937255 |
| 591.7312407 | 0.029553927 | 609.22 | 0.029125628 | 0.025935998 |
| 597.164025 | 0.033709948 | 617.29 | 0.033154222 | 0.029922314 |
| 602.0179849 | 0.037865969 | 624.81 | 0.037166652 | 0.033895374 |
| 606.4171355 | 0.04202199 | 631.90 | 0.041163046 | 0.037854669 |
| 610.44864 | 0.04617801 | 638.64 | 0.045143533 | 0.041799879 |
| 649.9906563 | 0.108942408 | 720.80 | 0.103406776 | 0.099632942 |
| 673.7367725 | 0.171706806 | 789.42 | 0.158461495 | 0.154328395 |
| 691.4283247 | 0.234471204 | 853.55 | 0.210642704 | 0.206173864 |
| 705.7875042 | 0.297235602 | 915.57 | 0.26023554 | 0.255441966 |
| 718 | 0.36 | 976.48 | 0.3074847 | 0.302372239 |

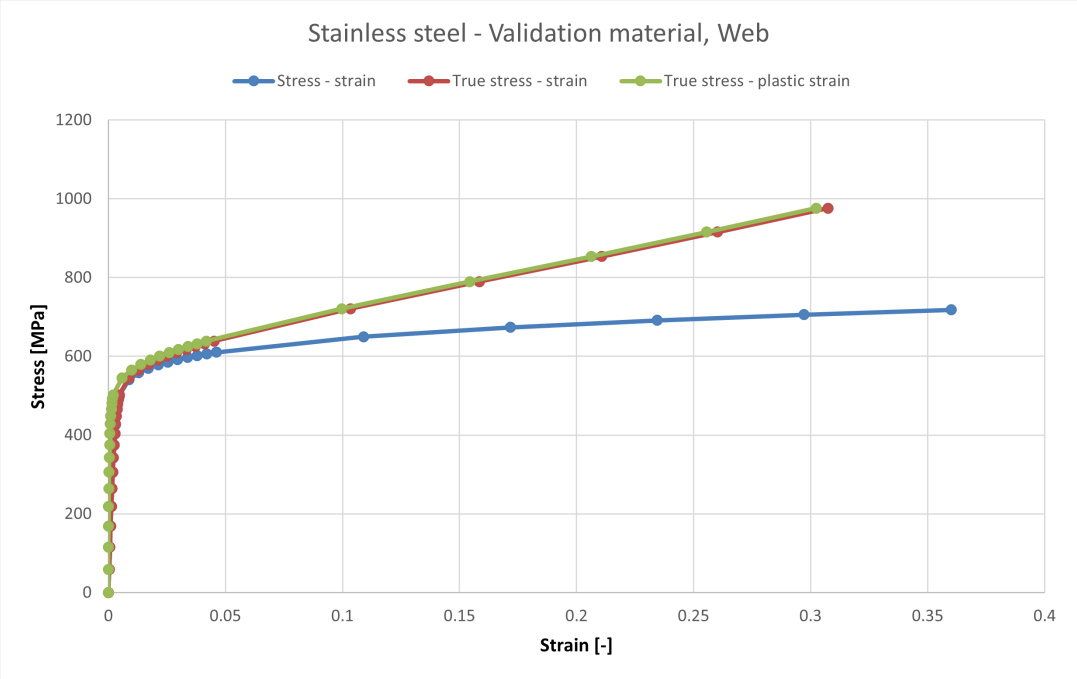


**Figure C.7:** *Stress-strain curves for the structural stainless steel used by Zhou et al. (2021) in the web*

**Table C.8:** *Material data for the structural stainless steel used by Zhou et al. (2021) in the flanges*

| | | |
|---|---|---|
| $f_y$ | 490 | MPa |
| $f_u$ | 673 | MPa |
| $E$ | 201000 | MPa |
| $A$ | 29 | % |
| $n$ | 7.08 | % |
| $m$ | 3.55 | % |
| $\varepsilon_{su}$ | 0.29 | [-] |

| $\sigma\ [MPa]$ | $\varepsilon\ [-]$ | $\sigma_{true}\ [MPa]$ | $\varepsilon_{true}\ [-]$ | $\varepsilon_{true,pl}\ [-]$ |
|---|---|---|---|---|
| 0 | 0 | 0.00 | 0 | 0 |
| 58.87500649 | 0.000295854 | 58.89 | 0.00029581 | 2.81317E-06 |
| 115.3561168 | 0.000591708 | 115.42 | 0.000591533 | 1.72825E-05 |
| 168.3103838 | 0.000887562 | 168.46 | 0.000887169 | 4.90602E-05 |
| 217.0929786 | 0.001183416 | 217.35 | 0.001182717 | 0.000101374 |
| 261.3843084 | 0.00147927 | 261.77 | 0.001478177 | 0.000175834 |
| 301.1018908 | 0.001775124 | 301.64 | 0.001773551 | 0.000272872 |
| 336.3333883 | 0.002070978 | 337.03 | 0.002068837 | 0.000392071 |
| 367.2828078 | 0.002366833 | 368.15 | 0.002364036 | 0.000532433 |
| 394.2278292 | 0.002662687 | 395.28 | 0.002659148 | 0.000692593 |
| 417.4870258 | 0.002958541 | 418.72 | 0.002954173 | 0.000870978 |
| 437.3956384 | 0.003254395 | 438.82 | 0.003249111 | 0.001065931 |
| 454.2884369 | 0.003550249 | 455.90 | 0.003543961 | 0.001275796 |
| 468.4882148 | 0.003846103 | 470.29 | 0.003838725 | 0.001498974 |
| 480.2985925 | 0.004141957 | 482.29 | 0.004133403 | 0.00173396 |
| 490 | 0.004437811 | 492.17 | 0.004427993 | 0.001979363 |
| 529.317034 | 0.008431841 | 533.78 | 0.008396491 | 0.005740869 |
| 544.6533035 | 0.012425871 | 551.42 | 0.012349303 | 0.009605915 |
| 554.8321355 | 0.0164199 | 563.94 | 0.016286552 | 0.013480868 |
| 562.5942459 | 0.02041393 | 574.08 | 0.020208359 | 0.017352245 |
| 568.9333105 | 0.02440796 | 582.82 | 0.024114846 | 0.021215245 |
| 574.3272959 | 0.02840199 | 590.64 | 0.028006132 | 0.025067627 |
| 579.0445085 | 0.03239602 | 597.80 | 0.031882334 | 0.028908188 |
| 583.2512868 | 0.03639005 | 604.48 | 0.035743569 | 0.032736226 |
| 587.0582 | 0.04038408 | 610.77 | 0.039589952 | 0.036551315 |
| 590.5426553 | 0.044378109 | 616.75 | 0.043421598 | 0.040353191 |
| 619.784179 | 0.093502488 | 677.74 | 0.089385836 | 0.086014017 |
| 638.1519822 | 0.142626866 | 729.17 | 0.13332988 | 0.12970217 |
| 652.0186457 | 0.191751244 | 777.04 | 0.175423859 | 0.171557968 |
| 663.3404055 | 0.240875622 | 823.12 | 0.215817277 | 0.211722138 |
| 673 | 0.29 | 868.17 | 0.254642218 | 0.250322965 |

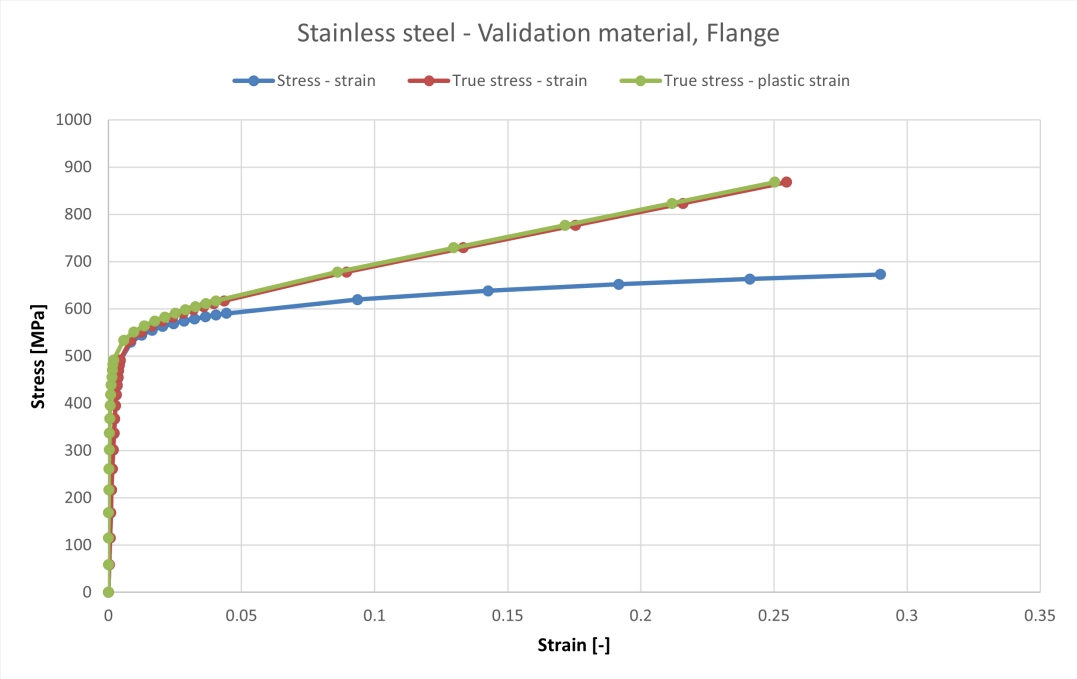


**Figure C.8:** *Stress-strain curves for the structural stainless steel used by Zhou et al. (2021) in the flanges*

**Table C.9:** *Material data for the reinforcement stainless steel used by Zhou et al. (2021)*

| | | |
|---|---|---|
| $f_y$ | 938 | MPa |
| $f_u$ | 1116 | MPa |
| $E$ | 201000 | MPa |
| $A$ | 2.4 | % |
| $n$ | 4.81 | % |
| $m$ | 3.94 | % |
| $\varepsilon_{su}$ | 0.024 | [-] |

| $\sigma\ [MPa]$ | $\varepsilon\ [-]$ | $\sigma_{true}\ [MPa]$ | $\varepsilon_{true}\ [-]$ | $\varepsilon_{true,pl}\ [-]$ |
|---|---|---|---|---|
| 0 | 0 | 0 | 0 | 0 |
| 89.02389157 | 0.000444444 | 89.06 | 0.000444346 | 1.24393E-06 |
| 176.5620866 | 0.000888889 | 176.72 | 0.000888494 | 9.2949E-06 |
| 261.588552 | 0.001333333 | 261.94 | 0.001332445 | 2.92744E-05 |
| 343.3007258 | 0.001777778 | 343.91 | 0.001776199 | 6.51992E-05 |
| 421.0739411 | 0.002222222 | 422.01 | 0.002219757 | 0.000120206 |
| 494.4425507 | 0.002666667 | 495.76 | 0.002663117 | 0.000196644 |
| 563.0846473 | 0.003111111 | 564.84 | 0.003106282 | 0.00029615 |
| 626.8063617 | 0.003555556 | 629.04 | 0.00354925 | 0.000419722 |
| 685.5252297 | 0.004 | 688.27 | 0.003992021 | 0.000567806 |
| 739.2530841 | 0.004444444 | 742.54 | 0.004434597 | 0.000740375 |
| 788.0791581 | 0.004888889 | 791.93 | 0.004876977 | 0.000937017 |
| 832.154033 | 0.005333333 | 836.59 | 0.005319161 | 0.001157011 |
| 871.6749171 | 0.005777778 | 876.71 | 0.00576115 | 0.001399403 |
| 906.8725666 | 0.006222222 | 912.52 | 0.006202944 | 0.001663067 |
| 938 | 0.006666667 | 944.25 | 0.006644543 | 0.001946765 |
| 970.5682181 | 0.007333333 | 977.69 | 0.007306575 | 0.002442467 |
| 992.1125293 | 0.008 | 1000.05 | 0.00796817 | 0.002992799 |
| 1008.215597 | 0.008666667 | 1016.95 | 0.008629327 | 0.003569857 |
| 1020.997117 | 0.009333333 | 1030.53 | 0.009290047 | 0.00416305 |
| 1031.540391 | 0.01 | 1041.86 | 0.009950331 | 0.004766969 |
| 1040.477628 | 0.010666667 | 1051.58 | 0.010610179 | 0.005378457 |
| 1048.210034 | 0.011333333 | 1060.09 | 0.011269592 | 0.005995514 |
| 1055.007781 | 0.012 | 1067.67 | 0.011928571 | 0.00661679 |
| 1061.061136 | 0.012666667 | 1074.50 | 0.012587116 | 0.007241338 |
| 1066.508892 | 0.013333333 | 1080.73 | 0.013245227 | 0.007868466 |
| 1080.94145 | 0.015466667 | 1097.66 | 0.015348277 | 0.009887282 |
| 1092.232274 | 0.0176 | 1111.46 | 0.017446914 | 0.011917284 |
| 1101.468695 | 0.019733333 | 1123.20 | 0.019541155 | 0.013953074 |
| 1109.264994 | 0.021866667 | 1133.52 | 0.02163102 | 0.015991613 |
| 1116 | 0.024 | 1142.78 | 0.023716527 | 0.018031034 |

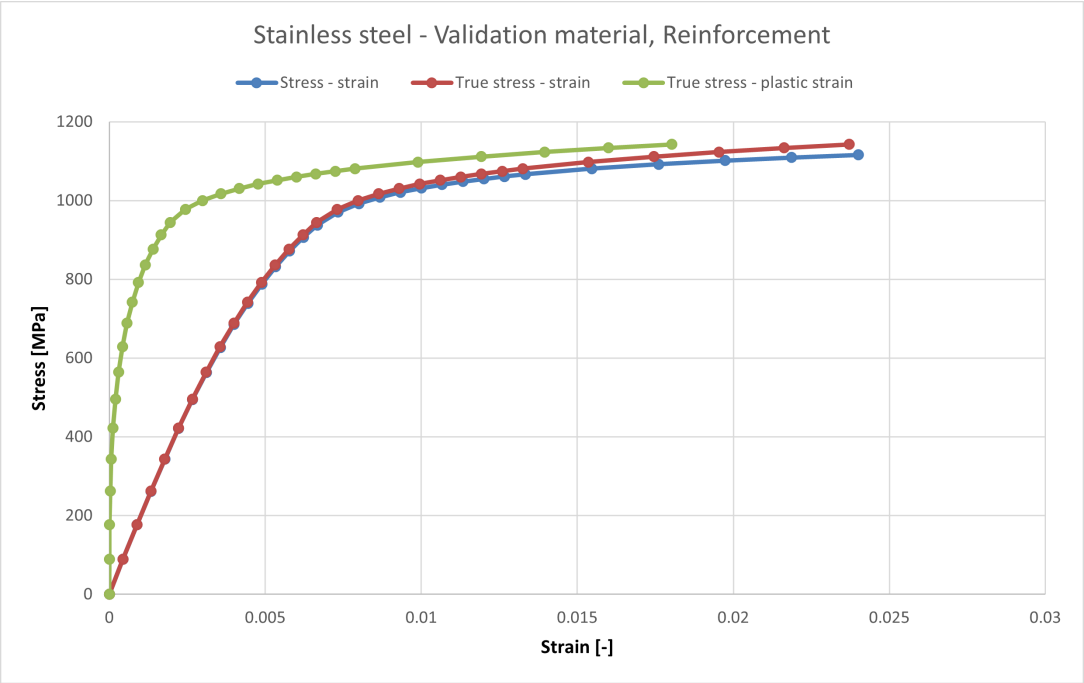


**Figure C.9:** *Stress-strain curves for the reinforcement stainless steel used by Zhou et al. (2021)*

**Table C.10:** *Material data for the structural steel 1.4162*

| | | |
|---|---|---|
| $f_y$ | 450 | MPa |
| $f_u$ | 650 | MPa |
| $E$ | 200000 | MPa |
| $A$ | 30 | % |
| $n$ | 8 | % |
| $m$ | 2.94 | % |
| $\varepsilon_{su}$ | 0.3 | [-] |

| $\sigma\ [MPa]$ | $\varepsilon\ [-]$ | $\sigma_{true}\ [MPa]$ | $\varepsilon_{true}\ [-]$ | $\varepsilon_{true,pl}\ [-]$ |
|---|---|---|---|---|
| 0 | 0 | 0 | 0 | 0 |
| 56.06363672 | 0.000283333 | 56.07952141 | 0.000283293 | 2.89559E-06 |
| 109.6814985 | 0.000566667 | 109.7436514 | 0.000566506 | 1.77879E-05 |
| 159.7022653 | 0.00085 | 159.8380123 | 0.000849639 | 5.04489E-05 |
| 205.488631 | 0.001133333 | 205.7215181 | 0.001132692 | 0.000104084 |
| 246.7464521 | 0.001416667 | 247.0960096 | 0.001415664 | 0.000180184 |
| 283.4288719 | 0.0017 | 283.910701 | 0.001698557 | 0.000279003 |
| 315.6626748 | 0.001983333 | 316.2887391 | 0.001981369 | 0.000399925 |
| 343.6894885 | 0.002266667 | 344.468518 | 0.002264102 | 0.000541759 |
| 367.8198924 | 0.00255 | 368.7578332 | 0.002546754 | 0.000702965 |
| 388.3989645 | 0.002833333 | 389.4994282 | 0.002829327 | 0.00088183 |
| 405.7815502 | 0.003116667 | 407.0462361 | 0.00311182 | 0.001076589 |
| 420.3154045 | 0.0034 | 421.7444768 | 0.003394233 | 0.001285511 |
| 432.3304238 | 0.003683333 | 433.9228409 | 0.003676566 | 0.001506952 |
| 442.1324004 | 0.003966667 | 443.8861922 | 0.00395882 | 0.001739389 |
| 450 | 0.00425 | 451.9125 | 0.004240994 | 0.001981432 |
| 482.4057271 | 0.008075 | 486.3011534 | 0.008042572 | 0.005611066 |
| 496.6497769 | 0.0119 | 502.5599093 | 0.011829752 | 0.009316952 |
| 506.6282422 | 0.015725 | 514.5949713 | 0.015602643 | 0.013029668 |
| 514.5035559 | 0.01955 | 524.5621004 | 0.019361353 | 0.016738543 |
| 521.0965343 | 0.023375 | 533.2771658 | 0.023105989 | 0.020439603 |
| 526.815226 | 0.0272 | 541.1446002 | 0.026836654 | 0.024130931 |
| 531.8946305 | 0.031025 | 548.3966614 | 0.030553453 | 0.02781147 |
| 536.4835021 | 0.03485 | 555.1799522 | 0.034256489 | 0.031480589 |
| 540.6824627 | 0.038675 | 561.593357 | 0.037945862 | 0.035137896 |
| 544.5630168 | 0.0425 | 567.706945 | 0.041621675 | 0.03878314 |
| 580.8255714 | 0.094 | 635.4231751 | 0.089840704 | 0.086663588 |
| 604.2129462 | 0.1455 | 692.1259299 | 0.135841223 | 0.132380593 |
| 622.212189 | 0.197 | 744.7879902 | 0.179818427 | 0.176094487 |
| 637.1253092 | 0.2485 | 795.4509485 | 0.221942831 | 0.217965576 |
| 650 | 0.3 | 845 | 0.262364264 | 0.258139264 |

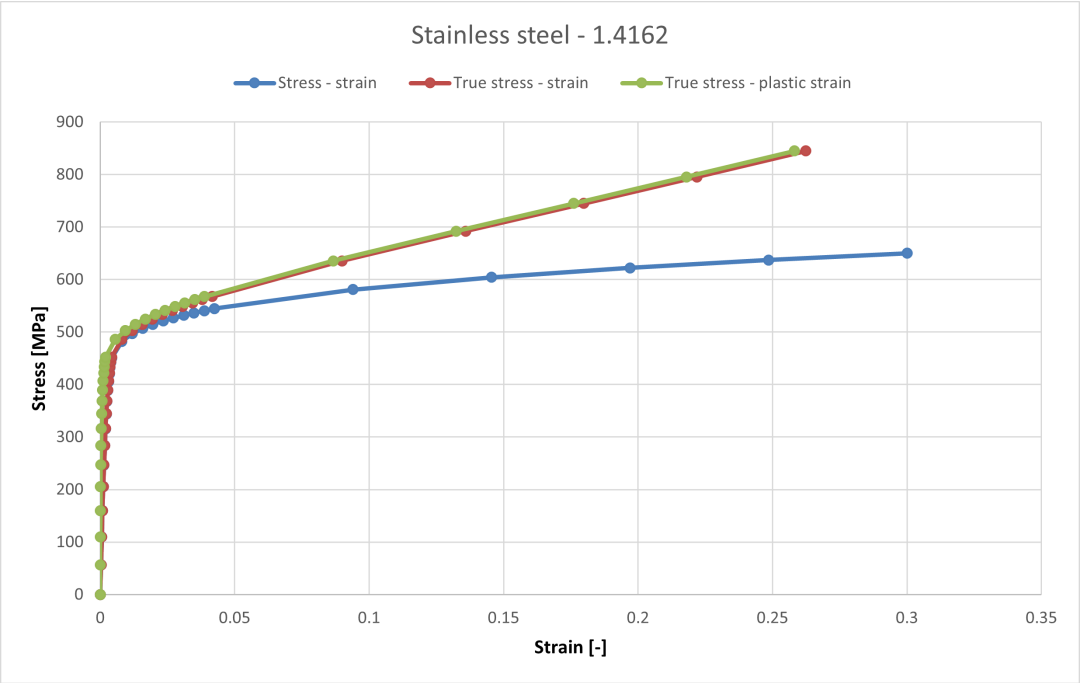


**Figure C.10:** *Stress-strain curves for the structural stainless steel 1.4162*

# D

# Beam designs and results from the tool

## D.1 Beam design results

**Table D.1:** *Geometries and results for beams with corrugated web, stainless steel and strain hardening*

| Beam type | C - SS - CSM | | | |
|---|---|---|---|---|
| Geometry | | | | |
| $b_{fu}$ [mm] | 300 | 465 | 300 | 578 |
| $t_{fu}$ [mm] | 12 | 20 | 12 | 23 |
| $b_{fl}$ [mm] | 496 | 465 | 647 | 578 |
| $t_{fl}$ [mm] | 20 | 20 | 23 | 23 |
| $t_w$ [mm] | 7 | 7 | 5 | 5 |
| $h_w$ [mm] | 1400 | 1400 | 900 | 900 |
| $\alpha$ [°] | 36 | 36 | 36 | 36 |
| $a_1$ [mm] | 95 | 95 | 70 | 70 |
| $a_3$ [mm] | 55 | 55 | 30 | 30 |
| Results | | | | |
| $t_{w,eff}$ [mm] | 0 | 0 | 0 | 0 |
| $A_{steel}$ [mm$^2$] | 23320 | 28400 | 22981 | 31088 |
| $NA$ [mm] | 63.9 | 83.7 | 83.7 | 117.5 |
| $Mpl$ [kNm] | 9991 | 9999 | 9992 | 9992 |
| $\sigma_m$ [MPa] | 563 | 550 | 539 | 526 |
| $\sigma_{max}$ [MPa] | 582 | 567 | 553 | 540 |
| C = Corrugated web, SS = Stainless steel, CSM = Continued strength method | | | | |

**Table D.2:** *Geometries and results for beams with corrugated web, stainless steel, strain hardening and partial web contribution*

| Beam type | C - CS - CSM - PW | | | | |
|---|---|---|---|---|---|
| Geometry | | | | | |
| $b_{fu}$ [mm] | 300 | 506 | 300 | 623 | 300 |
| $t_{fu}$ [mm] | 12 | 20 | 12 | 21 | 12 |
| $b_{fl}$ [mm] | 548 | 506 | 634 | 623 | 575 |
| $t_{fl}$ [mm] | 20 | 20 | 23 | 21 | 40 |
| $t_w$ [mm] | 8 | 8 | 6 | 6 | 8 |
| $h_w$ [mm] | 1200 | 1200 | 900 | 900 | 510 |
| $\alpha$ [°] | 36 | 36 | 36 | 36 | 36 |
| $a_1$ [mm] | 120 | 120 | 90 | 90 | 120 |
| $a_3$ [mm] | 50 | 50 | 50 | 50 | 10 |
| Results | | | | | |
| $t_{w,eff}$ [mm] | 0.8 | 0.8 | 0.6 | 0.6 | 2.8 |
| $A_{steel}$ [mm$^2$] | 24160 | 29840 | 23582 | 31566 | 30680 |
| $NA$ [mm] | 72.1 | 96.4 | 84.7 | 118 | 120 |
| $Mpl$ [kNm] | 10006 | 10001 | 9997 | 9999 | 10008 |
| $\sigma_m$ [MPa] | 553 | 541 | 539 | 526 | 513 |
| $\sigma_{max}$ [MPa] | 569 | 557 | 553 | 540 | 525 |

C = Corrugated web, SS = Stainless steel,
CSM = Continued strength method, PW = Partial web contribution

**Table D.3:** *Geometries and results for beams with corrugated web, stainless steel and elastic perfectly plastic material behaviour*

| Beam type | C - SS - EPP | | | |
|---|---|---|---|---|
| Geometry | | | | |
| $b_{fu}$ [mm] | 300 | 508 | 300 | 541 |
| $t_{fu}$ [mm] | 12 | 21 | 12 | 21 |
| $b_{fl}$ [mm] | 585 | 508 | 627 | 541 |
| $t_{fl}$ [mm] | 20 | 21 | 20 | 21 |
| $t_w$ [mm] | 6 | 6 | 8 | 8 |
| $h_w$ [mm] | 1520 | 1520 | 1400 | 1520 |
| $\alpha$ [°] | 36 | 36 | 36 | 36 |
| $a_1$ [mm] | 90 | 90 | 110 | 110 |
| $a_3$ [mm] | 50 | 50 | 50 | 50 |
| Results | | | | |
| $t_{w,eff}$ [mm] | 0 | 0 | 0 | 0 |
| $A_{steel}$ [mm$^2$] | 24420 | 30456 | 27340 | 33922 |
| $NA$ [mm] | 57.8 | 80.6 | 61 | 85.9 |
| $Mpl$ [kNm] | 9995 | 9992 | 9991 | 10000 |
| $\sigma_m$ [MPa] | 450 | 450 | 450 | 450 |
| $\sigma_{max}$ [MPa] | 450 | 450 | 450 | 450 |
| C = Corrugated web, SS = Stainless steel, EPP = Elastic perfectly plastic | | | | |

**Table D.4:** *Geometries and results for beams with flat webs*

| Beam type | F - SS - CSM | | F - CS - EPP | |
|---|---|---|---|---|
| Geometry | | | | |
| $b_{fu}$ [mm] | 300 | 300 | 300 | 300 |
| $t_{fu}$ [mm] | 12 | 12 | 12 | 12 |
| $b_{fl}$ [mm] | 300 | 300 | 300 | 300 |
| $t_{fl}$ [mm] | 12 | 12 | 12 | 12 |
| $t_w$ [mm] | 12 | 15 | 12 | 15 |
| $h_w$ [mm] | 1194 | 1080 | 1300 | 1199 |
| Results | | | | |
| $t_{w,eff}$ [mm] | 12 | 15 | 12 | 15 |
| $A_{steel}$ [mm$^2$] | 21528 | 23400 | 23232 | 25185 |
| $NA$ [mm] | 97.7 | 105.1 | 89.9 | 97.3 |
| $Mpl$ [kNm] | 10001 | 9999 | 9993 | 9996 |
| $\sigma_m$ [MPa] | 540 | 534 | 460 | 460 |
| $\sigma_{max}$ [MPa] | 556 | 550 | 460 | 460 |
| F = Flat web, SS = Stainless steel, CS = Carbon steel, CSM = Continued strength method, EPP = Elastic perfectly plastic | | | | |

## D.2 Additional validation

**Table D.5:** *Geometries and materials used in test by Zhou et al. (2021) for validation of the design tool*

| Beam | Zhou |
|---|---|
| $t_c$ [mm] | 100 |
| $b_c$ [mm] | 600 |
| $b_{fu}$ [mm] | 90 |
| $t_{fu}$ [mm] | 8 |
| $b_{fl}$ [mm] | 90 |
| $t_{fl}$ [mm] | 8 |
| $h_w$ [mm] | 159 |
| $t_w$ [mm] | 5 |
| $A_{steel}$ [mm$^2$] | 2235 |
| $A_w/Asteel$ | 35.6% |
| $A_{fl}/A_{steel}$ | 32.2% |
| Steel | Experimental (Flange), see Table 6.2 |
| Concrete | Experimental ($f_{ck}$ = 42 MPa) |

**Table D.6:** *Geometries and materials used in simulations by Ali and Abudaher (2022) for validation of the design tool*

| Beam | G1 | | G2 | | 100-262-1 | |
|---|---|---|---|---|---|---|
| | F | C | F | C | F | C |
| $t_c$ [mm] | 181 | | 181 | | 320 | |
| $b_c$ [mm] | 1524 | | 2184.4 | | 4925 | |
| $b_{fu}$ [mm] | 184.2 | | 184.6 | | 800 | 850 |
| $t_{fu}$ [mm] | 19.6 | | 19.6 | | 42 | 45 |
| $b_{fl}$ [mm] | 362 | | 182.6 | | 1200 | 1225 |
| $t_{fl}$ [mm] | 19.7 | | 19.6 | | 55 | 50 |
| $h_w$ [mm] | 758.8 | | 760.4 | | 1953 | 1955 |
| $t_w$ [mm] | 8.5 | | 8.9 | | 17 | 6 |
| $a_1$ [mm] | - | 120 | - | 120 | - | 120 |
| $a_3$ [mm] | - | 70 | - | 70 | - | 70 |
| $\alpha$ [°] | - | 36 | - | 36 | - | 36 |
| $A_{steel}$ [mm$^2$] | 17191.52 | | 13925.48 | | 132801 | 111230 |
| $A_w/A_{steel}$ | 37.5% | | 48.6% | | 25.0% | 10.5% |
| $A_{fl}/A_{steel}$ | 41.5% | | 25.7% | | 49.7% | 55.1% |
| Steel | 1.4162 | | | | | |
| Concrete | C30/37 | | C50/60 | | C35/45 | |

# E

# Finite element simulation results

## E.1 Validation

**Table E.1:** *FE results for the validation*

| **Validation beam** | | |
|---|---|---|
| Displacement ($U_3$) [$mm$] | Load [$kN$] | Moment [$kNm$] |
| 0 | 0 | 0 |
| 0.623086 | 0.999926 | 1.999852 |
| 1.2462 | 1.99971 | 3.99942 |
| 2.18094 | 3.4991 | 6.9982 |
| 3.58319 | 5.74757 | 11.49514 |
| 5.68761 | 9.10826 | 18.21652 |
| 8.84753 | 14.0334 | 28.0668 |
| 13.5902 | 21.2731 | 42.5462 |
| 20.7125 | 31.6373 | 63.2746 |
| 27.8534 | 41.2264 | 82.4528 |
| 29.6439 | 43.4889 | 86.9778 |
| 31.437 | 45.6904 | 91.3808 |
| 33.2315 | 47.8319 | 95.6638 |
| 35.9266 | 50.95 | 101.9 |
| 38.6248 | 53.9424 | 107.8848 |
| 41.3286 | 56.7921 | 113.5842 |
| 45.3937 | 60.799 | 121.598 |
| 49.4827 | 64.3998 | 128.7996 |
| 53.5844 | 67.7246 | 135.4492 |
| 57.697 | 70.7968 | 141.5936 |
| 61.8204 | 73.6284 | 147.2568 |
| 65.9556 | 76.2227 | 152.4454 |
| 70.1179 | 78.5056 | 157.0112 |
| 74.3122 | 80.4276 | 160.8552 |
| 78.5152 | 82.1693 | 164.3386 |
| 82.7196 | 83.8023 | 167.6046 |
| 83.771 | 84.1962 | 168.3924 |
| 84.8226 | 84.5842 | 169.1684 |

| | | |
|---|---|---|
| 86.4022 | 85.149 | 170.298 |
| 88.7717 | 85.9689 | 171.9378 |
| 91.1419 | 86.7614 | 173.5228 |
| 93.5137 | 87.5268 | 175.0536 |
| 95.8854 | 88.2718 | 176.5436 |
| 98.2557 | 89.0035 | 178.007 |
| 100.629 | 89.7037 | 179.4074 |
| 103.001 | 90.3849 | 180.7698 |
| 105.372 | 91.0542 | 182.1084 |
| 107.743 | 91.7092 | 183.4184 |
| 110.112 | 92.3459 | 184.6918 |
| 112.482 | 92.9642 | 185.9284 |
| 114.853 | 93.5656 | 187.1312 |
| 117.231 | 94.1339 | 188.2678 |
| 120.809 | 94.9169 | 189.8338 |
| 124.387 | 95.6619 | 191.3238 |
| 127.965 | 96.3814 | 192.7628 |
| 131.547 | 97.0593 | 194.1186 |
| 135.129 | 97.7089 | 195.4178 |
| 138.713 | 98.3402 | 196.6804 |
| 142.298 | 98.9544 | 197.9088 |
| 145.884 | 99.5483 | 199.0966 |
| 149.472 | 100.115 | 200.23 |
| 153.064 | 100.651 | 201.302 |
| 156.66 | 101.162 | 202.324 |
| 160.256 | 101.655 | 203.31 |
| 163.855 | 102.123 | 204.246 |
| 167.456 | 102.553 | 205.106 |
| 171.063 | 102.951 | 205.902 |
| 174.672 | 103.325 | 206.65 |
| 178.283 | 103.676 | 207.352 |
| 181.891 | 103.988 | 207.976 |
| 185.486 | 104.24 | 208.48 |
| 185.541 | 104.238 | 208.476 |
| 185.597 | 104.24 | 208.48 |
| 185.652 | 104.243 | 208.486 |
| 185.736 | 104.248 | 208.496 |
| 185.862 | 104.255 | 208.51 |
| 186.051 | 104.266 | 208.532 |
| 186.24 | 104.277 | 208.554 |
| 186.428 | 104.287 | 208.574 |
| 186.617 | 104.298 | 208.596 |
| 186.899 | 104.312 | 208.624 |
| 187.039 | 104.318 | 208.636 |

| | | |
|---|---|---|
| 187.177 | 104.318 | 208.636 |
| 187.211 | 104.317 | 208.634 |
| 187.245 | 104.314 | 208.628 |
| 187.279 | 104.307 | 208.614 |
| 187.314 | 104.292 | 208.584 |
| 187.349 | 104.249 | 208.498 |
| 187.381 | 104.09 | 208.18 |
| 187.413 | 103.767 | 207.534 |
| 187.442 | 103.448 | 206.896 |
| 187.472 | 103.123 | 206.246 |
| 187.499 | 102.717 | 205.434 |
| 187.507 | 102.596 | 205.192 |
| 187.515 | 102.447 | 204.894 |
| 187.523 | 102.264 | 204.528 |
| 187.531 | 102.031 | 204.062 |
| 187.537 | 101.656 | 203.312 |
| 187.541 | 101.234 | 202.468 |
| 187.549 | 100.95 | 201.9 |
| 187.556 | 100.708 | 201.416 |
| 187.568 | 100.408 | 200.816 |
| 187.579 | 100.084 | 200.168 |
| 187.591 | 99.8021 | 199.6042 |
| 187.604 | 99.5943 | 199.1886 |
| 187.623 | 99.3956 | 198.7912 |
| 187.65 | 99.2329 | 198.4658 |
| 187.679 | 99.1384 | 198.2768 |
| 187.708 | 99.0863 | 198.1726 |
| 187.751 | 99.055 | 198.11 |
| 187.815 | 99.0512 | 198.1024 |
| 187.912 | 99.0746 | 198.1492 |

## E.2 Case study

**Table E.2:** *FE results for the case study, Beam 1*

| **Case study, Beam 1 (C-SS)** | | |
|---|---|---|
| Displacement ($U_3$) $[mm]$ | Load $[kN]$ | Moment $[kNm]$ |
| 0 | 0 | 0 |
| 0.138123 | 0.999995 | 10.999945 |
| 0.276247 | 1.99998 | 21.99978 |
| 0.483433 | 3.49993 | 38.49923 |

| | | |
|---|---|---|
| 0.794215 | 5.74982 | 63.24802 |
| 1.26039 | 9.12454 | 100.36994 |
| 1.95967 | 14.1864 | 156.0504 |
| 3.0086 | 21.7787 | 239.5657 |
| 4.58206 | 33.1658 | 364.8238 |
| 6.94237 | 50.244 | 552.684 |
| 10.4831 | 75.8552 | 834.4072 |
| 15.8027 | 113.578 | 1249.358 |
| 23.7808 | 168.8 | 1856.8 |
| 35.7593 | 248.858 | 2737.438 |
| 53.777 | 360.931 | 3970.241 |
| 80.9492 | 507.14 | 5578.54 |
| 108.409 | 623.304 | 6856.344 |
| 136.363 | 707.016 | 7777.176 |
| 165.318 | 752.108 | 8273.188 |
| 194.279 | 785.588 | 8641.468 |
| 223.31 | 812.105 | 8933.155 |
| 252.39 | 834.232 | 9176.552 |
| 281.501 | 853.224 | 9385.464 |
| 310.7 | 869.375 | 9563.125 |
| 339.952 | 883.718 | 9720.898 |
| 369.226 | 896.887 | 9865.757 |
| 398.509 | 909.055 | 9999.605 |
| 427.797 | 920.363 | 10123.993 |
| 457.08 | 930.976 | 10240.736 |
| 486.364 | 940.964 | 10350.604 |
| 515.654 | 950.448 | 10454.928 |
| 545.015 | 959.178 | 10550.958 |
| 552.395 | 961.151 | 10572.661 |
| 554.261 | 961.565 | 10577.215 |
| 556.137 | 961.943 | 10581.373 |
| 558.018 | 962.298 | 10585.278 |
| 559.91 | 962.611 | 10588.721 |
| 561.815 | 962.873 | 10591.603 |
| 563.729 | 963.095 | 10594.045 |
| 564.209 | 963.146 | 10594.606 |
| 564.689 | 963.194 | 10595.134 |
| 565.17 | 963.241 | 10595.651 |
| 565.651 | 963.285 | 10596.135 |
| 566.129 | 963.343 | 10596.773 |
| 566.605 | 963.409 | 10597.499 |
| 567.082 | 963.472 | 10598.192 |
| 567.558 | 963.539 | 10598.929 |
| 568.033 | 963.61 | 10599.71 |

| | | |
|---|---|---|
| 568.509 | 963.679 | 10600.469 |
| 568.984 | 963.749 | 10601.239 |
| 569.457 | 963.829 | 10602.119 |
| 569.93 | 963.908 | 10602.988 |
| 570.403 | 963.987 | 10603.857 |
| 570.876 | 964.064 | 10604.704 |
| 571.35 | 964.141 | 10605.551 |
| 571.821 | 964.227 | 10606.497 |
| 572.297 | 964.299 | 10607.289 |
| 572.774 | 964.365 | 10608.015 |
| 573.251 | 964.429 | 10608.719 |
| 573.734 | 964.477 | 10609.247 |
| 574.214 | 964.534 | 10609.874 |
| 574.696 | 964.582 | 10610.402 |
| 575.197 | 964.524 | 10609.764 |
| 575.699 | 964.461 | 10609.071 |
| 576.203 | 964.368 | 10608.048 |
| 576.712 | 964.231 | 10606.541 |
| 577.217 | 964.115 | 10605.265 |
| 577.724 | 963.968 | 10603.648 |
| 578.231 | 963.819 | 10602.009 |
| 578.738 | 963.662 | 10600.282 |
| 579.246 | 963.506 | 10598.566 |
| 579.749 | 963.432 | 10597.752 |
| 580.247 | 963.478 | 10598.258 |
| 580.742 | 963.574 | 10599.314 |
| 581.237 | 963.666 | 10600.326 |
| 581.731 | 963.769 | 10601.459 |
| 582.224 | 963.875 | 10602.625 |
| 582.717 | 963.982 | 10603.802 |
| 583.21 | 964.085 | 10604.935 |
| 583.703 | 964.184 | 10606.024 |
| 583.827 | 964.208 | 10606.288 |
| 583.951 | 964.233 | 10606.563 |
| 584.074 | 964.256 | 10606.816 |
| 584.076 | 964.268 | 10606.948 |
| 584.078 | 964.279 | 10607.069 |
| 584.078 | 964.281 | 10607.091 |
| 584.078 | 964.284 | 10607.124 |
| 584.079 | 964.287 | 10607.157 |
| 584.079 | 964.288 | 10607.168 |
| 584.079 | 964.288 | 10607.168 |

**Table E.3:** *FE results for the case study, Beam 2*

| **Case study, Beam 2 (C-SS)** | | |
|---|---|---|
| Displacement ($U_3$) [$mm$] | Load [$kN$] | Moment [$kNm$] |
| 0 | 0 | 0 |
| 0.160022 | 0.999994 | 10.999934 |
| 0.320044 | 1.99998 | 21.99978 |
| 0.560078 | 3.49993 | 38.49923 |
| 0.920132 | 5.74981 | 63.24791 |
| 1.46022 | 9.12453 | 100.36983 |
| 2.27036 | 14.1864 | 156.0504 |
| 3.4856 | 21.7785 | 239.5635 |
| 5.30852 | 33.1656 | 364.8216 |
| 8.04305 | 50.2434 | 552.6774 |
| 12.1451 | 75.8539 | 834.3929 |
| 18.3089 | 113.509 | 1248.599 |
| 27.5526 | 168.682 | 1855.502 |
| 41.434 | 248.559 | 2734.149 |
| 62.317 | 360.19 | 3962.09 |
| 93.826 | 505.154 | 5556.694 |
| 125.726 | 618.863 | 6807.493 |
| 158.227 | 699.388 | 7693.268 |
| 191.807 | 743.169 | 8174.859 |
| 225.336 | 776.744 | 8544.184 |
| 258.96 | 803.479 | 8838.269 |
| 292.675 | 825.618 | 9081.798 |
| 326.47 | 844.34 | 9287.74 |
| 360.329 | 860.639 | 9467.029 |
| 368.798 | 864.445 | 9508.895 |
| 377.269 | 868.166 | 9549.826 |
| 389.982 | 873.598 | 9609.578 |
| 409.054 | 881.417 | 9695.587 |
| 428.128 | 888.866 | 9777.526 |
| 447.198 | 895.963 | 9855.593 |
| 466.269 | 902.784 | 9930.624 |
| 485.342 | 909.344 | 10002.784 |
| 513.945 | 918.764 | 10106.404 |
| 542.563 | 927.64 | 10204.04 |
| 543.459 | 927.906 | 10206.966 |
| 544.355 | 928.171 | 10209.881 |
| 545.251 | 928.435 | 10212.785 |
| 546.147 | 928.698 | 10215.678 |
| 547.043 | 928.961 | 10218.571 |
| 547.94 | 929.223 | 10221.453 |
| 548.837 | 929.484 | 10224.324 |

| | | |
|---|---|---|
| 549.733 | 929.744 | 10227.184 |
| 550.63 | 930.003 | 10230.033 |
| 551.53 | 930.252 | 10232.772 |
| 552.431 | 930.5 | 10235.5 |
| 553.331 | 930.745 | 10238.195 |
| 554.233 | 930.989 | 10240.879 |
| 555.134 | 931.23 | 10243.53 |
| 556.037 | 931.47 | 10246.17 |
| 556.939 | 931.707 | 10248.777 |
| 557.847 | 931.925 | 10251.175 |
| 558.76 | 932.127 | 10253.397 |
| 559.675 | 932.32 | 10255.52 |
| 560.593 | 932.502 | 10257.522 |
| 561.515 | 932.67 | 10259.37 |
| 562.468 | 932.717 | 10259.887 |
| 563.395 | 932.87 | 10261.57 |
| 564.314 | 933.048 | 10263.528 |
| 565.229 | 933.244 | 10265.684 |
| 566.143 | 933.442 | 10267.862 |
| 567.062 | 933.622 | 10269.842 |
| 567.98 | 933.808 | 10271.888 |
| 568.895 | 934 | 10274 |
| 569.812 | 934.189 | 10276.079 |
| 570.73 | 934.373 | 10278.103 |
| 571.643 | 934.574 | 10280.314 |
| 572.557 | 934.771 | 10282.481 |
| 573.477 | 934.95 | 10284.45 |
| 574.398 | 935.123 | 10286.353 |
| 575.315 | 935.312 | 10288.432 |
| 576.233 | 935.497 | 10290.467 |
| 577.153 | 935.676 | 10292.436 |
| 578.075 | 935.848 | 10294.328 |
| 578.998 | 936.017 | 10296.187 |
| 579.918 | 936.197 | 10298.167 |
| 580.835 | 936.383 | 10300.213 |
| 581.755 | 936.563 | 10302.193 |
| 582.677 | 936.736 | 10304.096 |
| 583.601 | 936.903 | 10305.933 |
| 583.833 | 936.944 | 10306.384 |
| 584.064 | 936.985 | 10306.835 |
| 584.296 | 937.026 | 10307.286 |
| 584.528 | 937.066 | 10307.726 |
| 584.76 | 937.105 | 10308.155 |
| 584.992 | 937.144 | 10308.584 |

| | | |
|---|---|---|
| 585.222 | 937.19 | 10309.09 |
| 585.452 | 937.235 | 10309.585 |
| 585.683 | 937.28 | 10310.08 |
| 585.686 | 937.299 | 10310.289 |
| 585.687 | 937.304 | 10310.344 |
| 585.688 | 937.311 | 10310.421 |
| 585.688 | 937.313 | 10310.443 |
| 585.689 | 937.314 | 10310.454 |
| 585.689 | 937.316 | 10310.476 |
| 585.689 | 937.316 | 10310.476 |

**Table E.4:** *FE results for the case study, Beam 3*

| **Case study, Beam 3 (C-SS)** | | |
|---|---|---|
| Displacement ($U_3$) [$mm$] | Load [$kN$] | Moment [$kNm$] |
| 0 | 0 | 0 |
| 0.167882 | 0.999994 | 10.999934 |
| 0.335766 | 1.99998 | 21.99978 |
| 0.587592 | 3.49993 | 38.49923 |
| 0.965333 | 5.7498 | 63.2478 |
| 1.53195 | 9.12449 | 100.36939 |
| 2.38189 | 14.1863 | 156.0493 |
| 3.65684 | 21.7784 | 239.5624 |
| 5.56932 | 33.1652 | 364.8172 |
| 8.4382 | 50.2425 | 552.6675 |
| 12.7419 | 75.8518 | 834.3698 |
| 19.2099 | 113.32 | 1246.52 |
| 28.9088 | 168.297 | 1851.267 |
| 43.4766 | 247.626 | 2723.886 |
| 65.393 | 357.913 | 3937.043 |
| 98.4865 | 499.189 | 5491.079 |
| 132.04 | 607.44 | 6681.84 |
| 166.388 | 679.334 | 7472.674 |
| 201.455 | 722.791 | 7950.701 |
| 236.447 | 757.562 | 8333.182 |
| 271.564 | 785.749 | 8643.239 |
| 306.767 | 809.385 | 8903.235 |
| 341.979 | 830.364 | 9134.004 |
| 377.2 | 849.222 | 9341.442 |
| 412.427 | 866.377 | 9530.147 |
| 447.649 | 882.212 | 9704.332 |
| 482.875 | 896.925 | 9866.175 |

| | | |
|---|---|---|
| 518.118 | 910.656 | 10017.216 |
| 553.368 | 923.503 | 10158.533 |
| 562.185 | 926.594 | 10192.534 |
| 564.39 | 927.357 | 10200.927 |
| 567.698 | 928.495 | 10213.445 |
| 572.665 | 930.177 | 10231.947 |
| 577.638 | 931.825 | 10250.075 |
| 582.628 | 933.402 | 10267.422 |
| 587.672 | 934.777 | 10282.547 |
| 592.731 | 936.089 | 10296.979 |
| 597.757 | 937.513 | 10312.643 |
| 605.302 | 939.611 | 10335.721 |
| 616.648 | 942.644 | 10369.084 |
| 619.49 | 943.38 | 10377.18 |
| 622.331 | 944.118 | 10385.298 |
| 626.588 | 945.233 | 10397.563 |
| 632.999 | 946.821 | 10415.031 |
| 639.403 | 948.419 | 10432.609 |
| 645.804 | 950.024 | 10450.264 |
| 655.404 | 952.418 | 10476.598 |
| 669.819 | 955.933 | 10515.263 |
| 684.246 | 959.361 | 10552.971 |
| 698.73 | 962.591 | 10588.501 |
| 720.49 | 967.252 | 10639.772 |
| 753.128 | 973.968 | 10713.648 |
| 785.791 | 980.297 | 10783.267 |
| 793.962 | 981.82 | 10800.02 |
| 802.136 | 983.317 | 10816.487 |
| 814.418 | 985.426 | 10839.686 |
| 814.611 | 985.458 | 10840.038 |
| 814.613 | 985.473 | 10840.203 |
| 814.617 | 985.495 | 10840.445 |
| 814.618 | 985.496 | 10840.456 |
| 814.618 | 985.498 | 10840.478 |
| 814.619 | 985.501 | 10840.511 |
| 814.619 | 985.505 | 10840.555 |
| 814.619 | 985.506 | 10840.566 |
| 814.619 | 985.506 | 10840.566 |

**Table E.5:** *FE results for the case study, Beam 4*

| **Case study, Beam 4 (F-SS)** |
|---|

| Displacement ($U_3$) [$mm$] | Load [$kN$] | Moment [$kNm$] |
|---|---|---|
| 0 | 0 | 0 |
| 0.190943 | 0.999993 | 10.999923 |
| 0.381886 | 1.99997 | 21.99967 |
| 0.668303 | 3.49991 | 38.49901 |
| 1.09793 | 5.74976 | 63.24736 |
| 1.74238 | 9.12439 | 100.36829 |
| 2.70908 | 14.186 | 156.046 |
| 4.15917 | 21.7778 | 239.5558 |
| 6.33439 | 33.1638 | 364.8018 |
| 9.59743 | 50.2394 | 552.6334 |
| 14.4939 | 75.7886 | 833.6746 |
| 21.8499 | 113.291 | 1246.201 |
| 32.8894 | 168.276 | 1851.036 |
| 49.4755 | 247.636 | 2723.996 |
| 74.4475 | 358.07 | 3938.77 |
| 112.19 | 500.915 | 5510.065 |
| 150.488 | 612.966 | 6742.626 |
| 189.59 | 692.984 | 7622.824 |
| 229.404 | 747.997 | 8227.967 |
| 269.609 | 789.372 | 8683.092 |
| 310.159 | 821.174 | 9032.914 |
| 350.848 | 847.812 | 9325.932 |
| 391.657 | 870.38 | 9574.18 |
| 401.869 | 875.558 | 9631.138 |
| 412.087 | 880.548 | 9686.028 |
| 427.421 | 887.72 | 9764.92 |
| 450.449 | 897.832 | 9876.152 |
| 473.51 | 907.198 | 9979.178 |
| 496.61 | 915.885 | 10074.735 |
| 502.392 | 917.975 | 10097.725 |
| 508.174 | 920.036 | 10120.396 |
| 511.428 | 921.176 | 10132.936 |
| 513.259 | 921.809 | 10139.899 |
| 516.008 | 922.745 | 10150.195 |
| 520.141 | 924.1 | 10165.1 |
| 526.5 | 925.391 | 10179.301 |
| 532.866 | 926.662 | 10193.282 |
| 539.277 | 927.768 | 10205.448 |
| 545.773 | 928.555 | 10214.105 |
| 552.451 | 928.792 | 10216.712 |
| 559.008 | 929.628 | 10225.908 |
| 565.489 | 930.743 | 10238.173 |
| 571.915 | 932.024 | 10252.264 |

| | | |
|---|---|---|
| 581.553 | 933.918 | 10273.098 |
| 595.957 | 936.845 | 10305.295 |
| 617.517 | 941.182 | 10353.002 |
| 639.099 | 945.275 | 10398.025 |
| 660.71 | 949.116 | 10440.276 |
| 682.348 | 952.723 | 10479.953 |
| 687.758 | 953.603 | 10489.633 |
| 693.171 | 954.465 | 10499.115 |
| 701.26 | 955.77 | 10513.47 |
| 707.34 | 956.696 | 10523.656 |
| 713.443 | 957.547 | 10533.017 |
| 714.974 | 957.747 | 10535.217 |
| 715.357 | 957.797 | 10535.767 |
| 715.931 | 957.869 | 10536.559 |
| 716.794 | 957.975 | 10537.725 |
| 717.66 | 958.073 | 10538.803 |
| 718.528 | 958.162 | 10539.782 |
| 719.393 | 958.261 | 10540.871 |
| 720.256 | 958.367 | 10542.037 |
| 721.122 | 958.464 | 10543.104 |
| 721.339 | 958.488 | 10543.368 |
| 721.342 | 958.503 | 10543.533 |
| 721.345 | 958.517 | 10543.687 |
| 721.35 | 958.538 | 10543.918 |
| 721.35 | 958.538 | 10543.918 |

**Table E.6:** *FE results for the case study, Beam 5*

| **Case study, Beam 5 (F-CS)** | | |
|---|---|---|
| Displacement ($U_3$) $[mm]$ | Load $[kN]$ | Moment $[kNm]$ |
| 0 | 0 | 0 |
| 0.190943 | 0.999993 | 10.999923 |
| 0.381886 | 1.99997 | 21.99967 |
| 0.668303 | 3.49991 | 38.49901 |
| 1.09793 | 5.74976 | 63.24736 |
| 1.74238 | 9.12439 | 100.36829 |
| 2.70908 | 14.186 | 156.046 |
| 4.15917 | 21.7778 | 239.5558 |
| 6.33439 | 33.1638 | 364.8018 |
| 9.59743 | 50.2394 | 552.6334 |
| 14.4925 | 75.8447 | 834.2917 |
| 21.8361 | 114.235 | 1256.585 |

| | | |
|---|---|---|
| 32.8538 | 171.779 | 1889.569 |
| 49.3857 | 258.006 | 2838.066 |
| 74.1951 | 387.144 | 4258.584 |
| 111.498 | 578.299 | 6361.289 |
| 170.875 | 725.705 | 7982.755 |
| 186.108 | 745.417 | 8199.587 |
| 201.406 | 762.079 | 8382.869 |
| 216.762 | 776.48 | 8541.28 |
| 232.207 | 788.69 | 8675.59 |
| 247.656 | 799.712 | 8796.832 |
| 263.096 | 810.129 | 8911.419 |
| 286.302 | 824.014 | 9064.154 |
| 309.469 | 836.995 | 9206.945 |
| 332.599 | 849.202 | 9341.222 |
| 355.71 | 860.61 | 9466.71 |
| 378.846 | 871.091 | 9582.001 |
| 401.962 | 880.992 | 9690.912 |
| 407.736 | 883.379 | 9717.169 |
| 413.51 | 885.737 | 9743.107 |
| 422.175 | 889.17 | 9780.87 |
| 427.058 | 891.031 | 9801.341 |
| 434.405 | 893.695 | 9830.645 |
| 445.446 | 897.459 | 9872.049 |
| 462.037 | 902.761 | 9930.371 |
| 486.948 | 910.193 | 10012.123 |
| 493.208 | 911.876 | 10030.636 |
| 499.521 | 913.318 | 10046.498 |
| 505.941 | 914.275 | 10057.025 |
| 512.417 | 915.01 | 10065.11 |

**DEPARTMENT OF ARCHITECHTURE AND CIVIL ENGINEERING**
**CHALMERS UNIVERSITY OF TECHNOLOGY**
Gothenburg, Sweden
www.chalmers.se


CHALMERS
UNIVERSITY OF TECHNOLOGY